# Development of Lab-on-a-chip Devices for Automated Zebrafish Embryo Bioassay

A thesis submitted in fulfilment of the requirements for the degree of Doctor of Philosophy

Feng Zhu

BSc (Hon)

School of Applied Sciences

College of Science Engineering and Health

RMIT University

May 2016

# Declaration

I certify that except where due acknowledgement has been made, the work is that of the author alone; the work has not been submitted previously, in whole or in part, to qualify for any other academic award; the content of the thesis/project is the result of work which has been carried out since the official commencement date of the approved research program; any editorial work, paid or unpaid, carried out by a third party is acknowledged; and, ethics procedures and guidelines have been followed.

Feng Zhu

May 2016

# Acknowledgements

This thesis would not have been possible without many people. I would like to express my deepest gratitude to my supervisor, Professor Donald Wlodkowic, for offering me the opportunity to join his innovative and exciting research. We first met each other in Auckland and moved to Melbourne together to seek the life we want and the research we enjoy. He has always been very helpful and supportive throughout my PhD years. His passion for research and attitude of life inspired me during my tough times. I feel extremely fortunate to be his student.

I would also like to show my appreciation to my collaborators. I thank Dr Jan Kaslin and Dr Timo Friedrich from Monash University for their help in fish embryo toxicity tests; Professor Philip Crosier and Dr Chris Hall from University of Auckland for introducing me to the zebrafish community; and Dr Danial Baker from Vancouver Island University for his help in embryo metabolism experiments. All the collaborations were successful and productive.

Special thanks go to my colleagues. I thank Dr Jin Akagi for teaching me microfluidics and fabrication; Dr Niall Macdonald for teaching me 3D modelling; and Dr Khashayar Khoshmanesh for his help with computational fluidic simulations. Without their guidance, my journey would have been rougher and tougher.

Last but not least, I would like to thank my family and friends for their encouragement and unconditional support when I need it the most. To my fellow group members, I wish them all the best with their studies.

# Table of Contents

# List of Figures

# List of Tables

# Abstract

Zebrafish embryos have become one of the most popular model systems in biomedical and environmental research. However, current testing protocols using conventional multiwell plates rely heavily on time-consuming and labour-intensive manual handing. Static culture environments and low-throughput data collection are outdated with regards to meet the requirements of modern compound library screening. Herein, this research presents steps towards the development of a miniaturised and automated system for manipulating zebrafish embryos by using both innovative microfluidic lab-on-a-chip technologies and three-dimensional printing technologies.

Four steps were taken to achieve this goal: (i) 3D printing technologies were explored to fabricate the lab-on-a-chip device. While 3D printing provided rapid manufacture of devices with high definition and optical transparency, as evidenced by SEM and confocal microscopy results, it caused significant toxicity in fish embryos after long-term exposure. (ii) The toxicity profile of a selection of 3D printing polymers was then extensively investigated using standard biotests. A chemical analysis was performed to reveal the compounds contributing to the toxicity. (iii) To avoid the use of toxic materials, a chip-based embryo trapping array was fabricated using biocompatible material PMMA. The chip allowed for automatic embryo loading, continuous reagent perfusion, and convenient image acquisition. The device was validated using both CFD simulations and biological experiments using reference toxicants. In addition, the embryo chip device was further developed to enable real-time metabolic level detection. (iv) A miniaturised and automated imaging platform, together with the high-throughput embryo trapping array and customised fluidic actuators, were prototyped.

# Publications

Research carried out during this study has already been published in peer-reviewed international journals. The following journal articles comprise the major parts of this thesis.

[1] Zhu, F., Skommer, J., Huang, Y., Akagi, J., Adams, D., Levin, M., Hall, C. J., Crosier, P. S., and Wlodkowic, D., "Fishing on chips: Up-and-coming technological advances in analysis of zebrafish and Xenopus embryos," Cytometry Part A, 85(11), 921-932 (2014)

[2] Zhu, F., Skommer, J., Macdonald, N. P., Friedrich, T., Kaslin, J., and Wlodkowic, D., "Three-dimensional printed millifluidic devices for zebrafish embryo tests," Biomicrofluidics, 9(4), 046502 (2015)

[3] Zhu, F., Friedrich, T., Nugegoda, D., Kaslin, J., and Wlodkowic, D., "Assessment of the biocompatibility of three-dimensional-printed polymers using multispecies toxicity tests," Biomicrofluidics, 9(6), 061103 (2015)

[4] Zhu, F., Wigh, A., Friedrich, T., Devaux, A., Bony, S., Nugegoda, D., Kaslin, J., and Wlodkowic, D., "Automated Lab-on-a-Chip Technology for Fish Embryo Toxicity Tests Performed under Continuous Microperfusion (µFET)," Environmental Science & Technology, 49(24), 14570-14578 (2015)

[5] Zhu, F., Baker, D., Skommer, J., Sewell, M., and Wlodkowic, D., "Real-time 2D visualization of metabolic activities in zebrafish embryos using a microfluidic technology," Cytometry Part A, 87(5), 446-450 (2015)

[6] Zhu, F., Hall, C. J., Crosier, P. S., and Wlodkowic, D., "Interfacing Lab-on-a-Chip Embryo Technology with High-Definition Imaging Cytometry," Zebrafish, 12(4), 315-318 (2015)

# Nomenclature

| Symbol | Description |
|---|---|
| µ_ | micro |
| µFET | microfluidic fish embryo toxicity |
| µTAS | microfluidic total analysis system |
| 1-HCHPK | 1-hydroxycyclohexyl phenyl ketone |
| 2D | two-dimensional |
| 2PP | two photon polymerisation |
| 3D | three-dimensional |
| ABS | acrylonitrile butadiene styrene |
| AFM | atomic force microscopy |
| ARM | advanced RISC machines |
| °C | Celsius degree |
| CAD | computer aided design |
| CFD | computational fluid dynamics |
| CMOS | complementary metal–oxide semiconductor |
| Da | Dalton |
| DCM | dichloromethane |
| DFC | Dreve Fototec 7150 Clear |
| DMD-PP | digital micromirror device-based projection printing |
| DMSO | dimethyl sulfoxide |
| dpf | day post fertilisation |
| $EC_{50}$ | half maximal response |
| EDM | electrical discharge machining |
| EGFP | enhanced green fluorescent protein |
| Em | emission wavelength |
| EWOD | electrowetting-on-dielectric |
| Ex | excitation wavelength |
| FC | Form Clear |
| FDM | fused deposition modelling |
| FET | fish embryo toxicity |
| FPGA | field programmable gate array |
| fps | frame per second |
| FRIM | fluorescence ratiometric imaging |
| g | gram |
| GC | gas chromatography |
| h | hour |
| HPDFO | high power density focusing optics |
| hpf | hour post fertilisation |
| HTS | high-througput screening |
| ID | inner diameter |
| iFET | sub-lethal fish embryo toxicity |
| ISV | inter-segmental vessel |
| ITO | indium tin oxide |
| L | litre |
| LBM | laser beam machining |

| | |
|---|---|
| $LC_{50}$ | medium lethal concentration |
| LED | light-emitting diode |
| LOC | lab-on-a-chip |
| LPT | Lagrangian particle tracking |
| lux | lumen per square metre |
| m | metre |
| M | molar |
| m_ | milli |
| MEMS | microelectricalmechanical systems |
| min | minute |
| MJM | multi-jet modelling |
| MMA | methyl methacrylate |
| MS | mass spectrometry |
| n_ | nano |
| NMR | nuclear magnetic resonance |
| OD | outer diameter |
| OECD | Organisation for Economic Co-operation and Development |
| Pa | pascal |
| PC | personal computer |
| PDMS | polydimethylsiloxane |
| PLA | polylactic acid |
| PMMA | poly(methyl methacrylate) |
| psi | pounds per square inch |
| PTFE | polytetrafluoroethylene |
| PTU | 1-phenyl-2-thioures |
| PUR | polyurethane |
| PVC | polyvinyl chloride |
| RIE | reactive ion etching |
| RISC | reduced instruction set computer |
| ROI | region of interest |
| rpm | revolution per minute |
| s | second |
| SEM | scanning electron microscopy |
| SLA | stereolithography |
| SLS | selective laser sintering |
| sp. | species |
| TMS | tricaine mesylate |
| USB | universal serial bus |
| UV | ultraviolet |
| VIS | visible light spectrum |
| VJC | VisiJet Crystal |
| VJSL | VisiJet SL Clear |
| W | watt |
| WXC | Watershed 11122XC |
| φ | the diameter of a circular section |

# 1 Introduction

## 1.1 Small model organism bioassays

Bioassays, or biological assessments, are one of the standardised scientific experiments used in drug discovery and ecotoxicology. They are used for a range of biological specimens from cells or tissues (in vitro) to live plants or animals (in vivo), to determine the activity or toxicity of a substance, such as a drug, protein, or unknown toxicant.

Whilst *in vitro* bioassays are simple, fast, and cheap, their test results are usually inconsistent with the human clinic trials. On the other hand, animal testing using mouse and chicken produce trustworthy results, but they are too expensive to screen a large number of samples. Therefore, small model organisms have merged to bridge the existing gap.

### 1.1.1 A brief introduction of small model organisms

In general, small model organisms are multicellular animals ranging in size from 50 µm to 2000 µm, including invertebrates and small vertebrates[1]. Commonly used invertebrate organisms are nematodes (*Caenorhabditis elegans*) and fruit flies (*Drosophila melanogaster*)[2]. They have been serving in biomedical laboratories for many decades and are still being actively used in high-throughput screening[2]. Being invertebrate animal models, they are low in cost, allow for easy genetic modification, and have no concerns of animal ethics. However, they bear some intrinsic disadvantages in that they do not have certain genes and organs for specific human disease studies. They are also evolutionarily distant from mammals, which has led to some false results.

Crustaceans, such as brine shrimp (*Artemia sp.*) and fresh water daphnids (*Daphnia sp.*), are aquatic invertebrate animal models extensively used for acute and chronic toxicity tests in ecotoxicology[3-5]. Bioassays testing on such organisms feature low cost, simple test procedures, and require a low degree of expertise. These bioassays also have relatively high adaption and sensitivity in various test conditions. In addition, with off-the-shelf test kits availability, these animals can be culture and maintenance free, which is a huge advantage for researchers[5]. Sub-lethal and behavioural responses could also be detected for different research purposes[6-9].

Zebrafish (*Danio rerio*) and clawed African frogs (*Xenopus sp.*) are vertebrate small model organisms with more complex organs, such as kidneys and a cardiovascular system, that invertebrate organisms lack. They also have a higher genetic similarity to human, compared to invertebrates. Moreover, recent advances in developing genetic tools has broaden their applications in biomedical research[10-13]. Also, development of behaviour analysis technologies has facilitated behaviour investigations in these species on a molecular basis[14-19].

Among all the small model organisms, zebrafish has become one of the most popular. Within only a few decades, it has gone from being a hobby fish to a mainstream model organism employed by scientists in a wide variety of scientific research[20]. Nevertheless, in recent years, there has been increasing concern with regard to animal welfare and research ethics, so that using adult fish for research experiment is largely discouraged. Fortunately, using early stage zebrafish, namely embryo and larvae, involves fewer ethical concerns and thus they are replacing adult zebrafish in many bioassays.

### 1.1.2 Zebrafish embryos as an animal model

Zebrafish embryos are only slightly larger in size than many invertebrate organisms, making them easy to handle manually in the laboratory, as well as capable of performing well in automated high-throughput screenings. They also survive with simple and cost effective husbandry and exhibit a large brood size that facilitates rapid and efficient bioassays. As a replacement of adult fish, zebrafish embryos can be effectively applied in many type of research. For example, zebrafish embryos are widely used in identifying lead compounds for biological targets during drug discovery[21, 22] and bio-active natural compound discovery[23-27]; they also play an important role in drug discovery preclinical toxicity tests[28-31], and in tumour studies using transgenic zebrafish reporter lines[32-39]. In addition, zebrafish embryo bioassays have remarkable applications in environmental research, particularly for assessment of aquatic toxins[40-43].

In fact, using zebrafish embryos is not only an excellent alternative to using adult fish, they also have their own advantages over adult fish. For instance, zebrafish embryos have transparent chorions and skins that enables non-evasive observation of most important

organs and cardiovascular systems. Furthermore, embryos are in early developmental stages, which are believed to be more sensitive to most chemical compounds.

Standard chemical test protocols for using zebrafish embryos have recently been established by OECD[44], also known as the Fish Embryo Acute Toxicity (FET) test. Zebrafish embryos have been validated as being able to test a variety of substances with diverse solubilities, volatilities, and hydrophobicities[44].

### 1.1.3 Challenges in current FET assays

In spite of the importance of zebrafish embryo models, standard FET tests are conducted on 24-well microtitre plates, which demand iterative manual manipulation of specimens and fluids[1, 45, 46]. Using such a method is time-consuming and labour intensive due to iterative manual pipetting. Fragile embryos can also easily be damaged during manual transferring. Moreover, static culture conditions require a substantial amount of compound solution, which is very costly for some applications, e.g. testing new therapeutic drugs. Furthermore, culturing embryos in a static environment can unfavourably bias the toxicity test results due to, for example, toxicant adsorption to the test chamber and bystander effects. Lastly, it is rather difficult to precisely position and immobilise specimens for high-resolution imaging in a microtitre plate. All above, these factors act as hurdles for high-throughput testing and lead to analytical error.

## 1.2 Microfluidics and Lab-on-a-Chip

Not surprisingly, many efforts and achievements have already been made to reform the current testing protocols. Apart from simple modifications of conventional multiwell plates[47], novel designs using microfluidic Lab-on-a-Chip (LOC) technologies have proven to greatly elevate laboratory automation and analysis. This section introduces lab-on-a-chip technologies and their applications in manipulation of zebrafish embryos.

### 1.2.1 A brief introduction to lab-on-a-chip

Lab-on-a-chip is a miniaturisation technology that integrates several laboratory functions onto a small piece of chip, which is only a few square centimetres in size. The core of a lab-

on-a-chip device is a microfluidic system that manipulates a tiny amount of fluid (usually tens of microliters) to perform chemical and biological analyses.

There are many benefits that lab-on-a-chip devices can offer us. Firstly, the consumption of reagents is greatly reduced. By using miniaturised animal culturing chambers with close-loop fluid circuits, a few hundred microliters of compound is usually enough for the entire assay, which is very favourable for high-throughput screenings. Secondly, lab-on-a-chip devices provide a flow-through condition for animal culture, which overcomes the drawbacks of testing in a static condition, such as adsorption or evaporation. Thirdly, micro channels in the chip device can be designed to function as many essential laboratory equipment, including pumps, valves, and mixers. By integrating these features, chip devices become miniaturised, portable, and convenient for clinical and environmental studies in the field.

Moreover, lab-on-a-chip devices are usually associated with microelectrical mechanical systems (MEMS) that allow various sensors to be embedded to monitor fundamental parameters, including pressure, light, and conductivity. Embedded electrical or hydraulic actuators allow users to manipulate small droplets of reagents, air bubbles, and even small live organism. Apart from micro techniques, integrating robotic actuators with computational vision technologies has been attempted to automate the whole experimental process from reagent preparation to image analysis.

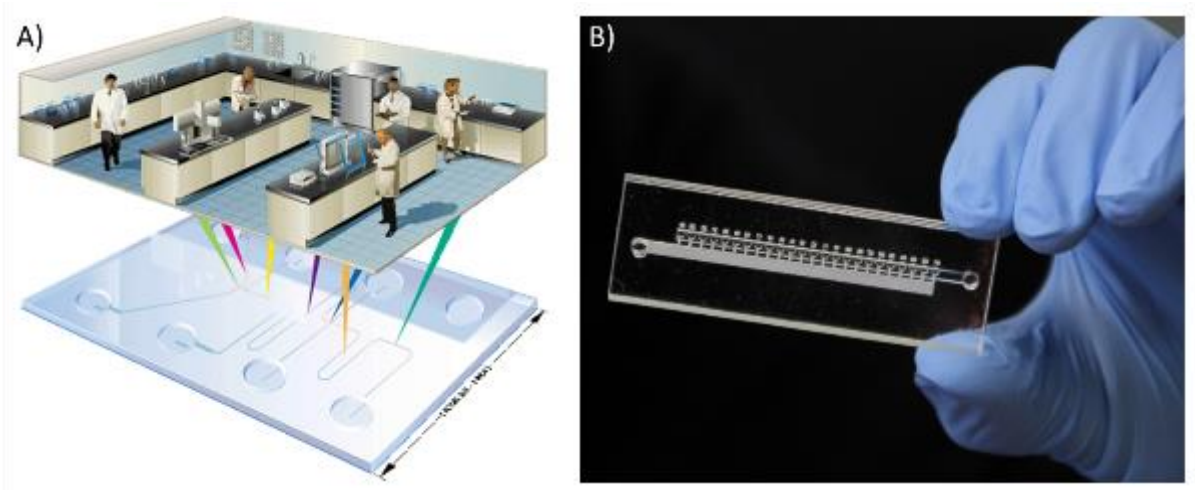


*Figure 1.2.1 Microfluidics and lab-on-a-chip. A) A conceptual image describing a microfluidic lab-on-a-chip device. Several laboratory functions are integrated onto a miniaturised chip through micro fluidic flows. The Image is sourced from a website[48]. B) An example of a lab-on-a-chip device. The size*

*of this chip was exactly same as a conventional glass microscope slide. The Image is sourced from a website[49].*

### 1.2.2 Lab-on-a-chip and zebrafish embryos

The applications of microfluidic lab-on-a-chip technologies in zebrafish embryo laboratory automation have been extensively explored by many researchers. Herein, I summarise the current and upcoming lab-on-a-chip devices and platforms that greatly improved specimen manipulation, fluidic regulation, and imaging acquisition. I present a brief introduction for each device in terms of their features, fabrication approaches, and utilities, as well as their limitations.

**Segmented flow microculture**

One of the earliest designs was the micro fluid segment technique[50]. This system comprised of a Teflon (PTFE) tubing coil, an integrated camera, and a PC controlled syringe pump[50] (Figure 1.2.2 A-B). It introduced zebrafish embryos by carrying medium (perfluoromethyldecalin, PP9) from an assay plate into the tube for imaging, where fluid flow and image recording were controlled by software[50]. In this way, zebrafish embryos were trapped in each fluidic segment and thus could be imaged individually inside the tubing. Despite of iterative dipping of the tube into the assay plate to alternatively aspirate embryos and carrying medium, the flow system and imaging system can work continuously, which can be applied for automation[50]. Interestingly, air bubbles that are inevitably introduced when changing the dipping wells were also useful for providing segment stability[50]. The limitation of this design was inadequate image quality due to the images being taken through a curved surface (the tubing).

**Digital EWOD microfluidics**

In addition to hydraulic force, a microfluidic device using electrokinetic force for transporting zebrafish embryos has been presented[51] (Figure 1.2.2 C-D). This device used electrowetting-on-dielectric (EWOD) techniques that could move an embryo-contained droplet in a gap between two plates[51]: the top plate acted as a common ground electrode; and the bottom plate had electrodes beneath a dielectric layer to manipulate droplet movement[51]. The surface of both plates were coated with hydrophobic material for easier movement[51]. Furthermore, a droplet-based on-chip dechorionation was performed by

mixing an embryo-contained droplet with a digestive agent (Pronase) droplet[51]. In addition, such mixing techniques were also useful for mixing laminar flows on microfluidic devices[52, 53].

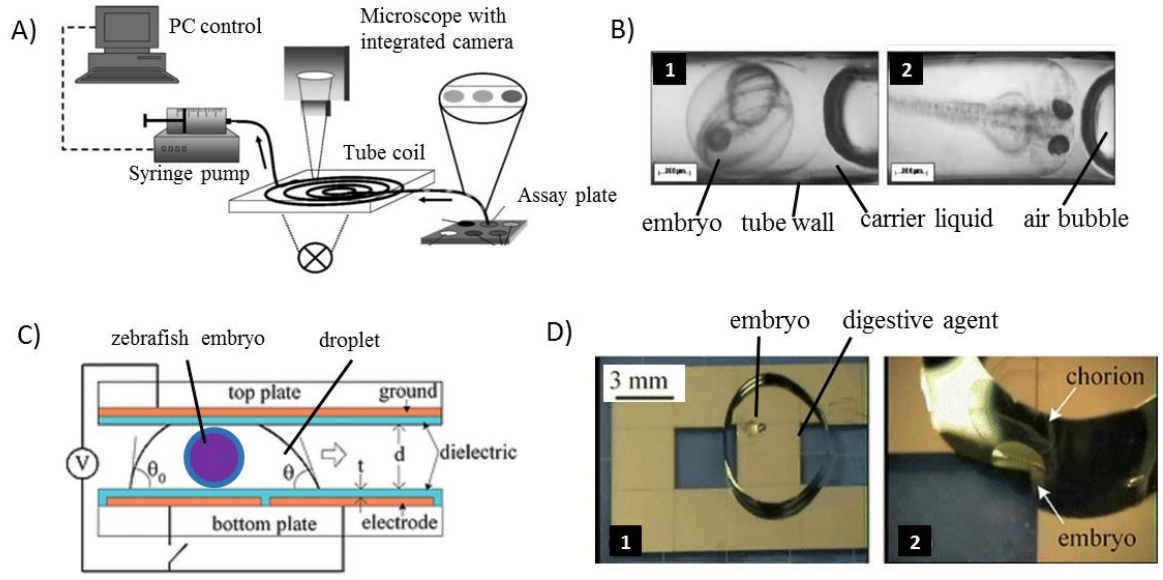


*Figure 1.2.2 Microfluidic technologies for manipulating zebrafish embryos. (A) – (B) Segmented flow microculture platform for zebrafish embryo development studies[50]. (Reproduced from Ref 50 with permission from The Royal Society of Chemistry). (C) – (D) Electrowetting device for moving zebrafish embryos[51]. (Reproduced from Ref 51 with permission from The Royal Society of Chemistry).*

**Chip-based device for embryo culture**

Using lab-on-a-chip technologies in design and fabrication, miniaturised chip-based devices have been applied to zebrafish embryo manipulation and on-chip embryo culture. Such techniques could also provide versatile functions and utilities for specific studies. Shen and co-workers presented a microfluidic chip to immobilise zebrafish embryo, with only a limited surface area of the embryo exposed to test compounds for growth factor experiments[54]. The chip was made of two layers of polydimethylsiloxane (PDMS). The top layer had a funnel-shaped aperture to immobilise the embryo; and the bottom layer contained a micro channel to deliver fluidic samples[54]. During operation, the chip was submerged in a Petri dish containing fish medium, and a gravity-driven pump was used to deliver test compounds via the micro channel[54]. When the embryo docked into the aperture, it could separate two phases of liquid[54]. While maintaining embryo viability, only the bottom part of the embryo was exposed to the test compounds. Although such a device

worked well in proof-of-concept experiments, it had limitations in high-throughput feasibility, namely embryos had to be manually positioned at the aperture using conventional pipetting. Furthermore, the design using two layers of PDMS had difficulties to be converted to a high-throughput device because the alignment would be a big issue, due to large pieces of PDMS layer bonding together, especially when both layers contain small features.

A microfluidic flow-through system was developed by Wielhouwer and co-workers (Figure 1.2.3 A). It featured an embedded heating system[55]. The device was made from three layers of bonded borosilicate glass[55]. It had two sets of flow-through systems: one for buffering solutions in on-chip embryo culture and the other for warm water keeping the desired temperature for embryo growth[55]. The embryo culturing chambers were smaller than the wells in conventional 96-well microtitre plates, but they were large enough for a hatched larvae to swim around[55]. This device facilitated on-chip flow-through culturing without an incubator meanwhile it provided real-time imaging accessibility. In particular, during the proof-of-concept culturing test, the authors observed that a high flow rate (6 µL per well per minute) can suppress the hatching rate of the embryo[55], however, a substantial flow rate (2-4 µL per well per minute) was necessary to deliver oxygen[55].

A chip-based microfluidic embryo array integrated with a concentration gradient generator was reported by Yang and co-workers[56] (Figure 1.2.3 B). This chip was made of three bonded glass plates – the top plate contains micro channel networks that were fabricated by photolithography; the middle plate contained seven embryo culture chambers that were drilled with a drill-bit; and the bottom layer simply acts as a base[56]. In experiment, embryos were manually transferred into the culturing chambers and each chamber can hold several embryos[56]. Interestingly, the chip was designed to lean around 20° to discharge waste and gain enough oxygen prior to applying drug solutions so that no tubing was required for the device[56]. Two syringe pumps can deliver drug and medium solution via concentration gradient micro channels to the chamber inlets, providing a series of concentrations over the culturing chambers[56]. For continuously flow-through on-chip culture, the chip needs to lean 20° again for the same reasons[56]. The device was designed for rapid drug toxicity tests, however, one chamber for each concentration is not optimal. Although each chamber can host multiple embryos, an overcrowded chamber is not ideal for culturing, nor for imaging.

In addition, the chip fabrication that using photolithography is complicated and uneconomical. Fabrication also involves using the dangerous chemical hydrofluoric acid (HF), which is unfavourable.

There was another chip-based microfluidic perfusion platform presented together with an embedded concentration gradient generator[57] (Figure 1.2.3 C). This prototype described by Choudhury et al. was similar to the device reported by Yang and co-workers[56], but differed in fabrication method and some other details. The chip device consisted of three different layers – an oxygen permeable and removable polyurethane membrane as a cover; a crystal silicon wafer with fluidic channels and embryo culturing chambers as a core; and a glass bonded to a silicon layer as a base[57]. Drug solution and media solution from syringe pumps created gradient concentration via microfluidic mixing channels; different mixing ratios generated different concentrations of drug solution[57]. There were eight chambers for embryo culture; each chamber had an independent inlet and outlet with specified drug concentration[57]. The culture chambers were rather small, which constrained embryos from moving freely, but was readily used for high magnification imaging. The inner surface of the micro channels were hydrophilic to minimise potential air bubbles[57]. Such a device was ready for flow-through culturing and real-time high resolution imaging, and could be used for dose-dependent chemical screenings. However, the chip only provided one embryo chamber per concentration, that is insufficient for bioassays. The fabrication for the core layer using photolithography was complicated and involved using hydrofluoric acid (HF), a method that is rather dangerous. Device set-up was also inconvenient, including manually dispensing embryos for loading and handling a 100 µm thick membrane as a cover for the chip at every use.

Another novel device with enhanced fluidic actuation capabilities was reported in a brief communication by Zheng and co-workers[58]. This device was fabricated using elastomeric PDMS layers to form embryo culture chambers. In addition to functioning as a microwell plate, it featured an embedded monolithic micro-valve system that was controlled pneumatically by actuators (Figure 1.2.3 D)[58]. This flow manipulation system can dynamically renew the medium within 10 second[58]. The device was still short of completion, but the monolithic micro-valve design has potential for many applications, including drug and anaesthetic solution delivery.

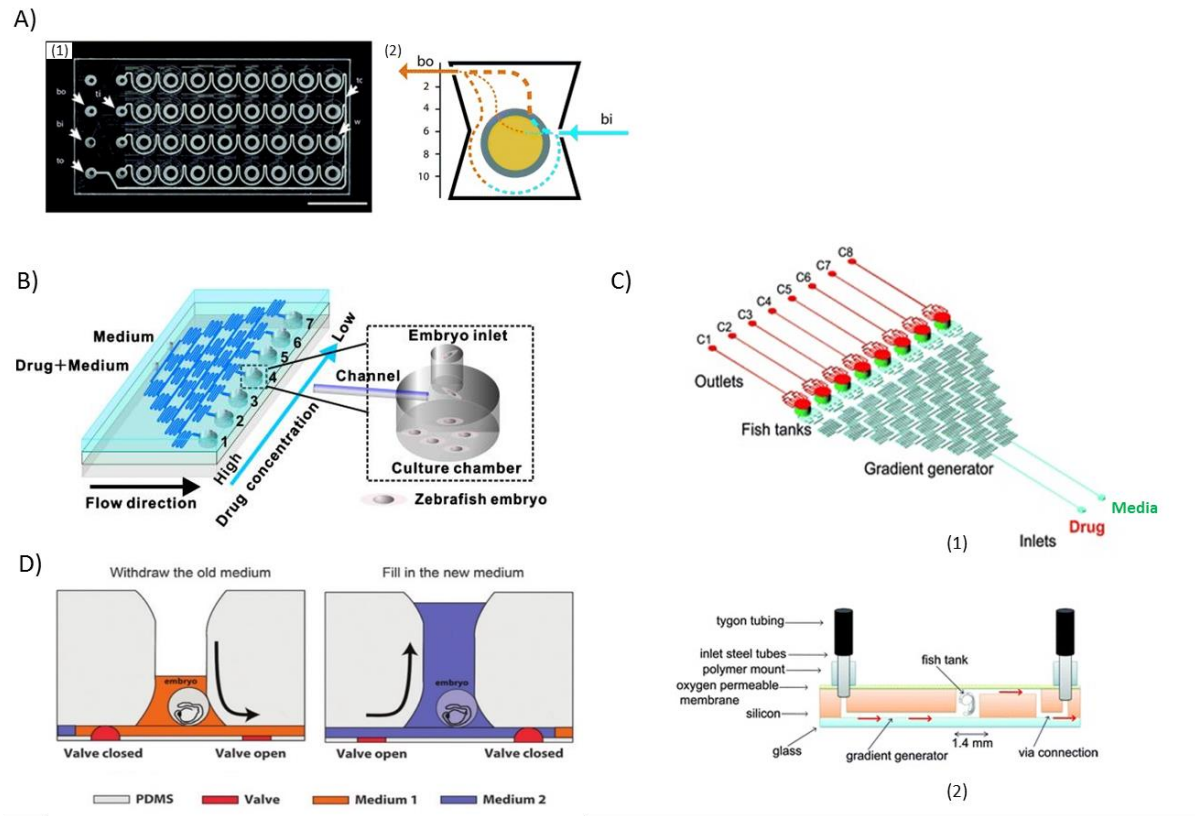


*Figure 1.2.3 Microwell chip-based embryo culture devices. (A) Microwell based microfluidic flow-through system[55]. (Reproduced from Ref 55 with permission from The Royal Society of Chemistry). (B) Microfluidic embryo array integrated with a concentration gradient generator from Yang et al[56]. (Reproduced from Ref 56 with permission from AIP Publishing LLC) (C) Microfluidic embryo array integrated with a concentration gradient generator from Choudhury et al[57]. (Reproduced from Ref 57 with permission from The Royal Society of Chemistry) (D) The schematic diagram of the microwell chip with embedded valves that enable instant fish medium exchange[58]. (Reproduced from Ref 58 with permission from The Royal Society of Chemistry).*

**Hydrodynamic fluid trap embryo arrays**

All the designs discussed above involve manually transferring embryos into the culturing chamber. For high-throughput screening processes, this is undesirable as the embryos are fragile and can be easily damaged during pipetting. To solve this issue, a miniaturised embryo array was reported for automated trapping, immobilisation, and on-chip perfusion using only hydrodynamics[59, 60] (Figure 1.2.4 A-B). The design concept was based on an anterior work reported by Tan and Takeuchi[61] for single cells trapping and immobilisation using hydrodynamic forces. Here, the chip was made of two layers: the top layer was a PDMS block containing fluidic channels and 48 embryo traps; the bottom layer was a

conventional microscope glass slide[59]. The PDMS layer was made through replica moulding. Afterwards, the PDMS layer was bonded to a glass microscope slide using oxygen plasma surface activation[59]. A peristaltic pump connected to the outlet of the channel, providing a passive hydrodynamic force; meanwhile the channel inlet was connected to PTFE Teflon tubing that can aspirate embryos from a reservoir[59]. All the embryo traps were sequenced along the main loading channel so that once an embryo docks to a trap, the following embryo would skip the occupied trap and move towards the next available trap[59]. After loading, test compounds could be introduced into the channel in the same manner as embryo loading[59]. Such hydrodynamic designs facilitate rapid and automatic loading, immobilisation and perfusion. The constrained embryo traps also enabled high magnification imaging. Based on this chip design, an automatic image analysis algorithm was presented to detect embryo anomalies during their on-chip development[62].

**Actively actuated 3D embryo arrays**

Akagi and co-workers also developed a microfluidic device for real-time analysis of transgenic zebrafish embryos[63, 64] (Figure 1.2.4 C). This multi-layer chip was made of four poly(methyl methacrylate) (PMMA) sheets, comprises of loading and suction channels, 20 embryo traps, and a heating manifold[64]. All the channels and traps were laser cut or engraved separately and then thermally bonded together in an oven[64]. The embryo loading and trapping combines hydrodynamic and gravitational forces: embryos were aspirated from a reservoir via a tubing, and then they were driven along the loading channel using suction force that was created at the outlet of the chip using a piezoelectric ultrasonic pump. When embryos flowed above the traps, they gravitationally sank into the traps assisted by suction force from micro suction channels that were located beneath the traps[64]. The trapped embryo acted as a spacer so that the following embryo could not enter into a same trap. Following trapping, compound solution can be delivered from the loading channel to each docked embryo[64]. The U shaped heating manifold that surrounds the embryo traps introduces flowing warm water and provides the proper temperature for embryo on-chip culture[64]. This design facilitated rapid device fabrication, automated embryo loading, trapping, and perfusion.

Based on this work, an integrated automation platform was then presented[65]. Apart from the microfluidic chip, the authors integrated a microfluidic actuator, a temperature

regulator, and image acquisition units[65]. All the units were controlled by a Field Programmable Gate Array (FPGA)-based embedded microcontroller[65], which made the system approach a higher level of automation. Another modification and development of the original design was focused on achieving a higher degree of integration[66]. The authors added a drug delivery manifold with another piezoelectric pump to the chip so that embryo loading and drug delivery were controlled separately with an integrated servo pinch valve[66]. Furthermore, they used an optically transparent indium tin oxide (ITO) heater to replace the previous flow-through heating manifold[66]. Moreover, a USB fluorescent microscope (Dino-lite) was also integrated for imaging together with a LED illumination and polarisation base[66]. In addition, a motorised rack and pinion drive was embedded into the stage that drives the chip for imaging[66]. All the units were controlled by PC and microcontrollers[66]. Together with embedded sample and waste bottles, the author managed to minimise the size of the platform to as large as a restaurant tray, which means it was portable for field studies (Figure 1.2.4 D).

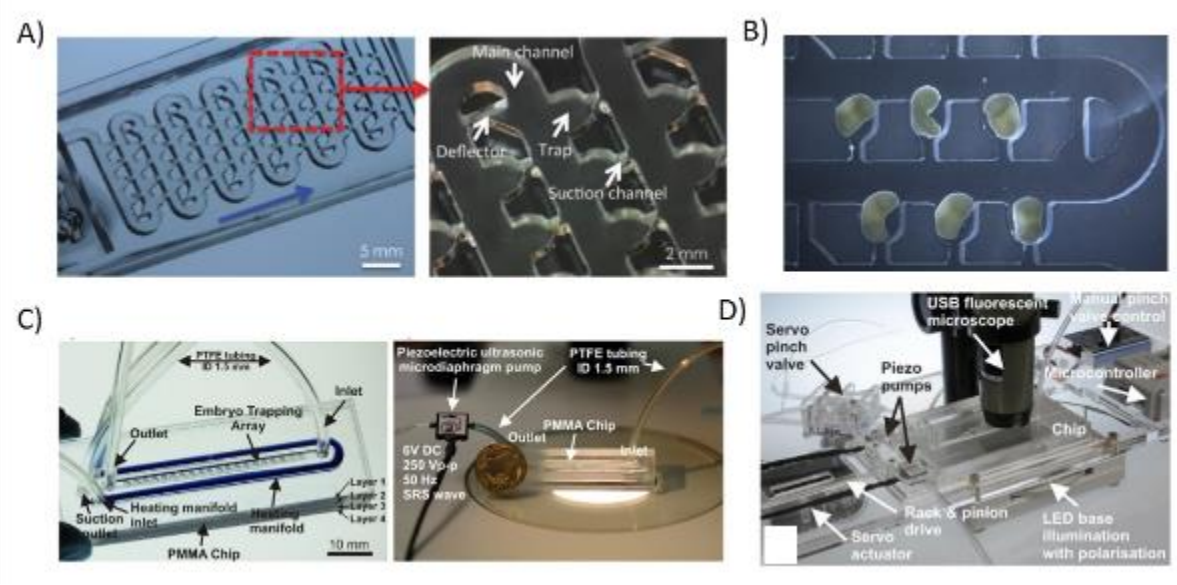


*Figure 1.2.4 Hydrodynamically and actively actuated embryo trapping array. (A) A twisted channel hydrodynamic embryo trapping array[59](Reproduced from Ref 59, no permissions were required). (B) A modified twisted channel embryo trapping array for Xenopus oocytes[67](Reproduced from Ref 67, no permissions were required). (C) A 3D multilayer linear embryo trapping array embedded with a heating manifold[64]. (Reproduced from Ref 64 with permission from Elsevier) (D) A highly integrated platform for zebrafish embryo bioassays[66] (Reproduced from Ref 66, no permissions were required).*

Letamendia and co-workers developed and presented a fully automated high-throughput zebrafish embryo screening system[68]. This robotic system comprised of a master PC, an embryo sorter, two liquid handling devices, an automatic incubator, a plate feeder, a plate transporter, and an imaging system with software[68]. Such fully motorised and automated system offered comprehensive functions for high-throughput screening, including embryo dispensation, compound delivery, culturing, imaging, and data analysis[68]. After sorting, embryos could be dispensed into a multiwell microtitre plate within 3-5 minutes[68]. Then the two liquid handling devices were capable of operating in parallel to deliver test samples for screening[68]. Afterwards, a microscope with a camera scanned the microtitre plate well by well and acquires images by imaging software[68]. Finally, a customised image analysis software processed the images and generates the results directly in Excel and Word formats[68].

**Vertebrate automated screening technology (VAST)**

Recently an advanced innovative vertebrate automated screening technology (VAST) was reported for fully automated high throughput screening[69, 70] (Figure 1.2.5). This highly integrated platform could load zebrafish larvae from either a multiwell microtitre plate or a reservoir into a detection tube, where the system could recognise larvae from air bubbles and debris[69]. Afterwards, the larvae moved into a capillary tube that was capable of automatically adjusting larvae's position and orientation from any angles for automated imaging. After experiments, the larvae could be recovered either into a multiwell plate or a reservoir[69]. Because of the precise positioning and orientating system, the image resolution could reach to cellar level[70]. The ultimate completion platform was also motorised with a multi-thread system that could process multiple animals simultaneously[70]. The authors also optimised the capillary tube material with ultra-thin borosilicate that facilitates confocal and fluorescent imaging[70]. This technology greatly facilitated *in vivo* specimen manipulation and subcellular organ imaging.

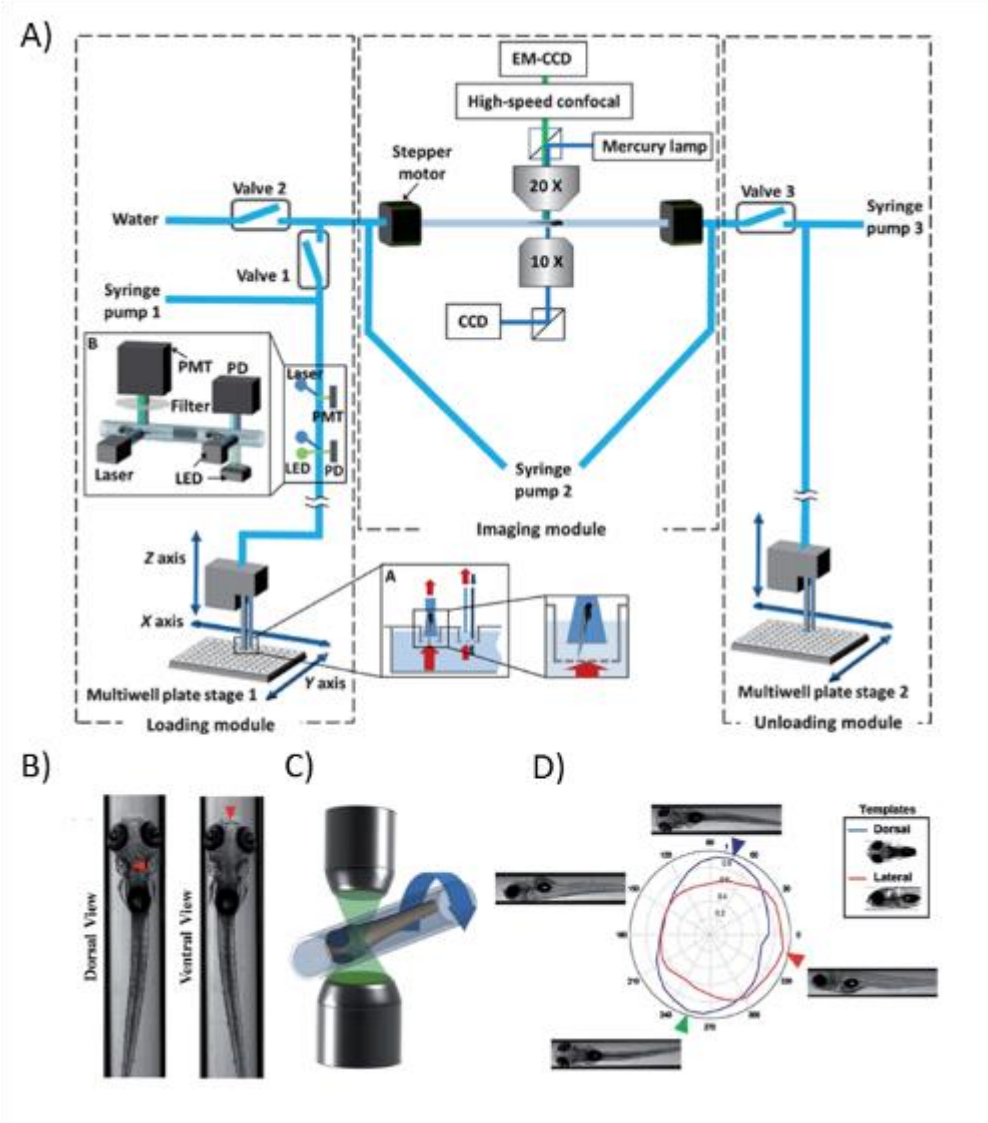


*Figure 1.2.5 VAST platform for high-throughput zebrafish larvae manipulation and image detection[70]. (A) The schematic diagram of the Vertebrate Automated Screening Technology (VAST) system. (B) – (D) in a microcapillary tube, larvae orientation can be easily adjusted for imaging. (Reproduced from Ref 76 with permission from The Royal Society of Chemistry)*

### 1.2.3 Challenges in lab-on-a-chip

Despite the growing interest and demand of lab-on-a-chip technologies in small model organism assays, lab-on-a-chip has not yet been widely adopted in practice compared with other flourishing fields using LOC technologies. This phenomenon is referred to as the workshop-to-bench gap[71]. One of the major reasons is that prototyping and fabrication of millilitre scale lab-on-a-chip devices for accommodating small model organisms are expensive and difficult to achieve using standard fabrication methods, such as mechanical machining and lithography. Another important reason is that many of the lab-on-a-chip

devices or systems are not user-friendly, and require substantial know-how and an engineering background to operate and maintain the system.

The way to solve the problems is to develop a simple and affordable fabrication methods for making lab-on-a-chip devices. A significant amount of work needs to be accomplished in exploring optimal approaches utilising advanced technologies, including those derived from microelectronics industry[72].

## 1.3 Fabrication of lab-on-a-Chip devices

Not all microfabrication methods are suitable for making a lab-on-a-chip devices. Firstly, lab-on-a-chip devices or microfluidic devices are meant to be miniaturised. Fabrication methods with high feature definitions are required. Secondly, the devices usually contain three dimensional structures with over hanging fluidic channels in an enclosed configuration, which many conventional subtractive manufacturing methods cannot achieve. Thirdly, the fabrication process needs to be relatively simple and inexpensive as most lab-on-a-chip devices are developed in laboratories with limited engineering resources.

In this section, I briefly discuss rapid microfabrication methods for making lab-on-a-chip devices, and emphasise on a cutting-edge technology: 3D printing.

**Photolithography and Softlithography**

Photolithography was one of the most successful technologies in microfabrication of industrial semiconductors and microelectronics. It can fabricate features below 1 µm. Nevertheless, for most microfluidic lab-on-a-chip devices, this resolution is overkill. Furthermore, the fabrication is very time-consuming when making large features (> 250 µm).

To improve the fabrication process, soft lithography was introduced by Qin and co-workers [73-75]. In their protocol, photolithography was only used to make a master mould with patterned structures on the stamp. Afterwards the authors used elastomeric material polydimethylsiloxane (PDMS) for replica moulding. The cast PDMS blocks can be bonded to other PDMS blocks, as well as other silicon-based surfaces such as glass. Because the mould can be reused and the PDMS is very cheap to obtain, the fabrication time and cost were

greatly reduced (Figure 1.3.1). This technology is so good that after nearly two decades, despite some disadvantages, including the complexity of making a master mould and multi-layer assembly, soft lithography is still a widely used technique in prototyping lab-on-a-chip devices.

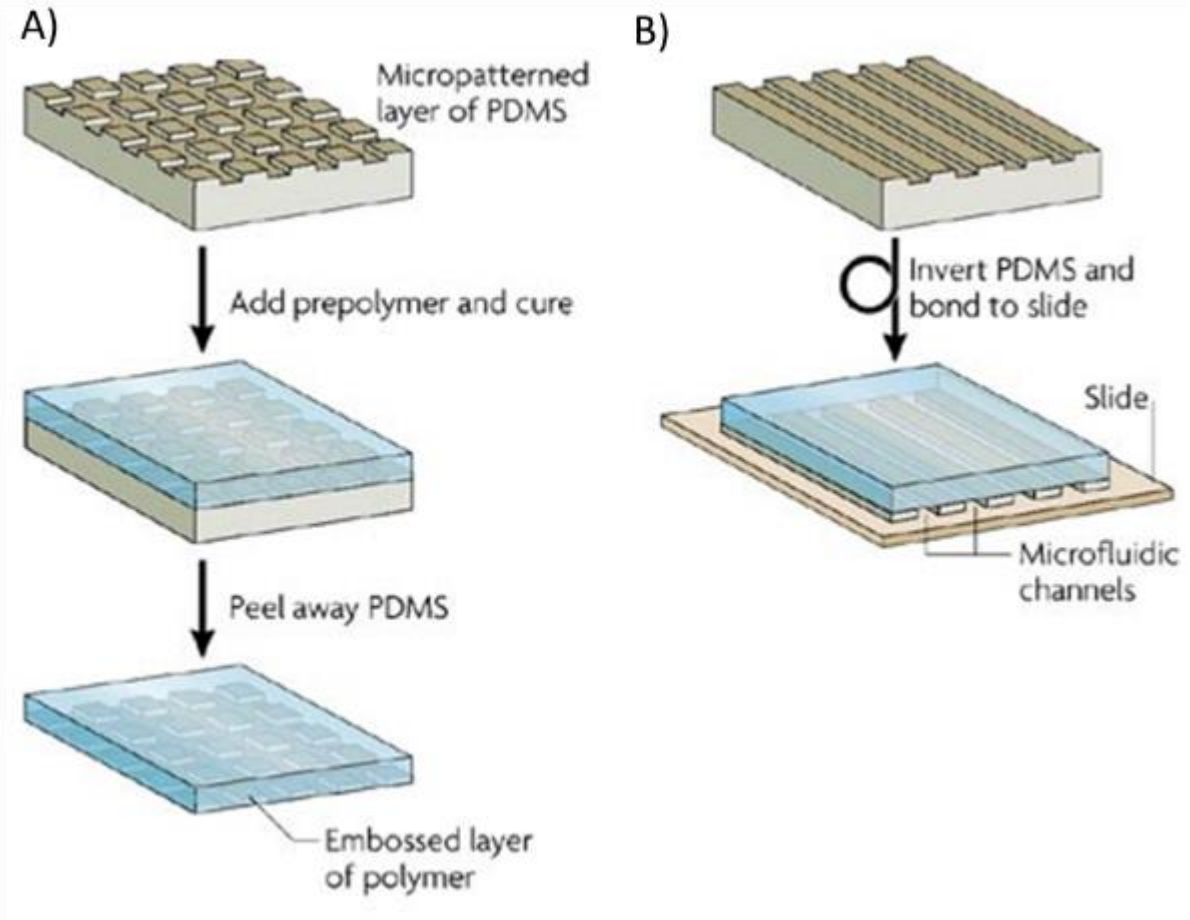


*Figure 1.3.1 Principle of PDMS soft lithography[76]. A casing is placed around the master mould, and liquid PDMS is poured over the mould. The PDMS is degassed under vacuum, and is later heated in an oven to harden. Cast PDMS is peeled off the master and then bonded to a flat substrate to enclose the microchannels to form a complete microfluidic device. The mould can be reused, and thus new devices can easily be made repetitively and quickly. (Reproduced from Ref 76 with permission from Nature Publishing Group)*

**Laser beam machining**

Cutting, grinding, and punching are essential techniques for fabrication. However, conventional machining methods using mechanical force to remove unwanted materials may influence the fabrication accuracy through the deposition of waste materials on the surface[72]. The feature resolution is also limited by the spot size of the tools. Hence new

technologies using non-contact machining methods have been developed. For example, electrical discharge machining (EDM) is a well-developed fabrication process based on melting and vaporisation of materials by electrical sparks generated between the parts and the tools[72]. The drawback of this technology is that it can only function effectively with conductive materials such as metals. The fabrication process is also time-consuming and expensive.

Laser beam machining (LBM) melts and vaporises materials by heat generated from a high energy laser source[72]. The beam shape is controlled by optical lenses to sharply focus on a small spot on the surface of the object. The optical lenses also determine the resolution and the precision of the laser. The laser power can easily fabricate with wood, fabric, and plastics and a high energy laser source is also able to fabricate with metals (Figure 1.3.2).

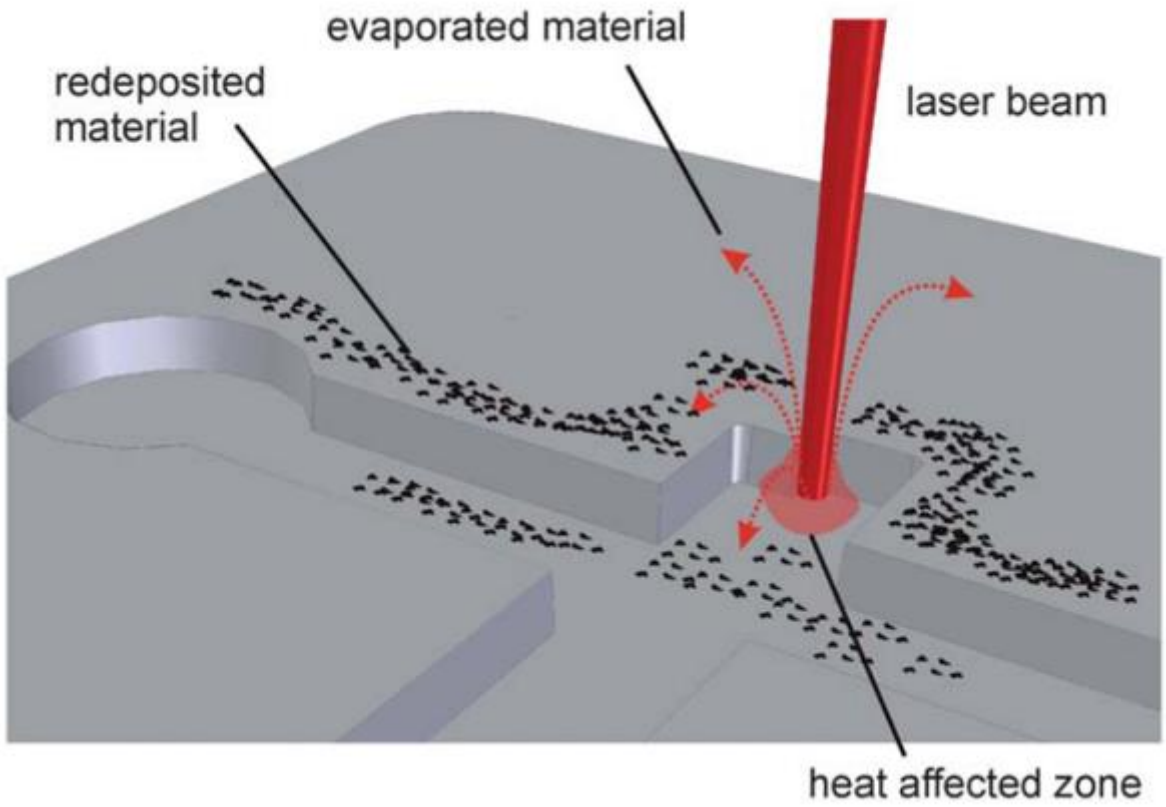


*Figure 1.3.2 Principle of direct laser micromachining[77]. A laser beam scans throughout the material. The laser creates a small heated area where the material will be evaporated. In this way, the unwanted material is expelled from the fabrication area in gaseous form, preventing the risk of material re-deposition on the surfaces and the resulting increase in surface roughness. (Reproduced from Ref 77 with permission from The Royal Society of Chemistry)*

Apart from two-dimensional fabrication, such as cutting and grinding, laser-fabricated plastic sheets can be assembled and thermally bonded together and form three dimensional structures. Furthermore, such a technique can be used to fabricate master moulds for soft lithography[59].

### 1.3.1 Three dimensional (3D) printing

Three dimensional printing, a.k.a. 3D printing, is an additive manufacturing process. The name is sometimes misleading because many other additive manufacturing technologies are also capable of creating three dimensional structures by stacking two-dimensional planes and assembling them in a third dimension. Yet, they are often called as 2.5-dimensional (2.5D) manufactures. The main feature that stands out the genuine 3D printing is that it can make an object with arbitrary shaping in all dimensions[77]. The widely accepted definition of 3D printing specifically refers to the technology that selectively solidifies materials on a three-dimensional building stage. With few exceptions, most of them are building on a layer-on-layer basis. The 3D printing technology has been commercially available for more than two decades, but only recently, when the original patent expired, were great advances in developing 3D printing technologies achieved. At present, there are several different 3D printing types on the market.

**Stereolithography (SLA)**

Stereolithography is the classical method of 3D printing developed by Hull in 1986[78]. In practice, fabrication takes place in a container filled with photosensitive resin. A radical stimulation (usually a UV laser) is used to scan and cure the resin at the surface of the building platform in the resin tank. After the surface layer hardens, the building platform will shift one layer so the laser will be focused on curing the next layer of the object. This process is repeated until the entire structure is cured.

Currently, there are two different types of SLA printers: the bath configuration and the bat configuration[77]. The bath configuration is the conventional set-up. The laser is sourced from the top while the building platform submerges in the resin bath. The platform continuously moves downwards during the printing. In this method, however, the printable height of the object is limited to the depth of the resin tank. In contrast, the bat configuration is more advanced and widely accepted[77]. In this printing method, the laser comes from the bottom

of the resin tank and the printing pad is hanged over and pulled away from the resin tank during the printing. By this way, the printed object is positioned upside down when finish, but the height of the object is independent from the depth of the resin tank[79, 80] (Figure 1.3.3).

SLA features high resolution, smooth surfaces, and acceptable printing speed. It is now globally applied in industrial prototyping processes. Many 3D printing technologies are derived from SLA and are often compared with it.

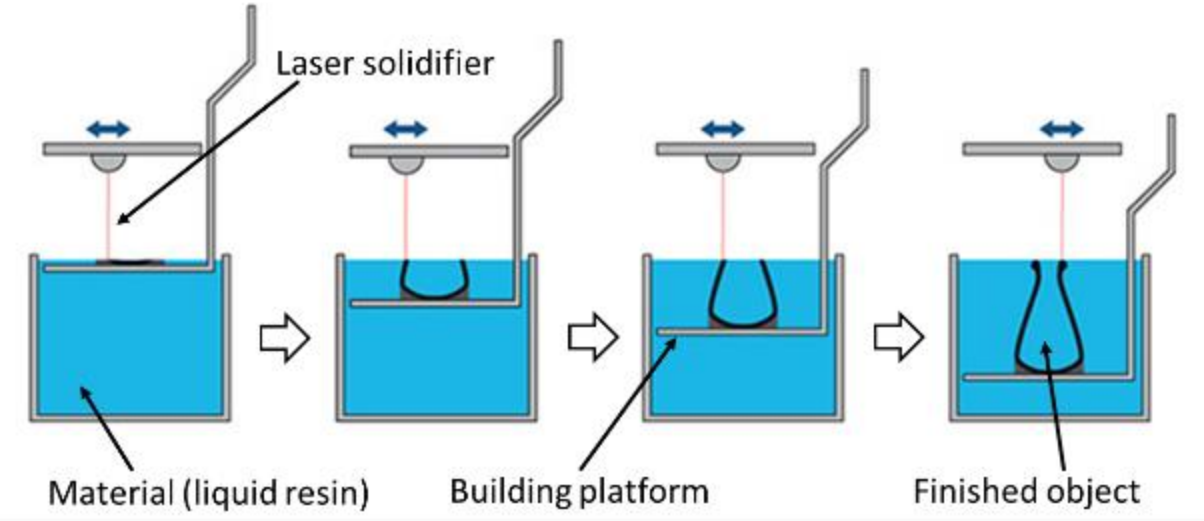


*Figure 1.3.3 Principle of Stereolithography (SLA) with bath configuration. The figure is adapted from a webpage[81].*

**Digital micromirror device-based projection printing (DMD-PP)**

This is a technology similar to the SLA, however, instead of using a laser to scan the shape of the printing object, it uses a projection system together with a digital mirror that can reflect the light to cure an entire layer simultaneously, where unwanted printing areas are digitally masked[82]. Besides, it is sometimes unnecessary to move the printing stage in DMD-PP because the focus depth can be automatically adjusted by tilting the convex lens equipped with the printer[83]. As a result, this technology can greatly reduce the printing time and it is believed to be the next generation of SLA[77].

**Two photon polymerisation (2PP)**

Two photon polymerisation is a direct writing technology. During the printing, two photons are absorbed by the photo initiator for the polymerisation reaction to begin from both sides directly within the volume of the resin[82, 84]. Because the resin is transparent, the focus of the laser beam can be controlled by adjusting the laser beam energy and the number of applied pulses[84]. Despite the fact that printing speed is decreased in 2PP, the printing resolution is greatly improved by avoiding contact to the oxygen and having a much smaller laser spot size[84].

**Multi-jet modelling (MJM)**

Also known as **Inkjet (Polyjet) 3D printing**, MJM is a technology that is similar to conventional paper printers. The MJM printer usually has cartridges that contain printing materials, including photosensitive resins, plastic granules, or wax. The print head embeds multiple nozzles that are capable of jetting tiny drops of resins, melted plastics, or wax on to the printing pad. Once the droplets are cured by UV or thermally hardened on the printing platform, the printing stage moves downwards a step for building of the next layer on top of the previous one. By using multiple nozzles jetting picolitre droplets, this printing method gains high resolution and printing speed[82]. It also uses wax (which can be melted away later) as a support material for printing over hung structures, rather than print an additional supportive structure (which could to be manually removed later) in SLA technology. The only drawback for MJM is that cleaning out the wax is tedious and troublesome when printing certain structures. Although there are some water soluble support materials available now, the cleaning procedure is actually still difficult. The so-called water soluble supports also require some special solvents provided by the manufacturer to be dissolved, with the assist of constant tumbling in a specifically designed support cleaning apparatus.

**Fused deposition modelling (FDM)**

Also known as **Fused filament fabrication (FFF)**, FDM is one of the most widely used 3D printing technologies at present. It uses a heating nozzle to melt thermoplastic filaments that are continuously fed into the extruder. Because there is only one nozzle for each polymer, melted polymers are dropped as threads onto the printing platform and then solidified on top of each another layer. After one layer is finished, the printing stage moves down one step for building the next layer. Depending on the manufacturer of the printer, it

also can have more than one nozzle to be able to print different materials together. This straightforward printing rational welcomes an extensive selection of materials (thermoplastics) for use in fabrication, as well as making itself relatively inexpensive. Its resolution, however, is also restricted by this printing method as it creates gaps formed from two adjacent molten polymer threads. The gaps result in a rough surface when finish and often cause leakage when containing liquids (Figure 1.3.4).

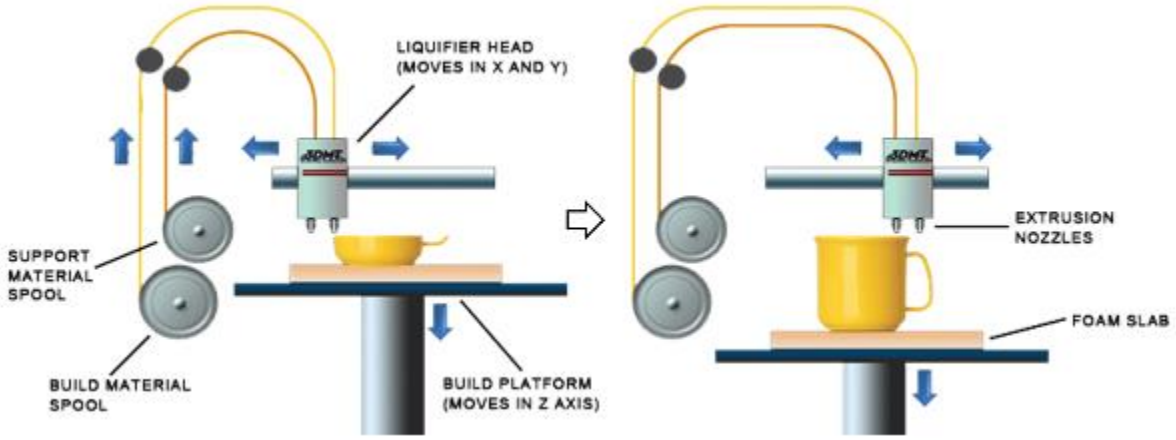


*Figure 1.3.4 Principle of Fused deposition modelling (FDM). The figure is adapted from a webpage[85].*

**Selective laser sintering (SLS)**

Selective laser sintering is a powder 3D printing technology[77]. There is powder reservoir filled with metal, ceramic, or polymer powders, continuously feeding a powder slider. On the printing platform, the slider spreads a thin layer of material powder smoothly and evenly. A laser is then used to selectively heat and fuse the powder particles into a bulk object. The most advantageous feature of technology over others is that it can print metals and ceramics, while other 3D printings can only work with plastics. Unlike resins or thermoplastics, metal and ceramic powders are not compressible, so there is no support structure needed to printing over hanging structures. The residue powder, however, is still difficult to remove from small and narrow structures.

**Bioprinting**

Bioprinting provides a solution that allows cells and biomaterials to be arranged together in a specific structure[82]. The printing methods, as well as materials, vary between different printer manufacturers, but they typically use combinations of other 3D printing technologies

(such as DMD-PP[86] and MJM[87]) together with cells, hydrogels, or other viscous biocompatible materials in fabrications.

To sum up, each of the 3D printing technologies has its highlights and drawbacks and there are different applications for each technology. The table below outlined the characteristics of each aforementioned 3D printing technology (Table 1-1):

*Table 1-1 Comparison of 3D printing technologies*

| **Type** | **Material(s)** | **Resolution** | **Speed** | **Cost** | **Feature(s)** |
|---|---|---|---|---|---|
| SLA | Photoresist resin | <100 µm | Medium | Medium | High resolution |
| DMD-PP | Photoresist resin | <100 µm | Fast | Medium | Rapid fabrication |
| 2PP | Photoresist resin | <100 nm | Slow | High | Ultra-resolution; Truly 3D structure |
| MJM | Photoresist resin; Thermal polymer | <100 µm | Medium | Medium | Use of multiple materials together |
| FDM | Thermal polymer | >200 µm | Fast | Low | Simple and cheap; multiple materials; without support |
| SLS | Metal; Ceramics | <100 µm | Medium | Medium | Use of metal as material |
| BIO | Cell; Hydrogel | <100 µm | Slow | High | Use of cells as material |

### 1.3.2 Applications of 3D printing in making lab-on-a-chip devices

Comparing all major microfabrication techniques, 3D printing features high resolution, capability for making complex structures, and a simple and inexpensive fabrication process. Recent advances of 3D printing technologies have gained a growing interest in the biological and biomedical communities, and the applications of this technology in making microfluidic and lab-on-a-chip devices are being explored.

**Master mould fabrication**

The first application for microfluidics that used 3D printing involved making master moulds for elastomer casting. Back in 2002, McDonald and co-workers attempted to produce master moulds for microfluidic device fabrications with PDMS[88]. A Thermojet 3D printer (3D

Systems) using multi-jet moulding (MJM) technology was used in this study. At that time, however, the resolution for the printer was only 250 µm, which was not enough to make normal microfluidic devices, so only large channels (>250 µm) were tested in printing. As a result, the printed surface was so rough that the optical transparency was limited. The mould was also too soft, especially after being thermally cured with PDMS. Despite all these disadvantages, many positive prospects were foreseen, including simplicity in fabrication, large scale manufacturing, and fast but not labour intensive operation.

Eight years after MJM was well developed, Bonyar and co-workers once again investigated the difficulty, resolution, and fabrication speed of using a new MJM 3D printer to construct moulds for PDMS replica moulding[89, 90]. In computer aided designs (CAD), they drew a few rectangular channels and then printed them out by using an Objet Geometries Eden 250 printer. This 3D printer had two printing modes, namely "glossy" and "matt". They found that although the "glossy" mode printed fully transparent parts with smoother surfaces, the printing accuracy was actually very poor, and vice versa for the "matt" mode. Interestingly, despite the manufacturer's claims that the 3D printer had a sub 100 µm resolution, in practice, only those structure that are larger than 200 µm (for "matt") and 400 µm (for "glossy") were reliably built with accuracy. However, neither of these modes were actually useful for making complex microfluidic channels or devices directly (Figure 1.3.5).

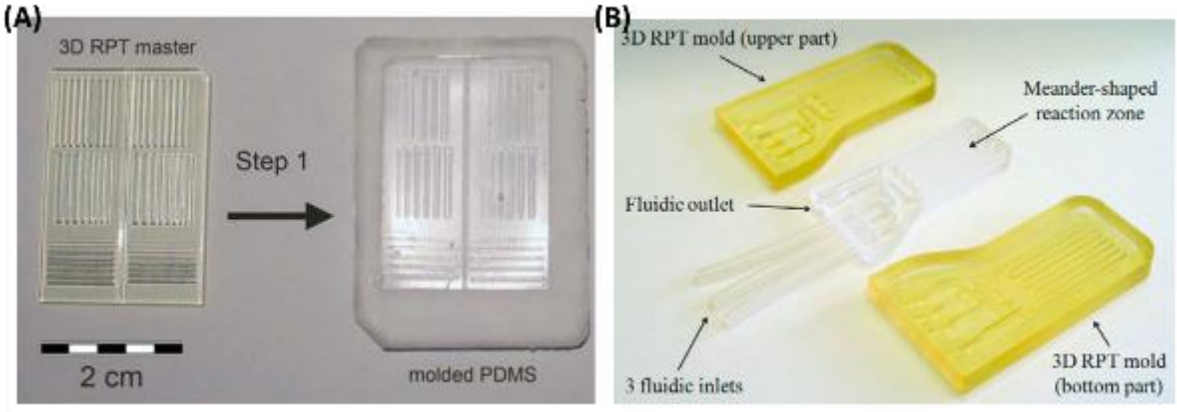


*Figure 1.3.5 3D printing for making master moulds. A) From left to right: A 3D printed master mould; a negatively moulded PDMS layer; and a positively moulded epoxy mould[90]. (Reproduced from Ref 90 with permission from Springer). B) A PDMS microfluidic cell lysis chamber moulded from 3D printed master moulds[89]. (Reproduced from Ref 89 with permission from Elsevier)*

**3D printed microfluidic interconnections**

Dealing with leakage is an instinctive problem in microfluidics. Three dimensional printing is capable of solving the issue by printing a fluidic interface with embedded connectors. Han and co-workers first reported a so-called microfluidic-system-interface (MSI) technology that can interconnect to complex microfluidic systems[91]. They used a SLA 3D printer to make an interface layer containing O-ring ports and fluid manifolds. This layer was then glued to the top surface of a glass microfluidic device. With this set-up, the system withstood up to 116 psi during testing. Unfortunately, by using glue to irreversibly bond the interface onto the chip, the fabrication method became complicated again, which lost the advantage from using 3D printing.

Paydar and co-workers also reported a 3D printed interface that contained a flexible gasket, an embedded O-ring, and a rigid clamp[92]. Tubing were directly connected to the interface and docked to the chip device by clamping the interface at the connection port. This design was tested with the goal of being able to hold a dead-end pressure up to 60 psi. However, in a subsequent test with the same prototype, the interface failed at 36 psi in a 12 hour test. This suggested that the clamping mechanism has its limitation for use in long-term experiments. This problem would be magnified further for applications such as long-term culture of small model organisms.

Au and co-workers attempted to solve this problem by directly integrating 3D printed Luer connectors into the design of chip devices[93]. They made their microfluidic chips with female Luer connector embedded while the tubing was connected to commercially available male Luer connectors. Thanks to modern SLA technology, the printing resolution was high enough to create the three dimensional helix structures on the Luer connectors. From their test, the desired dimensions fit very well to the practically measured sizes (Figure 1.3.6). The authors also demonstrated acceptable optical transparency of 3D printed channels compared with glass microscope slides using fluorescent cells. Interestingly, the authors stated that the "resolution" defined as minimum printable feature, is not equivalent to the minimum printable channel in microfluidics. Despite the convincing report, the capabilities of desktop 3D printers to fabricate complex microchannels still require more investigations on different microfluidic devices.

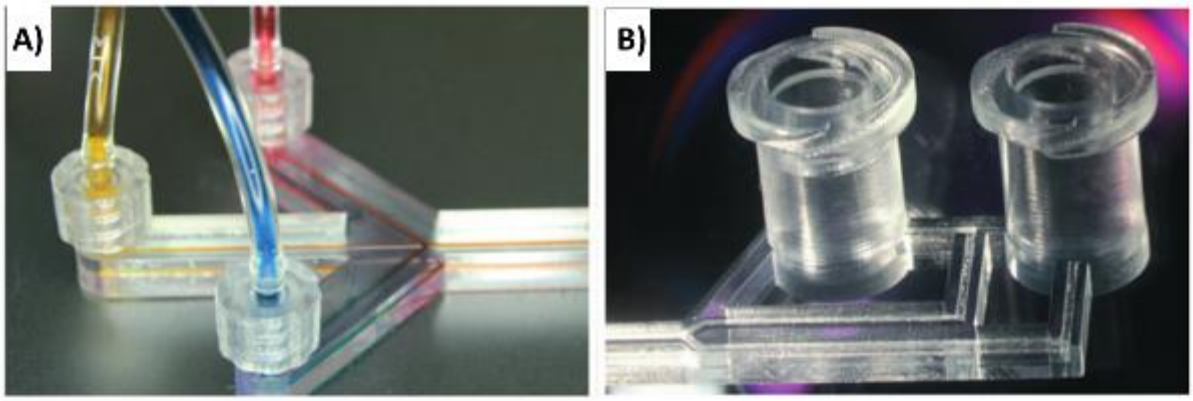


*Figure 1.3.6 3D printing for making fluidic interconnectors[93]. A) Male Luer connectors interconnecting with 3D printed microchannels. B) 3D printed female Luer connectors integrated on the chip device. (Reproduced from Ref 93 with permission from The Royal Society of Chemistry)*

**Monolithic lab-on-a-chip devices**

Using 3D printing technologies to fabricate monolithic lab-on-a-chip devices was reported by many research groups. Compared to conventional PDMS casting technology, although 3D printing has many advantages during the fabrication process, in practice, it still has issues such as low resolution, rough surface, and difficulties in post processing procedures. Thus the current 3D printing technologies are well suited to make devices in millimetre scale, rather micrometre scale. Also, it is critical to choose a suitable 3D printing technology for different device designs.

Preechaburana and Filippini pioneered a feasibility study for printing monolithic microfluidic devices[94]. In this report, a series of microfluidic manifolds in arbitrary positive, negative, and suspended 3D geometries were created. The authors described the substantial capabilities of 3D microfabrication methodology to fabricate 3D micro structures in a concise and affordable way. In a highlight of this study, the authors managed to 3D print a cantilever structure for fluid mixing purposes in a stream of flow. By using a DMD-PP 3D printer, all the microstructures were fabricated within 5 minutes. Unfortunately, the printing system only supported a maximum working area of 4 $mm^2$ at the highest resolution mode, which is insufficient for most monolithic microfluidic devices.

Bonyar and colleagues presented a monolithic fluid mixer and homogeniser for gynaecological cervical sample storage and pre-processing[89]. The authors took full advantages of 3D printing to make microfluidic device that were inexpensive and

disposable, so the device was capable of separating deoxyribonucleic acid (DNA) and protein from cervical samples and delivering them from a clinic to a laboratory. In addition, the authors also showed some flexibilities in using 3D printing technologies; they customised a holder platform for a surface Plasmon resonance imaging instrument. The process from the design all the way through the fabrication occurred within a day, which avoided tedious purchase order procedures from the original manufacturer. However, the authors failed to provide any biological assay results from the bio device, thus its actual functionality is still unknown.

Shallan and co-workers demonstrated how to use DMD-PP 3D printing technology to fabricate microfluidic devices with different functions[95]. The authors fabricated their devices by using a miniaturised DMD-PP 3D printer with a printable stage of merely 43 mm × 27 mm × 180 mm (x × y × z), specialised for making microfluidic devices. Apart from mixing the fluids, the devices fabricated with high resolution were able to generate concentration gradients, extract droplets, and even undertake electrophoresis (Figure 1.3.7 A). Unfortunately, no topological studies of the printing surface were conducted in this paper. It is rather crucial to show these important parameters when using and testing cheap 3D printers.

Kitson and co-workers reported a few 3D printed microfluidic “reactionware” devices for chemical synthesis[96]. The devices were printed on a desktop 3D printer using FDM technology. By using polypropylene (PP) as the printing material, the devices were tolerant to a wide range of organic and inorganic chemical reactions, including reductive amination, alkylation, and large polyoxometalate synthesis. This methodology allows customised reaction wares’ design and fabrication so that it offers greater freedom to the chemistry communities (Figure 1.3.7 B). This work proved that chemical reagents were stable when exposed with 3D printed materials. However, the compatibility of using such devices for containing biological samples has not yet been tested.

Rogers and co-workers presented a 3D printed microfluidic device with membrane based valves[97]. The membrane was printed together with the chip device and functioned well at 20 psi. Interestingly, the fabrication was performed on a normal SLA 3D printer, but the authors used a tailored resin formula for specific hydrophilicity requirements. Moreover, such 3D printed devices allowed direct bonding with a range of commonly used materials,

including glass and PDMS, which broaden the application of this device even further. Unfortunately, the material selected for 3D printing was not optically transparent. This largely limited its application in biological assays.

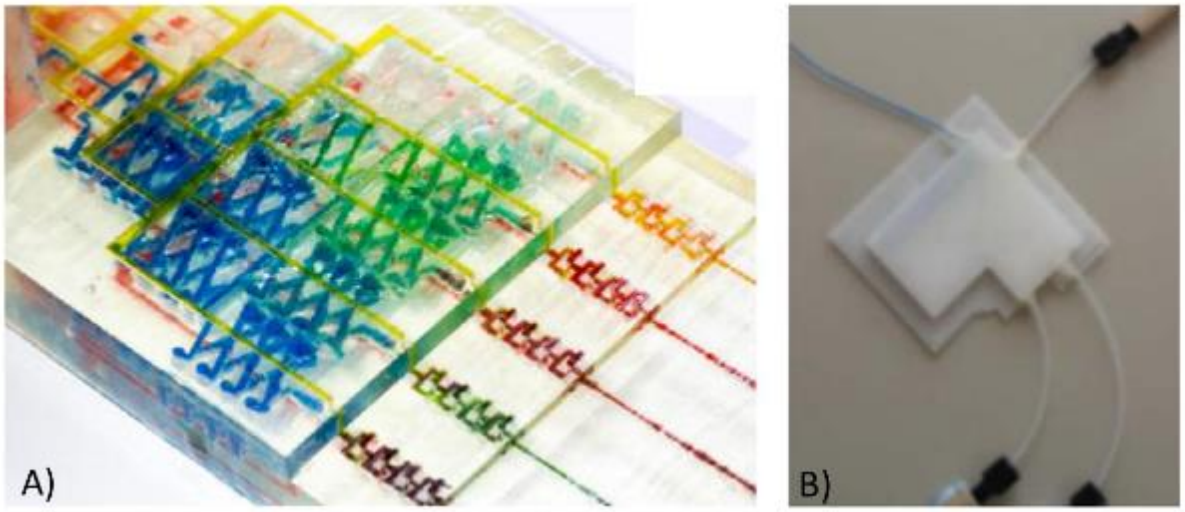


*Figure 1.3.7 3D printing for making monolithic chip devices. A) A 3D printed device filled with coloured solutions to show the different fluidic layers[95]. (Reproduced from Ref 95 with permission from © 2014 American Chemical Society). B) A 3D-printed reactionware used for polyoxometalate syntheses[96]. (Reproduced from Ref 96 with permission from The Royal Society of Chemistry)*

**3D printed lab-on-a-chip device with integrated features**

Apart from making monolithic devices, 3D printing also help fabrication with integrated features. For example, a 3D printed helix thread structure on the chip device provides capability of interconnecting additional parts easily but without leaking. Being able to integrate fine parts patches the weak point of not being able to precisely fabricate complex small features in current 3D printing technologies. Lab-on-a-chip devices become more versatile with integration of mechanic, electronic, and photonic parts for different research.

Anderson and co-workers fabricated a 3D printed high-throughput fluidic device for studying drug transport and cell viability in a parallel manner[98]. The device comprised eight parallel channels. Each channel had independent fluidic controls enabling eight independent tests in the same time. The device was also designed to allow integration of commercially available membrane inserts for different drug delivery test during dynamic flow through the system (Figure 1.3.8 A). On the other hand, the author pointed out that among the 17 available materials for the Object Connex 3D printer, only one was tested as being

biocompatible with medical approval. The need for a comprehensive biocompatibility test on commercially available 3D printing materials is thus extremely urgent.

Begolo and co-workers introduced a miniaturised pumping mechanism for microfluidic studies[99]. This 3D printed device not only served as a fluidic interface, but also could produce positive or negative pressure flow by compression or expansion of gases. In practice, up to 300 µL of reagent could be pumped into a chip device by using the pumping mechanism. In response to criticisms regarding the complexity of using lab-on-a-chip devices, the authors herein demonstrated that this device was so user-friendly that even a six-year-old child was able to operate the device after minimal training (Figure 1.3.8 B). Unfortunately, this design could only manipulate a small amount of fluid (20 µL), which is not enough for a normal bioassay on small model organisms.

Erkal and colleagues reported two 3D printed microfluidic devices with integrated electrodes for oxygen level measurement and ATP detection[100]. In both cases, the electrodes were encapsulated in cured epoxy resin and inserted into plastic fitting bolts. The bolts were then screwed into a 3D printed device with embedded threads. With different electrodes and coatings, the first device successfully detected dopamine and nitric oxide concentrations in flow injection analyses. The second device managed to detect oxygen levels in a stream of flowing biological samples (Figure 1.3.8 C). Again, this work lacked biological experiment verification and its reliability was also not demonstrated.

Walczak and Adamski explored the use of MJM technology to fabricate microfluidic structures[101]. They investigated several printers for their printing quality and optimised printing protocols. Although the authors managed to fabricate a chip device with integrated optical fibre and a spectrophotometric chip that is capable of detecting UV/VIS spectra of loaded fluids, they found that the minimum dimension for a microfluidic channel to be 3D printed properly was around 200 µm. This proved that current 3D printing technologies are only applicable for making fluidic devices in millimetre scales, rather than micrometre scales, which is suitable for devices accommodating small model organisms.

Bhargava and co-workers developed a microfluidic system with 3D printed discrete components[102]. Much like LEGO blocks, each 3D printed part had male and female connectors, together with fluid channels. They could be easily assembled into a fully

functional device in any desired configuration. The drawback of this concept is that the final assembly could be very complex for certain fluidic manifolds and leakage could also be a problem as the final assembly size becomes larger (Figure 1.3.8 D).

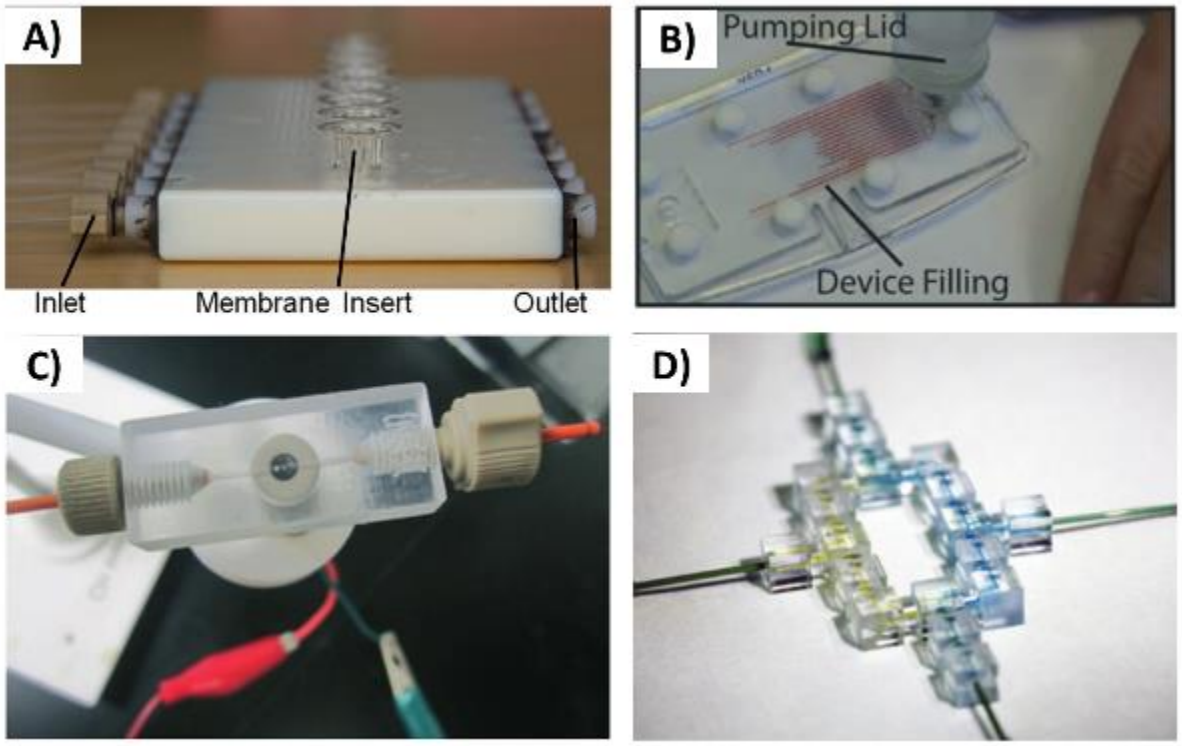


*Figure 1.3.8 3D printing for making microfluidic complexes. A) A 3D printed device with inserted membrane[98]. (Reproduced from Ref 98 with permission from © 2013 American Chemical Society). B) A 3D printed device with a self-pumping lid delivering coloured fluid[99]. (Reproduced from Ref 99 with permission from The Royal Society of Chemistry). C) A 3D printed device with integrated Pt-electrode, electrode leads and interconnectors[100]. (Reproduced from Ref 100 with permission from The Royal Society of Chemistry). D) A fluidic system combined with discrete elements[102]. (Reproduced from Ref 102, no permissions were required)*

### 1.3.3 Challenges in 3D printing

3D printing technologies have been extensively studied with regard to fabrication of microfluidic lab-on-a-chip devices. Despite promises of rapid and user-friendly fabrication processes, using 3D printing is still challenging for most microfluidics applications. The printing quality, especially the surface roughness, has not yet been properly evaluated. It is known that different 3D printers using different materials result in various finish qualities and optical transparencies. As microfluidic chip-devices require high quality fabrication, a comprehensive assessment in printing quality is necessary. Moreover, despite the fact that

most 3D printed lab-on-a-chip devices are designed for biological studies, the general toxicity profile of 3D printing materials remains largely unknown. As many 3D printing materials are developed by individual companies and their chemical composites are protected, the assessment could be performed using bioassays on selected model organisms.

## 1.4 Thesis aim and objectives

The presented research is aimed to address all the challenges described above, namely:

i) Evaluation of the feasibility of using 3D printing to fabricate a lab-on-a-chip device for zebrafish embryo bioassays.

ii) Investigation of the toxicity profile of a range of common 3D printing materials and finding the compounds contributing to the toxicity

iii) Design and development of a new microfluidic lab-on-a-chip device that allows automated zebrafish embryo arraying and long-term culturing, without material toxicity issues.

iv) Integration of technologies and prototyping a miniaturised, automated, and multi-functioned system to manipulate zebrafish embryos for high-throughput bioassays.

In particular, Chapter 2 provides general methods used throughout the thesis, including chemistries, animal cultures, and fabrications. Each objective listed above is completed and described in Chapter 3 to Chapter 6, where experimental results and discussions are presented. The thesis is concluded in Chapter 7 with an outlook of future research directions.

# 2 Materials and Methods

This chapter describes the materials used in the experiments, including reagents for biological tests, as well as materials for device fabrication. This chapter also presents methods in prototyping, animal culture, and data acquisition and analysis.

## 2.1 Chemicals and materials

### 2.1.1 Chemicals for toxicity test

**Copper sulphate pentahydrate** ($CuSO_4 \cdot 5H_2O$) and **caffeine** were purchased from Sigma-Aldrich, Australia as solid powders. Solutions were prepared by dissolving solids in E3 medium in volumetric flasks, followed by serial dilutions.

**1-Hydroxycyclohexyl phenyl ketone** (1-HCHPK; Sigma-Aldrich, Australia) was dissolved in dichloromethane (Sigma-Aldrich, Australia) at a ratio of 600:1 (w/v) as a stock solution. Working solution was prepared by serial dilutions using E3 medium. Vehicle control was prepared by adding dichloromethane into E3 medium.

**Dimethyl sulfoxide** (DMSO), **phenol, ethanol,** and **nicotine** were purchased from Sigma-Aldrich, Australia as liquids. Solutions were prepared by adding test chemicals into E3 medium in volumetric flasks, followed by serial dilutions.

Anti-angiogenesis drugs **AV951** (Tivozanib; Symansis Ltd., Auckland, New Zealand) and **Sunitinib** (Sutent; Sapphire Bioscience Ltd., New South Wales, Australia) were dissolved in DMSO as stock solutions. Working solutions were prepared by serial dilution using E3 medium. Vehicle control was prepared by adding DMSO into E3 medium.

### 2.1.2 Biological culture media

**Algae culture medium** (MLA medium) was prepared as shown below in Table 2-1. The final culture medium (working solution) was then autoclaved.

*Table 2-1 MLA medium formulation*[103]

| Constituents | Working solution (mg/L) |
|---|---|
| 1. $MgSO_4 \cdot 7H_2O$ | 49.1 |
| 2. $NaNO_3$ | 170 |
| 3. $K_2HPO_4$ | 34.8 |
| 4. $H_3BO_3$ | 2.4 |
| 5. $Na_2EDTA$ | 4.56 |
| 6. $FeCl_3 \cdot 6H_2O$ | 1.58 |
| 7. $NaHCO_3$ | 18 |
| 8. $MnCl_2 \cdot 4H_2O$ | 0.36 |
| 9. $CuSO_4 \cdot 5H_2O$ | 0.01 |
| 10. $ZnSO_4 \cdot 7H_2O$ | 0.022 |
| 11. $CoCl_2 \cdot 6H_2O$ | 0.01 |
| 12. $Na_2MoO_4 \cdot 2H_2O$ | 0.006 |
| 13. $H_2SeO_3$ | 0.0012 |
| 14. $CaCl_2 \cdot 2H_2O$ | 29.4 |
| 15. $Na_2SO_3$ | 12.6 |
| 16. Thiamine HCl | 0.1 |
| 17. Biotin | 0.0005 |
| 18. Cyanocobalamin (Vitamin $B_{12}$) | 0.0005 |

**Duckweed culture medium** (Hoagland's E-medium) was prepared as demonstrated below in Table 2-2. The final culture medium (working solution) was then autoclaved.

*Table 2-2 Hoagland's E-medium formulation*

| Constituents | Working solution (mg/L) |
|---|---|
| 1. $MgSO_4 \cdot 7H_2O$ | 246 |
| 2. $Ca(NO_3)_2 \cdot 4H_2O$ | 542.8 |
| 3. $KH_2PO_4$ | 68 |
| 4. $KNO_3$ | 252.5 |
| 5. $H_3BO_3$ | 1.43 |
| 6. $MnCl_2 \cdot 4H_2O$ | 0.91 |
| 7. $ZnSO_4 \cdot 7H_2O$ | 0.11 |
| 8. $Na_2MoO_4 \cdot 2H_2O$ | 0.045 |
| 9. $CuSO_4 \cdot 5H_2O$ | 0.045 |
| 10. $FeCl_3 \cdot 6H_20$ | 9.68 |
| 11. EDTA | 30 |

**Daphnia culture medium** contained $NaHCO_3$ (67.75 mg/L), $CaCl_2 \cdot 2H_2O$ (294 mg/L), $MgSO_4 \cdot 7H_2O$ (123.25 mg/L), and KCL (5.75 mg/L) in Milli-Q water.

**Rotifer culture medium** contained $NaHCO_3$ (96 mg/L), $CaSO_4 \cdot 2H_2O$ (120 mg/L), $MgSO_4 \cdot 7H_2O$ (123 mg/L), and KCL (4 mg/L) in Milli-Q water.

**Ceriodaphnia culture medium** contained $NaHCO_3$ (96 mg/L), $CaSO_4 \cdot 2H_2O$ (60 mg/L), $MgSO_4$ (60 mg/L) and KCL (4 mg/L) in Milli-Q water.

**Zebrafish embryo culture medium (E3)** contained NaCl (292.5 mg/L), KCl (12.67 mg/L), $CaCl_2$ (36.62 mg/L), $MgSO_4$ (39.72 mg/L), and methylene blue (0.002% v/v) in Milli-Q water.

## 2.2 Biological specimens

### 2.2.1 Plant culture and biotests

**Microalgae**

Fresh water microalgae *Selenastrum capricornutum (a.k.a Pseudokirchneriella subcapitata)* beads were obtained from the Algaltoxkit-F ™ (MicroBioTest Inc., Belgium) biotest kit. Tubes containing storage medium and algal beads were kept in a refrigerator at 4 °C until use. When preparing the algae stock, algal beads were dissolved in the "Matrix dissolving medium" provided in the test kit. To assist this de-immobilising process, vigorous hand shaking was exercised followed by centrifugation at 3000 rpm for 10 minutes. After pouring out the supernatant, the remaining algae were resuspended homogenously in the algal culture medium. The resultant algal suspension was incubated in a 500 mL Erlenmeyer flask filled with 100 mL of culture medium placed on a rotatory mixer and illuminated continuously by LED light under 10,000 lux at 22 °C for 72 hours.

Prior to the experiment, the concentration of algae stock was determined using a TC-20 ™ automated cell counter (Bio-rad, Australia). The algal suspension was then diluted at least 10 times by the respective test compound solutions, and were then pipetted into standard 24-well plates with 2 mL per well. Each concentration had 5 replicates. From each well, 100 µL of algae test solution was transferred into standard 96-well plates to measure the optical density (OD) at 670 nm using a microplate reader (PolarStar Omega, BMG Labtech,

Offenburg, Germany). The culturing 24-well plate was placed on a rotatory mixer and illuminated continuously by LED light under 10,000 lux at 22 °C for up to 96 hours. Every 24 hours, 100 µL of algae test solution was transferred into standard 96-well plates to measure the OD as described above.

**Duckweed**

Duckweed (*Lemna minor*) was obtained from a culture collection held in the RMIT University Bundoora West Campus, Victoria, Australia. Collected plants were transferred into a container filled with duckweed culture medium and illuminated continuously by LED light under 10,000 lux at 25 °C. Test plants were acclimated in this condition for at least three weeks before experiments. In the tests, duckweed with a same number of fronds were transferred into 250 mL beakers filled with 100 mL medium/test compound solutions. Each concentration had 3 replicates. The beakers were then wrapped in aluminium foil and covered by a transparent thin plastic film. All the beakers were illuminated continuously by LED light under 10,000 lux at 25 °C for up to 7 days. At the end of days three, five, and seven, the number of frond in each beaker was manually counted. At the end of experiment, the fresh weight of the duckweed from each beaker was measured.

### 2.2.2 Invertebrate culture and biotests

**Artemia cysts and larvae**

Marine crustacean *Artemia franciscana* cysts were obtained from the Artoxkit-M™ (MicroBioTest Inc., Belgium) biotest kit. Vials containing dry cysts were kept at 4 °C until use. When hatching, cysts were incubated in a Petri dish filled with filtered sea water (pH= 8.0 ± 0.5) and illuminated continuously by LED light under 3000 lux at 25 °C for 30 hours. After 23 hours of incubation, hatched larvae were manually selected and kept incubating, while unhatched cysts were discarded. In experiments, artemia larvae were pipetted into standard 24-well plates. Each plate contained 1 mL of medium/test compound solution and 10 artemia larvae. Each concentration had 5 replicates. The test plate was then incubated in darkness at 25 °C for 24 hours. At the end of the test, animal mortality was manually counted under a stereomicroscope.

**Daphnia ephippia and neonates**

Fresh water crustacean *Daphnia magna* ephippia were obtained from the Daphtoxkit-F *Magna* ™ (MicroBioTest Inc., Belgium) biotest kit. Vials containing storage medium and ephippia were kept in a refrigerator at 4 °C until use. When hatching, ephippia were rinsed by pre-aerated daphnia culture medium to remove any storage medium. Rinsed ephippia were then incubated in a hatching Petri dish filled with daphnia culture medium and illuminated continuously by LED light under 6000 lux at 22 °C for 80 hours. After 72 hours of incubation, spirulina powder was sprinkled into the hatching Petri dish for pre-feeding. In experiments, neonates were pipetted into a special 24-well plate provided in the test kit. Each test well contained 10 mL of medium/test compound solution and 5 neonates. Each concentration had 4 replicates. The plate was then covered with Parafilm and incubated in darkness at 20 °C for up to 48 hours. Every 24 hours, animal mortality was manually counted under a stereomicroscope.

**Rotifer cysts and neonates**

Fresh water rotifer *Brachionus calyciflorus* cysts were obtained from the Rotoxkit-F ™ (MicroBioTest Inc., Belgium) biotest kit. Vials containing dry cysts were kept at 4 °C until use. When hatching, cysts were incubated in a special 36-well plate obtained from the test kit. The hatching wells were filled with pre-aerated rotifer culture medium and illuminated continuously by LED light under 3000 lux at 25 °C for 18 hours. After 16 hours of incubation, hatched neonates were manually selected and kept incubating, while unhatched cysts were discarded. The experiments started within 18 hours of incubation. In experiments, rotifers were pipetted from the hatching wells into the test wells of the 36-well plate. Each test well contained 0.3 mL of medium/test compound solution and 5 neonates. Each concentration had 6 replicates. The plate was then covered with Parafilm and incubated in darkness at 25 °C for 24 hours. At the end of the test, animal mortality was manually counted under a stereomicroscope.

**Ceriodaphnia ephippia and neonates**

Fresh water crustacean *Ceriodaphnia dubia* ephippia were obtained from the Ceriodaphtoxkit-F Acute ™ (MicroBioTest Inc., Belgium) biotest kit. Vials containing storage medium and ephippia were kept in a cool dry place at 20 °C until use. When hatching, ephippia were rinsed with pre-aerated ceriodaphnia culture medium to remove any storage

medium. Rinsed ephippia were then incubated in a hatching Petri dish filled with culture medium and illuminated continuously by LED light under 6000 lux at 25 °C for 80 hours. In experiments, neonates were pipetted into standard 24-well plates. Each test well contained 1 mL of medium/test compound solution and 10 neonates. Each concentration had 3 replicates. The plate was then covered with Parafilm and incubated in darkness at 25 °C for 24 hours. At the end of the test, animal mortality was manually counted under a stereomicroscope.

**Amphipod**

Adult amphipods *Allorchestes compressa* were collected from ashore sea grass in Swan Bay, Victoria, Australia. Collected animals were maintained in glass tanks filled with filtered sea water at temperature of 20 ± 1 °C with a 12 hour light/dark cycle. Amphipods were left to acclimate for at least two weeks prior to experiments. In the test, amphipods were pipetted into standard 24-well plates. Each test well contained 2 mL of medium/test compound solution and 2 amphipods. Each concentration had 5 test wells. The plate was then incubated at 20 ± 1 °C with a 12 hour light/dark cycle for up to 72 hours. Every 24 hours, animal mortality was manually counted under a stereomicroscope.

### 2.2.3 Vertebrate culture and biotests

Vertebrate animal experiments were conducted with approvals from the University of Auckland Animal Ethics Committee, the RMIT University Animal Ethics Committee, and the Monash University Animal Ethics Committee.

**Zebrafish husbandry and embryo culture**

Adult wild type zebrafish were kept in a circulating aquatic system on a 14 hour light and 10 hour dark cycle. The environmental temperature was maintained at 27.5 ± 0.5 °C and the pH was held at 7.5-8.0. Fish were fed twice daily, once with live crustaceans *Artemia sp.* and once with dry fish food granule. Daily monitoring was exercised and standard water quality parameters (pH, ammonia, nitrite, nitrate, carbon hardness, and general hardness) were measured.

Zebrafish embryos were obtained from pair-wise mating and natural spawning of the adult zebrafish. Adult fish were randomly grouped in a 1:1 male to female ratio in a separate fish tank and left overnight. Female adult fish naturally spawned eggs when the light was turned

on the following morning. Embryos were harvested within an hour of spawning and were transferred to embryo culture medium (E3).

Wild type embryos were incubating at 28 °C in a Petri dish filled with E3 medium until use. Any debris and unfertilised embryos were manually removed at 3 hour post fertilisation (hpf). When using transgenic *Tg(fli1:EGFP)* embryos, harvested embryos were incubated at 22 °C for 16 hours. Prior to experiments, homozygous-recessive and heterozygous embryos were manually removed. The density of embryos held in the Petri dish was kept around 50 per dish. Besides, culture medium (E3) that contained 0.003% 1-phenyl-2-thioures (PTU; Life technologies Corp., California, USA) was used to inhibit the natural formation of the pigment that optically blocks the observation of inter-segmental vessel (ISV). At the end of experiments, 0.2 mg/mL of Tricaine mesylate (TMS) was added into the culture medium to temporarily anaesthetise the embryo from spontaneous movement inside the chorion.

Static fish embryo toxicity (FET) tests were performed according to the OECD animal test protocol[44]. In experiments, 20 fertilised embryos at 5 hour post fertilisation (hpf) were dispensed into 24-well plates with one embryo per well. Test compound, positive control, or negative control solutions were then pipetted into the test wells with 2 mL per well. The 24-well plate were covered by Parafilm-M and incubated in darkness at 28 ± 1°C for up to 48 hours.

Chip-based fish embryo toxicity (µFET) tests were conducted with a slight modification from the FET test protocol[44]. In experiments, 21 embryos at 5 hour hpf were loaded into each culturing chamber on the microfluidic chip made of PMMA. The device was connected to a fluid reservoir containing 40 mL of test compound, positive control, or negative control via PUR tubing. Such system was continuously perfused in a closed-loop regimen at flow rate of 400 µL/min. Embryos were immobilised on the chip device and incubated in darkness at 28± 1°C for up to 48 hours.

In 3D printed chip device experiment, 24 embryos at 5 hour post fertilisation were loaded into each culturing chamber of the microfluidic chip made from different 3D printing materials. The device was connected to a fluid reservoir containing 40 mL of embryo medium via silicon tubing. The system was continuously perfused in a closed-loop regimen at flow rate of 400 µL/min. Embryos were immobilised on the chip device and incubated in

darkness at 28± 1°C for up to 72 hours. At the end of experiments, embryos were unloaded from the chip device into a Petri dish where embryonic development was observed under a stereomicroscope.

**Zebrafish larvae**

Zebafish larvae were obtained from hatched zebrafish embryos. Zebrafish embryos normally hatch around 48 hpf under the incubation conditions described in section 2.5.1. Hatched larvae were kept incubating until use.

In larval toxicity experiments, larval zebrafish at 5 days post fertilisation (dpf) were manually transferred into standard 24-well plates. Each test well of the 24-well plate contained 2 mL of medium/test compound solution and one zebrafish larvae. Each concentration had 5 replicates. The plate was then covered with Parafilm and incubated in darkness at 28 ± 1 °C for up to 48 hours. Every 24 hours, the number of unviable animals was manually counted under a stereomicroscope.

In zebrafish larvae behaviour tests, larval fish at 7 days post fertilisation (dpf) were used. The day prior to the experiment, test larvae were fed with live paramecium (*Paramecium caudatum*; Southern biological, Victoria, Australia) to keep them active. In experiments, larval fish were pipetted into standard 24-well plates with one larvae per well. Each test well contained 1 mL of embryo medium/test solution. Locomotion activity analysis was performed using the Zebrabox behaviour recording system and associated analysis software (ViewPoint, France). The tracking experiment was conducted on a 4 min light and 4 min dark cycle for 64 minutes at temperature of 25 ± 1 °C. A LED light pad and an infrared camera were equipped for light stimulation and dark imaging, respectively. Assessment of sub-lethal behavioural effects was performed by tracking the movement (total distance moved) of each larvae during alternating periods of 240 seconds of light and dark.

## 2.3 Scoring criteria for zebrafish embryo biotests

Based on the OECD testing protocol (FET), four lethal end-points were recorded every 24 hours: (i) coagulation; (ii) lack of somite formation; (iii) lack of tail detachment from the yolk; and (iv) lack of heartbeat[44].

Furthermore, a new method (iFET) developed by Wigh and co-workers was applied to score sub-lethal biomarkers and teratogenicity[104]. This method introduced 9 new parameters: (i) abnormal eye development; (ii) pericardial oedema; (iii) lack of pigmentation; (iv) defects in blood circulation; (v) head abnormalities; (vi) tail abnormalities; (vii) heart abnormalities, (viii) spine abnormalities; and (ix) yolk abnormalities[104]. These sub-lethal parameters were also checked every 24 hours.

The iFET index integrated lethal and sub-lethal endpoints observed from the experiment. It can be quantitated using the following formula[104]:

$$\text{iFET index} = \frac{(9 \text{ x } \text{N}_\text{D}) + \sum_1^N N_{SL}}{9 \text{ x N}} \text{x} 100\%$$

Where N = total number of test embryos; $N_D$ = number of dead embryos (FET lethal endpoints); $N_{SL}$ = number of sub-lethal biomarkers recorded from each embryo (iFET sub-lethal endpoints, a total of 9 for each embryo). The iFET index was expressed as a percentage of embryos that shows lethal and/or sub-lethal abnormalities.

## 2.4 Design and fabrication

### 2.4.1 Infrared laser machining

The design and modelling of microfluidic lab-on-a-chip devices were performed using the CorelDraw X3 (Corel Corp., Ontario, Canada) software package. For multilayer devices, each layer was fabricated separately in poly(methyl methacrylate) (PMMA) – a transparent thermoplastic - using a non-contact 30W $CO_2$ infrared laser machining system (VLS 3.50, Universal Laser Systems, Scottsdale, Arizona, USA). The system was equipped with high power density focusing optics (HPDFO) that has a 40 μm elliptical beam spot (Figure 2.4.1).

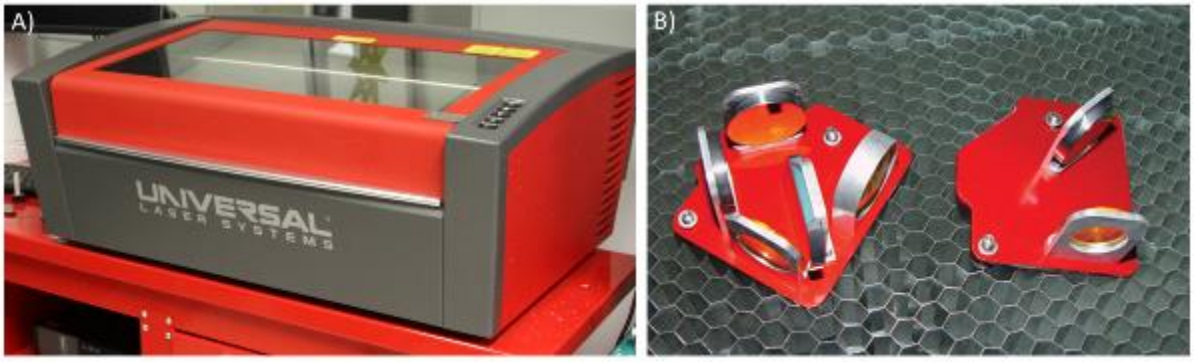


*Figure 2.4.1 Laser cutting system. A) VLS 3.50 infrared $CO_2$ laser cutting system. B) Lenses: left – High Power Density Focusing Optics (HPDFO) lens with a beam spot size of 40 µm; right – Standard lens with a beam spot size of 100 µm.*

Fabricated PMMA slides were manually aligned, sandwiched by, in the sequence of, standard microscope glass slides, metal slides, and C-clamps. It was then thermally bonded in a fan assisted oven at 120 °C for 1.5 hours.

### 2.4.2 Soft lithography

The master mould was designed and fabricated using laser machining as described in section 2.4.1. The mould was then used for replica moulding with poly(dimethylsiloxane) (PDMS; Sylgard 184; DowCorning Corp., Midland, Michigan, USA). The PDMS elastomer base and curing agent were mixed at a ratio of 10:1 (w/w). The mixture was poured onto a master mould, followed by the degassing process at 40 Torr to remove air bubbles completely.

The de-bubbled PDMS mixture was cured thermally in a fan assisted oven at 70 °C for 1.5 hours. The hardened PDMS layer was then carefully peeled off from the master mould. The inlet and outlet of the device were bored by a 3 mm diameter biopsy punch. The resulting PDMS block was bonded to a standard glass microscope slide using oxygen plasma generated by a reactive ion etching system (RIE; CS-1701 RIE Plasma Cleaning System, March, Concord, Massachusetts, USA) in a clean room.

### 2.4.3 Three dimensional (3D) printing

The design and modelling of 3D printed objects were performed using the SolidWorks 2013 (Dassault Systems SolidWorks Corp., USA) software package. All designs were saved as STL file and were then processed by the respective 3D printers' software.

**Multi-jet moulding (MJM) fabrication**

HD3500 Plus (3D Systems, USA) high definition 3D printer was used for MJM fabrication. It features a 25 µm x-y resolution and 16 µm z-layer thickness. VisiJet Crystal (3D System, USA) resin together with VisiJet S300 Support Wax (3D System, USA) was used for fabrication according to the standard operating procedures. The following post-processing procedure was conducted to remove the support wax from the printed parts: (i) heating in the oven at 65 °C to melt and scrap out large chunks of wax; (ii) soaking in warm vegetable oil in an ultrasonic bath at 55°C with a pumping flow at 70 mL/min; and (iii) rinsing and flushing with Decon90 detergent to clean out any residual wax and oil. Furthermore, to achieve a desirable level of optical transparency, the surface of the device was polished using 10.3 µm grit pads followed by 9 µm diamond paste (Mold Makers 9-STD GREEN; Boride Engineered Abrasives, USA) with high-quality modelling heads (Dremel, USA).

**Stereolithography (SLA) fabrication**

Multiple SLA systems were selected including: (i) Viper Pro (3D System, USA) using Watershed 11122XC (DSM Somos, USA) resin or Dreve Fototec 7150 Clear (Dreve Otoplastik GmbH, Germany) resin; (ii) ProJet 7000HD (3D Systems, USA) using VisiJet SL Clear (3D Systems, USA) resin, and (iii) Form 1 using Form Clear (FormLabs, USA) resin. The first two systems are characterised by 25 µm x-y resolution and 50 µm z-layer thickness, while the third system has 300 µm x-y resolution and 50 µm z-layer thickness. All prototyping was performed according to manufacturer's standard operating procedure, including flushing and resining with 99% isopropyl alcohol to remove un-polymerised resins. In addition, prototypes fabricated from the Form1 printer were exposed to UV light at emission wavelength of 350 nm in a standard tissue culture hood for 12 hours to harden the polymer. To achieve a desirable level of optical transparency, the surface of the device printed in Dreve Fototec 7150 Clear or Form Clear resins was mechanically polished by using 10.3 µm grit pads followed by 9 µm diamond paste polishing (Mold Makers 9-STD GREEN; Boride Engineered Abrasives, USA) with high-quality modelling heads (Dremel, USA).

**Fused Deposition Modelling (FDM) fabrication**

Makerbot Replicator 2 (MakerBot, Brooklyn, New York City, USA) desktop 3D printer with poly(lactic acid) (PLA) and uPrint SE (Stratasys, Edina, Minnesota, USA) with acrylonitrile butadiene styrene (ABS) were used for FDM fabrication. In addition to the standard

processing procedure, post-processing treatment was performed manually to remove any support materials and printing residues.


*Figure 2.4.2 3D printers used in this study. From left to right: ProJet 3500HD is a MJM 3D printer using VisiJet Crystal material together with VisiJet S300 support wax. ViperPro is a SLA 3D printer using Watershed 11122XC resin or Dreve FotoTec Clear resin. ProJet 7000HD is also a SLA 3D printer using VisiJet SL Clear resin. And Form 1 is a SLA 3D printer as well using Form Clear resin. All the printing materials are specifically used for only their designated 3D printers.*

## 2.5 Electricals and actuators

Dynamixel MX-64T robotic actuators (Robotis Ltd., Irvine, California, USA) were used in making 3D printed peristaltic pumps. Each actuator was equipped with an on-board 32bit 72 MHz Cortex M3 microcontroller, contact-less magnetic encoders and TTL 2.0 bus. The actuators were controlled by a CM-530 microcontroller (Robotis Ltd.) based on 32-bit ARM Cortex M3 architecture. The programing of the actuators was performed in a native RoboPlus environment (Robotis Ltd.). In addition, Dynamixel AX-12A servo actuators (Robotis Ltd.) were used in making a moving stage for imaging in the integrated device.

Miniplus Evolution peristaltic pumps equipped with MFI pump heads (Gilson Inc., Middleton, Wisconsin, USA) was used in the device validation test. A water bath (Julabo Labortechnik GmbH, Seelbach, Germany) was used for incubation when hatching organisms.

## 2.6 Tubing

Polyurethane (PUR) tubing, silicon tubing and luer connectors (John Morris Scientific Pty. Ltd., Australia) were used for connecting peristaltic pumps. They all have an inner diameter of 1/16" (1.58 mm) that allows zebrafish embryos to pass through. Polyvinyl chloride (PVC) tubing (Gilson Inc., Middleton, Wisconsin, USA) was used inside the peristaltic pumps. This flexible tubing has an inner diameter of 1.02 mm that provides the desired flow rates ranging from 0.1 mL/min to 7.0 mL/min.

## 2.7 Imaging

**Stereomicroscopy** and time-lapse imaging were conducted using Nikon SMX18 (Nikon Corp., Tokyo, Japan) equipped with a Retiga ™ 4000DC cooled CCD camera and Nikon Eclipse TiE epifluorescence microscope equipped with a cooled DS-Qi1Mc CDD camera. A standard FITC/GFP filter cube (Nikon Corp.) was used to acquire fluorescence images of *Tg(fli1a:EGFP)* zebrafish embryos. The systems were controlled by a native NIS-Elements Ar software package.

**Confocal laser scanning microscopy** was performed on a Leica SP5 (North Ryde, New South Wales, Australia) with a FLUOTAR 10x dry objective lens. Focus-stack imaging was performed in steps of 5 µm. Bidirectional scan was performed with 3 line average at 8 bit and 200 Hz scan speed. A 488 nm Argon laser was used at 30% power for excitation. The emission signals were received from 498 nm to 651 nm.

**Miniaturised USB microscopy** (AM7013MT Dino-Lite Premier, Dino-Lite, AnMo Electronics Corp., New Taipei City, Taiwan) was used for brightfield imaging and video recording. This microscope was equipped with a 5 megapixal colour CMOS sensor and variable magnifications of up to 200x, supporting video acquisition up to 15 frame per second (fps). The illumination was supplied by 8 embedded LED lights, which were controlled by the operating software (DinoCapture2.0; AnMo Electronics Corp.). Time-resolved image acquisition was fully programmable through the software user interface.

**Scanning electron microscopy (SEM)** was performed using a FEI Quanta 200 ESEM (2002) (FEI Company, Hillsboro, Oregon, USA) operated at 20.0 kV with a 5.0 Spot size in high vacuum. Before sampling into the SEM, samples were coated with Au/Pd using an in-house

sputter coater operating at 15 mA for 2 minutes. The object stage was tilted to 39° for stereoscopic imaging.

**Optical profilometry** images were taken from BRUKER ContourGT-I 3D Optical Microscope (Bruker Corp., Billerica, Massachusetts, USA). Stitching was enabled to obtain a final bounding box of 0.5 mm x 0.5 mm with 20% overlapping area.

## 2.8 Oxygen gradient imaging

Oxygen detection was accomplished by a Presens® VisiSens ™ system (PreSens Precision Sensing GmbH, Germany) that receives fluorescence signals from sensor foils via a miniaturised digital microscope. Image acquisition was supported by native software (VisiSens Analytical 1, ver. 1.13) capable of capturing 1.3 megapixel images at up to 0.5 frames per second (fps). The oxygen level was calculated by comparing the fluorescence readings from the calibration with signals detected from the oxygen sensor foil.

## 2.9 Computational fluid dynamics (CFD) simulation

The CFD simulation was conducted using the ANSYS 15.0 software package (ANSYS Inc., Canonsburg, PA, USA). Simulation was initiated after importing 3D models created from SolidWorks software into Fluent 15.0 software to generate mesh. Virtual zebrafish embryos were modelled as rigid spheres 1 mm in diameter. The flow rate was set at 400 µL/min from the inlet port. Trypan blue was virtually used as a model for mass transfer simulation. Flow velocity, pressure and shear stress on the surface of the embryos were calculated.

## 2.10 Gas chromatography-mass spectrometry (GC-MS)

The GC-MS experiment was performed on an Agilent HP 6890 Gas chromatography system with an Agilent 5973 Mass spectrometer (Agilent Technologies Australia Pty. Ltd., Forest Hill, Victoria, Australia). The system was controlled in a native ChemStation software environment. The instrumental conditions are listed below in Table 2-3:

*Table 2-3 GC-MS instrumental conditions*

| | |
|---|---|
| **GC** | |
| Injection mode | Split |
| Split ratio | 20:1 |
| Injection volume | 1 µL |
| Injection port temperature | 250 °C |
| Carrier flow | Helium at 17.54 psi |
| Temperature ramp | 40 °C for 1 min, 10 °C/min, 325 °C final for 4.30 min |
| Column | DB-5ms, 0.25 mm x 30.0 m x 0.25 µm |
| **MS** | |
| Acquisition mode | Scan |
| EMV Mode | Relative |
| Relative voltage | 47 |
| Resulting EM Voltage | 1035 |
| Low mass | 50 |
| High mass | 550 |
| Mass source | 230 °C, maximum 320 °C |

## 2.11 Data analysis and control

**Image analysis** was conducted using ImageJ (Wayne Rasband, Research Services Branch, National Institute of Mental Health, Bethesda, Maryland, USA). **Video processing** was executed using Adobe Premiere Pro CC software (Adobe Systems Inc., San Jose, California, USA). **Embryonic video analysis** was performed on a Danio Scope 1 (Noldus, Wageningen, The Netherlands). **Behavioural video analysis** was performed on ZebraBox (ViewPoint, Lyon, France). **Data analysis** was done using GraphPad Prism 5 (GraphPad Software Inc., La Jolla, California, USA) and ToxRat (ToxRat Solutions GmbH, Alsdorf, Germany) software. A standard ANOVA model was applied to perform independent comparisons for each test compound concentration with significance set at $p < 0.05$.

All experiments were performed in at least independent 3 replicates per concentration, unless otherwise indicated. All control measurements were provided in detail, where appropriate, for context and/or figure legends.

# 3 Three dimensional printed lab-on-a-chip device for zebrafish embryo biotest

## 3.1 Introduction

This chapter describes using high-definition 3D printing systems to fabricate optical-transparent lab-on-a-chip devices with complex fluidic geometries for zebrafish embryo bioassays. As mentioned in Chapter 1, the spread of lab-on-a-chip technology is inhibited by complicated manufacture methods requiring significant engineering expertise. The main objective of this project was to investigate the feasibility of using 3D printing to simplify and accelerate fabrication of microfluidic lab-on-a-chip devices, with an equal or better fabrication quality. To compare with conventional fabrication methods, a design of a microfluidic zebrafish embryo trapping array fabricated in PDMS was selected as the control. The chip device was then prototyped using four off-the-shelf 3D printers and five associated printing materials.

To assess the printing quality, I tested the printing accuracy and completion of complex geometries. Surface topology analysis was performed using scanning electron microscopy, optical profilometery, and atomic force microscopy. Optical transparency was tested with both bright field microscopy and fluorescence microscopy. The device functionality was examined by loading zebrafish embryos hydrodynamically. Lastly, I investigated the biocompatibility of 3D printed devices for live embryo cultures for an extended period of time.

## 3.2 Design and fabrication

The original lab-on-a-chip device was designed and fabricated by Akagi and co-workers (Figure 3.2.1)[59]. It was a 2D (one-layer) fluidic system fabricated from Polydimethylsiloxane (PDMS). It consisted of three major modules: (i) the twisted main loading channel, (ii) the array of embryo traps, and (iii) the array of suction channels.

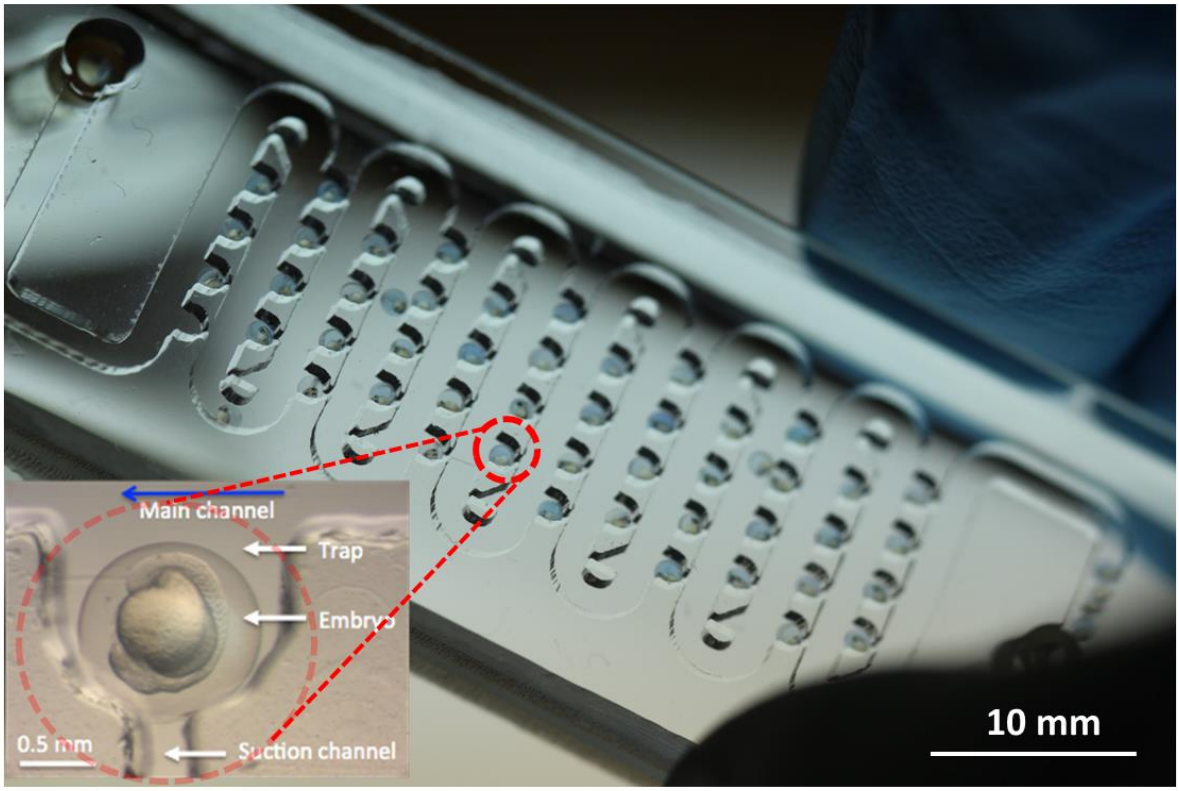


*Figure 3.2.1 A lab-on-a-chip device for zebrafish embryo trapping[59]. Key features are depicted. The body of the chip was made of polydimethylsiloxane (PDMS), with a bottom sealing layer made of glass. This chip will be converted to a 3D printed chip in this chapter.*

To convert the 2D chip into 3D, a computer aided design (CAD) was built (Figure 3.2.2). The dimensions of the fluidic system in the 3D chip were exactly same as the ones in 2D chip with total internal volume of approximately 825.9 µL. The corners of the 3D chip were rounded to reduce the usage of the materials. The top and bottom sealing layer were designed to be 500 µm in thickness, offering optical transparency and leaving an overhead of material to be removed in the post-printing polishing procedure. In addition to the 2D chip design, two barb connection ports were embedded to the 3D chip for leak-free and user-friendly tubing interconnections.

To enable a detailed evaluation of the inner structure of the device, prototypes without the top sealing layer were also manufactured. An additional 2D control chip made of PMMA thermal plastic by infrared laser micromachining was also fabricated. The detailed manufacturing and post-processing procedures of all chips can be found in Chapter 2.

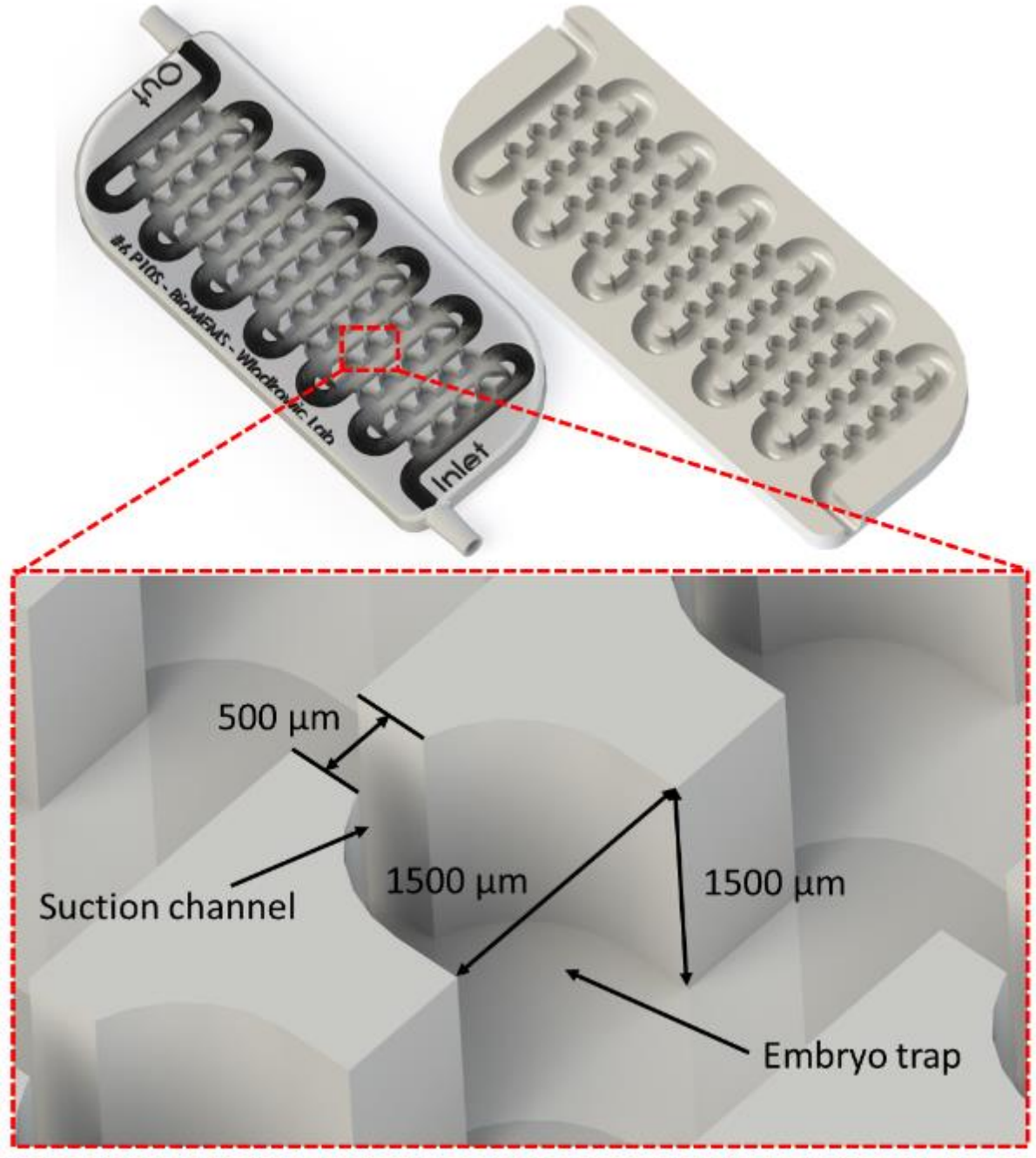


*Figure 3.2.2 3D computer aided design (3D CAD) rendered model of the chip device. Left: a monolithic device with integrated interconnection ports; Right: An open-lid chip for analysing 3D printing quality assessments; Bottom: Magnified view of the microfluidic embryo trapping system. All theoretical dimensions are depicted. They were used as references when assessing the printing quality.*

## 3.3 Appearance and accuracy

First, I investigated the feature production quality of the chip device. Chip devices were printed in VisiJet Crystal (VJC), Watershed 11122XC (WXC), Dreve Fototec 7150 Clear (DFC), VisiJet SL Clear (VJSL), or Form Clear (FC) materials. The 3D printing of all chip devices were successful as monolithic devices with no further bonding needed, whereas the control chips made in PDMS and PMMA required plasma and thermal bonding, respectively. The finishes of 3D printed devices were comparable to the control chips, with minor surface polishing required in only the VJC, DFC, and FC chips. Although all 3D printing polymers were named "crystal" or "clear", they all bear with some colour tint. For example, VisiJet Crystal (VJC) polymer was yellow; Watershed XC11122 (WXC) polymer was blue. However, after polishing, the colour of the chips changed to green because of the use of green polishing paste.

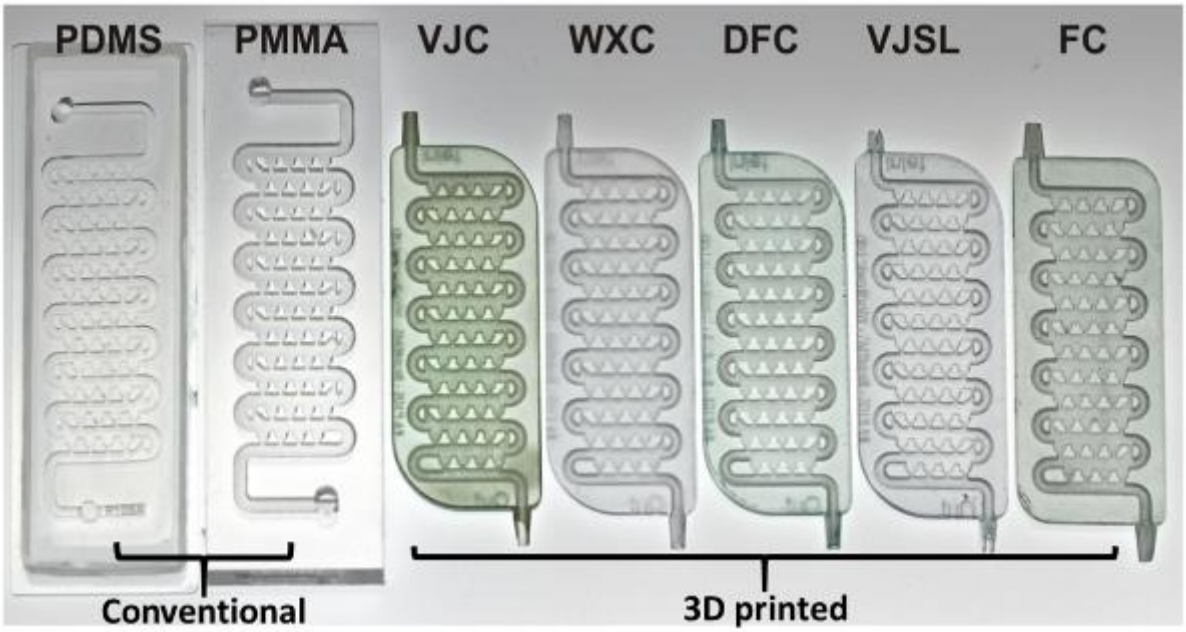


*Figure 3.3.1 A photograph depicting embryo trapping arrays from different fabrication methods. i) chips fabricated using soft lithography (PDMS, elastomer) and infrared laser micromachining (PMMA, thermoplastic) as controls; ii) 3D printed chips fabricated using Multi-Jet Modelling (MJM; in VisiJet Crystal resin) and Stereolithography (SLA; in Watershed 11122XC, Dreve Fototec 7150 Clear, VisiJet SL Clear and Form Clear resins).*

The printing accuracy was assessed by comparing the designated dimension with the actual dimension of a small feature on the chip. The smallest feature on the chip was the width of

the suction channel (500 µm) (Figure 3.2.2). In practice, despite some variations, the printing accuracy was satisfactory across most 3D printing chips with less than 10% variation (Figure 3.3.2). The exceptions were the chips made from PDMS and Form Clear (FC). PDMS is an elastic polymer so accuracy is lost during the moulding and de-moulding processes. However, the poor accuracy observed in the FC was considered to be related to the printing quality of the 3D printer.

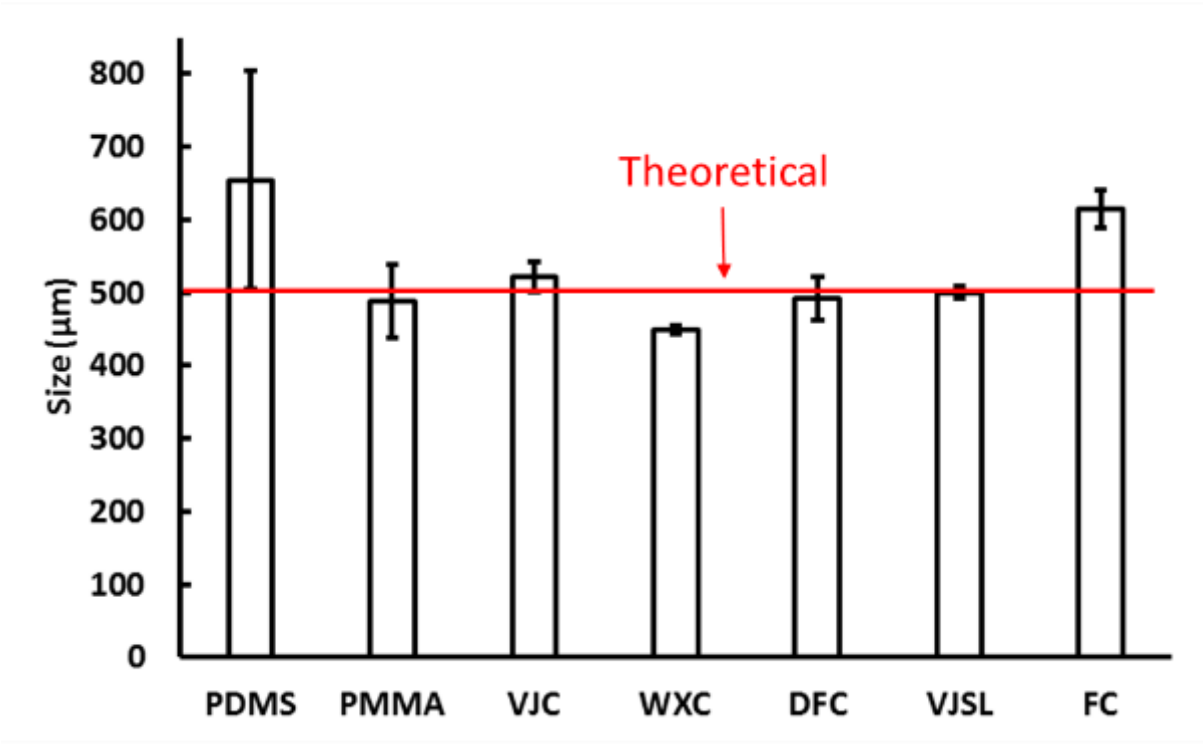


*Figure 3.3.2 Comparison of the feature size deviations across different chips. The suction channel designed in CAD to be 500 µm in width was fabricated in all 3D prototyped chips. Apart from the chips made of PDMS and Form Clear, the fabrication of other chips were relatively accurate and precise.*

The printing quality of the embedded connection nozzles was also examined. Due to the thin wall of the connectors, some of them broke during attempts to connect hard tubing, such as Teflon (PTFE) or polyurethane (PUR) tubing (Figure 3.3.1). No difficulties were experienced when connecting soft tubing, like silicon or polyvinylchloride (PVC) tubings. This result indicates that these 3D printing polymers (epoxy resins) are hard and brittle.

The embedded connectors offer user-friendly interconnections, but the quality of the sealing remained unclear. To elucidate the answer to this question, a dead-end pressure

holding test was performed. The connector was found to be able to withhold a fluidic maximum pressure of up to 30 psi (figure 3.3.3). This result demonstrates a seamless fluidic connection that is more than sufficient for a microfluidic perfusion system.

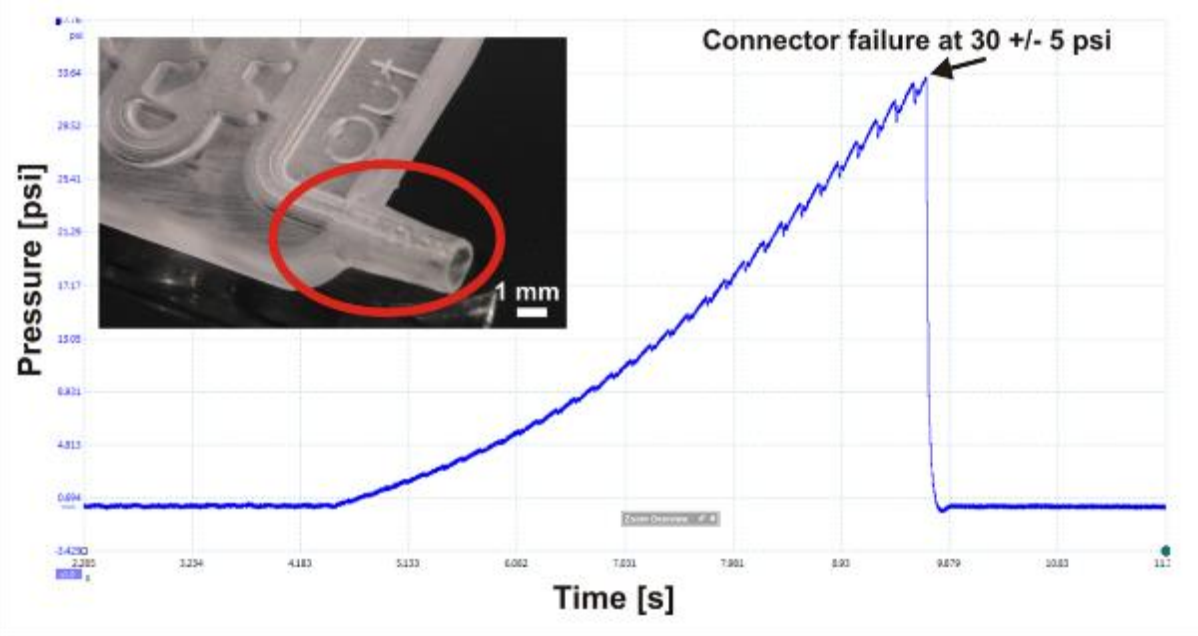


*Figure 3.3.3 An embedded barb connector fabricated during 3D printing allowed leak-free and convenient fluidic interconnections. The fluidic seal between the connector and silicon tubing was capable of withstanding a peak pressure of up to 30 psi.*

## 3.4 Surface properties

The surface properties of the chip device are important because they heavily affect the microfluidic chip performance. For example, a rough surface has a significantly larger surface area that causes extra compound adsorption onto the surface. Moreover, a turbulent flow instead of a laminar flow will be created by the rough surface. Most importantly, a rough surface scatters light and thus reduces optical transparency. In this regard, a detailed topological assessment of 3D printed devices was performed. To improve the resolution and sensitivity, all chip devices had to be coated with gold, and thus only the chips without the lid layer were used here.

### 3.4.1 Scanning Electron Microscopy

The surface roughness of 3D printed lab-on-a-chip devices was first analysed under a scanning electron microscope (SEM), allowing us to visually compare the difference among

surfaces (Figure 3.4.1). The VJSL chips had a very smooth surface after printing and was comparable with the control PDMS chip. WXC and DFC chips had characteristic lattices patterns on their surface, as they were fabricated from a same 3D printer. The VJC was revealed to have a coarse surface. The surface of the FC chip was the worst with obvious gaps existing in the surface.

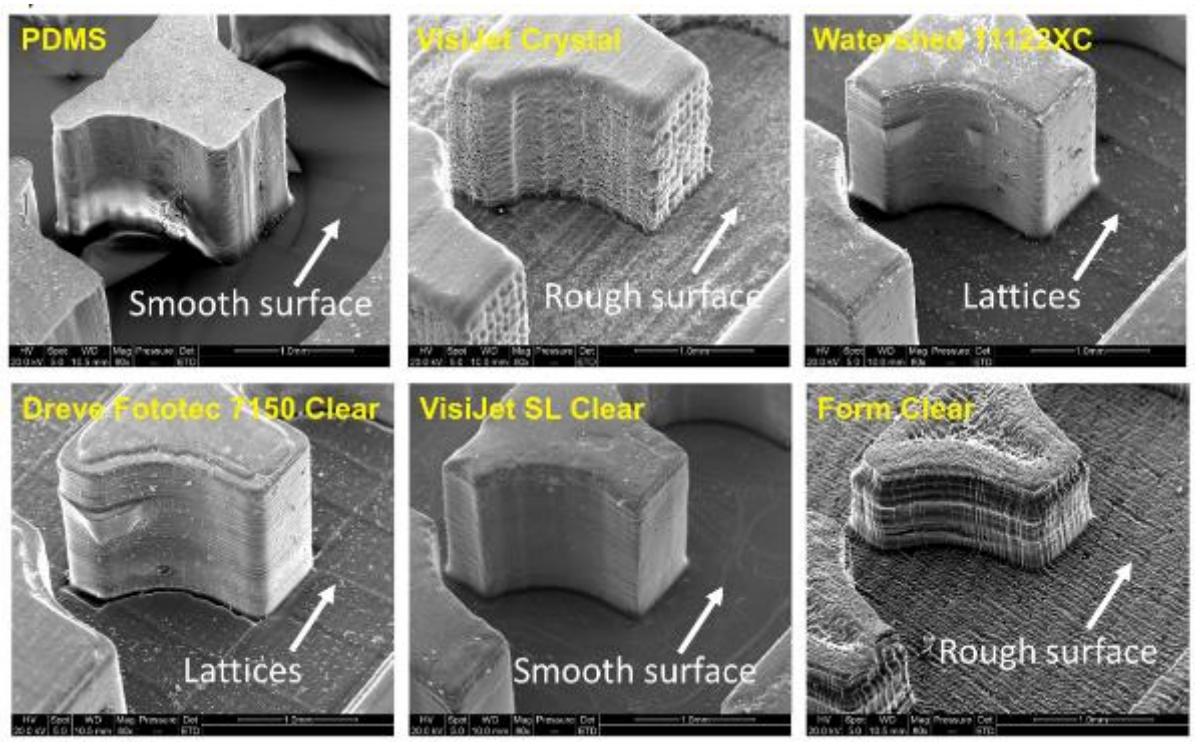


*Figure 3.4.1 Comparison of topographic surfaces of a single embryo trap in the chip using scanning electron microscope (SEM). Rough surfaces were observed in VisiJet Crystal and Form Clear chips. PDMS and VJSL chips presented smooth surfaces. Published in Ref 105. Reproduced with permission from AIP Publishing LLC.*

Next I magnified the view and looked at the vertical wall of the embryo trap (Figure 3.4.2). In the control PDMS chip, there is a large residue due to the moulding process during fabrication. In all 3D printed chips, traces from the building of each layer can be clearly observed. The VJSL chip had a smooth vertical surface without any residues, and the WXC and DFC chips again had a similar printing quality with minor unpolymerised residues. Because of the printing principles, the VJC chip fabricated in a MJM 3D printer had a rough surface caused by melting of the raw polymer. The FC chip had a problem with aligning each layer accurately. As a result, the finished structure was deformed and the surface looked very bumpy.

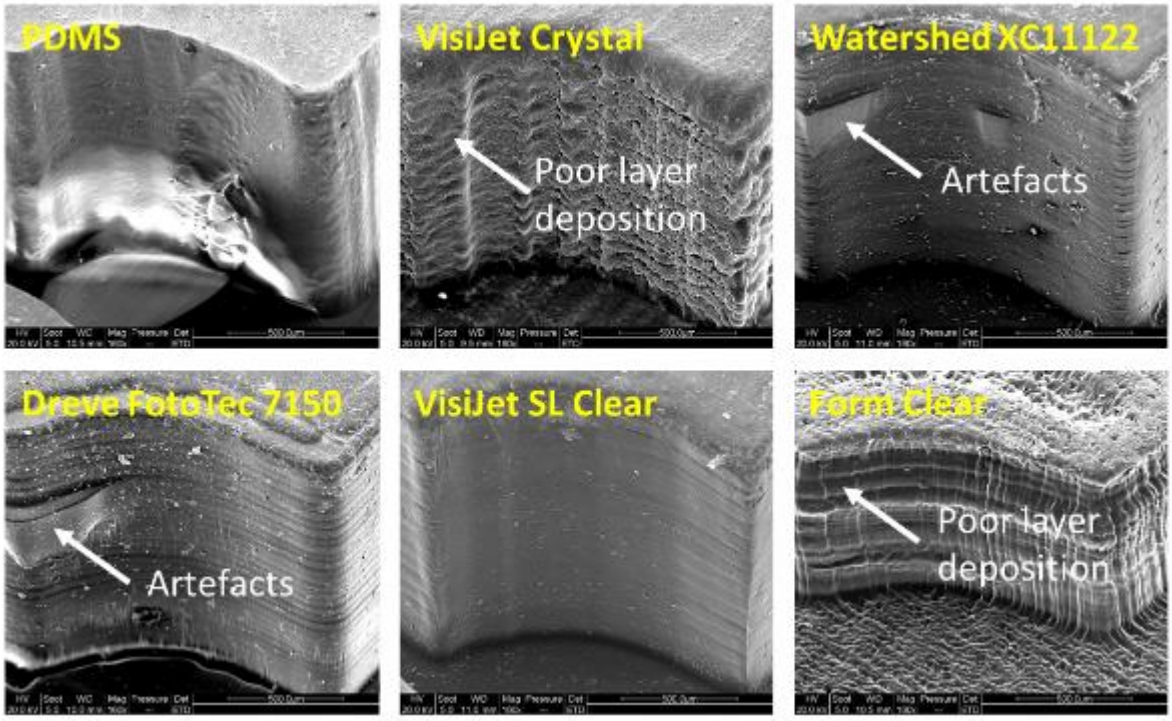


*Figure 3.4.2 Comparison of topographic surfaces using SEM, showing the vertical surface of the embryo trap. Note that layer deposition can be observed in all 3D printed chips. Poor layer deposition in VisiJet Crystal chip was due to the printing principle (MJM); in the Form Clear chip it was because of poor layer alignment. Artefacts (unpolymerised resin) were left on Watershed XC and Dreve FotoTec chips.*

Afterwards I magnified the view of the top surface of 3D printed structures (Figure 3.4.3). Small dents as a result of air bubble residues were observed in the control PDMS chip. This was due to insufficient degassing time during the PDMS fabrication procedure. Residual resin materials were left on the top surfaces of WXC, DFC, and VJSL chips, making the top surfaces not as flat as the bottom surface. In particular, the building of the top surface in the FC chip was not successful, as the material collapsed in the centre of the structure, leaving a large indentation on a porous surface.

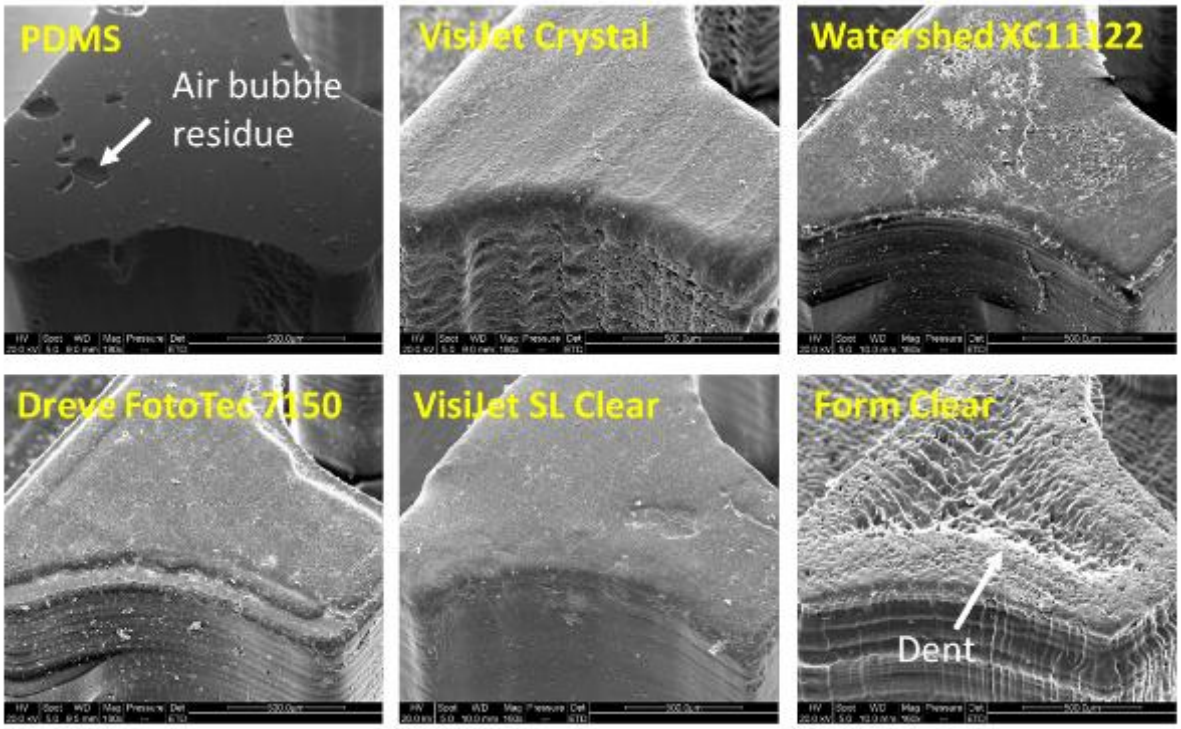


*Figure 3.4.3 Comparison of topographic surfaces using SEM, showing the top surface of the embryo trap. Most 3D printed chips achieved a relatively smooth surface, with the exception of the Form Clear chip where structural deformation was observed.*

### 3.4.2 Optical profilometry

To quantify the surface analysis, I applied 2D and 3D topographic surface mapping technology using optical profilometry. In practice, representative areas of 500 x 500 µm from the bottom and top surfaces of the chip devices were scanned by a laser beam. As a result, the surface roughness was presented as a heat map where the areas in green were set as a reference panel, the red areas were peaks and the blue areas were valleys. In the end, the height of each unit area were statistically organised and presented as a Gaussian distribution.

The result of the control PDMS chip showed a lot of green and flat areas with occasional crests, demonstrating that the surface of the PDMS chip was indeed very flat. The Gaussian distribution of the height plotted a curve with a small variance (Figure 3.4.4).

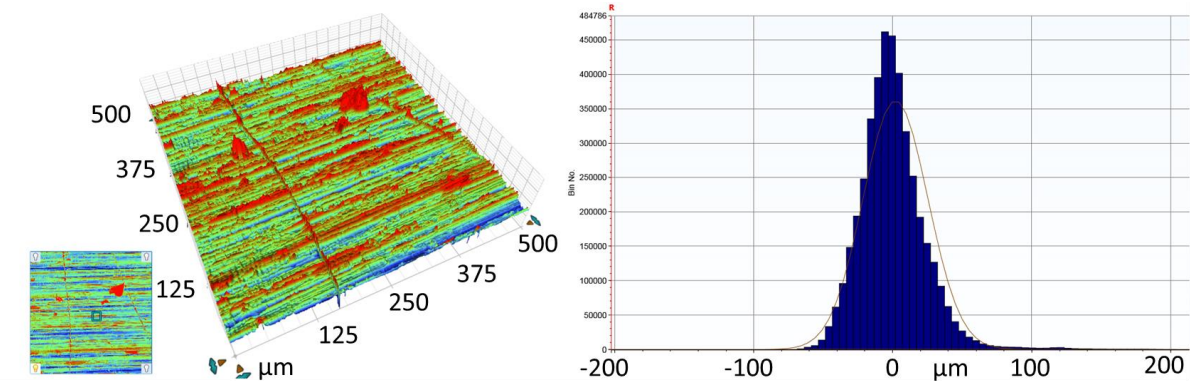


*Figure 3.4.4 Quantitative analysis of topological surfaces from a microfluidic structure fabricated in PDMS (left) and the Gaussian distribution of surface roughness (median feature height) (right). Note that the relatively smooth surface from the PDMS chip resulted in a small variance in the distribution curve. Published in Ref 105. Reproduced with permission from AIP Publishing LLC.*

In contrast to the PDMS chip, the FC chip showed a map with randomly distributed peaks and trenches. There are even white (no data) areas in the map, meaning that the height variation was too large to detect. The distribution curve was also deformed and had a large variation (Figure 3.4.5).

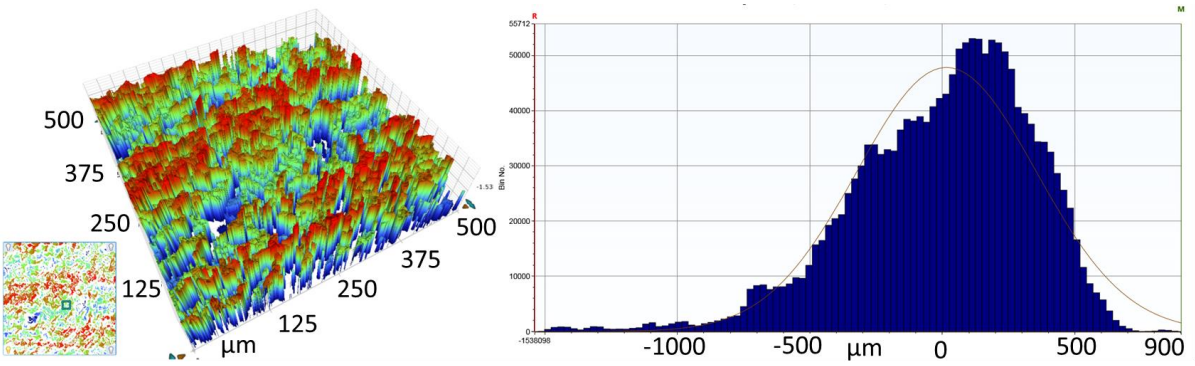


*Figure 3.4.5 Quantitative analysis of topological surfaces from a microfluidic structure fabricated in Form Clear (left) and the Gaussian distribution of surface roughness (median feature height) (right). Note that the rough surface from the FC chip leads to a large variation in the distribution curve.*

Among all 3D printed chips, the VJSL chip showed a similarly flat surface as the control PDMS chip, except for a few scratches and ridges. The distribution of the heights was also very narrow and tight. The difference in median height between PDMS chip and VJSL chip was less than 5% (Figure 3.4.6).

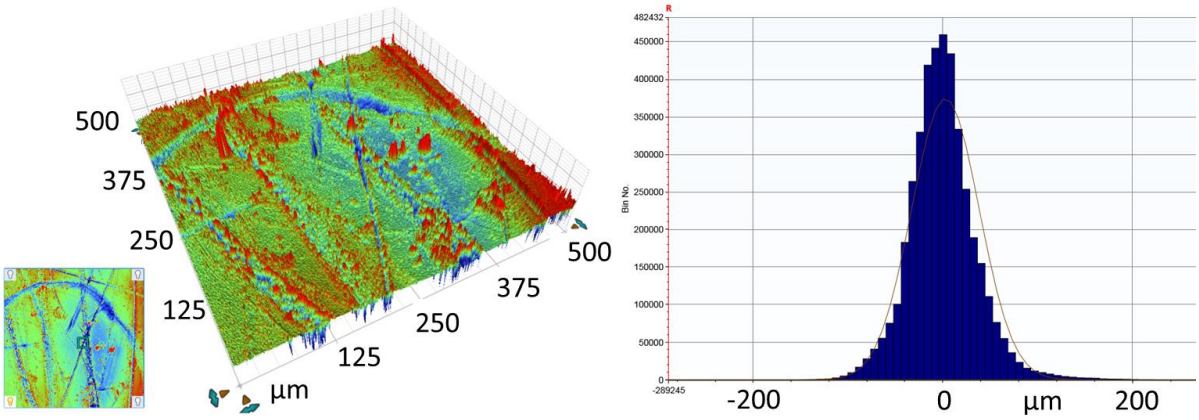


*Figure 3.4.6 Quantitative analysis of topological surfaces from a microfluidic structure fabricated in VisiJet SL Clear (left) and Gaussian distribution of surface roughness (median feature height) (right). Despite some scratches, the surface of the VJSL chip was relatively flat as evidenced by the small variation in the distribution curve. Published in Ref 105. Reproduced with permission from AIP Publishing LLC.*

### 3.4.3 Atomic Force Microscopy

To assess the surface properties at an even higher magnification, atomic force microscopy was utilised. This technology is able to reveal the surface topological properties as tiny as a few nanometres. Because AFM has a very limited imaging depth of field and scanning area that are designed for investigating smooth surfaces rather relatively rough surfaces created by 3D printing, this experiment was then terminated and was only briefly described and discussed here. Nevertheless, the result indicated that 3D printed surfaces are generally too rough that beyond the scale of what AFM is capable to measure. Here, I presented the result from a relatively flat VJSL chip.

A representative area of 10 x 10 µm, which is the largest detectable size, from the VJSL chip was selected for AFM imaging. The result again proved that the VJSL chip had a flat surface with a maximal variation of less than 0.2 µm.

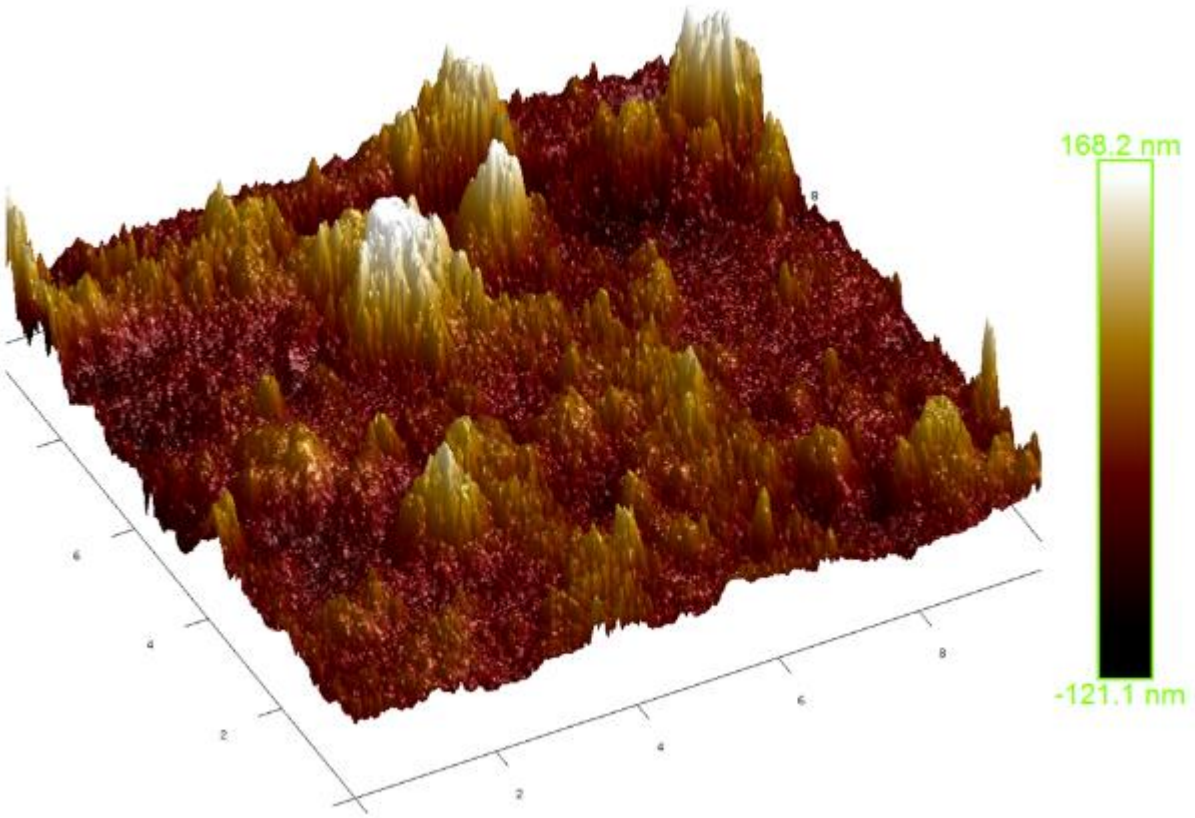


*Figure 3.4.7 Qualitative analysis of topographic surfaces using atomic force microscopy (AFM). A representative image of a 10 x 10 µm section was taken from a microfluidic channel fabricated in VisiJet SL Clear (left). Note the maximal roughness variation was less than 0.2 µm.*

## 3.5 Optical properties

Zebrafish embryo bioassays rely on high resolution images to analyse any phenotypic responses. The accessibility of high quality images from lab-on-a-chip devices is thus of the utmost important. In this regard, all 3D printed chip devices were made of optically transparent or "clear" materials. Moreover, the surface roughness described above also played an important role in optical properties. Herein, the imaging performance of the 3D printed chips was assessed with several commonly used microscopies.

### 3.5.1 Bright field microscopy

Zebrafish embryos were loaded into the chip devices, imaging under an upright stereomicroscope in the bright field (Figure 3.5.1). The result showed that the lab-on-a-chip devices fabricated from different materials have dramatically different optical

transparencies, though they were all claimed to be transparent. Compared with the control PDMS chip, only the VJSL chip had a close transparency that clearly showed embryo sitting in the chip device. VJC, WXC, and DFC chips showed transparency to some extent, where the shape of the embryos could be seen but no details were readily observable. The DFC chip also presented black spots throughout the chip, further obstructing the imaging. The FC chip again performed so poorly that the embryo was barely noticeable. The body of the chip device also had perceptible "scan line" traces from the fabrication processes. To compensate for this problem, the chips lacking of optical transparency were further mechanically polished, but the improvement was very limited.

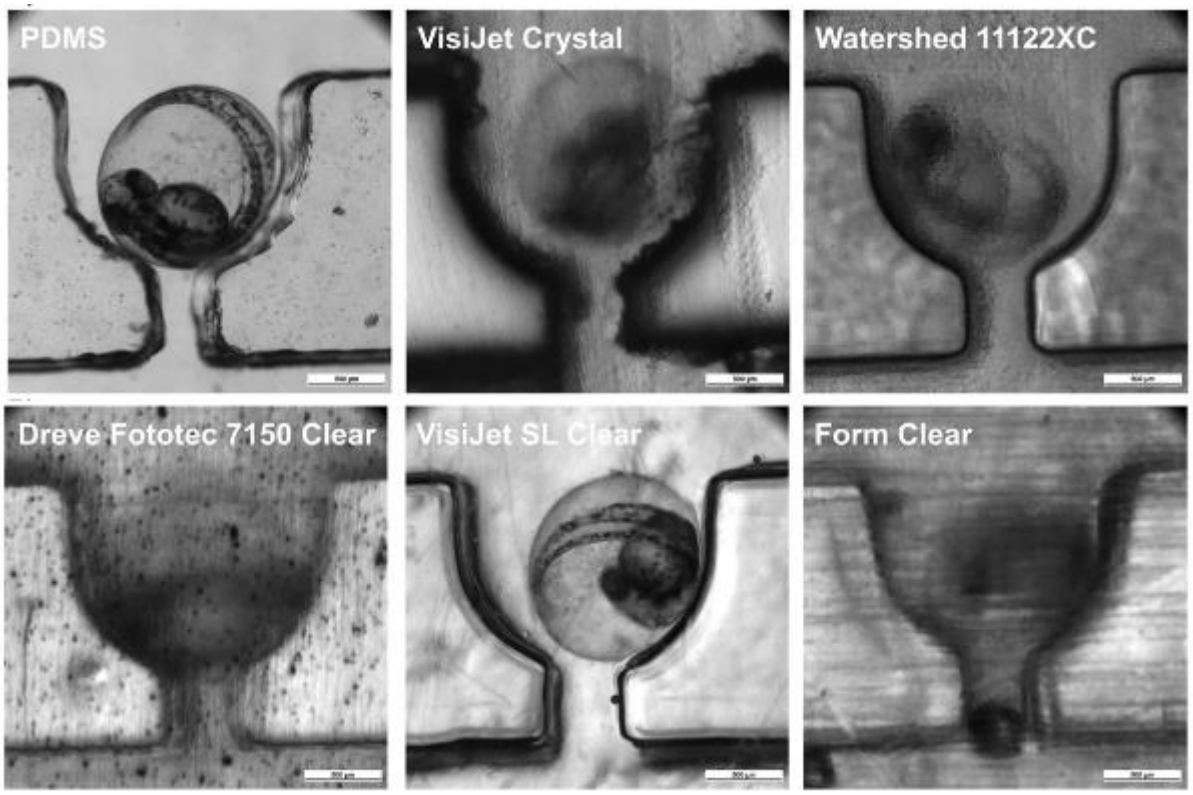


*Figure 3.5.1 Comparison of optical transparency of the chip devices in the presence of loaded embryos under a stereomicroscope. Only the chips made of PDMS and VisiJet SL Clear allowed an unobstructed view of live embryos. Published in Ref 105. Reproduced with permission from AIP Publishing LLC.*

### 3.5.2 Fluorescence microscopy

Zebrafish and embryos are popular animal models in biomedical applications because they allow simple genetic modification and can express fluorescent protein. Therefore, the suitability of 3D printed chips for fluorescence imaging of specimens was also examined. In

the experiment *Tg(fli1:EGFP)* transgenic zebrafish embryo (48 hpf) were loaded into the chip device and imaged under a popular fluorescence (FITC/GFP Ex 480 nm / Em 535 nm). This transgenic strain offers non-invasive observation of the blood vessel development expressing in enhanced green fluorescent protein (EGFP) in endothelial cells.

The result showed that all 3D printed chips bear substantial autofluorescence due to the material, interfering with the observation of small features such as the intersegmental vessels (Figure 3.5.2). Compared with the control PDMS chip, only the VJSL chip offered an acceptable level of visibility. The transparency of WXC chip was fine but contained too much background noise fluorescence. The remaining chips were not capable of imaging fluorescent zebrafish embryos at all.

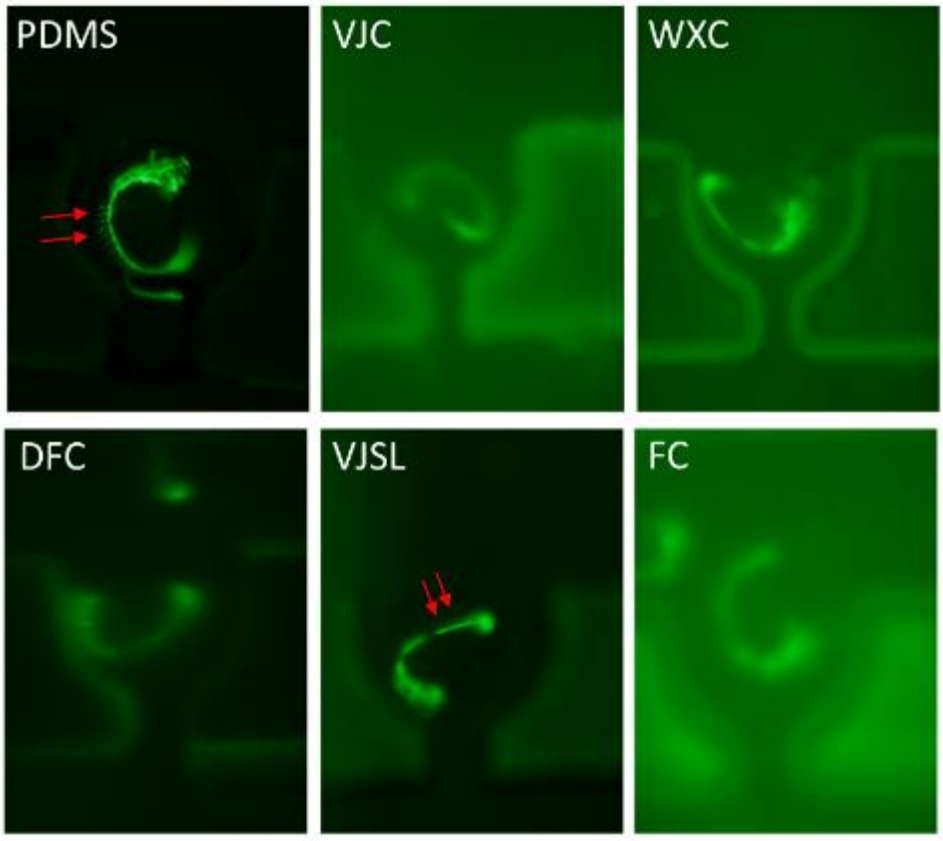


*Figure 3.5.2 Comparison of optical transparency of chip devices for fluorescent microscopy imaging. Epifluorescence imaging (GFP Ex 480 nm / Em 535 nm) of immobilised transgenic* Tg(fli1:EGFP*) zebrafish embryos (48 hpf) inside 3D printed microfluidic chip devices. All 3D printed chips showed auto fluorescence that interfered with imaging. Only the image from the VJSL chip was comparable with the control PDMS chip. Published in Ref 105. Reproduced with permission from AIP Publishing LLC.*

### 3.5.3 Focus stacking confocal microscopy

Because zebrafish embryos are close in shape to spheres, conventional microscopy cannot focus on the entire surface of the embryo. Hence, for high resolution imaging, focus stacking confocal microscopy is necessary. The confocal microscopy suppresses the signal outside the field of focus and only focuses on a very small depth of field. Multiple images were taken at different focal distances. Then, the focus stacking technology merges the images from all steps into one fully focused image.

In the experiment, confocal images were taken from the VJSL chip loaded with *Tg(fli1:EGFP)* zebrafish embryos (48 hpf), as well as from the PDMS chip as a control. Two channels i.e. bright field and fluorescence were merged together showing GFP highlighted blood vessels in the bright field. The VJSL chip once again showed a similar imaging quality as the control PDMS chip. Despite some shadows, the key features were reliably presented.

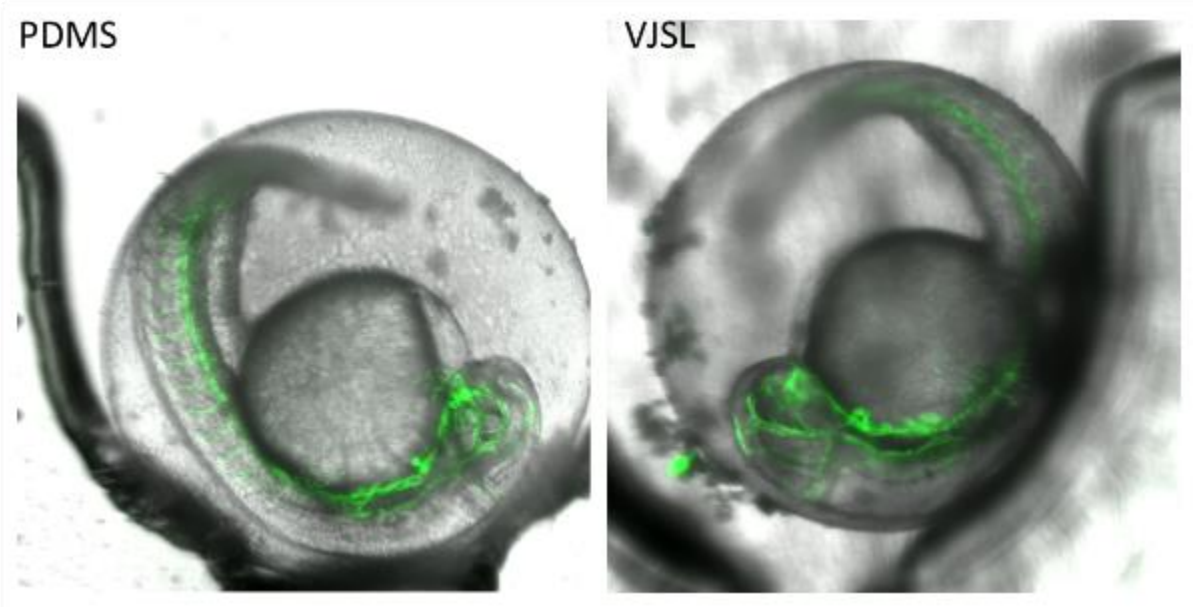


*Figure 3.5.3 Comparison of the PDMS chip with the VJSL chip in high-resolution stacked confocal imaging of live Tg(fli1:EGFP) zebrafish embryos. The image taken from the VJSL chip was comparable with the control PDMS chip.*

## 3.6 Embryo loading and immobilisation

Next, I investigated the functionality of 3D printed embryo trapping chips. The chip design exploited hydrodynamic forces enabling automated embryo trapping and immobilisation

(Figure 3.6.1)[59]. Hydrodynamic trapping is dependent on the geometry of the microfluidic systems, and even small obstructs in the system will affect the loading efficiency. In this regard, I tested how quality of fabrication affected the function of the chip devices under standard operation procedures.

In the experiment, wild type zebrafish embryos at 24 hfp were individually loaded into embryo trapping arrays at a flow rate of up to 2 mL/min. The trapping efficiency was calculated as the number of docked embryos over the number of injected embryos on the chip device.

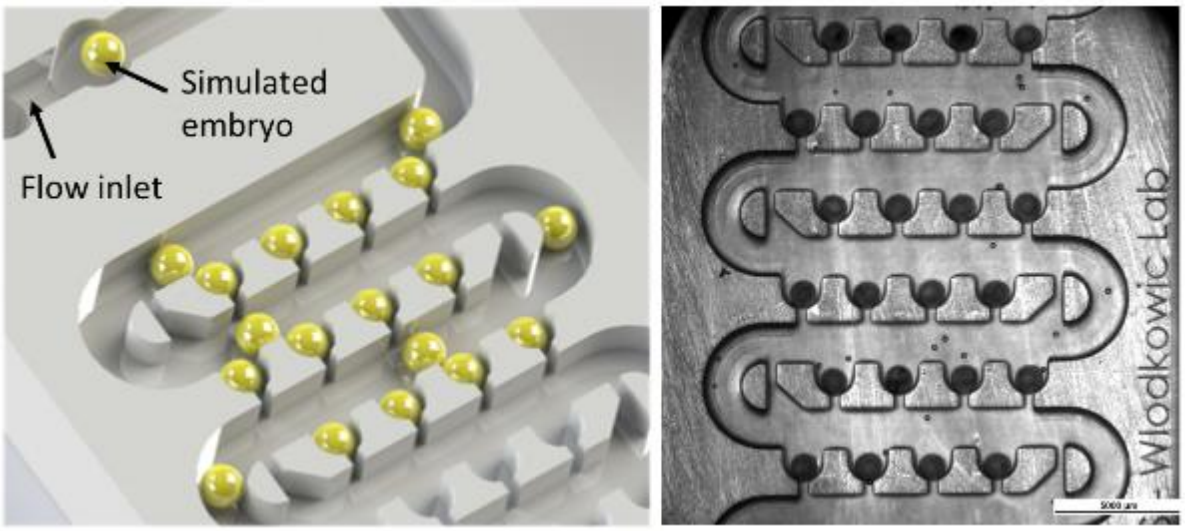


*Figure 3.6.1 Embryo loading and immobilisation. Left: CAD rendered cartoon depicting the embryo loading principle. Embryos were aspirated from a storage reservoir into the fluidic channel. Hydrodynamic force guided the embryo into the trap. Docked embryos act as spacers allowing the upcoming embryos to roll over towards the next available trap. Right: A macrograph showing all embryos were trapped in a 3D printed chip device.*

The result showed that embryo trapping efficiency was significantly affected by the quality of fabrication and surface roughness. Accordingly, trapping efficiencies in PDMS, PMMA, VisiJet Crystal, Watershed 11122XC, Dreve Fototec 7150 Clear, VisiJet SL Clear, and Form Clear chip prototypes averaged 81 ±3%, 87 ±2%, 48 ±8%, 79 ±1%, 100 ±0%, 98 ±2%, and 25 ±5%, respectively (Figure 3.6.2). Residues and support materials caused a lowered trapping performance of VJC chips fabricated by the MJM process. In contrast, a poor trapping efficiency from Form Clear chips suggested a low quality of feature fabrication and a rough surface due to imprecise layer composition. While, the outstanding embryo trapping

efficiency achieved by WXC, DFC and VJSL devices were supported by superior feature production and minimised surface roughness as demonstrated by SEM and optical profilometry.

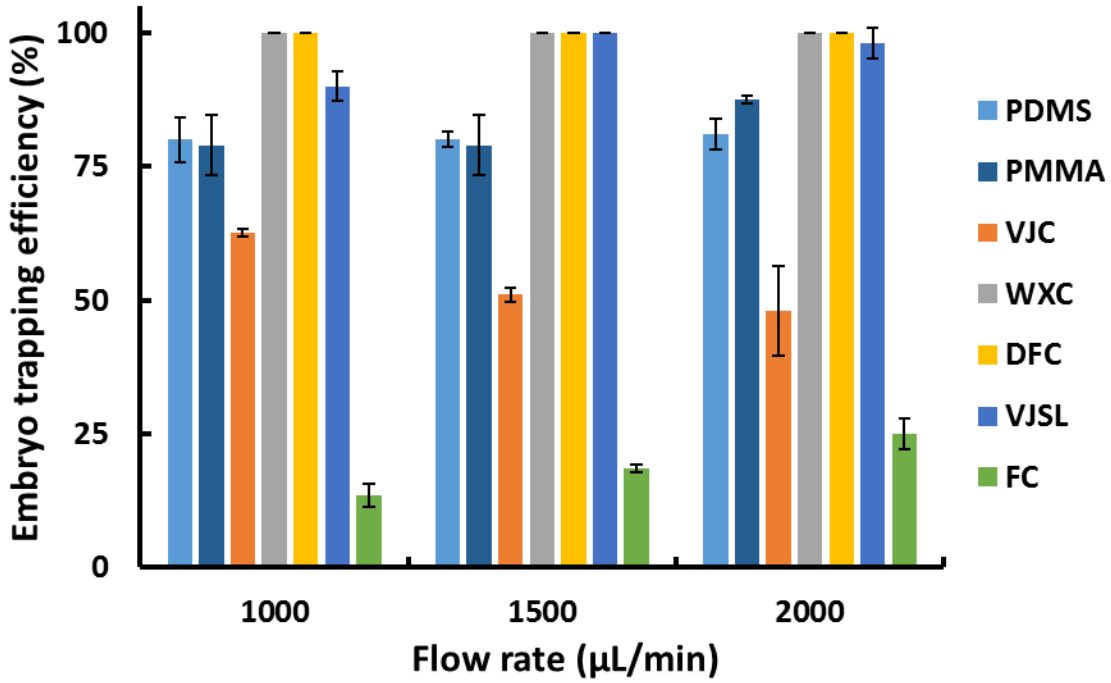


*Figure 3.6.2 Embryo trapping efficiency on 3D printed devices. Loading experiments were conducted at different flow rates as indicated. Note that the embryo trapping efficiency was significantly related to feature finish quality and surface roughness.*

## 3.7 Biocompatibility

In the last phase of assessment, the biocompatibility of the 3D printed chips for long term culture was investigated under a microperfusion environment. Zebrafish embryos are considered to be one of the most sensitive organisms to environmental deteriorations and can be readily applied to test chemical toxicity of solid substrata[39], and the 3D printed chip devices were indeed designed for zebrafish embryo bioassays.

In the experiments, wild-type zebrafish embryos at 6 hour post fertilisation (hpf) were loaded onto the chip devices and cultured under continuous microperfusion at a flow rate of 400 µL/min for up to 72 hours. The perfusion was performed in a closed loop circuit with a 40 mL reservoir contained fresh embryo medium. Embryo viability was observed every 24

hours, however, due to the limited visibility of some 3D printed chips, detailed characterisation of embryo developmental stages was not accessible. Therefore, at the end of the exposure experiment, embryos were unloaded from the chip devices onto Petri dishes for phenotypic analysis.

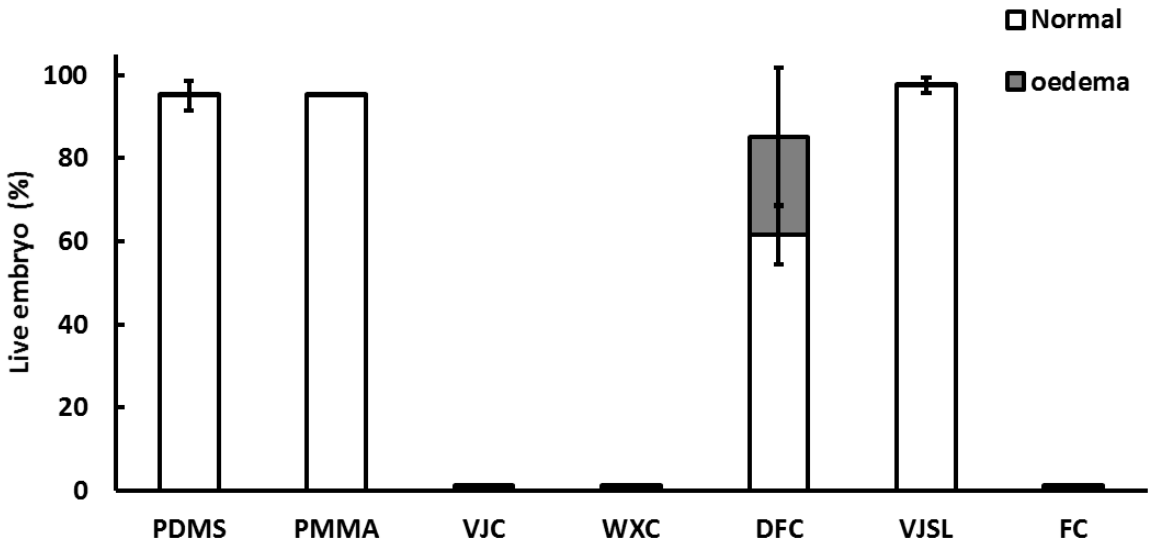


*Figure 3.7.1 Viability of zebrafish embryos cultured on microfluidic chip devices at 72 hour post fertilisation (hpf) under a continuous microperfusion of 400 µL/min. Note that only one 3D printed chip, the one made of VJSL polymer, showed a similar embryo viability to the control PDMS and PMMA chip devices.*

The result showed significant toxic effects for most 3D printed chips (Figure 3.7.1). 100% mortality was observed in VJC, WXC, and FC chips. The DFC chip was less toxic to the zebrafish embryos, but caused sublethal effects such as oedema. Compared with control PDMS and PMMA chips, only the VJSL chip was biocompatible with the embryos.

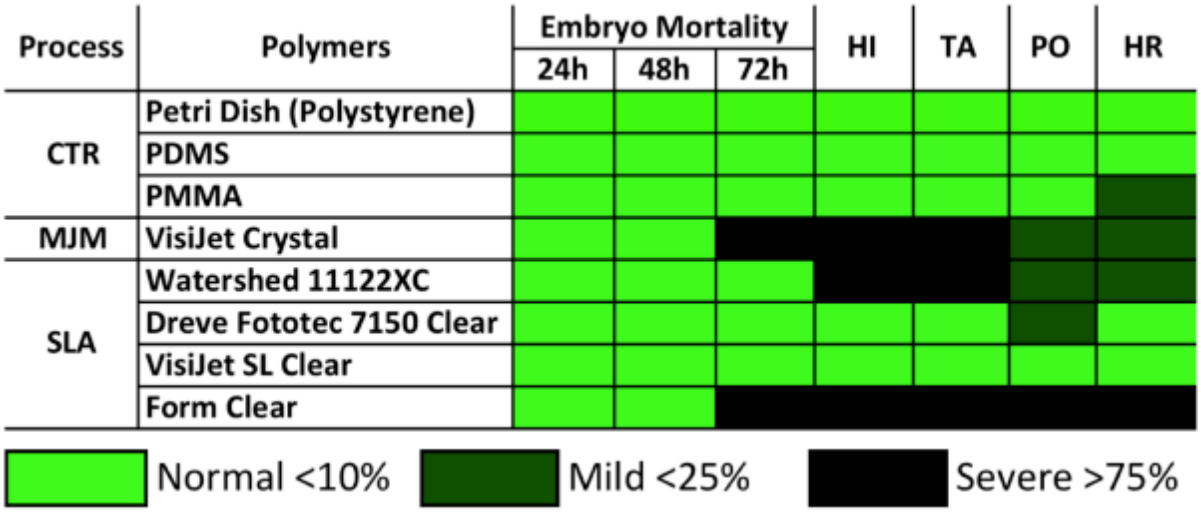


*Figure 3.7.2 Biocompatibility of microfluidic chips for long-term living zebrafish embryo bioassays under a continuous microperfusion of 400 µL/min. Matrix chart depicts cumulative teratogenic effects during a standard zebrafish embryo toxicity (FET) test. CTR – control; MJM – multi-jet-modelling; SLA – stereolithography; HI – hatching inhibition; TA – trunk abnormalities; PO – pericardial oedema; HR – heart rate abnormalities. Published in Ref 105. Reproduced with permission from AIP Publishing LLC.*

For the first 48 hours of the experiment, no embryo mortality was observed on any chip device. Lethal and sublethal effects were expressed between 48 and 72 hours of the experiment, suggesting a cumulative chronic toxicity effect rather than an accurate response (Figure 3.7.2). In survived embryos, different developmental abnormalities among different 3D printed chips were observed (Figure 3.7.3), indicating different toxic ingredients contained in different 3D printing materials.


*Figure 3.7.3 Critical developmental abnormalities in cultured zebrafish embryos observed in chip-based devices fabricated using 3D printing.*

## 3.8 Summary and discussion

The implementation of lab-on-a-chip (LOC) technologies for *in situ* analysis of small model organisms and their embryos is attracting an increasing amount of interest from the biomedical community. However, the development of microfluidic lab-on-a-chip devices for small model organisms is rather limited compared with other burgeoning fields. This is due to the difficulty of rapid prototyping and manufacturing millilititre scale LOC devices with complex three dimensional structures that can accommodate large organisms in flow-through conditions. I postulate that the advanced 3D printing technology is capable of solving this problem. However, so far no reports have investigated the biological implications of small model organisms or embryo culturing in 3D printed devices.

Despite the rapid developing of 3D printing technology on the market, the printing resolution and quality varies dramatically. Materials suitable for making biomicrofluidic lab-on-a-chip devices are so far limited to photoresist resins, as they are the only optically transparent materials used by current 3D printers. However, most photoresist resins were not initially designed for applications in aqueous environments because they tend to swell significantly when in contact with water, and they were found being toxic to aquatic organisms[77]. Nevertheless, few commercially available materials, such as DSM Somos WaterShed XC11122, were reported to be biocompatible[77, 93].

In this study a range of 3D printing systems and their associated materials were selected to fabricate a zebrafish embryo trapping array. A comprehensive side-by-side evaluation of all prototypes was performed to test printing accuracy, surface roughness, and optical transparency. I also focused on the material biocompatibility by conducting zebrafish embryo bioassays, and found only one material that was nontoxic to the embryo over the testing period. It can be concluded that current 3D printing technology, especially stereolithography (SLA) and multi-jet modelling (MJM), provide a convenient and inexpensive way to fabricate complex lab-on-a-chip devices. However, one has to be very careful when choosing the printing system and materials. Many challenges remain in the current 3D printing technologies.

**Fabrication of 3D printed chips**

All the devices presented in the thesis were printed horizontally. During the prototyping, the FC chips had been attempted to be printed vertically. In general, printing vertically took much more time; and it resulted in a similar optical performance but a reduced accuracy in building the microfluidic channels. For these reasons, only the horizontally printing configuration was chosen to print all the chips in this study.

Although the 3D printing process is simple and so convenient that it can be achieved by one-click, most of technologies require post-processing procedures. For instance, the MJM fabrication process uses wax as a support in building hollow structures such as fluidic channels. Removing the support wax required complicated procedures, which are described in Chapter 2. During experiments, despite efforts to clean the fluidic channel, residue wax could not be completely eliminated (Figure 3.8.1). Wax granules blocked the small fluidic channel, which affected embryo loading efficiency; they also accumulated in the embryo traps, which prevented embryo docking (white arrows). So far, no solutions were found to address this issue.

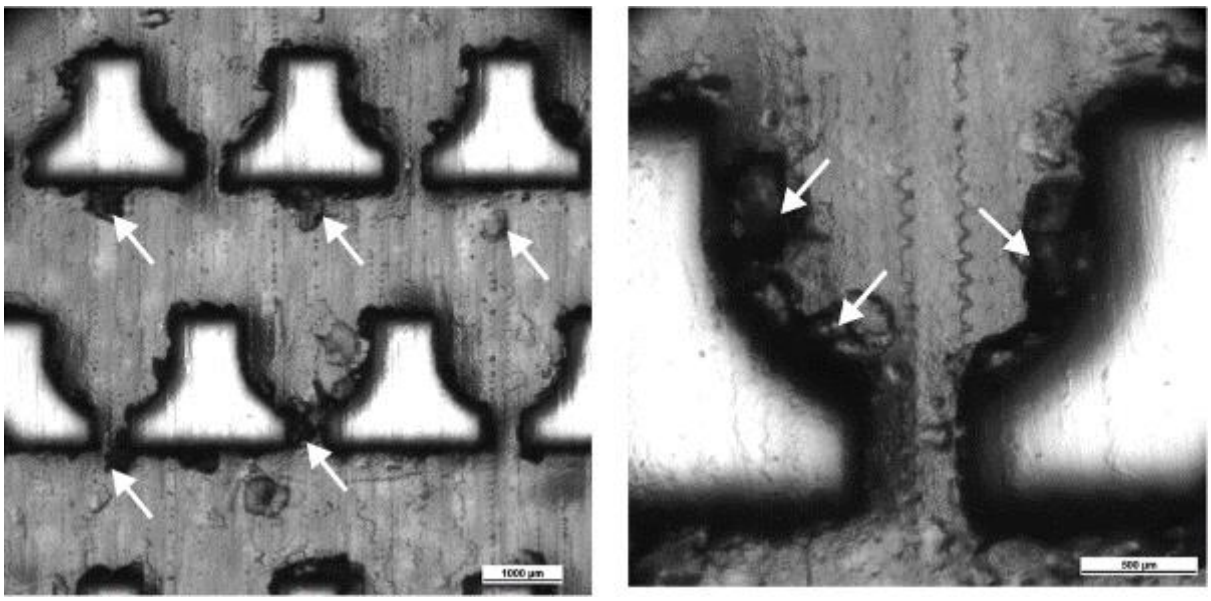

*Figure 3.8.1 Post-processing challenges associated with Multi-Jet modelling (MJM) fabrication of microfluidic chip-based devices. Left: Residues of VisiJet S300 Support Wax left behind during the fabrication process (white arrows); Right: Magnified view of a single embryo microtrap obstructed by significant VisiJet S300 Support Wax residue. Post-processing of MJM prototypes required several*

*subsequent steps to remove Support Wax as outlined in Chapter 2. Complete removal of wax residues proved impossible.*

A similar situation occurred during the SLA fabrication processes. To print a structure over the hollow spaces, unpolymerised resin (the printing material) were employed as the spacer. When finishing, excess resins need to be flushed out to achieve the designated structure. In the standard operation protocols, residue resins are cleaned by flushing with isopropanol followed by soaking the prototype in isopropanol for 10 minutes. In the end, the 3D printed chips needed to be hardened in a UV oven.

Unlike the support wax, unpolymerised resin is relatively easy to wash out using isopropanol (Figure 3.8.2). However, when the structure is complicated, the washing becomes ineffective. For example, when the fluidic channel is narrow or has a lot of sharp twists, isopropanol is unable to reach the residue. In practice, I found that applying air pressure can sometimes blow off the residue. Nevertheless, an overpowered pressure can damage the structure, as the 3D printed structures are relatively soft and prone to deform prior to the UV curing.

There are more difficulties when a 3D printed chip had residual resin remaining in the channel during UV curing. The UV light would harden the excessive resin and block the fluidic manifold permanently. It is necessary to clean the channel very carefully before the final curing.

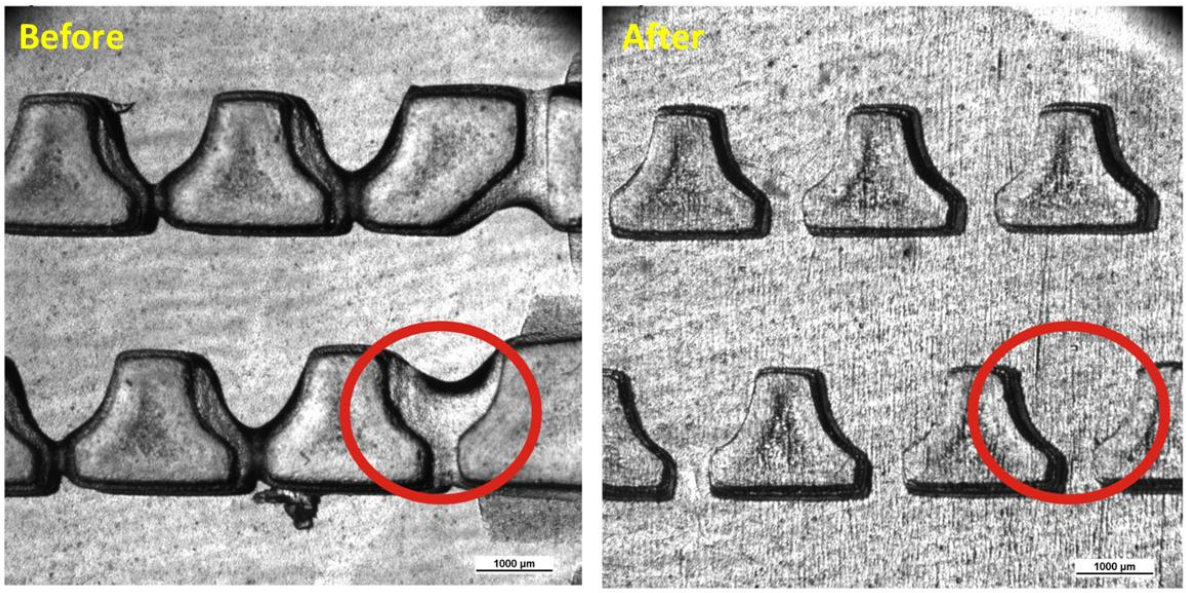


*Figure 3.8.2 Post-processing challenges associated with stereolithography (SLA) fabrication of*

*microfluidic chip-based devices. Left: Non-polymerized SLA resin residues obstructing channels with high fluidic resistance (red circle); Right: Removal of non-polymerized SLA resin residues with isopropyl alcohol ensures proper geometry of the microfluidic circuitry.*

**Autofluorescence**

Autofluorescence is a natural emission of light where the molecules of material absorb excitation light without artificial addition of fluorescent markers. Strong autofluorescence obstructs observation of fluorescent markers in target specimens, as described above. Choosing materials should be done very carefully for experiments using fluorescent specimens because different polymers have different autofluorescence intensities at different wavelengths. For example, VisiJet SL Clear chip had low to moderate autofluorescence from the excitation wavelengths ranging from 458 nm to 514 nm, but it had an extremely high response to the excitation wavelength at 633 nm (Figure 3.8.3).

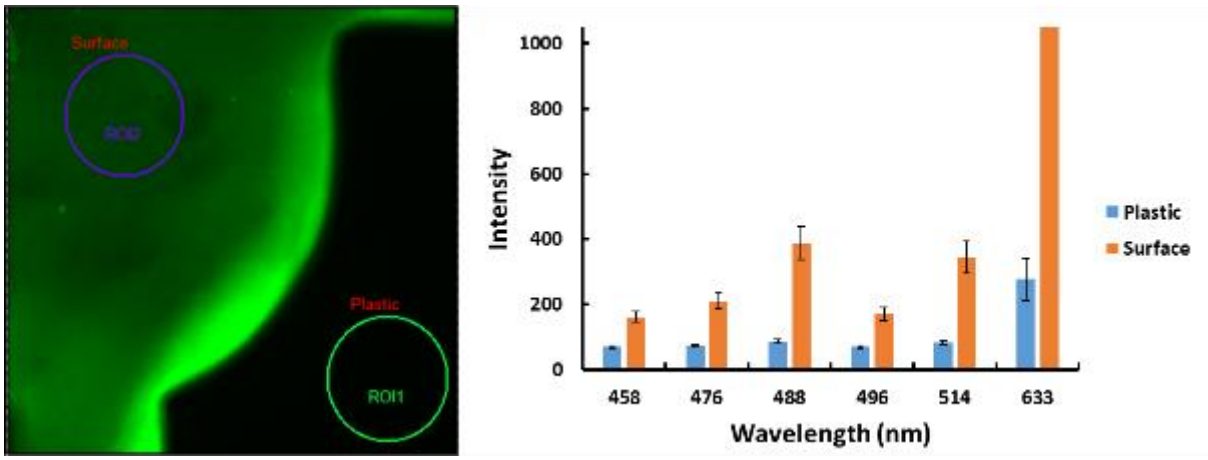


*Figure 3.8.3 Detection of autofluorescence across a range of wavelengths on VisiJet SL Clear chip. Left: Region of interest (ROI) of the chip is depicted. "Plastic" denotes the solid part of the chip and the "Surface" denotes the hollow part (fluidic manifold) of the chip. Right: Intensities detected at different wavelengths. Surface areas have significantly higher autofluorescence than the plastic areas. The intensity of the fluorescence is dependent on the wavelength of the excitation light.*

**Other properties of the 3D printing materials**

To reveal other physical attributes of the 3D printing material, I have applied several treatments to the chips. In autoclave testing, the 3D printed prototypes were heated up to 140 °C under a standard pressure for 20 minutes. As a result, all 3D printed chips were cracked and no longer functional. In UV exposure experiments, 3D printed prototypes were

exposed to UV light in a standard cell culture hood for 24 hours. In the end of the experiment, the 3D printed chips were curved and had become hard and brittle. All 3D printed chips were also treated with 50% oxygen plasma twice, each time for 30 seconds. No visible damaged was caused.

**The biocompatibility issue**

So far, only a selection of photoresist resins and printing systems were evaluated for one biological model (zebrafish embryo), the results nevertheless pointed to serious biocompatibility issues for polymers commonly used in high-definition 3D printing. To understand the general toxicity profile of 3D printing materials, more ecotoxicological assays need to be performed on more 3D printing materials using more animal models. Preferably, chemical analysis of the toxic leachates would also be performed. I will continue discussing this topic in chapter 4.

# 4 Characterisation of 3D printing material toxicity

## 4.1 Introduction

A recent boom in three dimensional (3D) printing technologies has instigated a revolution of microfabrication and prototyping in science and engineering. In particular, bioengineering has benefited from 3D printing for making medical implants, including bones, ear moulds, and exoskeletons. Moreover, development of high-definition 3D printing technologies, such as Multi-jet moulding (MJM) and Stereolithography (SLA), has allowed the production of features as small as a few micrometres, capable of prototyping and fabrication of biomicrofluidic lab-on-a-chip devices. This incentive helped the biomedical researchers to close the gap between the need for prototyping bio-devices and their insufficiency in engineering expertise.

As discussed in the previous chapter, although high-definition 3D printing is able to rapidly fabricate biomicrofluidic devices for aquatic organism culture, the materials have the potential issue of lacking biocompatibility as per our primary test on zebrafish embryos. In this chapter, a comprehensive toxicity characterisation of numerous commonly used polymer materials in 3D printing applications was performed. Currently, there are dozens of materials on the market, and different printing systems use very different printing materials. In this study, I carefully selected a few popular materials as representatives for biocompatibility tests. For fused deposition modelling (FDM) printing systems, I selected acrylonitrile butadiene styrene (ABS) and polylactic acid (PLA); for Multijet moulding (MJM) printing systems, VisiJet Crystal (VJC) was picked; and for stereolithography (SLA) printing systems, Watershed XC11122 (WXC), Dreve Fototec Clear (DFC), VisiJet SL Clear (VJSL), and Form Clear (FC) photoresist resins were chosen.

## 4.2 Experimental design

I postulate that the material's toxicity derives from the leachate that comes from the surface of polymerised material, and/or unpolymerised residues left in the 3D printed prototypes. In this regard, the potential toxicants need to be extracted from the solid phase (3D printed objects) into aqueous phase (organism culture medium). In this experiment,

porous blocks fabricated in different 3D printing polymers were used for extraction (Figure 4.2.1 A). Each block had a surface area of 6,250 $mm^2$. Four 3D printed blocks were added into a glass bottle filled with 500 mL of respective organism culture medium for extraction. The extraction was conducted in darkness at 22 °C for 72 hours, with the assistance of a magnetic stir bar spinning at approximately 240 rpm. The resultant medium was considered to be concentrated 100% extract.

Material toxicity profiles were evaluated by using standardised bioassays according to OECD guidelines for testing of chemicals. Test aquatic organisms were selected and ranged from plants, invertebrates, and vertebrates. The biotests were conducted immediately after material extraction.

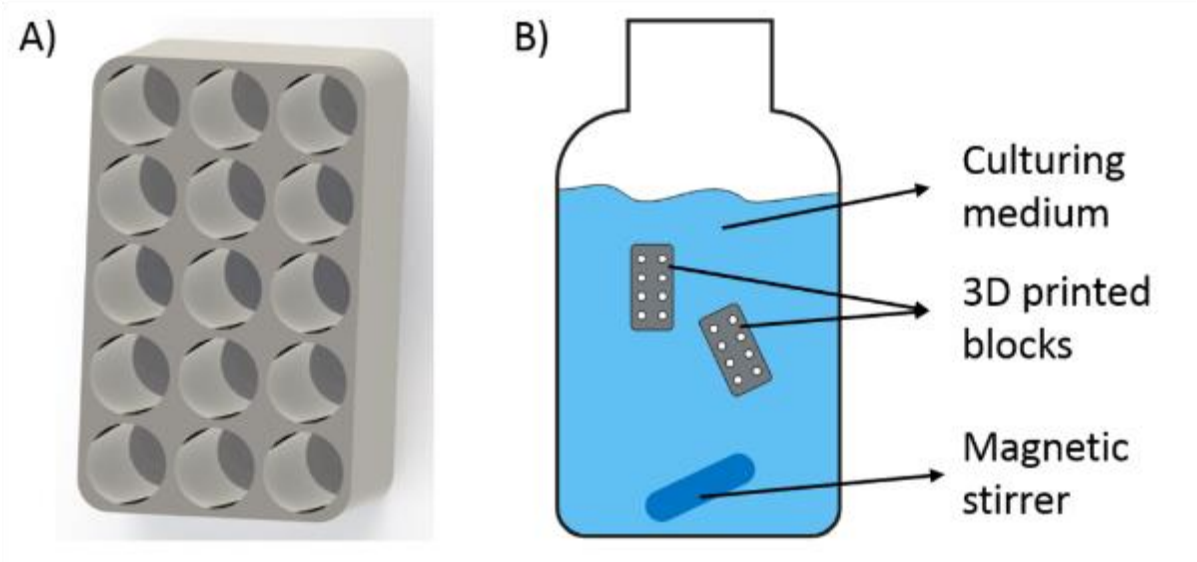


*Figure 4.2.1 A standardised preparation of water extracts for profiling polymer toxicity (A) CAD Design of the extraction structure, each block has a surface area of 6,250 $mm^2$. (B) Extraction cartoon. Four 3D printed blocks were added into culture medium with a magnetic stir bar and stirred for three days in a dark environment.*

## 4.3 3D printed polymer screening test

In the first phase of toxicity bioassays, 100% concentrated polymer extract was used to explore the toxic effects on a battery of aquatic model organisms.

### 4.3.1 Aquatic plants

Fresh water microalgae (*Selenastrum capricornutum*) responsed to the toxicity by a reduction in growth. Algae normally grow exponentially over a period of 72 hours[106]. Growth and growth inhibition were quantified from the measurement of algal cell number density as a function of time. As a result of testing, all 3D printing polymer extracts exhibited toxicity by inhibiting algal growth (Figure 4.3.1 A). In particular, while algae were still growing in ABS, PLA, and VJC treatments, algal cell density in all SLA polymer (WXC, DFC, VJSL, and FC) treatments decreased or remained unchanged. The result indicated that fresh water algae is very sensitive to 3D printing polymer extracts, especially the SLA material extracts, which were highly toxic to the algae.

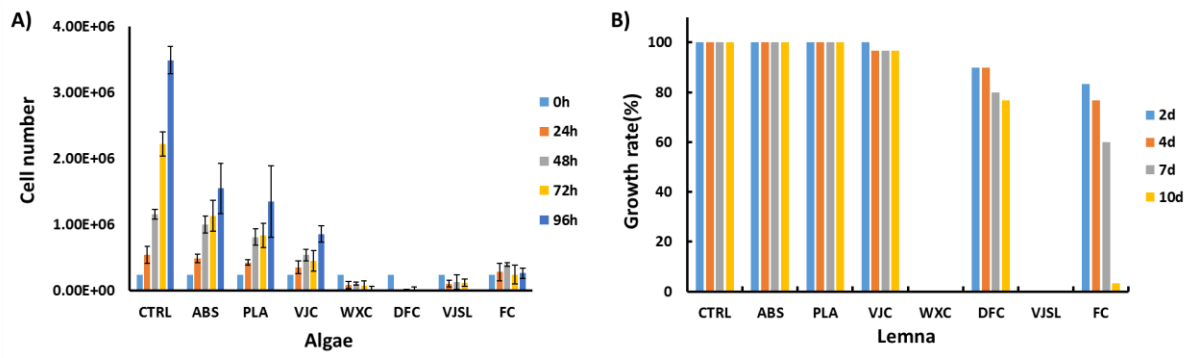


*Figure 4.3.1 3D printing polymer toxicity profiling using aquatic plants. 100% concentrated 3D printing material extracts were used. A) Toxicity biotest on fresh water algae. Cell numbers of each treatment were counted every 24 hours. Algal growth was inhibited in all treatments, including ABS and PLA. B) Toxicity biotest on lemna. Growth rates for each treatment were calculated. Lemna died in WXC and VJSL treatments after just two days. DFC and FC also showed chronic toxicities.*

Fresh water duckweed (*Lemna minor*) has been extensively studied as a standard toxicity model system. Growth and growth inhibition were quantified from the measurement of frond number as a function of time. In this experiment, I observed that ABS and PLA treatments were not toxic to the lemna; VJC and DFC treatments showed slight toxicity. The FC treatment had a chronic toxic effect on the lemna, whereas the WXC and VJSL killed lemna completely within 24 hours (Figure 4.3.1 B).

### 4.3.2 Marine invertebrates

Toxicity investigations were also performed with marine invertebrates. Brine shrimp *Artemia franciscana* is a commonly used species for ecotoxicological biotest. The artemia, however, is known for being less sensitive to many chemicals in comparison to other test species.

During experiments, it was indeed found that artemia were rather resistant to all the polymer treatments. By the end of 24 hours, all artemia survived the test (Figure 4.3.2 A). Significantly decreased survival rates were observed after 72 hour of exposure.

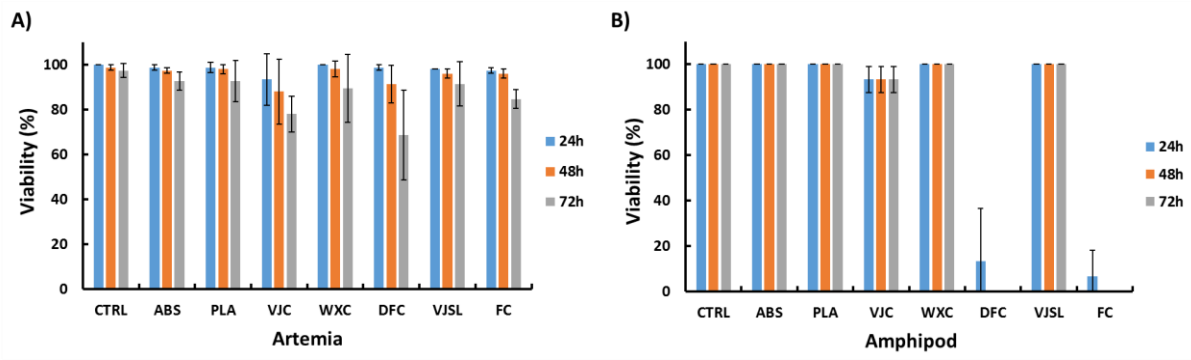


*Figure 4.3.2 Toxicity profiling using marine invertebrates. 100% concentrated 3D printing material extracts were used. Viabilities were calculated every 24 hours. A) Test on the marine crustacean artemia. Note that artemia was resistant to the toxicity from all the treatments. B) Test on the marine crustacean amphipod. Amphipods were very sensitive to DFC and FC extracts.*

Amphipods (*Allorchestes compressa*) were another marine crustacean species chosen for toxicity tests. They are more sensitive to environmental toxicants than artemias. In the experiment, amphipods were found very sensitive to two polymer treatments, DFC and FC, with 100% mortality within 24 hours of exposure (Figure 4.3.2 B). In other treatments, however, no significant toxicity was observed during 72 hours of exposure.

### 4.3.3 Freshwater invertebrates

Following up the marine invertebrates, I also tested the toxicity responses of freshwater species. Rotifer (*Brachionus calyciflorus)* has a favourably comparative sensitivity with other invertebrates currently used in aquatic toxicology. The data show that rotifers were found being very sensitive to SLA polymer (WXC, DFC, VJSL and FC) extracts (Figure 4.3.3 A). The FDM materials (ABS and PLA) and MJM material (VJC) were found non-toxic to this species.

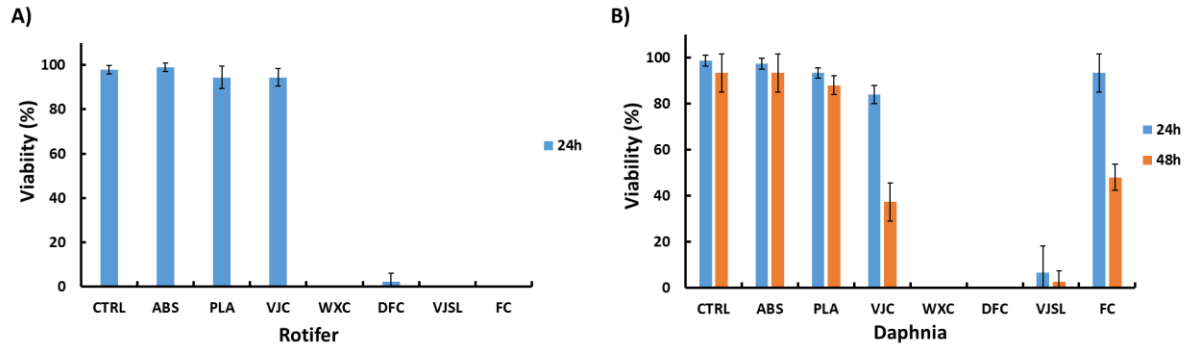


*Figure 4.3.3 Toxicity profiling using freshwater invertebrates. 100% concentrated 3D printing material extracts were used. Viabilities were calculated every 24 hours. A) Tests on rotifer. All SLA polymers (WXC, DFC, VJSL, and FC) were shown to be very toxic to this organism. B) Test on daphnia. WXC, DFC, and VJSL polymer extracts were very potent toxins to the daphnia, whereas the VJC and FC extracts showed moderate toxicities. Published in Ref 107. Reproduced with permission from AIP Publishing LLC.*

The freshwater planktonic crustacean *Daphnia magna* has been developed as a standard aquatic toxicity test for many years and has been approved by many international organisations, including OECD, ISO, and USEPA. It is one of the most commonly used species for determining the effects of xenobiotics in aquatic ecosystems. In this experiment, I observed that WXC, DFC, and VJSL treatments were very toxic to the daphnia that they were all killed within 24 hours of exposure (Figure 4.3.3 B). VJC and FC polymer extracts were moderately toxic to the daphnia, so that nearly 50% of them were dead after 48 hours of exposure. The ABS and PLA were inert to this species.

### 4.3.4 Freshwater vertebrates

Next, I investigated the toxicity profiles on vertebrate animal models, i.e. zebrafish embryos and larvae. In the primary test performed on a flow-through chip-based system, the 3D printing polymers were found to be lethal to the fish embryos after 72 hour of exposure (Chapter 4). In this experiment, biotests were performed in a static condition and the toxicity was found even higher, so that embryos were dead within 24 hours of exposure, except for ABS and PLA treatments, which were not toxic (Figure 4.3.4 A).

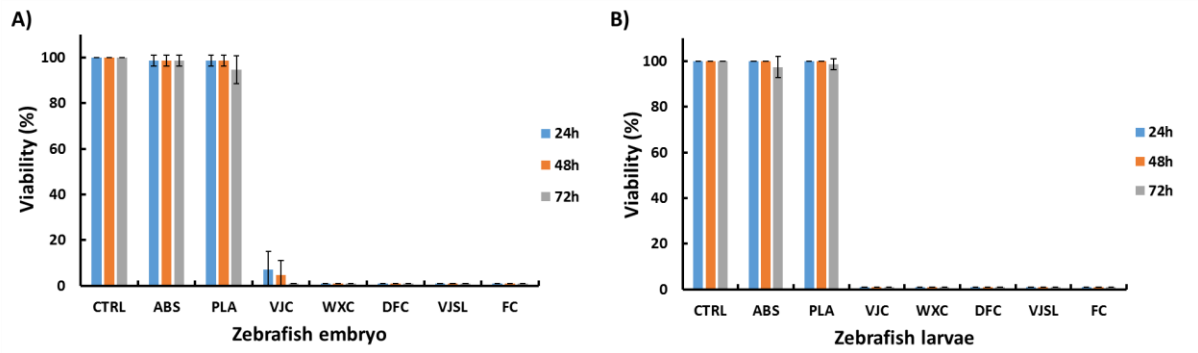


*Figure 4.3.4 Toxicity profiling using freshwater vertebrates. 100% concentrated 3D printing material extracts were used. A) Test on zebrafish embryo. B) Test on zebrafish larvae (7 dpf). Only two FDM materials (ABS and PLA) were nontoxic to the zebrafish. The toxicants apparently can penetrate the chorion of the embryo. Published in Ref 107. Reproduced with permission from AIP Publishing LLC.*

Zebrafish larvae at 7 days post fertilisation (dpf) were also used as a test organism. Compared with zebrafish embryos, the larvae are much more mature, with main organs developed and are expected to be more resistant to toxicants. On the other hand, hatched larvae have lost the protection from their chorion so that they actually might be more vulnerable to the toxicants. As a result of biotests, the toxicity response of zebrafish larvae was almost identical to the response of embryos. All polymer extracts, apart from ABS and PLA, were highly toxic to the zebrafish (Figure 4.3.4 B).

### 4.3.5 Zebrafish larvae behaviour

All aforementioned biotests were based on the mortality observed at the endpoint of the experiments. There is an alternate way to assess the toxicity by looking at animal behavioural parameters. Behavioural test using zebrafish larvae have been well developed on both the scientific side and the technological side. In particular, it has been established that behavioural parameters, such as travelled distance and active duration, precisely reveal animal's locomotion and response to the toxicants. Recently, a few innovative imaging systems have been developed for automated animal behaviour tracking and analysis. In this experiment, Zebrabox was used for video recording and analysis.

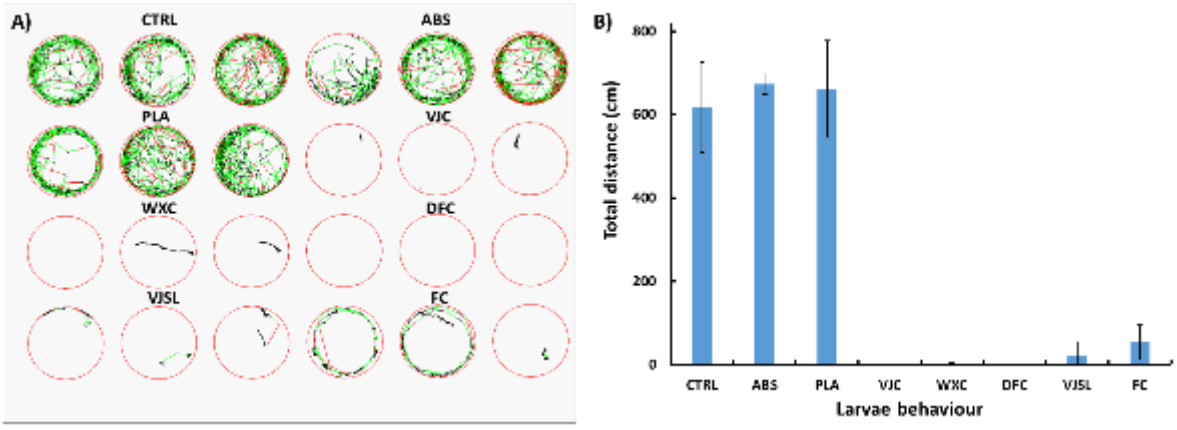


*Figure 4.3.5 Toxicity profiling based on zebrafish larvae behaviour studies. 100% concentrated 3D printing material extracts were used. A) Tracking of zebrafish larvae trajectories in test chambers. B) Total distance of larvae travelled in the test chambers. After just five minutes of exposure, the moving ability of the larvae were significantly inhibited in MJM (VJC) and SLA (WXC, DFC, VJSL and FC) material extracts. Published in Ref 107. Reproduced with permission from AIP Publishing LLC.*

In the 3D printing material toxicity tests, zebrafish larvae (7 dpf) were exposed to polymer extracts for one hour, during which their movement trajectories were recorded. In fact, after just 5 minutes of exposure, while all the zebrafish larvae were still alive, their locomotion activity were significantly inhibited in most treatments, except for ABS and PLA (Figure 4.3.5 A). The locomotion activity is directly related to the total travelled distance as shown in Figure 4.3.5 B. This result was in line with the mortality test results, demonstrating that only FDM materials (ABS and PLA) were inert to the zebrafish larvae.

## 4.4 Form Clear toxicity test

In the last section, I performed a comprehensive screening test on a range of model animals. The toxicity profiles of seven popular 3D printing materials were investigated. However, as an ecotoxicology study, the information was still insufficient because only one concentration was tested for each polymer. A dose response curve is required for understanding the potential effects on the test organisms and finding remediation methods.

An in-depth study of all polymers was impossible because the time input and cost would be considerably high. In this regard, I selected one material, Form Clear. The reason was that the Form Clear is specifically used by the Form series 3D printers. They are desktop 3D

printers that are markedly lower in cost than other 3D printing systems. Therefore, I expect that this material would be largely manufactured, and the waste material would hence also be extensively produced, causing potential environmental issues.

### 4.4.1 Acute toxicity test

In the Form Clear acute toxicity test, concentrated extract media were further diluted to 20%, 40%, 60%, 80%, and 100% fractions. Lemna, daphnia, zebrafish embryos and larvae were chosen as model organisms for mortality test. Toxicity curves and half-maximal response concentrations ($EC_{50}$) of each test organism were plotted and calculated using the Toxrat software.

In the lemna test, concentrated Form Clear extract caused a maximal 70% of growth inhibition, with the $EC_{50}$ at 77.4% dilution of the extract. Similarly, concentrated Form Clear caused only 50% mortality in daphnia. The dose response curve was relatively flat, meaning the daphnia were not very sensitive to the toxicants in the FC extract. To the contrary, zebrafish embryo and larvae were very sensitive to this polymer, as evidenced by their steep dose response curves. 100% mortalities were observed at 30% and 35% dilution of extract for embryo and larvae, respectively (Figure 4.4.1).

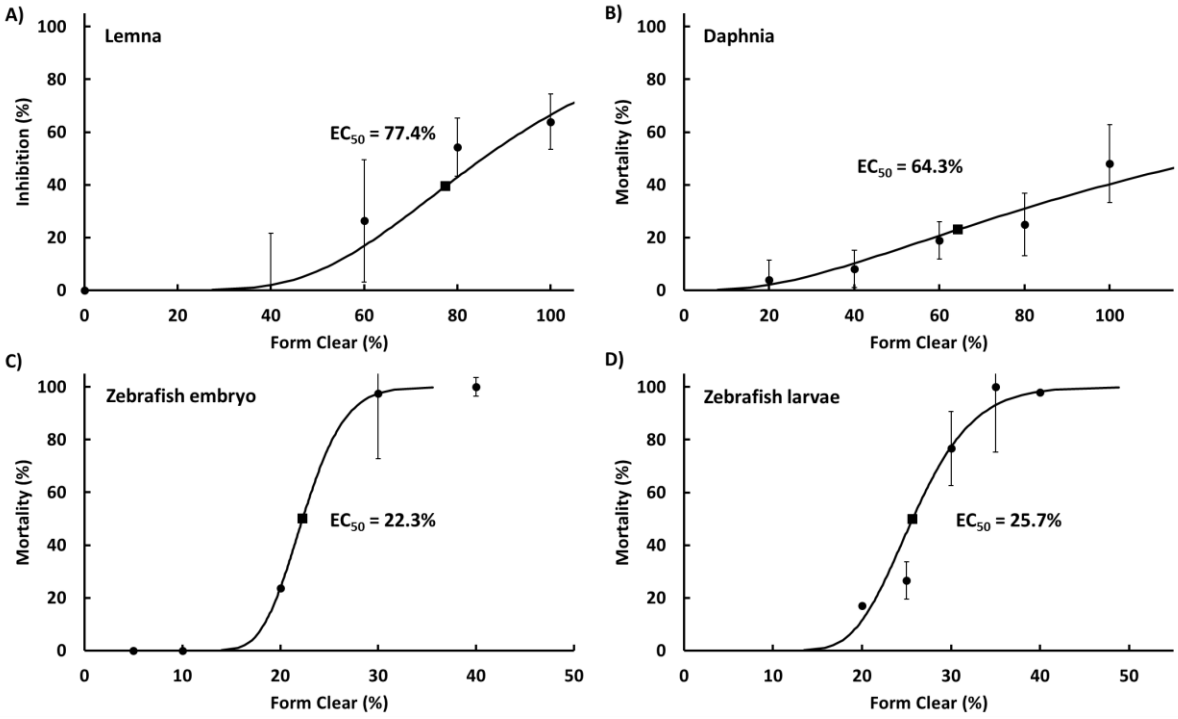

*Figure 4.4.1 Toxicity tests of Form Clear extract on model organisms: A) Lemna, B) Daphnia, C) zebrafish embryo and D) zebrafish larvae. Concentrated Form Clear extract was diluted for the test. Toxicity curves depicted the response of each test organism to different concentrations of the extract. Half-maximal response concentrations were calculated using the Toxrat software. Note that 100% mortality could not be achieved in the tests using Lemna or Daphnia. In the tests with zebrafish embryo or larvae, 100% of mortality was observed at a mere 40% dilution of the concentrated extract.*

### 4.4.2 Zebrafish larvae behaviour test

In addition to the mortality tests, zebrafish larvae behaviour tests were performed to reveal sublethal locomotor activity responses to lower concentrations. The experiment was performed by tracking the movement of each larvae during alternating periods of light and dark. After 64 minutes of exposure, the polymer extract was shown to be toxic to the fish larvae by inhibiting their moving ability, even in a the low concentration of 20% dilution (Figure 4.4.2 A). Zebrafish larvae normally are more active during the dark period than the light period. As the the concentration of the toxicant increased, the difference in moving distance between light and dark became insignificant (Figure 4.4.2 B). The habituation curve showed that zebrafish larvae had an instant locomotion change at the very beginning of the experiment. The moving distances in each concentation differed significantly during the first light/dark cycle. As the fish larvae adaped to the test environment, the behavioural differences among different concentrations became trivial (Figure 4.4.2 C). When analysing the percentage of change in the moving distance during the experiement, compared to the control, significant locomotion changes were found at concentrations higher than 40% dilution (Figure 4.4.2 D). The threshold of the toxicity is around 20% of dilution, which is in line with the result from the mortality test.

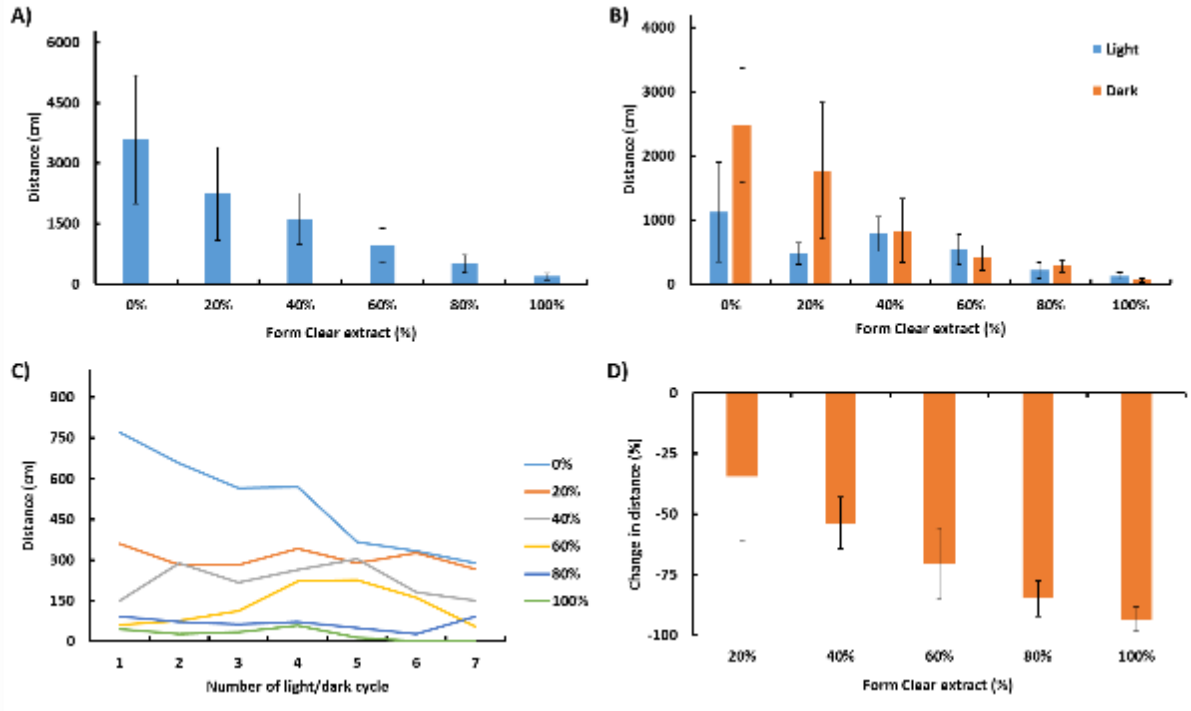


*Figure 4.4.2 Larval behaviour tests of Form Clear extract. 100% concentrated Form Clear extract was diluted for the tests. The behaviour test lasted for 64 min with a 4-min-light-4-min-dark cycle applied during the tests. A) Total distance travelled by larvae in the test chamber. B) Comparison between the distances travelled during the light and the dark. Zebrafish larvae were more active during the dark environment. C) Habituation curve of the larvae in every light/dark cycle. Zebrafish larvae had an instant response immediately after being exposed to the toxicants. However, they tended to recover over the exposure time. D) Percentage of change in total movement distance during the experiment. Significant changes were observed even at the lowest conentration.*

As a vision assistant, the record of larvae trajectories was presented in Figure 4.4.3. The trajectory lines were in three colours. Green lines are large movements with a burst speed larger than 20 cm/s. Red lines represents small movements with a burst speed between 7 and 20 cm/s. Black lines are trivial movements with a burst speed smaller than 7 cm/s. It is clear that embryo activity is negatively related to toxicant concentration. The embryo locomotion also decreased over the period of time.

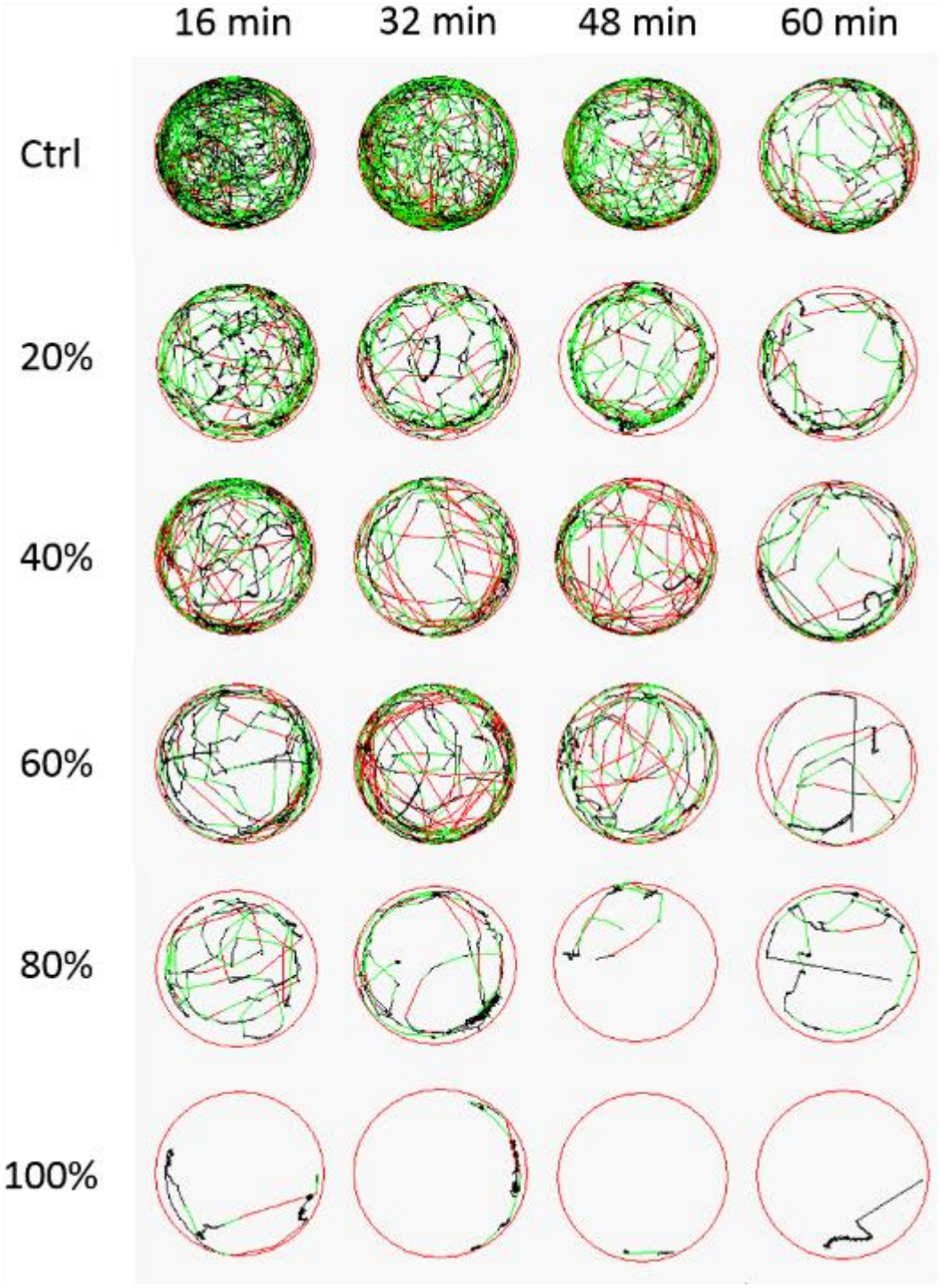


*Figure 4.4.3 Tracking of zebrafish larvae trajectories after exposure to the Form Clear material extract at different concentrations. Each circle depicted the larvae travelling trajectory in 16 minutes. Zebrafish larvae showed an instant behaviour change to the toxicant at different concentrations.*

## 4.5 Chemical analysis

So far, I have investigated the toxicity effect of 3D printing materials on aquatic model organisms, but the specific chemical compounds contributing to the toxicity have not yet been identified. Therefore, in the next phase of toxicity profiling, a chemical analysis was performed using gas chromatography (GC) with associated mass spectrometry (MS).

Generally, in GC-MS analysis, all compounds are injected into to a separation column. As the temperature ramps up, constituents with smaller molecular weight exit the column and are detected first, followed by heavier molecules. Peaks are then recorded on the graph according to their respective retention time. Afterwards, the separated compounds enter an MS detector, where compounds are electronically impacted and decomposed into smaller fragments. The molecular weights of all fragments work like a finger print for the original compound and can then be identified through comparison to compound libraries.

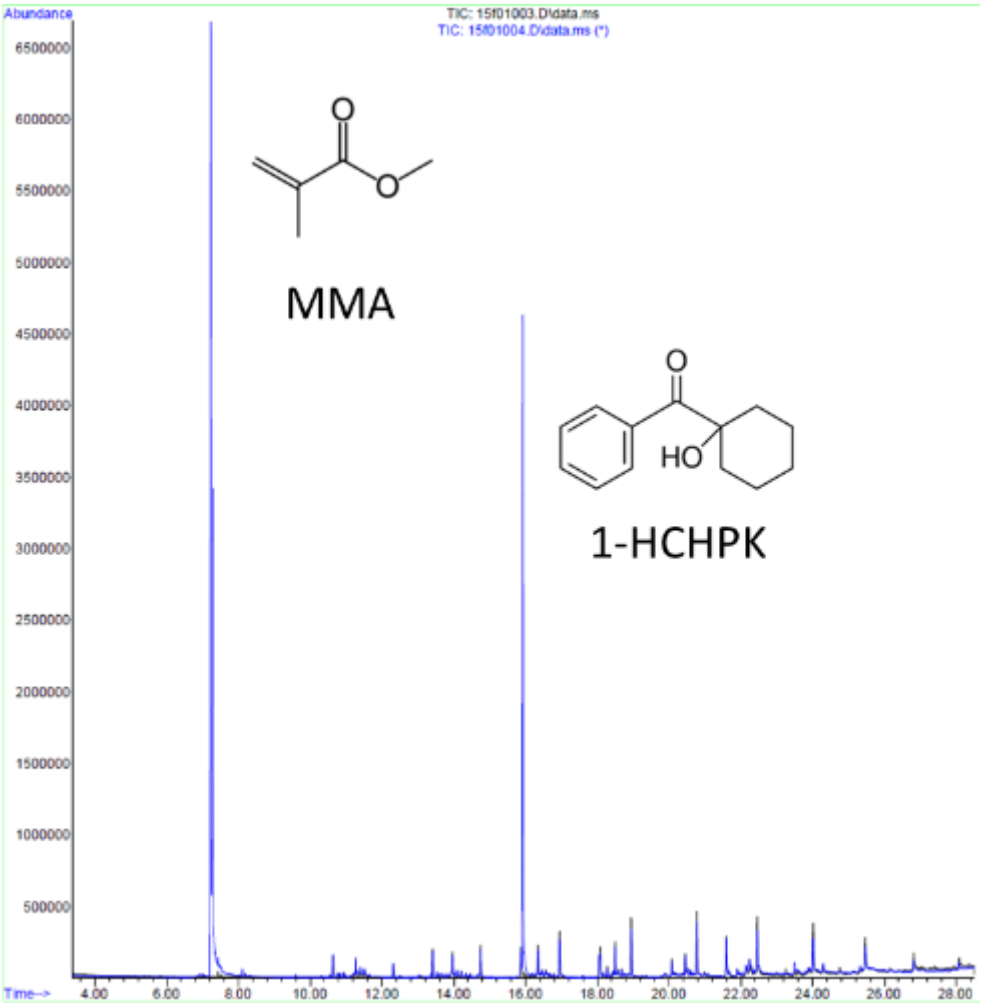


*Figure 4.5.1 Qualitative chemical analysis of Form Clear extract using GC-MS. Form Clear extracted water sample was further extracted into dichloromethane (DCM) for GC experiments. Two major peaks were detected. From the compound library, one compound was identified as methyl methacrylate (MMA) and the other one as 1-hydroxycyclohexyl phenyl ketone (1-HCHPK).*

During these experiments, I again used Form Clear polymer as an example. Before sampling, constituents existing in FC water extract were further extracted into a solvent dichloromethane (DCM). As a result of GC-MS analysis, apart from some small peaks that were actually the impurities from the solvent, two major peaks were found in the sample (Figure 4.5.1). The first one, with a retention time of 7.23 min, was identified as methyl methacrylate (MMA) and the second one, at a retention time of 15.92 min, was characterised as 1-hydroxycyclohexyl phenyl ketone (1-HCHPK) (Figure 4.5.1). The similarities of identified compounds compared with the compound library were 72% for MMA and 94% for 1-HCHPK.

Although the MMA is one of the major compounds in the raw material (unpolymerised resin), its MS identification score was only 72% which was not reliable enough to confirm its existence. Furthermore, I compared the unknown compound's MS spectrum with that of a standard MMA. As a result, their retention times were different under the same GC condition, and their MS spectra did not match each other. Based on this result, MMA was then excluded in the further study. Therefore, the actual compound responsible for this peak remained unknown. On the other hand, 1-HCHPK, with 94% similarity to the library, can be identified with high confidence. To confirm the presence of this compound in the sample, I again compared the retention times of the sample and the pure 1-HCHPK compound. Their retention times were found to match, as expected.

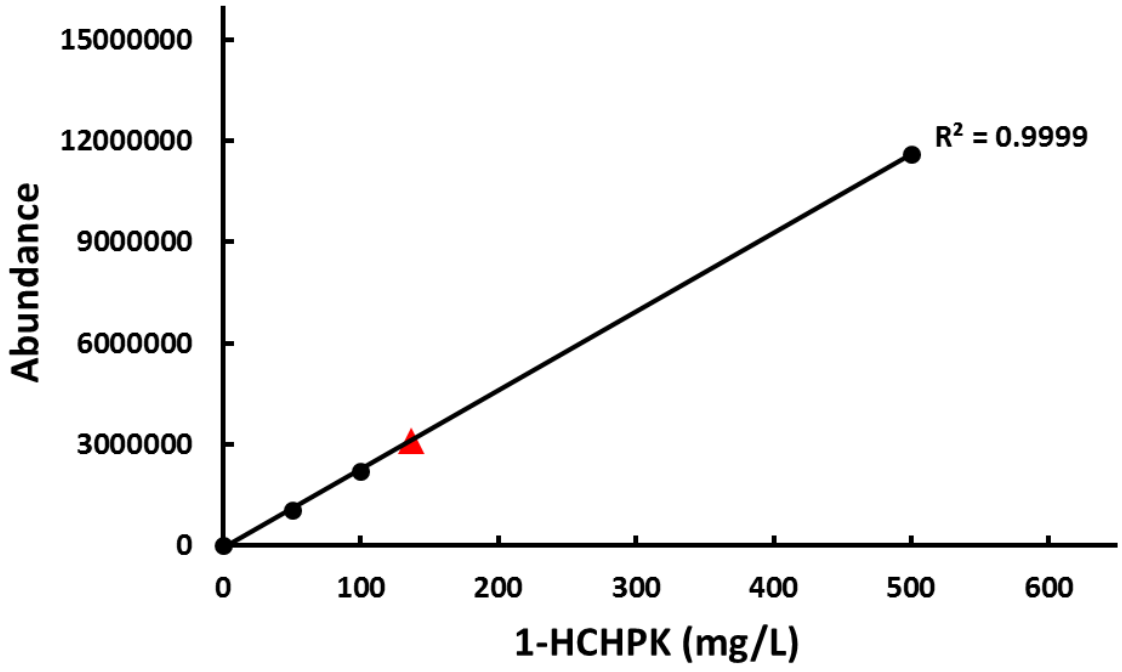


*Figure 4.5.2 Calibration curve of 1-hydroxycyclohexyl phenyl ketone (1-HCHPK) for GC quantitation. The concentration of the 1-HCHPK in the extract was determined to be 137 mg/L.*

Following up the qualitative analysis, a quantitation was performed to determine the concentration of 1-HCHPK in the water extract. A series of standards were prepared to generate a calibration curve. Excellent linearity was achieved, as shown in Figure 4.5.2. I then analysed the FC polymer extraction sample again and found the concentration of 1-HCHPK in the extract was 137 mg/L.

## 4.6 Identified compound verification

In the last section of the toxicity profiling, the toxicity of the identified compound (1-HCHPK) was tested to see if it was as effective as the original Form Clear extract. This is to verify whether the chemical analysis was properly performed. If the toxicity of 1-HCHPK was the same as the polymer extract, it could be concluded that the 1-HCHPK was the very compound that causes toxicity. Otherwise, it indicates that the chemical analysis was incomplete and that one or more unidentified toxicants existed in the sample, or that several chemicals have a synergetic effect on the overall toxicity.

### 4.6.1 Acute toxicity test

Toxicity verification biotests were performed on a few selected model organisms. In the mortality tests, lemna, daphnia, zebrafish embryos and larvae were chosen, identical to the Form Clear extract tests. Half-maximal response concentrations ($EC_{50}$) and toxicity curves of each species were calculated and plotted (Figure 4.6.1). For organisms that were not sensitive to the Form Clear extract, i.e. lemna and daphnia, they were also not very sensitive to 1-HCHPK. The maximal responses (100% mortality) were found at nearly 200 mg/L. Likewise, zebrafish embryo and larvae were very sensitive to the Form Clear extract, and they are also sensitive to 1-HCHPK. Toxicity curves for both embryo and larva were steep and the $EC_{50}$ value was around 45 mg/L.

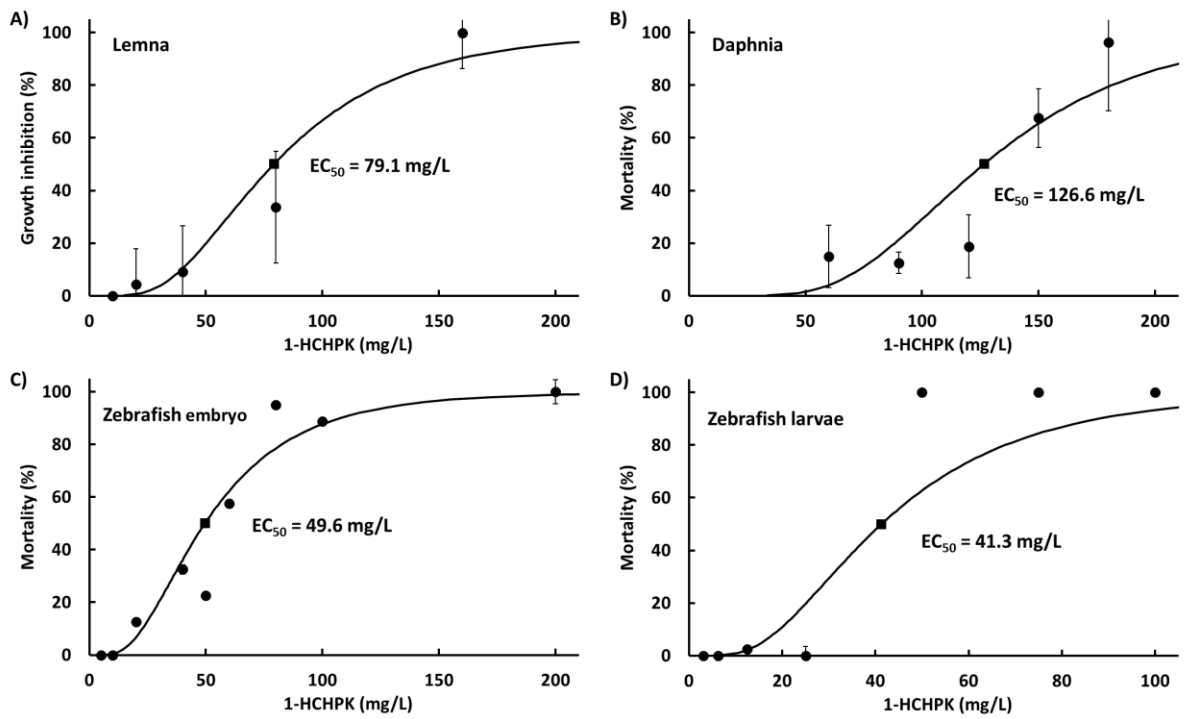


*Figure 4.6.1 Toxicity test of 1-HCHPK on model organisms. Toxicity curves depicted the response of each test organism to different concentrations of 1-HCHPK. Half-maximal response concentrations were calculated using the Toxrat software. Four model organisms A) lemna B) daphnia C) zebrafish embryo, and D) zebrafish larvae were used for the tests, same as the Form Clear extract tests, for comparison (Figure 4.4.1). The 1-HCHPK was indeed toxic to all test organisms at relatively low concentrations.*

### 4.6.2 Zebrafish larvae behaviour test

Zebrafish larvae behaviour tests were also performed for the toxicity verification test. Similarly, zebrafish larvae at 7 dpf were exposed to different concentrations of the toxicant for 64 min with a 4-min-light-4-min-dark cycle. Zebrafish larvae again displayed sensitive responses to the toxicant. Larval locomotor activity was significantly inhibited at 30 mg/L, in both light and dark environments (Figure 4.6.2 A&B). The habituation curve demonstrated an instantaneous response of larval fish to the toxicant exposure. Compared with the control, 1-HCHPK at 15 mg/L and 30 mg/L inhibited larvae mobility by more than 50%; the inhibition was close to 100% at higher concentrations (Figure 4.6.2). Comparing the percentage of change in travelled distance, I postulate that the toxicity threshold of toxic response is between 15 and 30 mg/L.

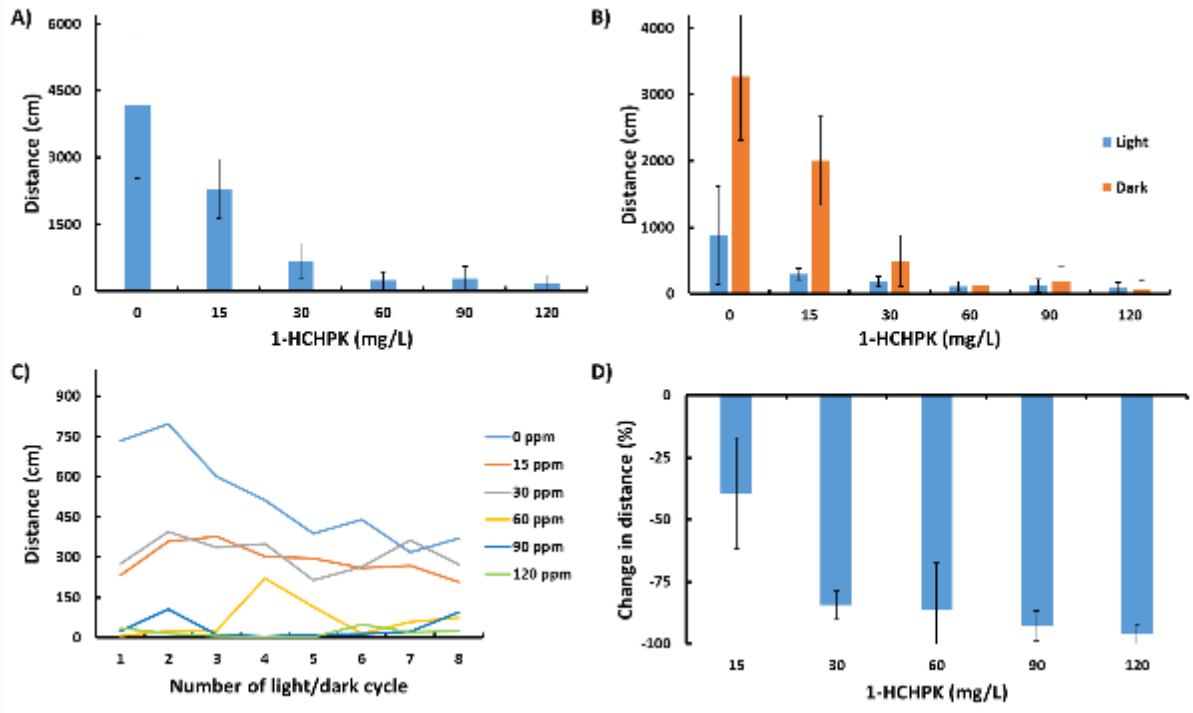


*Figure 4.6.2 Zebrafish larval behaviour test of 1-HCHPK. The behaviour tests were performed for 64 min with a 4-min-light-4-min-dark cycle. A) Total distance travelled by larvae in the test chamber. B) Comparison between the distances travelled during the light and the dark. C) Habituation curves of the larvae in every light/dark cycle. D) Percentage of change in total movement distance during the experiment.*

## 4.7 Summary and discussion

A recent revolution in high-definition 3D printing technologies has greatly facilitated fabrication of biomicrofluidic lab-on-a-chip devices. While fused deposition modelling (FDM), multi-jet moulding (MJM), and stereolithography (SLA) provide the capabilities to rapidly prototype miniaturised devices for small model organism culturing, the 3D printing material toxicity has not yet been extensively studied. In this chapter, a significant toxicity profiling was performed on a selection of widely used 3D printing materials by using biotests. In the first stage, the toxicity profiles of 7 selected materials were screened through the use of 8 model organisms. Secondly, I focused on one particular polymer, Form Clear. Standard bioassays were conducted according to OECD protocols and behavioural bioassays were carried out using zebrafish larvae. Thirdly, a chemical analysis was conducted to identify the compounds existing in the polymer extract and determine their

concentrations. Lastly, I verified the toxicity of the identified compound by performing biotests again. In summary, it was found that significant toxic effects were exhibited by a vast majority of MJM and SLA polymers, causing both lethal and sublethal (behaviour) effects on a range of aquatic organisms.

**Attribute of 1-HCHPK**

The toxic compound identified in the 3D printed polymer water extract was 1-HCHPK. It exists in the raw material (monomer resin) as a photo initiator which absorbs photons and initiates the polymerisation reaction. Photo initiators are being used in a broad range of plastic products, including food, biological and medical applications. In particular, Yamaji and co-workers found the presence of 1-HCHPK in the injection solution from polyethylene ampoules from three brands; and the MTT assay demonstrated that concentration of 1-HCHPK in the injection solution was cytotoxic[108]. This result is in line with the finding from this study.

**Limitation of the biotest**

Although eight model aquatic species, ranging from plants to vertebrates, were selected for the toxicity characterisation, it is probably still insufficient to understand the general toxic effects on the ecological system, especially after knowing that there is a huge variation among the response of all tested organisms to the toxic polymer extracts. For example, lemna was not very sensitive to DFC and FC polymers, but very sensitive to WXC and VJSL polymers; whereas amphipods were delicate with regard to DFC and FC polymers, but very resistant to WXC and VJSL polymers.

The number of tested polymers in this study was limited at seven, which was restricted by the funding, time, and printing facility availability. Provided that there are dozens of 3D printing materials on the market and new materials are being produced every year, the material coverage of the study was also inadequate. Therefore, caution is required for bioengineers who are willing to use MJM or SLA 3D printing to fabricate devices for biological utilities.

**Limitation of the chemical analysis**

In this study, chemical analysis was performed by GC-MS and two major peaks were detected from the extraction sample. One of the peaks hit the compound library and was successfully identified. However, the analysis had many limitations. To start with, GC-MS is only ideal for detecting polar and volatile (molecular weight < 300 Da) compounds. Any larger constituents existing in the sample would not be detected. Moreover, polymer extracted in water (aqueous phase) could not be injected into the instrument for direct analysis, they need to be extracted further into an organic solvent phase. Herein, I used dichloromethane (DCM) as the solvent because it is a widely used polar solvent. As water is also a polar solvent, any compounds dissolved in water theoretically should also dissolve in DCM. Nevertheless, there could have exceptions, resulting in the loss of some analytes. Furthermore, the further extraction was a liquid-liquid extraction. Analytes could easily be lost during this procedure, making the quantitation inaccurate. Finally, a better separation method like high pressure liquid chromatography (HPLC) could be utilised together with a more precise detection method like nuclear magnetic resonance (NMR) to identify trace compounds in the extract.

**Remediation and challenges**

Given the 3D printing principle and the material properties, I postulate that the toxicity came from unpolymerised residual resins left in the channels, and/or leachate from the surface of the polymerised material. In both cases, the biocompatibility issue could be remediated by iterative washing using fresh water and solvents. In the standard operating protocol, isopropanol was recommended to clean the residual resins through soaking and flushing for a short time. That was apparently not enough to wash away all the toxicants.

To prove this point, I have 3D printed a few single-well organism culture chambers (Figure 4.7.1). The size of the well was designed to be exactly same as the wells on a conventional 24-well microtitre plate. Zebrafish embryos were used as a test organism and cultured in the wells after a standard post-fabrication cleaning of the chamber. Not surprisingly, all embryos were died after 24 hours of exposure.

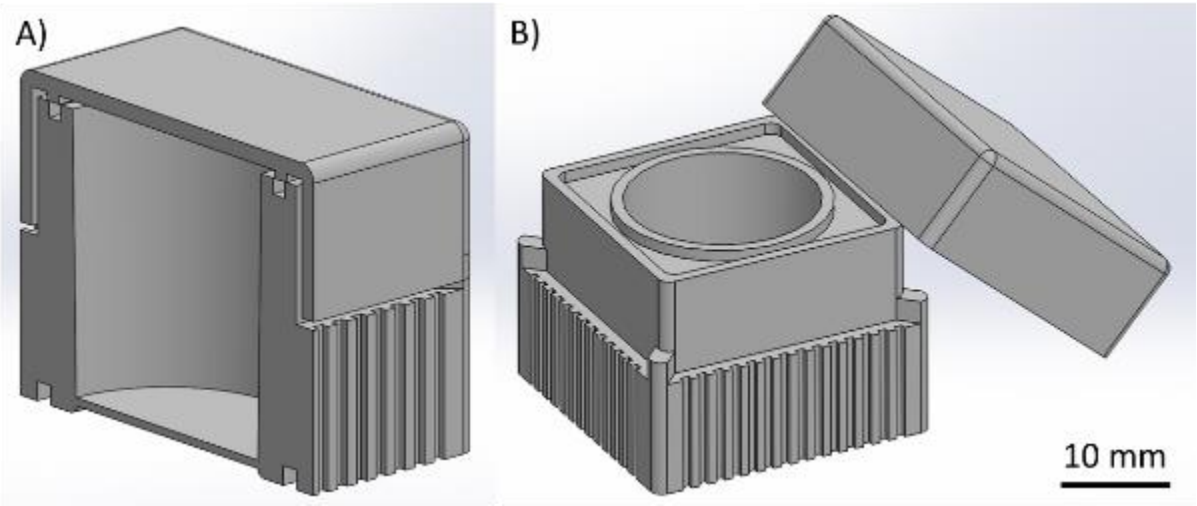


*Figure 4.7.1 CAD design of single-well organism culture chamber. (A) Cross-section view of the single well culture chamber. Note that the lid only loosely covered the chamber for air exchange. (B) Single well with the lid. The size of single-well was designed to be exactly same as the wells on conventional 24-well microtitre plate.*

In the test of washing, I soaked the 3D printed chip devices in 99% isopropanol for 24 hours each wash (Figure 4.7.2). After 24 hours of soaking, the zebrafish embryo viability increased dramatically from 0% to 75% in the devices fabricated by Dreve Fototec Clear resin. The toxicity was completely gone after three wash interactions and no further toxicants were released.

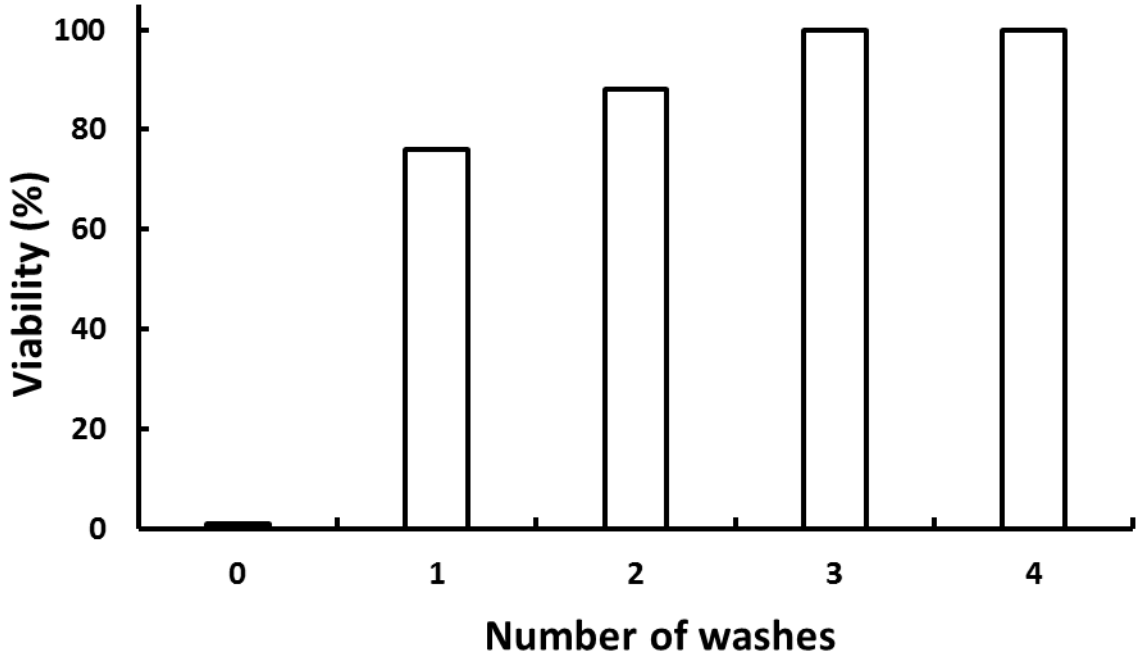


*Figure 4.7.2 Viability of zebrafish embryos cultured on prototypes made of Dreve FotoTec polymer resin at 72 hour post fertilisation (hpf).*

However, this remediation method has its drawbacks. Overly soaking the printed parts in isopropanol will soften the 3D printed material and damage delicate 3D printed structures, such as small channels and pillars. Thus, it is not ideal for lab-on-a-chip fabrication purposes. In experiments using other solvents, 99% ethanol increased the washing efficiency, but it caused more damage and the Watershed XC11122 material even completely dissolved after 24 hours.

Apart from washing, some other remediation methods was attempted including subsequent UV exposure of printed objects, plasma treatment of the surface of printed objects, and autoclave of the polymer extract. However, none of the methods were able to address the issue. Thus, to fabricate a biocompatible microfluidic lab-on-a-chip device for zebrafish embryos, a new manufacturing approach needs to be explored. This is demonstrated in the next chapter.

# 5 ZebraTox Chip: A lab-on-a-chip device for automated fish embryo toxicity assays

## 5.1 Introduction

This chapter describes the design, validation, and application of a pioneering lab-on-a-chip technology for automated zebrafish embryo toxicity bioassays utilised in drug discovery and ecotoxicology. The main objective was to develop a biocompatible and miniaturised embryo trapping array to load, isolate, and immobilise single embryos in a flow through environment. The chip device was made of optically transparent materials with no structural obstacles for a broad adaption of imaging systems and was suitable for high-throughput imaging. The microfluidic module facilitated continuous medium exchange and/or toxicant delivery under microperfusion during the period of embryo development.

To validate the microfluidic system, computational fluid dynamics simulations were performed, followed by experimental validations. For a proof-of-concept drug delivery test, two antiangiogenic compounds were tested on transgenic zebrafish embryos. To investigate the applicability of the microfluidic fish embryo toxicity test (µFET) in ecotoxicity testing, six reference toxicants were tested as model chemical stressors. I provide evidence that miniaturised µFET analysis opens a brand new alternative for inexpensive automation in aquatic ecotoxicity protocols. For innovative applications, I demonstrate that microfluidic devices with immobilised embryos offer great convenience for embryonic activity analysis in a flow through environment. Moreover, by integrating oxygen sensors onto the chip, a new function for the device was explored for visualised fish embryo metabolic analysis. Furthermore, I demonstrate that by expanding the embryo trapping array into a high density plate-like device, it can fulfil the requirement of high-throughput screening.

## 5.2 Design of the linear embryo trapping array

Zebrafish embryos are protected by an elastic spherical chorion with a diameter of 1 mm to 1.2 mm. They also bear a substantial amount of mass, 850 µg to 1050 µg, that leads to rapid gravitational-induced sedimentation and high translational and rotational momentum when moving. These features were initially considered as obstacles for manipulation in a

microfluidic system, but in this study, these very characteristics were utilised for embryo loading and immobilisation.

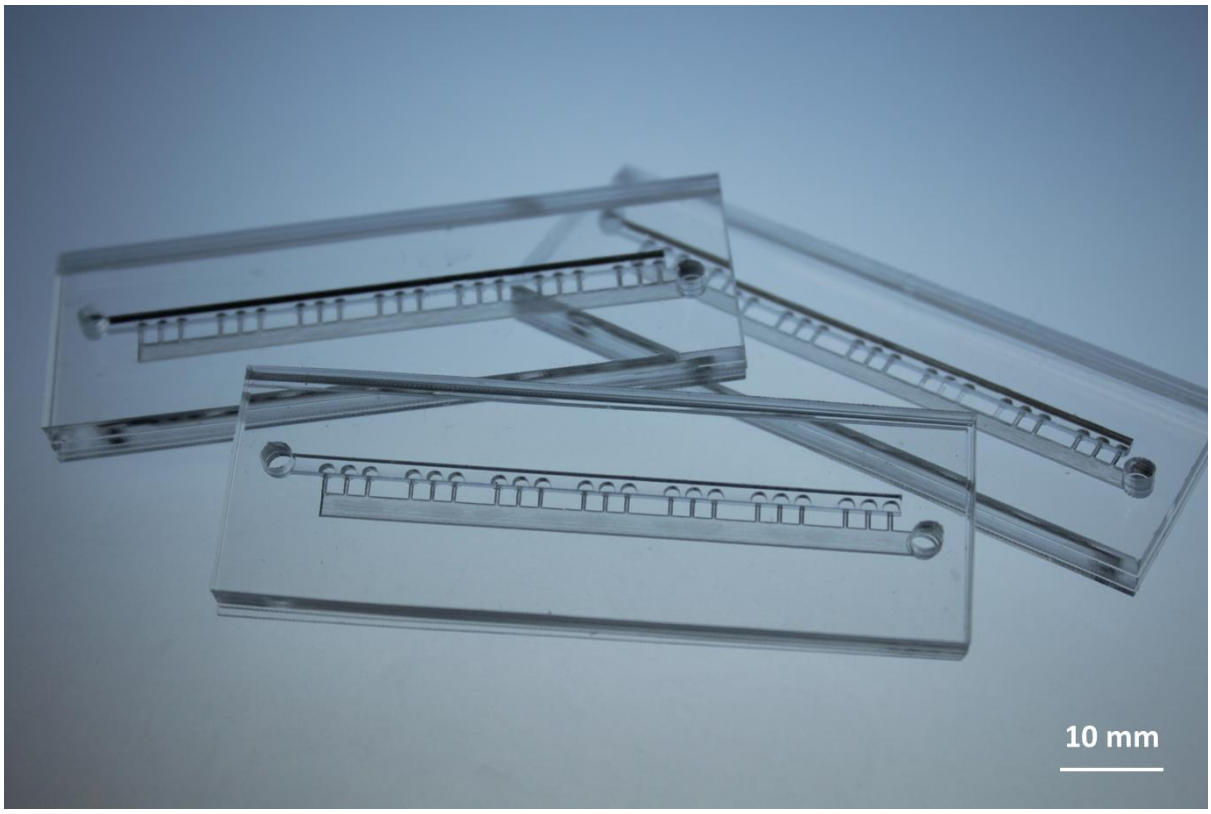


*Figure 5.2.1 Overview of miniaturised zebrafish embryo trapping arrays. The chip devices are made of optically transparent and biocompatible thermoplastic poly(methyl methacrylate) (PMMA). The size of the chips is identical to standard microscope glass slides.*

The size of the chip was designed to be to identical to standard microscope glass slides (75 mm x 25 mm, Figure 5.2.1). Each chip contained a microfluidic system consisting of five major components: an inlet port, a loading channel, an embryo array, a suction manifold, and an outlet port (Figure 5.2.2). The 21 embryos traps were clustered into 7 groups of three traps. Each group of three traps is positioned within a single well from a 96 well plate for high-throughput imaging (red dotted circle, Figure 5.2.2).

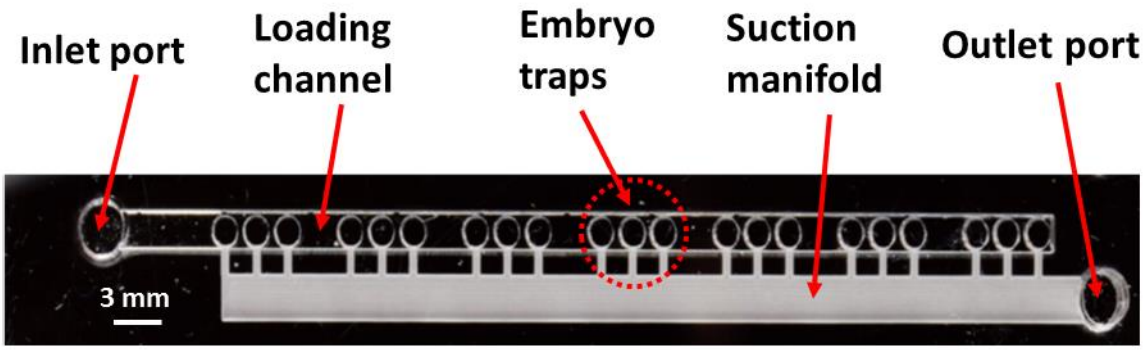


*Figure 5.2.2 Microfluidic manifold on the chip device. All main modules depicted. Embryo traps were clustered in seven groups. Each group consisted of three traps and featured a total circumference and distribution equal to the wells on standard 96-well microtitre plate. Published in Ref 109, Reprinted with permission from © 2015 American Chemical Society.*

The chip device comprised of five PMMA layers (Figure 5.2.3), with a total thickness of 7.3 mm. The top layer contained the inlet and the outlet of the chip; both of which were circular cuts with a diameter of 2.9 mm. The second layer held a loading channel (68 mm × 1.8 mm × 2.0 mm). This channel is not only for embryo loading, but also for toxicant delivery and post-culture embryo recovery. The third layer carried the top half of 21 embryo traps (φ 1.5mm × 0.7 mm); the fourth layer contain the bottom half of 21 embryo traps (φ 1.5mm × 0.5 mm) and the suction manifold. The suction manifold included a main suction channel (63 mm × 2.5 mm × 0.5 mm) and interconnection channels (0.3 mm × 1.6 mm × 0.5 mm) linking each embryo trap and the main suction channel. A suction force was created from the small channels to help embryo docking, immobilisation, and toxicant perfusion. To support unobstructed imaging capabilities from both upright and inverted cameras, the suction manifold was located on the side panel of the traps. The bottom layer was simply a sealing of the entire fluidic domain.

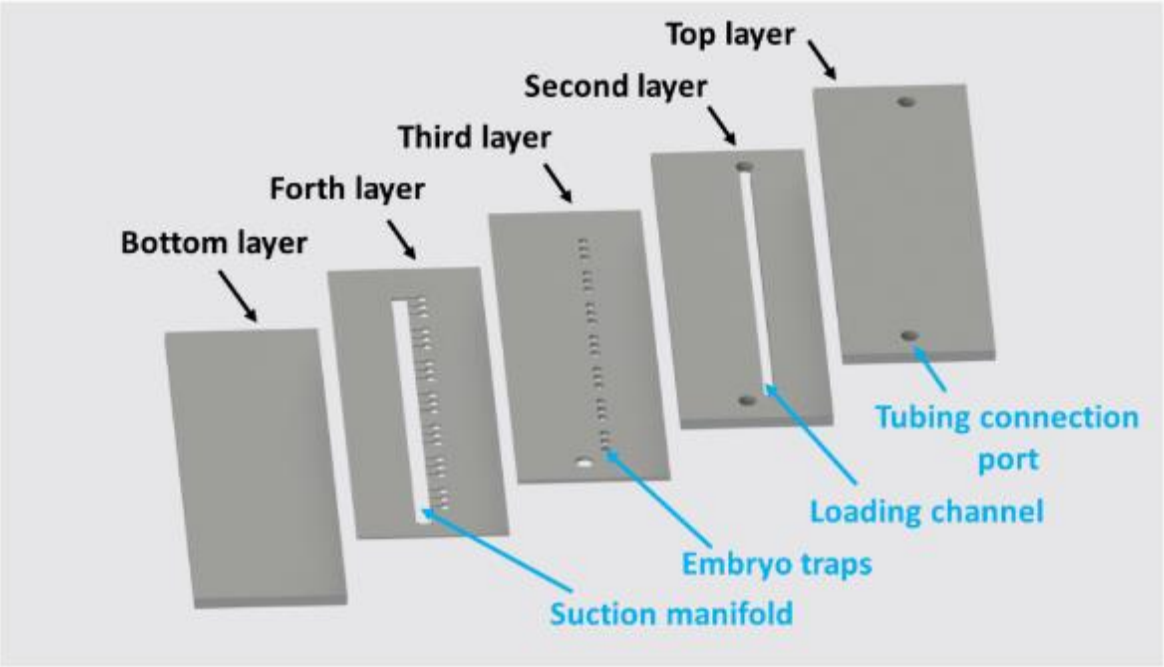


*Figure 5.2.3 Exploded view of the chip device. The chip comprised of 5 layers. The functions of each layer is depicted. Each layer was fabricated separately on a laser cutting machine. The five layers were then thermally bonded together in a fan assisted oven.*

After bonding all five layers together, a fluidic domain was then created as depicted in Figure 5.2.4. The total volume of the fluidic domain was 324 µL and the total surface area was 1012 $mm^2$.

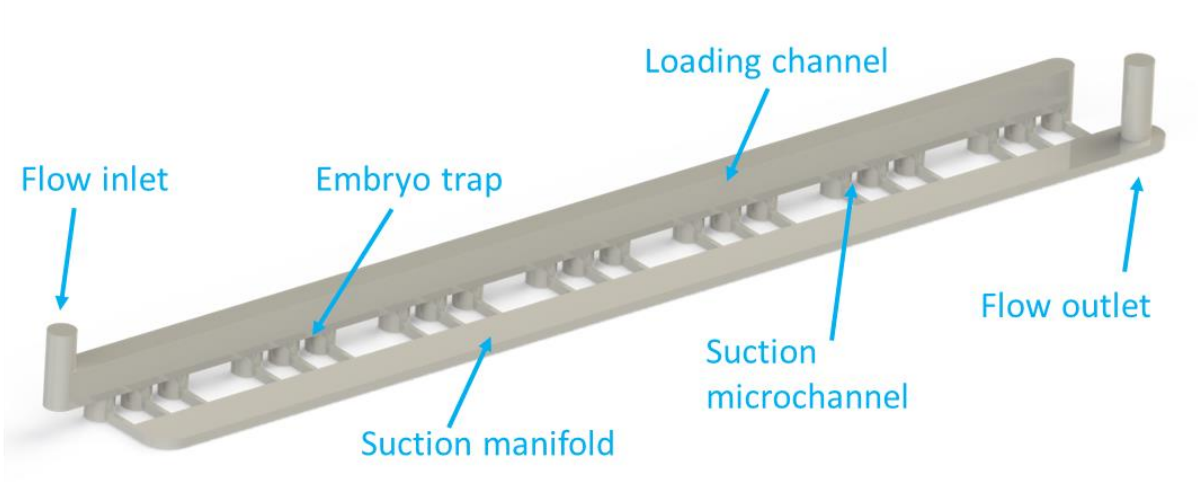


*Figure 5.2.4 CAD rendering of the fluidic domain of the chip device. The fluidic domain is the hollow part of the chip device. All features are depicted.*

The microfluidic system was designed for automatically trapping embryos with the one-embryo-in-one-trap concept. The trapping principle exploited both gravitational-induced sedimentation of embryos and low-pressure suction at the bottom of the device (Figure 5.2.5). When loading, a low pressure suction force from a peristaltic pump was applied constantly at the outlet of the chip. Embryos were first aspirated one by one at certain intervals from a reservoir to the inlet of the chip. As the embryos enter the chip, they were pulled to move forward along the loading channel because of the hydrodynamic force from the suction channel. When the embryos flowed over the embryo trap, they were deflected by the combination of gravitational force and suction force and hence sank into the embryo trap. As the docked trapped embryos were immobilised, they behaved as spacers occupying the trap, allowing subsequent embryos to roll freely across the trapped embryos and towards the next available trap. The process was repeated until all traps were occupied and the loading process was discontinued. Toxicant solutions could then be introduced via the flow inlet.

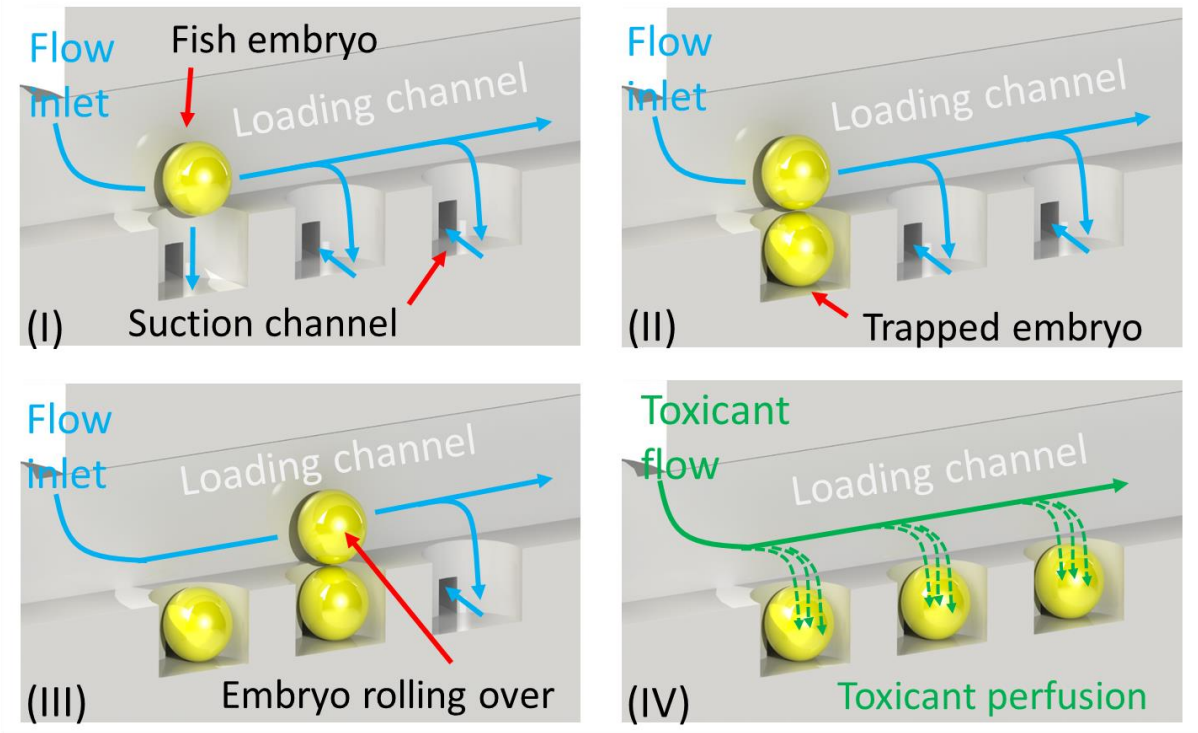


*Figure 5.2.5 3D cartoon depicting the principle of embryo trapping and immobilising on the chip. i) The system took advantage of combined gravitational-induced sedimentation and low pressure suction at the bottom of the embryo trap. Embryos fall into the embryo trap as they pass over. ii) and iii) Trapped embryos are immobilised, acting as spacers for following embryos to roll over the*

*occupied traps and toward next available trap. iv) After all embryos are trapped, drugs or toxicant can be introduced for on-chip bioassays. Published in Ref 109. Reprinted with permission from © 2015 American Chemical Society.*

In the case that one extra embryo is loaded into the microfluidic device, the embryo will stay in the end of the loading channel without being immobilised. However, this embryo will not interfere the embryo on-chip culture, nor the imaging of the embryos.

## 5.3 Simulation and validation

To predict the embryo trapping performance, the mass transfer uniformity, and the on-chip culture feasibility, computational fluid dynamics (CFD) simulations were performed followed by experimental validations.

### 5.3.1 Embryo trapping

The simulated fluidic streamlines demonstrated the flow velocities at different regions of the fluidic domain under a constant flow rate of 400 µL/min. The flow velocity was uniform at 4.3 mm/s along the embryo loading channel up to trap number 18. At the fluidic region of the last three embryo traps the flow velocity plummeted to nearly zero though the flow velocity elevated to 10 mm/s at the suction microchannel (Figure 5.3.1). This indicated that the embryo trapping could be difficult in the last three traps.

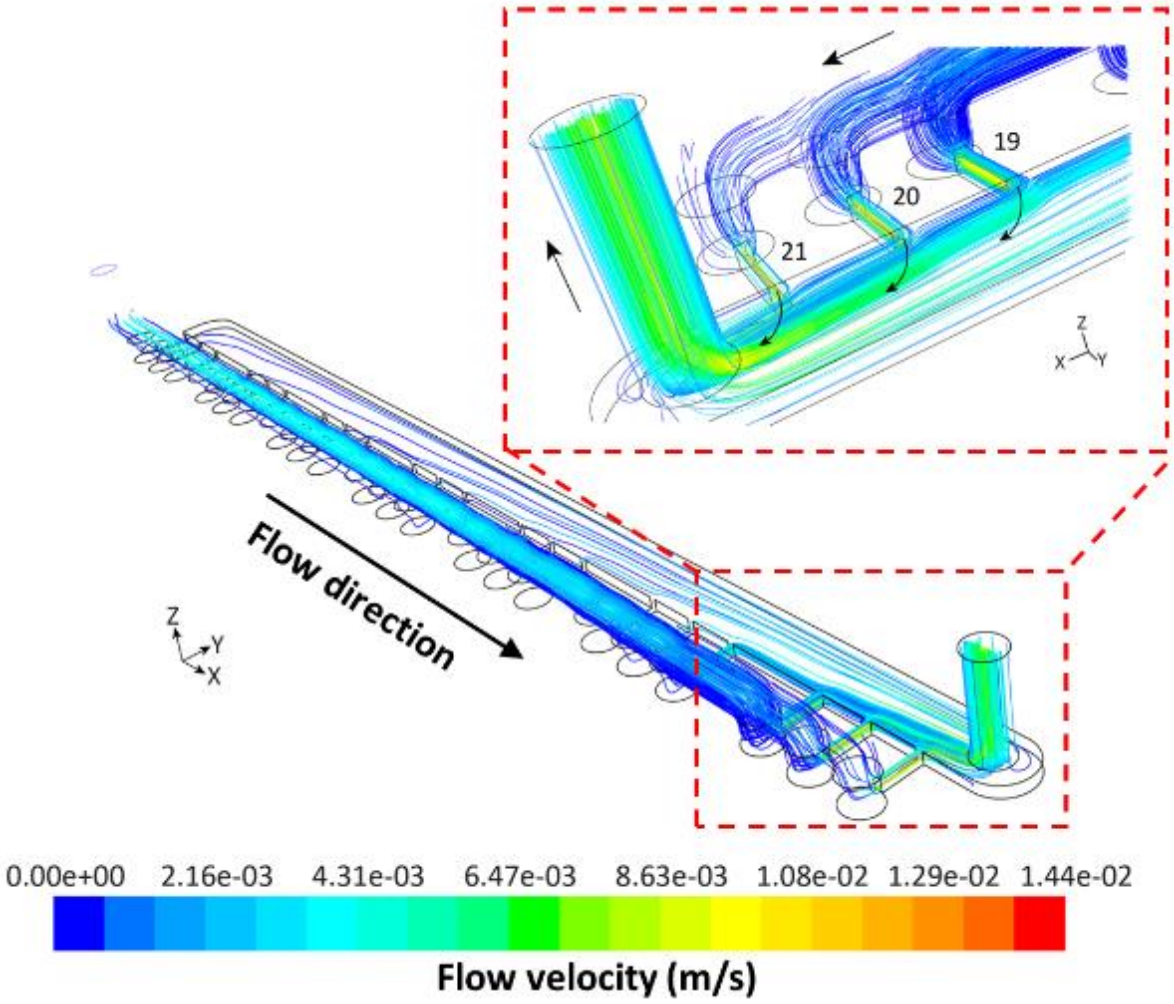


*Figure 5.3.1 Computational fluid dynamics (CFD) simulation predicting streamlines when flowing across the trapping array. Flow trajectory and the velocity along the fluidic domain are depicted. At the flow rate of 400 µL/min, most of main loading channel achieved a flow velocity of around 4 mm/s. Note that the flow velocity is dramatically decreases towards the last three embryo traps (trap number 19 to 21). Published in Ref 109. Reprinted with permission from © 2015 American Chemical Society.*

The Lagrangian particle tracking (LPT) model was applied to predict the embryo trapping trajectory. This model is often used to analyse small particles, such as dust, aerosol, or small bubbles, but here this model was used to predict zebrafish embryo behaviour under hydrodynamic and sedimentation forces. Simulated embryos were set as rigid spherical balls with a diameter of 1 mm, which is slightly smaller than the depth of the embryo trap (1.2 mm). As a result, the simulation indicated that when passing through the occupied wells embryos would roll on top of the trapped embryos, bounce, and continue rolling until they

dock into the next available trap (Figure 5.3.2). On top of that, LPT also predicted a sequential trapping of embryos.

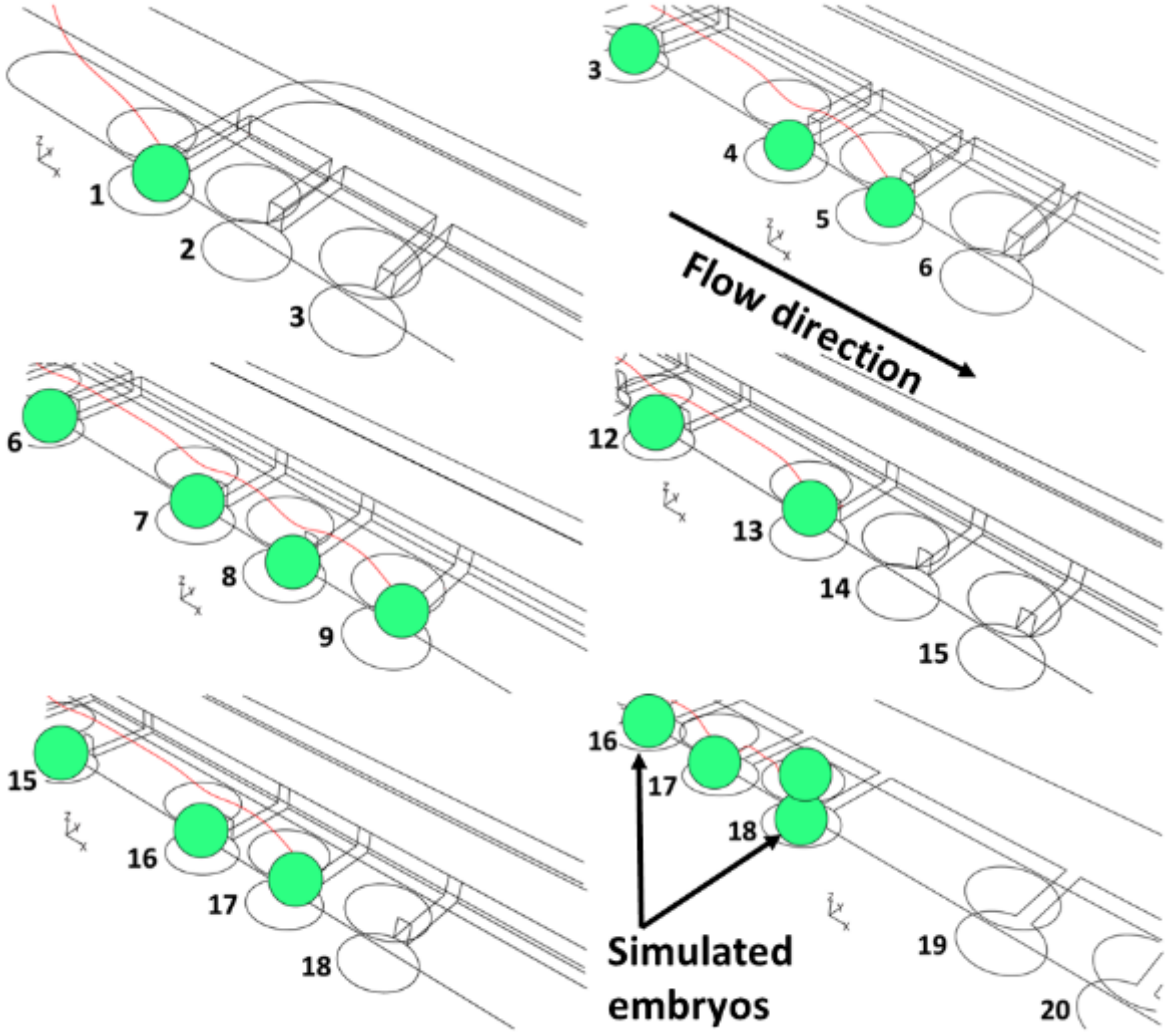


*Figure 5.3.2 Implementation of Lagrangian particle tracking simulation model to predict the trapping characteristics of the design. Embryos traps were numbered in sequence from the flow inlet. Embryo The red line depicts the trajectory of embryo movement along the loading channel. Published in Ref 109. Reprinted with permission from © 2015 American Chemical Society.*

In experimental validation, zebrafish embryo at 6 hour post fertilisation (hpf) were first stained with trypan blue for a better observation. To begin with, the chip device was primed with 99% ethanol to eliminate any visible air bubbles, followed by a thorough flushing out with embryo medium E3. Embryos were then aspirated from a reservoir into the chip one after another at an interval of 15 seconds. Although the embryo trapping did not occur in

the sequence predicted by the simulation, it indeed achieved 100% of trapping efficiency (Figure 5.3.3).

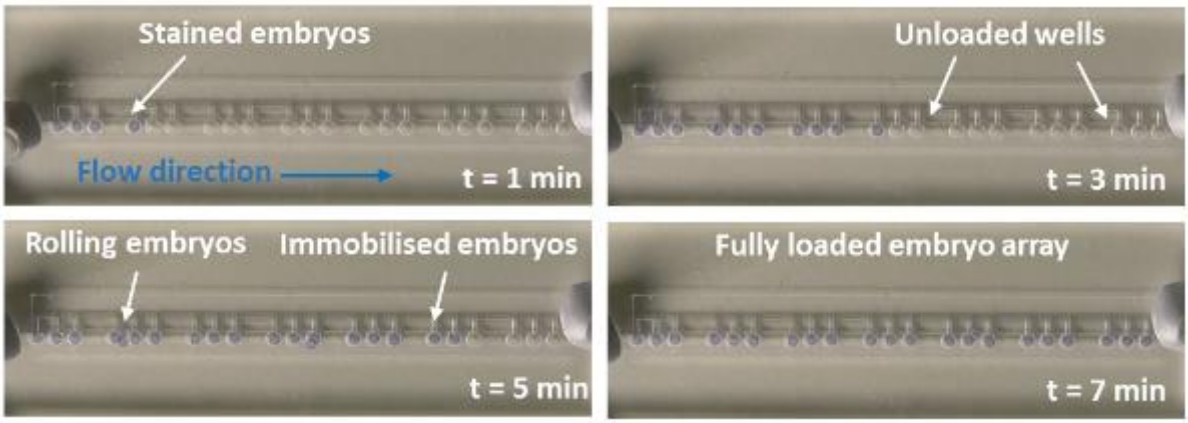


*Figure 5.3.3 Experimental validation of the particle tracking model. Embryos were stained with Trypan blue to highlight the embryo locations. The full loading took approximately 7 minutes depending on the flow rate and embryos aspiration gap. Note the excellent agreement of experimental embryo docking as compared with CFD simulations. Published in Ref 109. Adapted with permission from © 2015 American Chemical Society.*

The embryo trapping efficiency was tested under different flow rates (Figure 5.3.4). At low flow rates, the hydrodynamic force was insufficient to lead embryos through the channel due to the substantial mass of the embryos (sedimentation force >> hydrodynamic force). In contrast, when the flow rates were too high, all the embryos skipped the traps and were flushed into the end the loading channel (sedimentation force << hydrodynamic force). Eventually, an optimal flow rate of 400 µL/min was found to constantly achieve 100% trapping efficiency.

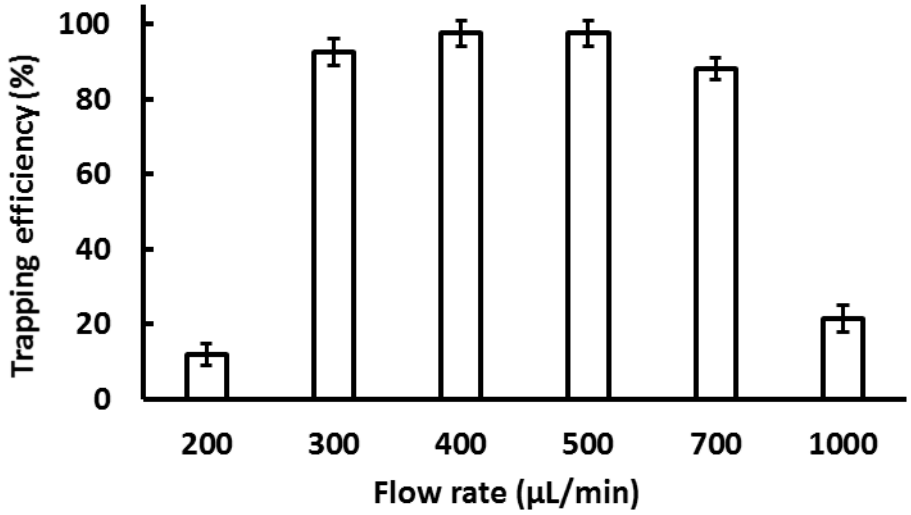


*Figure 5.3.4 Trapping efficiency at various flow rates (n ≥ 4).100% trapping efficiency can be achieved at flow rates between 300 and 700 µL/min. Trapping efficiency deteriorated at higher flow rates. This phenomenon was attributed to excessive velocity and momentum of the embryos that could not be compensated for by the suction manifold when trapping. Published in Ref 109. Reprinted with permission from © 2015 American Chemical Society.*

This chip device also allowed recovery of immobilised embryos. In practice, the chip can be turned upside down to release trapped embryo into the loading channel. A positive pressure could then be applied from the suction port to push all the embryo to leave the chip device.

### 5.3.2 Mass transfer

**Mass transfer on empty chip**

Constant delivery of toxicants with a uniform distribution to the immobilised zebrafish embryos is essential for long-term microperfusion studies in drug discovery and ecotoxicology. CFD simulations were performed to predict the uniformity of the mass transfer across the chip device (Figure 5.3.5). Trypan blue was set as the simulated dye. The simulation indicated that the medium exchange rate reached 100% in the embryo traps after 60 seconds of perfusion at a flow rate of 400 µL/min. It also predicted a unique perfusion pattern in the suction manifold, as the medium exchange rate at some part of the suction channel was very slow.

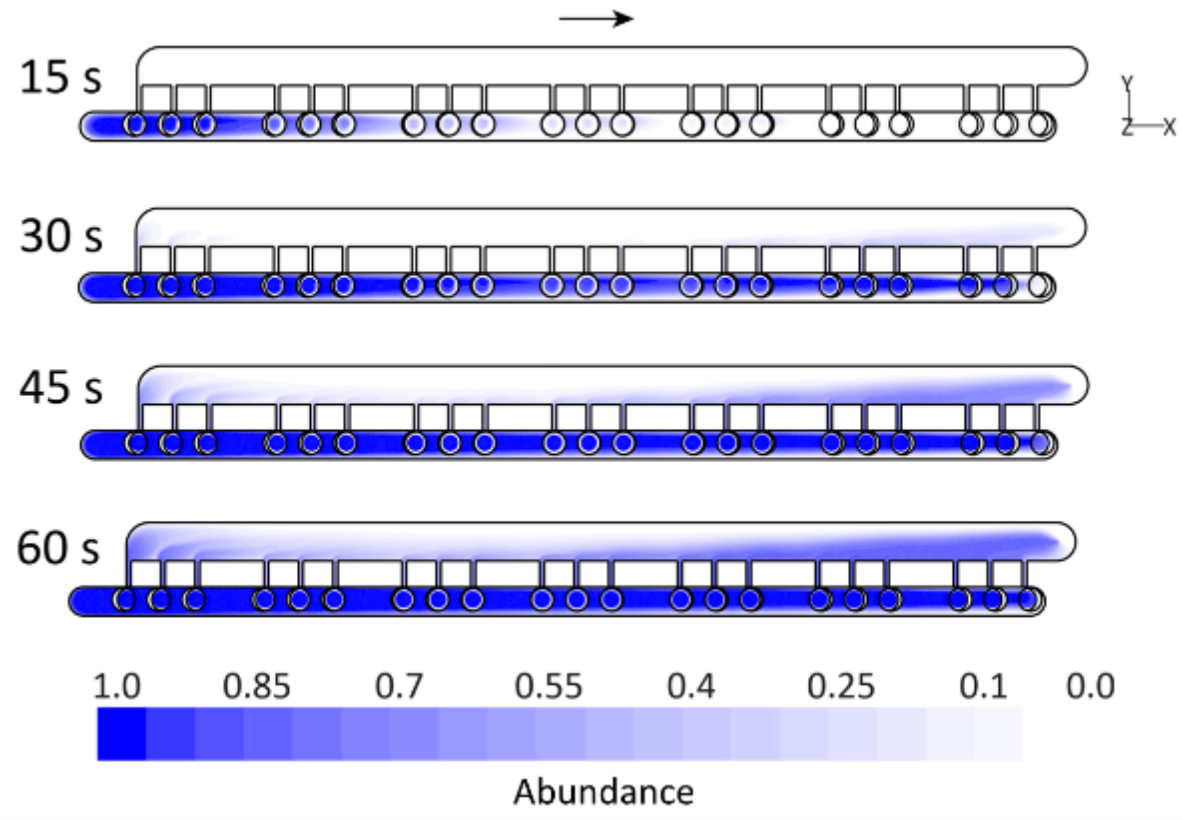


*Figure 5.3.5 CFD simulation predicted uniformity of mass transfer across the empty array. Trypan blue was chosen as a modelling compound. After 60 seconds of continuous perfusion at the flow rate of 400 µL/min, the medium exchange rate in the main loading channel reached 100%. Note the unique fluidic pattern in the suction manifold after 60 seconds of perfusion.*

During experimental validation, the chip was again primed with ethanol to eliminate air bubbles followed by flushing with embryo medium E3. Afterwards, 0.04% Trypan blue solution was perfused from the loading port at a flow rate of 400 µL/min. Images were taken every 15 seconds as a comparison of the simulation. In spite of a few seconds delay in medium exchange, the medium exchange rate was fast and the microperfusion pattern was in excellent agreement with the CFD prediction (Figure 5.3.6).

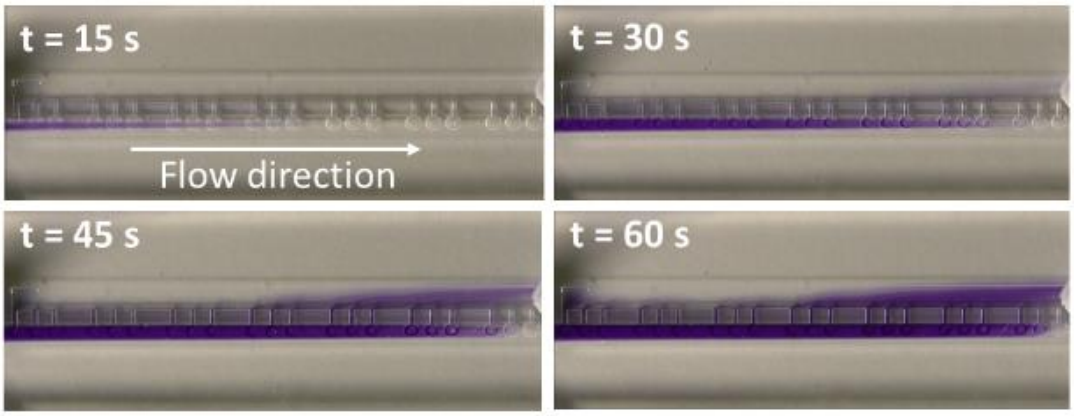


*Figure 5.3.6 Experimental validation of mass transfer in the empty chip. Chip was perfused with a 0.04% Trypan Blue at a volumetric flow rate of 400 µL/min. Images were taken at 15, 30, 45, and 60 seconds of perfusion. After 60 seconds of perfusion, 95% of the embryo traps achieved full medium exchange with trypan blue. The exception was the very last embryo trap. Note the fluidic pattern was identical between the simulation and the experiment.*

**Mass transfer on loaded chip**

The CFD simulations were also performed to predict the perfusion uniformity with docked embryos (Figure 5.3.7). Here, simulated embryos were set as rigid spherical balls with a 1 mm diameter. Trypan blue was used as a simulated solution perfusing at 400 µL/min. The prediction indicated that the medium exchange rate was rather fast that after 60 seconds, the surface of the embryos achieved more than 90% of medium exchange. It is worth noting that the upper hemisphere received more medium exchange than the lower hemisphere due to the suction microchannels locating in the bottom of the embryo traps. However, the exchange rate could still achieve 100% over the time.

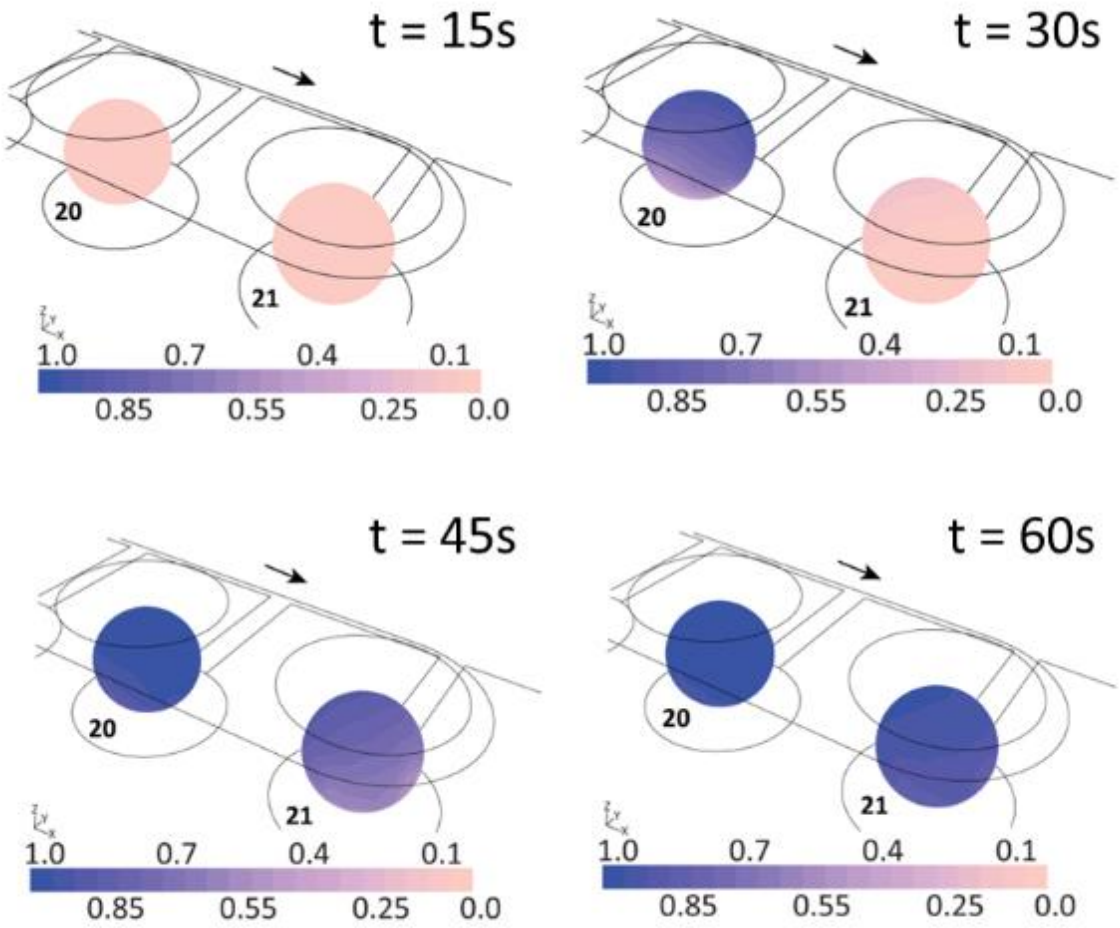


*Figure 5.3.7 Time-resolved CFD simulations of toxicant perfusion in the chip with fully loaded fish embryos, detailing traps numbered 20 and 21. Trypan blue was predicted to cover most of the embryo surface after 60 seconds of perfusion at flow rate of 400 µL/min.*

In experimental validation, zebrafish embryos at 6 hpf were loaded onto the chip device, followed by a microperfusion of 0.04% Trypan blue solution for 5 minutes. The Trypan blue was then washed out by embryo medium E3. As a result, all loaded embryos were stained by the blue dye with a relatively uniform intensity across all the traps (Figure 5.3.8). In some embryo trap however, higher staining intensities were observed because of variation in the size in the embryo population.

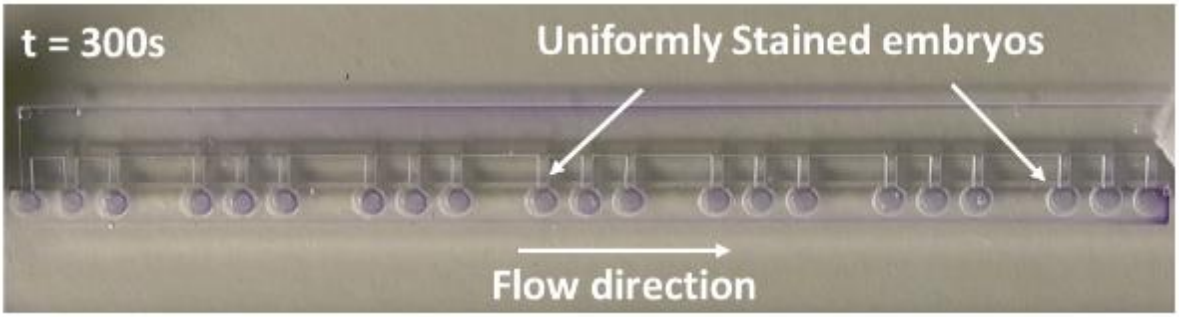


*Figure 5.3.8 Experimental validation of toxicant perfusion on the fully loaded chip device. Trypan Blue was perfused in the chip device at a flow rate of 400 µL/min for 300 seconds, followed by a washout with E3 embryo medium. Most trapped embryos remained in the traps and show uniform labelling of embryos across each cluster.*

### 5.3.3 Embryo on-chip culture

In the next stage, the biocompatibility of the chip microenvironment for embryo culture was evaluated under a continuous flow over an extended period of time. CFD was performed to predict the water pressure and shear stress exerting on the surface of immobilised embryos. Here, simulated embryos were set as rigid spheres with a 1 mm diameter sitting in the bottom of the embryo traps under a continuous flow rate of 400 µL/min.

As shown by calculations, the water pressure was evenly exerted onto the embryos, with a maximum pressure of 4.1 Pa at the top section and a minimum pressure of 3.5 Pa at the bottom section (Figure 5.3.9-A). The water pressure was mainly attributed to the flow from the loading channel, and was slightly compensated for by the flow from the suction microchannel. In contrast, the shear stress exerting on the embryos originated from the suction microchannel (Figure 5.3.9-B). The section directly facing the suction microchannel received a maximal shear stress of 0.1 Pa.

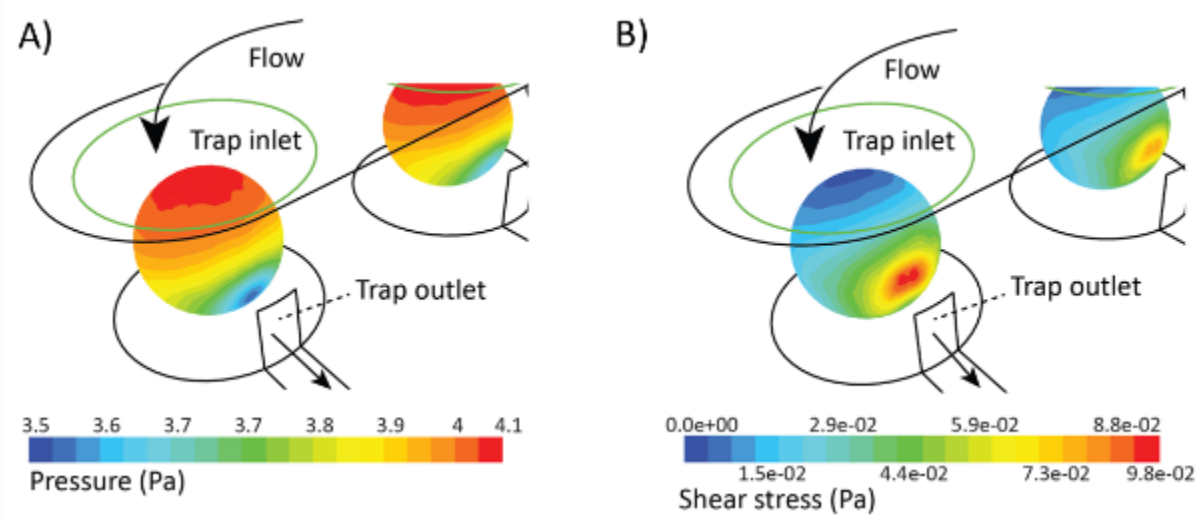


*Figure 5.3.9 CFD simulation of embryo microperfusion culture on the chip at flow rate of 400 µL/min A) Contours of water pressure exerted on immobilised embryos inside the trap. B) Contours of shear stress exerted on immobilised embryos inside the trap. Calculations were based on the embryos from the last two embryo traps. Published in Ref 109. Reprinted with permission from © 2015 American Chemical Society.*

It is rather difficult to physically measure water pressure and shear stress exerted on the zebrafish embryos in the chip microenvironment. Hence, experimental validation was performed by a long-term culture of zebrafish embryos in a microperfusion condition from a very early developmental stage until 48 hours post fertilisation (hpf) (Figure 5.3.10). Developing embryos reached all developmental staging criteria, including somite formation (12 hpf), eye buds formation (18 hpf), tail detachment (24 hpf), and pigmentation (48 hpf).

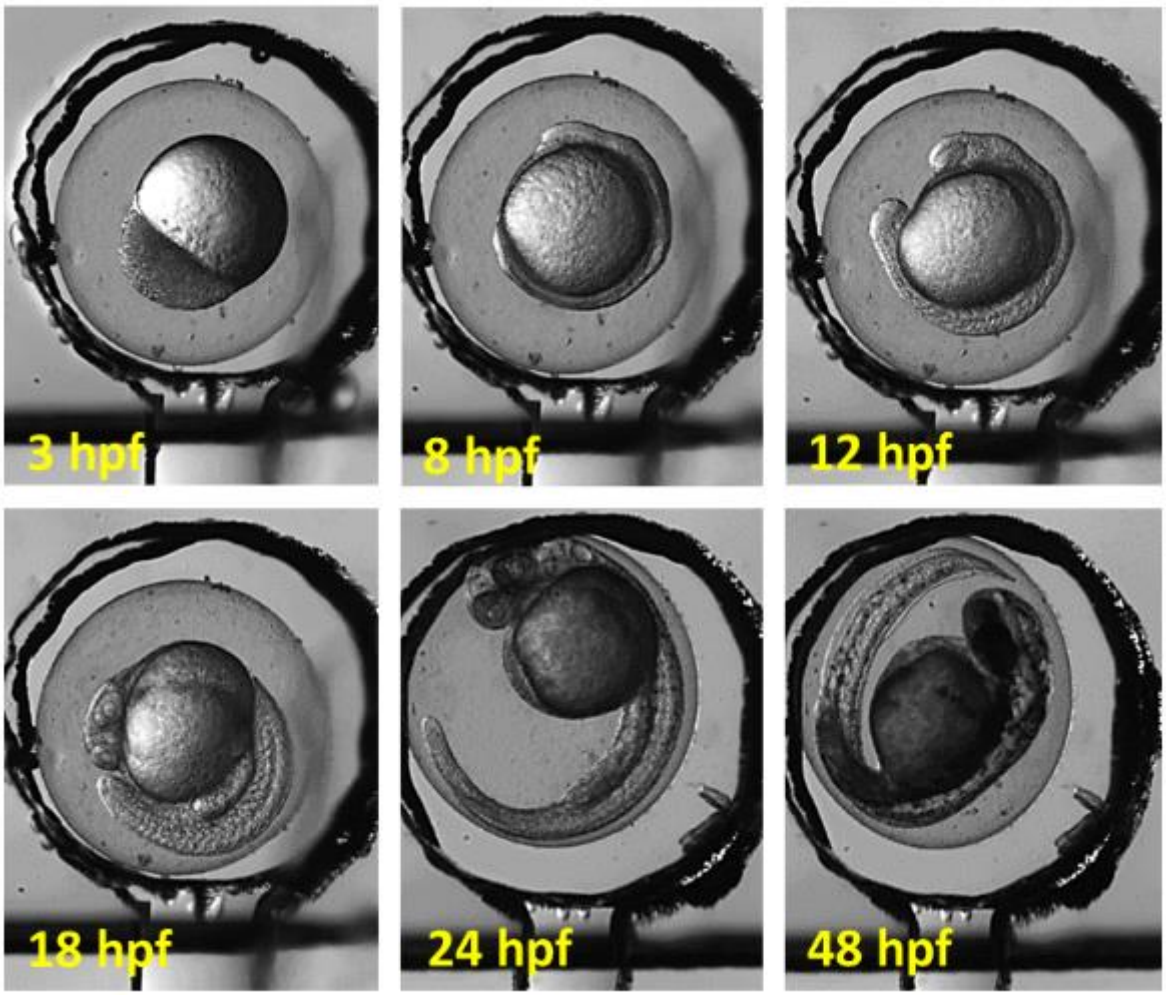


*Figure 5.3.10 Time-lapse images of developing zebrafish embryos over the duration of the experiment. Embryos were loaded on a chip at the flow rate of 400 µL/min, followed by on-chip culture under the same flow rate for up to 48 hours. Published in Ref 109. Reprinted with permission from © 2015 American Chemical Society.*

A normal and uniform development of embryos was observed across the living embryo array. Furthermore, a cumulative embryo survival test was conducted at different flow rates ranging from 0 to 1000 µL/min. Embryo survival rate during microperfusion experiments were statistically comparable with static Petri dish control experiments, except for those with extremely low flow rates (Figure 5.3.11). The decreased survival rates were due to the oxygen depletion inside the chip when the flow rate was too low to carry sufficient oxygen for the embryo in a chip that is made of gas non-permeable PMMA.

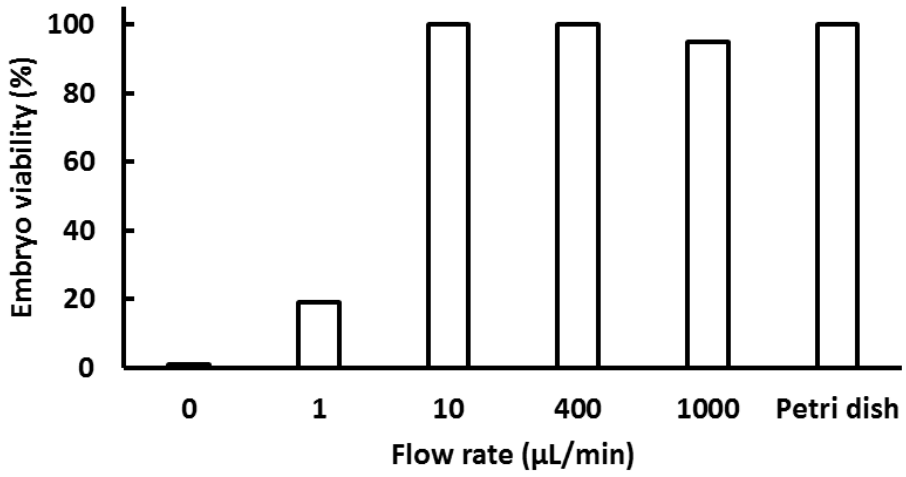


*Figure 5.3.11 Cumulative survival (72 hours) of zebrafish embryos perfused on chip at varying volumetric flow rates. Embryo viability on microperfusion experiments were comparable with static experiment on Petri dish. Low viability occurred in low flow rate experiments due to the oxygen depletion. Published in Ref 109. Reprinted with permission from © 2015 American Chemical Society.*

## 5.4 Imaging from the chip

The accessibility for imaging is one of the most important considerations when design lab-on-a-chip devices because, currently, the zebrafish embryo assays rely greatly on microscopy. In this regard, the chip device was designed to facilitate both upright and inverted imaging systems by assigning all fluidic channels to positions with no obstacles for imaging (Figure 5.4.1). The thickness of the chip device was also minimised for high magnification imaging. In particular, the minimum distance from the lens and the embryo was 1 mm from the bottom and 5 mm from the top. Hence the imaging from the bottom of the chip was preferred.

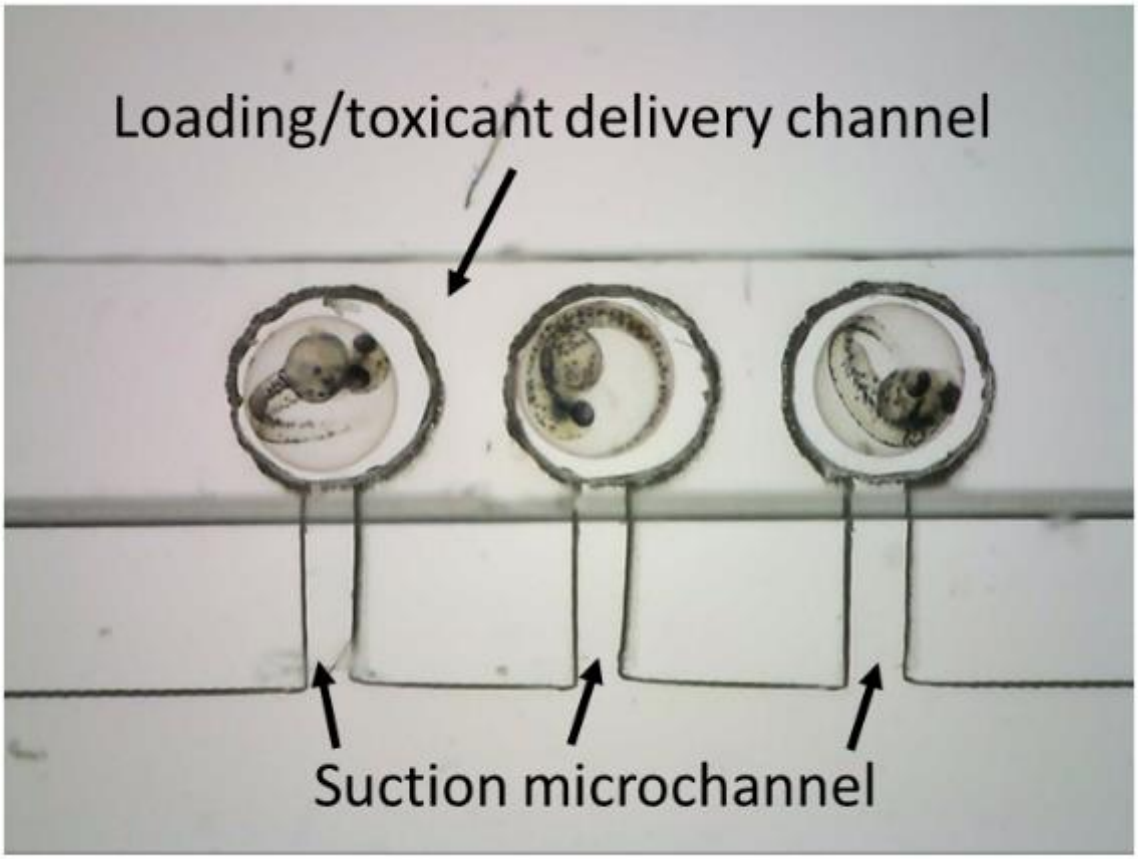


*Figure 5.4.1 Bright field image from the top of the chip device with immobilised zebrafish embryos at 48 hpf. There is no physical obstacles blocking imaging from either sides of the chip.*

Images from the chip device could to be taken, per cluster of three embryo traps, at a magnification of at least 30x. An image of the whole chip with detailed embryo features was also possible by stitching all sections together as shown in Figure 5.4.2.

*Figure 5.4.2 Bright field image from miniaturised Dino-Lite 5 MP USB microscope. Images of embryos were taken at a group of three and then stitched together and shown as an image of the whole chip.*

The chip device also fully supported fluorescence imaging from different imaging systems (Figure 5.4.3). In experimental validations, transgenic zebrafish *Tg(fli1:EGFP)* embryos with highlighted intersegmental vessels (red arrows) at 48 hpf were loaded onto the chip device. The blood vessel pattern of zebrafish embryos is highly characteristic during embryogenesis

and can be stained or genetically modified to allow visualisation under fluorescence microscopes [36, 37]. Fluorescence imaging were performed by i) Dino-Lite miniaturised fluorescent microscope ii) Trophos high-throughput image cytometer iii) Nikon SMZ1500 upright microscope, and iv) Nikon Eclipse TiE epifluorescence microscope. The features highlighted by green fluorescent protein (gfp) were all clearly present, even at low magnifications (with three embryos); and the intensity of autofluorescence from the PMMA chip was at an acceptable level.

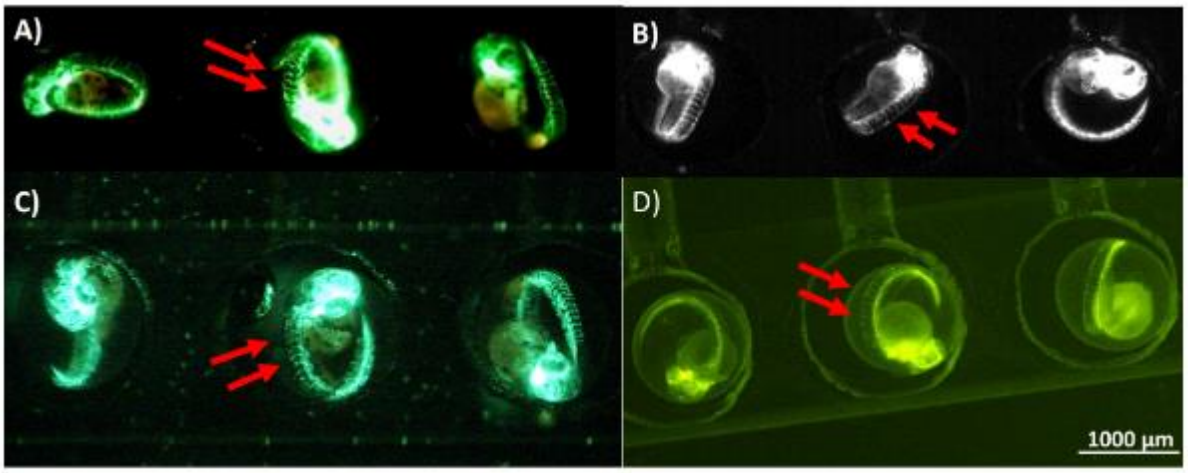


*Figure 5.4.3 Comparison of different fluorescence imaging systems on zebrafish embryo array with loaded Tg(fli1:EGFP) embryos. A) Miniaturised Dino-Lite 1.3 MP fluorescent USB microscope. B) TROPHOS plate RUNNER image cytometer. C) Upright microscope Nikon SMZ1500. D) Inverted microscope Nikon Eclipse TiE epifluorescence. Note that the intersegmental vessels (red arrow) were all clearly visible.*

## 5.5 On-chip anti-angiogenesis assays

Following the preliminary validation of the lab-on-a-chip fish embryo trapping array, I tested a couple of small molecular drugs as a proof-of-concept drug toxicity screening. Zebrafish embryos are protected by chorion (a layer of membrane surrounded the body) that resists large molecules, however, small molecular drugs are able to penetrate the chorion and affect embryos, causing mortality or developmental abnormalities[36]. In this experiment, two anti-angiogenesis drugs i.e. VEGFR1-3 inhibitor AV951 (Tivozanib) and VEGFR2/PDGFRβ inhibitor Sunitinib were selected for testing with transgenic zebrafish *Tg(fli1a:EGFP)* embryos on the chip device.

Prior to the experiment, 0.003% 1-phenyl-2-thioures (PTU) was added into the standard embryo culture medium E3. This compound not only inhibits the natural pigmentation of the embryo without any effects on their health, but also delays the embryo hatching time, allowing the embryos to be encapsulated within their chorion for an extended period of time[110]. At the endpoint of experiment, 0.2 mg/mL of Tricaine mesylate (TMS) was added into the culture medium to temporarily anaesthetise the embryo from spontaneous movement inside the chorion. This process was essential to obtain a better imaging quality with fluorescent images when the exposure time was very long.

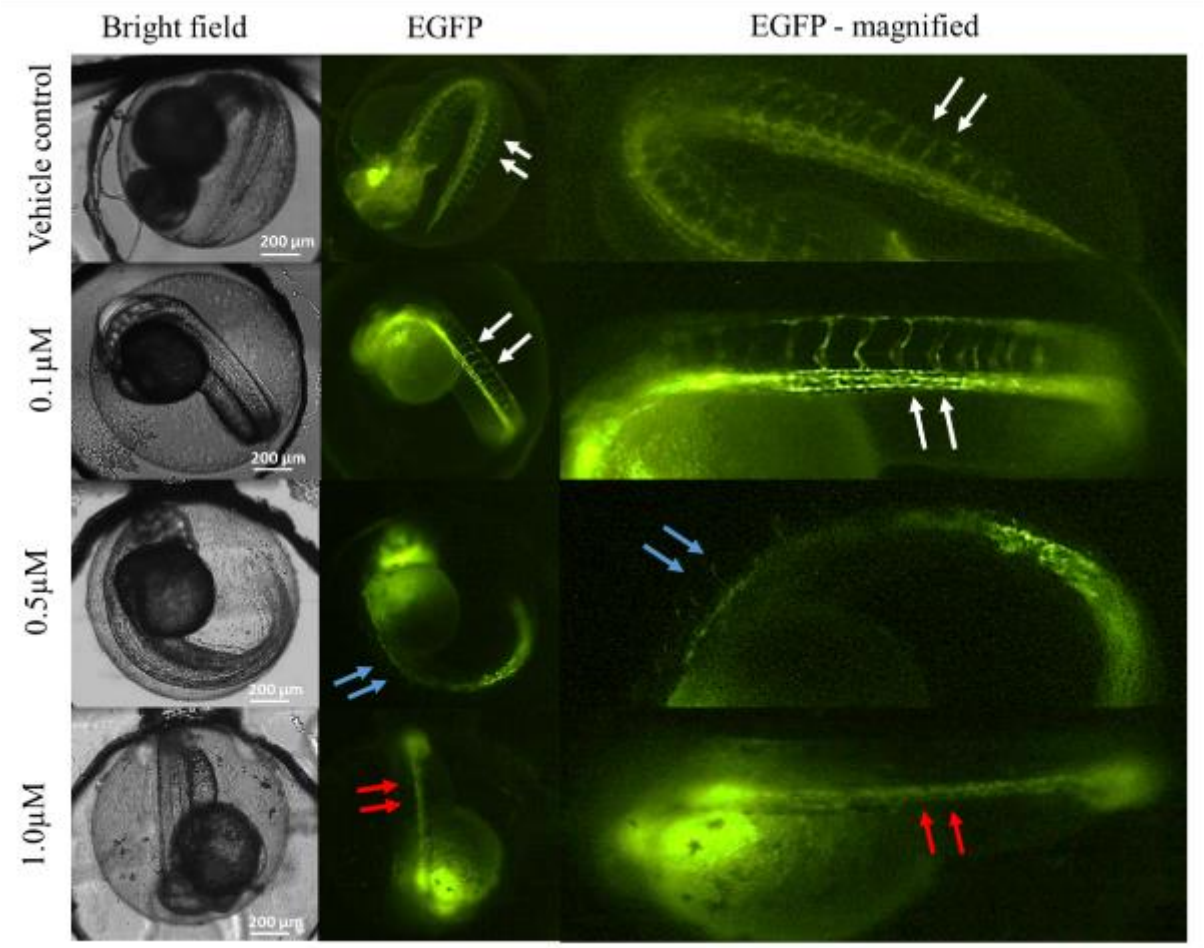


*Figure 5.5.1 Chip-based angiogenesis assay performed on Tg(fli1:EGFP) zebrafish embryos. Images were taken at 72 hours into the experiment with z-stack imaging. Embryos were anesthetised with Tricaine mesylate (0.1 mg/mL) when imaging. Vehicle control was DMSO. Microscopic visualisation of intersegment vessel (ISV) showed no inhibition, partial inhibition, and full inhibition of AV951 at 1.0, 0.5 and 0.1 µM respectively.*

Embryos at 16 hpf were loaded into the chip device under continuous perfusions of anti-angiogenesis drugs. At 72 hours post fertilisation (hpf), non-stimulated (control) zebrafish embryos developed normally in the chip device as evidenced by the presence of characteristic patterns of intersegmental vessels (ISV). Embryos treated with AV951 achieved 100% inhibition of ISV at 1 µM, partial inhibition at 0.5 µM, and no inhibition at 0.1 µM (Figure 5.5.1). Sunitinib showed no inhibition of ISV up to 50 µM, but showed 100% inhibition at 100 µM (Figure 5.5.2). By using TMS, using focus-stacking imaging technique, I was able to generate fully focused images on spherical embryos by merging multiple images taken at difference focus distances.

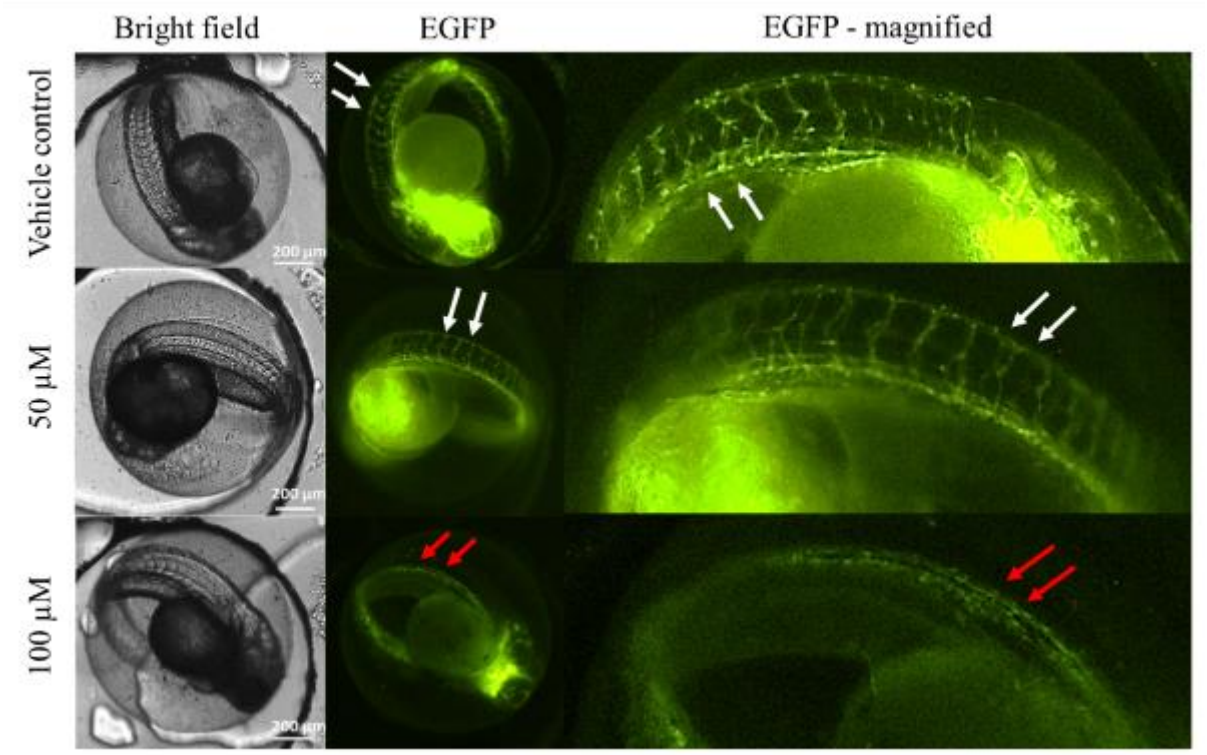


*Figure 5.5.2 Chip-based angiogenesis assay performed on Tg(fli1:EGFP) zebrafish embryos. Images were taken at 72 hours of experiment with focus-stack imaging. Embryos were anesthetised with Tricaine mesylate (0.1 mg/mL) when imaging. Microscopic visualisation of intersegment vessel (ISV) showing vehicle control (DMSO), no inhibition, and full inhibition of Sunitinib at 0, 50 and 100 µM, respectively.*

## 5.6 Microperfusion fish embryo toxicity (µFET) assays

Following the proof-of-concept drug toxicity screening test, the applicability of using microfluidic embryo array was investigated by performing fish embryo toxicity (FET) test based on a standard toxicity test protocol (OECD TG 236). This experiment was aimed at demonstrating that the fish embryo toxicity test performed on the microfluidic chip device is equal to, if not better than, the standard toxicity tests performed in static multiwell plates. I expected to see the microfluidic chip device overcome the limitations of standard toxicity tests.

To compare the performance between testing methods, medium lethal concentration ($LC_{50}$) by using FET protocol and half maximal response ($EC_{50}$) by using the iFET scoring criteria were calculated. To demonstrate the microfluidic system is applicable for a wide range of chemical compounds, I selected several commonly used reference toxicants to represent major classes of chemicals.

### 5.6.1 Test using FET protocol

I first used the standard fish embryo toxicity test (FET, OECD TG 236) protocol to test toxic compound. This protocol outlined four lethal endpoint of the experiment i.e. coagulation of embryo, lack of somite formation, non-detachment of tail, and lack of heartbeat (Figure 5.6.1). There are, however, no scoring criteria for sub-lethal effects and therefore the utility of this protocol is rather limited. In experiments, copper sulphate pentahydrate ($CuSO_4 \cdot 5H_2O$) was used as a reference toxicant for toxicity tests. Copper is known to be toxic to aquatic organisms at low concentrations. It causes mortality without significant sub-lethal or teratogenic effects.

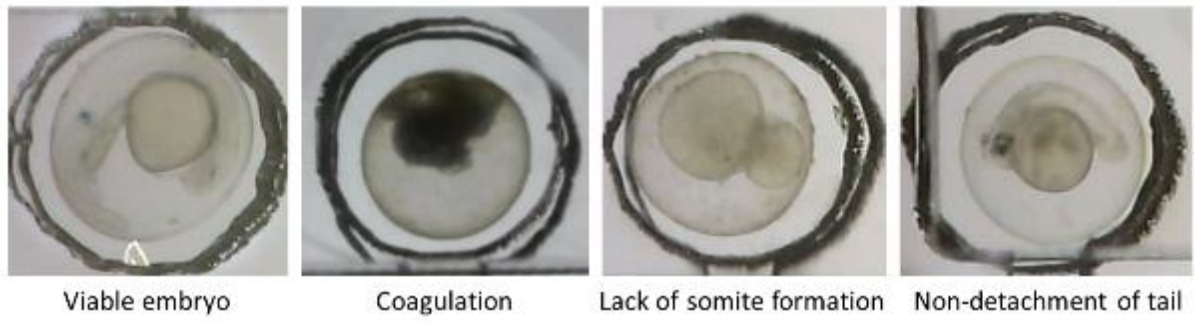


*Figure 5.6.1 Lethal endpoints of zebrafish embryo toxicity tests at 24 hpf compared with a viable embryo. Lethal endpoints of coagulation of embryo, lack of somite formation, and non-detachment*

*of tail were illustrated. Note that the fourth lethal endpoint. i.e. lack of heartbeat, was not applicable for embryos at 24 hpf.*

As a result of the biotest, embryo mortality in the microperfusion chip was in line with the mortality in the static culture plate (Figure 5.6.2). In particular, the $LC_{50}$ value was 0.8 mg/L on the chip device and 1.3 mg/L in the static wells.

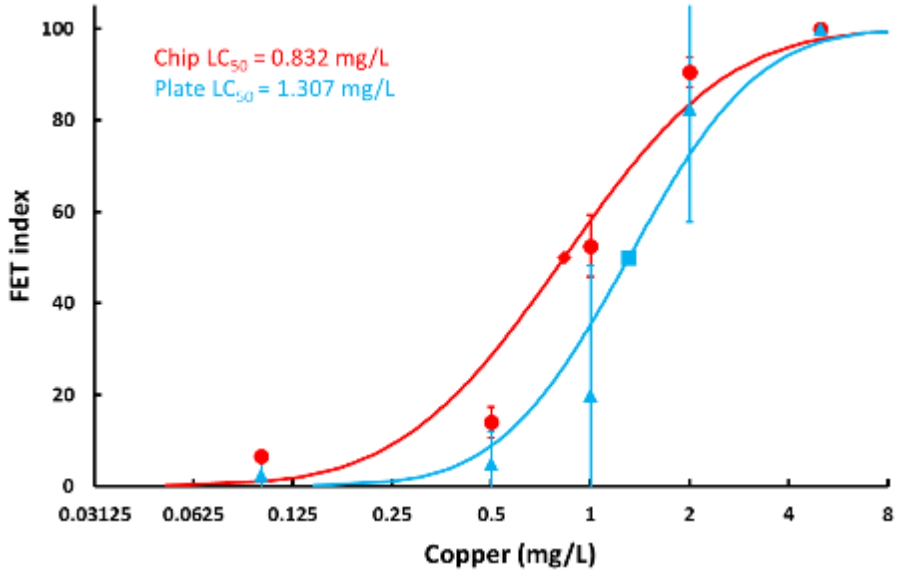


*Figure 5.6.2 Comparison between zebrafish embryo biotests performed in a microfluidic chip-device and conventional static culture plates. Chip experiments were performed under continuous microperfusion at a flow rate of 400 µL/min for 48 hours. Copper sulphate pentahydrate ($CuSO_4 \cdot 5H_2O$) was used as a reference chemical to cause mortality with no sublethal effects in the fish embryos. The FET index was calculated based on the standard FET assessment criteria. The FET index indicates the mortality of the test embryos. Published in Ref 109. Reprinted with permission from © 2015 American Chemical Society.*

### 5.6.2 Test using iFET protocol

Organic reference toxicants, such as phenol and caffeine, induce significant developmental abnormalities, but are not lethal to zebrafish embryos. Using FET endpoints in these cases are not appropriate. In this regard, the iFET protocol was used to improve the FET protocol to be able to test compounds causing sub-lethal effects on fish embryos. Apart from the four lethal endpoints from the FET protocol, iFET further introduced nine sub-lethal endpoints during the embryo development[104]. Those parameters are: i) pericardial oedema, ii) lack of pigmentation, iii) head abnormalities, iv) yolk abnormalities, v) tail abnormalities,

vi) abnormal eye development vii) spine abnormalities viii) defects in blood circulation, and ix) heart abnormalities (Figure 5.6.3).

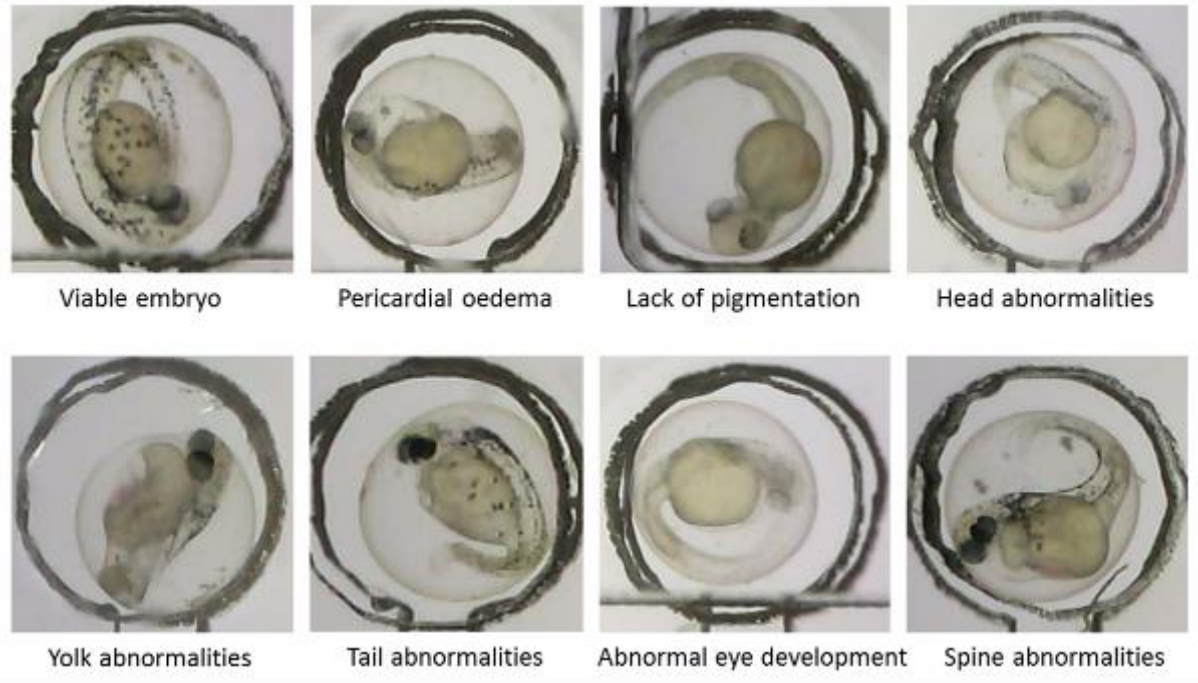


*Figure 5.6.3 Sub-lethal (iFET) endpoints of zebrafish embryo toxicity test at 48 hpf compared with a viable embryo. iFET endpoints of pericardial oedema, lack of pigmentation, head abnormalities, yolk abnormalities, tail abnormalities, abnormal eye development, and spine abnormalities are illustrated. Note that two of the iFET parameters, defect in blood circulation and heart abnormalities, were not depicted here because they require demonstration via video clips.*

In the tests with organic compounds, four reference toxicants, dimethyl sulfoxide (DMSO), ethanol, phenol and caffeine, were used. Comparing $EC_{50}$ values determined from microperfusion chip experiments with $EC_{50}$ from static plate experiments, the values are rather close between two experiments. This result confirmed that the zebrafish embryos cultured in a microperfusion condition on the lab-on-a-chip device are suitable for fish embryo toxicity test with a broad range of chemical compounds and toxicants (Figure 5.6.4).

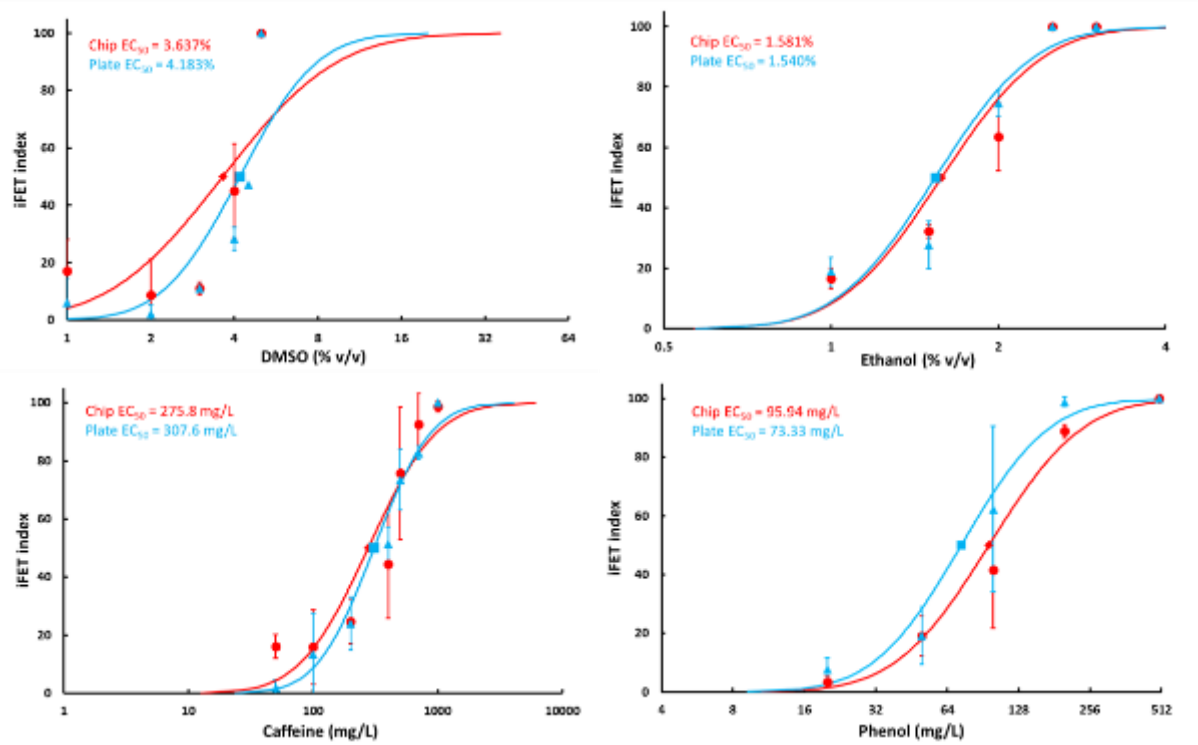


*Figure 5.6.4 Comparison between zebrafish embryo biotests performed in a microfluidic chip-device and conventional static culture plates. Chip experiments were performed under continuous microperfusion at a flow rate of 400 µL/min for 48 hours. DMSO, ethanol, caffeine, and phenol were used as reference chemicals that not only cause mortality, but also provoke sub-lethal effects on the fish embryos. The iFET method was used to score both lethal and sub-lethal effects based on the relevant criteria. Note that the $EC_{50}$ values were close between perfusion experiment and static experiment. Published in Ref 109. Adapted with permission from © 2015 American Chemical Society.*

### 5.6.3 iFET test with unstable compound

Despite the agreement with toxicity results in the above experiments, the model compounds selected were considered "easy" compounds that are very polar or moderately hydrophobic and they are likely to provide stable exposure concentrations both in a static exposure setup and in a microperfusion system. However, the static FET is particularly limited when the exposure concentrations at static conditions cannot be stably maintained, e.g. in case of hydrolysis, volatilisation, or absorption of the test compound to surfaces of exposure vessels. For these conditions, a pulse exposure is required and a microfluidic device could provide great advantages. To demonstrate that the microfluidic chip device provides more stable and reliable exposure, I chose nicotine as a representative compound.

Nicotine represents a challenge for toxicological assays due to the following reasons: Firstly, it is a common drug with an unquestionable and well-established toxicity. Secondly, its aromatic structure makes it prone to light degradation and oxidation, and, lastly, it is non-polar and not hydrated below 60 °C, which poses the challenge.

When testing the effects of nicotine in the microperfusion system, the iFET $EC_{50}$ obtained was 112 mg/L. In comparison, the iFET $EC_{50}$ for conventional systems was 185 mg/L, which is 1.65 times the detection limit observed using the microperfusion system (Figure 5.6.5). This result demonstrated that microperfusion system can have lower detection thresholds due to increased availability of non-polar and unstable compounds. This increase in sensitivity from using the microfluidic device as a testing platform presents strong advantages and is therefore a contribution to the advancement of the toxicological technology currently available.

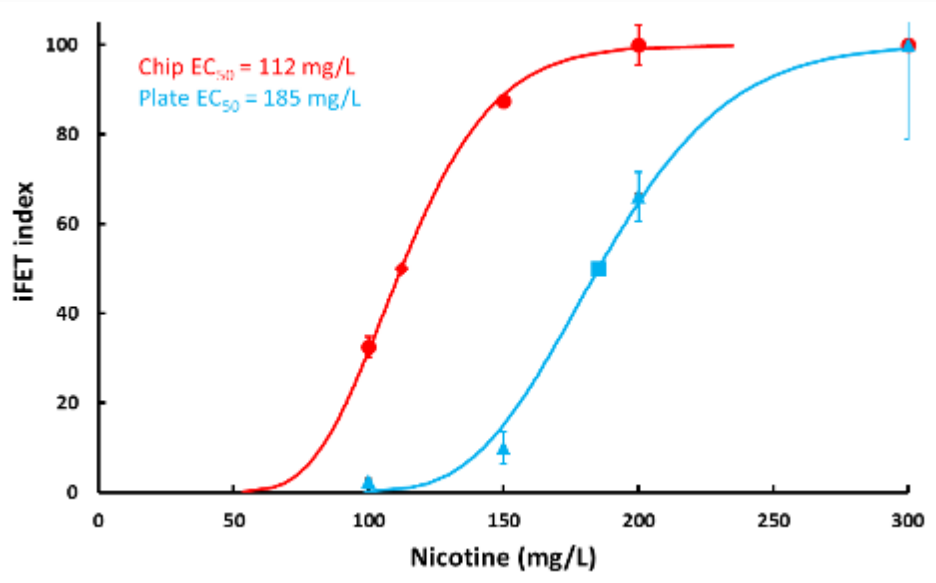


*Figure 5.6.5 Comparison between zebrafish embryo biotests performed in a microfluidic chip-device and conventional static culture plates. Chip experiments were performed under continuous microperfusion at a flow rate of 400 µL/min for 48 hours. Nicotine was used as an example of a class of unstable compounds. The iFET (lethal and sub-lethal/teratogenic) index was calculated based on the scoring criteria. Note that the $EC_{50}$ value was significantly lower in the perfusion experiment than in the static experiment. Published in Ref 109. Reprinted with permission from © 2015 American Chemical Society.*

## 5.7 Embryonic activity detection

The application of the embryo trapping array in embryonic behaviour studies was also explored. One of the greatest advantages of using zebrafish embryos is that their chorions are completely transparent, revealing the embryonic movement inside the chorion. Movements such as tail flicks, coilings, and convulsive behaviour starting as early as 17 hours post fertilisation (hpf) are important measurements in toxicology and pharmacology because they reflect the development of the nervous system and are highly susceptible to pharmacological manipulation.

To study the embryo behaviour, a video analysis software is required. In this study, DanioScope was used, as it is a non-invasive video analysis tool that investigates zebrafish embryo and larvae activity, cardiology, and morphology. For embryo activity study, DanioScope detects tail coils or convulsions.

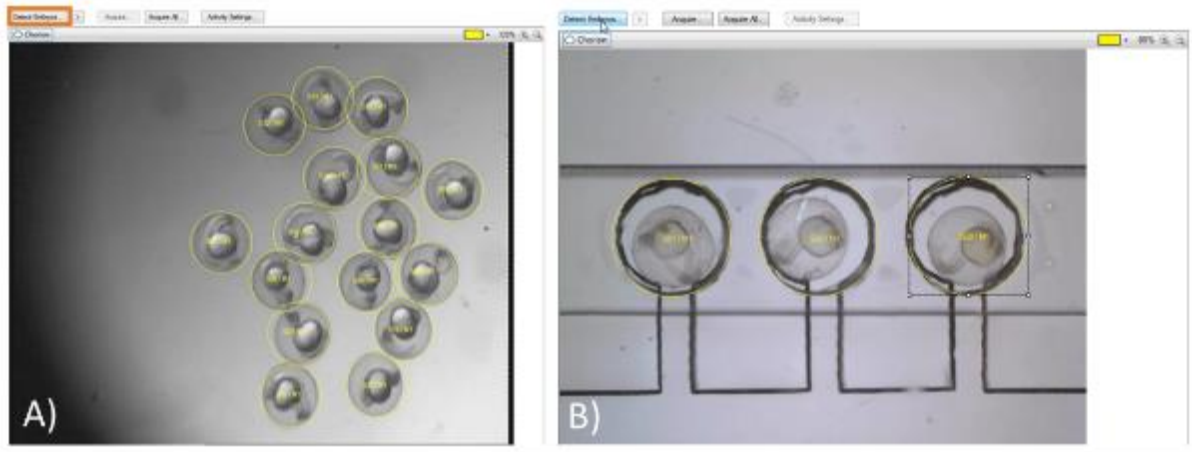


*Figure 5.7.1 Comparison of the embryo detection windows using DanioScope 1 software in video acquisition. A) A standard setup in a Petri dish. B) A setup using the lab-on-a-chip device. Embryos were positioned and immobilised on the chip device. The software successfully detected the region of interest (yellow circles) in the chip device without overlapping.*

Compared with a standard experimental setup in a Petri dish, embryos were spatially separated on the chip device (Figure 5.7.1). This accelerated the detection of the embryo chorion and reduced the error from overlapping embryos. Furthermore, the chip device provided a continuous microperfusion environment that prevented the evaporation of embryo medium during video acquisition. Moreover, because embryos were immobilised in the chip device, it minimised the external movements of the embryos that lead to a shift in

position, and allowed spatial encoding of each embryo during an extended period of time (Figure 5.7.2).

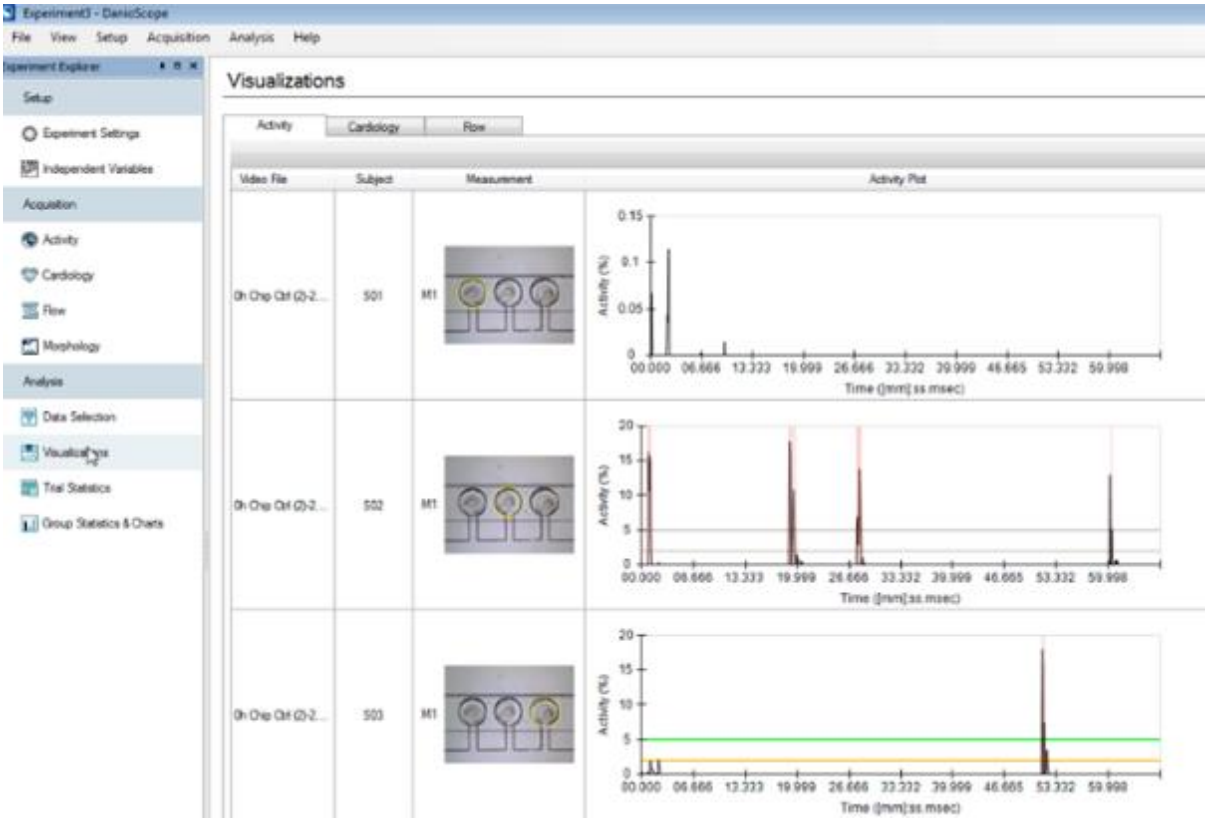


*Figure 5.7.2 User interface of the Danio Scope 1 in data analysis, plotting the charts of embryo activity over the period of 1 min. The software generated embryonic activity results based on every single detected embryos for the period of the video.*

In a proof-of-concept experiment, 5% dimethyl sulfoxide (DMSO) was used to stimulate the embryo activity over 24 hours, as DMSO is known to be mildly toxic to zebrafish embryos. Embryos at 24 hpf were loaded into the chip device under a continuous microperfusion at 400 µL/min. In comparison, a negative control (E3 medium, non-toxic embryo medium) and a positive control (Form Clear extract) experiment were also conducted in parallel (Figure 5.7.3).

A rapid stimulation in embryo activity was observed after just one hour of exposure to 5% DMSO solution, and the stimuli affected the embryonic activity over the next six hours. The embryo activity plummeted after 12 hours into the experiment. In comparison, in the negative control experiment the embryo's bursts of activity fluctuated around 3% in the

duration of the experiment; while in the positive control experiment, the embryo activity was constantly decreasing after an elevation in the first hour of perfusion.

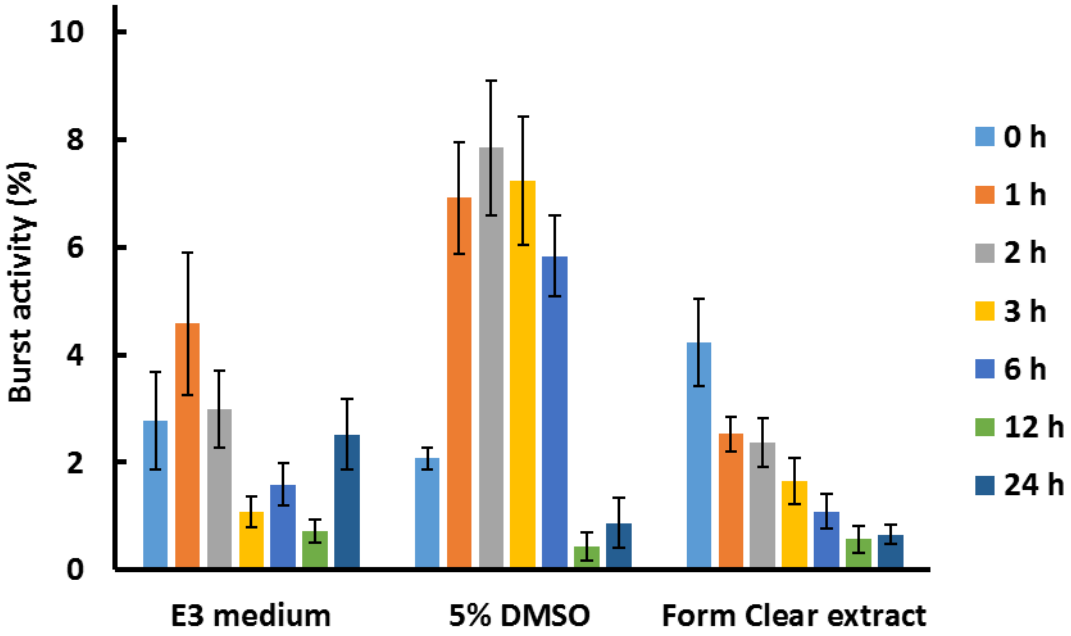


*Figure 5.7.3 Comparison of embryonic burst activities after toxicant exposure on chip-based device. Note the rapid activity stimulation in 5% DMSO after just one hour of exposure. Also note that a continuous activity decrease over the time occurred in the positive control experiment.*

## 5.8 Visualisation of metabolic activities in zebrafish embryos

Oxygen gradient is a physiological parameter for measuring the metabolic activity of the specimen. Progress in development of oxygen sensors has allowed visualised detections by luminescence as a result of excited molecular oxygen. However, all the tests were still conducted in small glass vessels containing a single organism, and, therefore, were not convertible to high-throughput screening assays.

A new technology named Fluorescence Ratiometric Imaging (FRIM) has recently been reported. It is based on real-time quantification of fluorescence signals sourced from a fluorescence sensor foil placed approximate to the specimen. This miniaturised system is capable of observing the patterns of aqueous oxygen gradients in real-time. In this section, a proof-of-concept microfluidic technology was demonstrated that integrated an oxygen

sensor foil into the fish embryo trapping array. Such a combination represents a new method to measure the oxygen gradient in a flow-through condition.

### 5.8.1 Design of the microfluidic device

A microfluidic chip-based device for zebrafish embryo metabolic activity detection was fabricated in poly(methyl methacrylate) (PMMA). PMMA is not only biologically compatible and optically transparent, but also gas impermeable which prevents passive oxygen exchange between the atmosphere and the fluidic environment. The oxygen sensor foil was fabricated by coating fluorescing substances onto a plastic sheet. The reference dye emits a constant green fluorescence signal; whereas the indicator dye emits fluorescence in response to reaction with oxygen. The sensor foil was capable of indicating the partial pressure of oxygen in an aqueous environment[111-113]. Therefore, to make the sensor fully functional, it needs to be in direct contact with the specimen.

The design concept of the chip device was very similar to the device described earlier, however, an extra layer was added to hold the oxygen sensor foil (Figure 5.8.1). The fluidic manifold was also slightly modified because of the restriction of the oxygen sensor foil size provided by the manufacturer. In particular, the chip device consisted of five modules: (i) a loading manifold (52 mm × 1.8 mm × 1.0 mm) for embryo loading, toxicant perfusion, and specimen recovery, (ii) an array of 18 miniaturised embryo traps (φ 1.5 mm × 1 mm) for individual embryo trapping and immobilisation, located beneath the loading channel, (iii) a suction manifold including a main suction channel (53 mm × 2.5 mm × 0.5 mm) and interconnection channels (0.3 mm × 1.6 mm × 0.5 mm) for each embryo trap, (iv) connection ports (φ 2.9mm) as inlet and outlet for direct tubing (1/16” OD) connections, and (v) a sensing manifold holding oxygen sensor foil sheets. Despite having an additional layer of oxygen sensor foil, the rational for embryo loading, immobilising, and on-chip culture remained the same as described in chapter 3 (Figure 5.8.1).

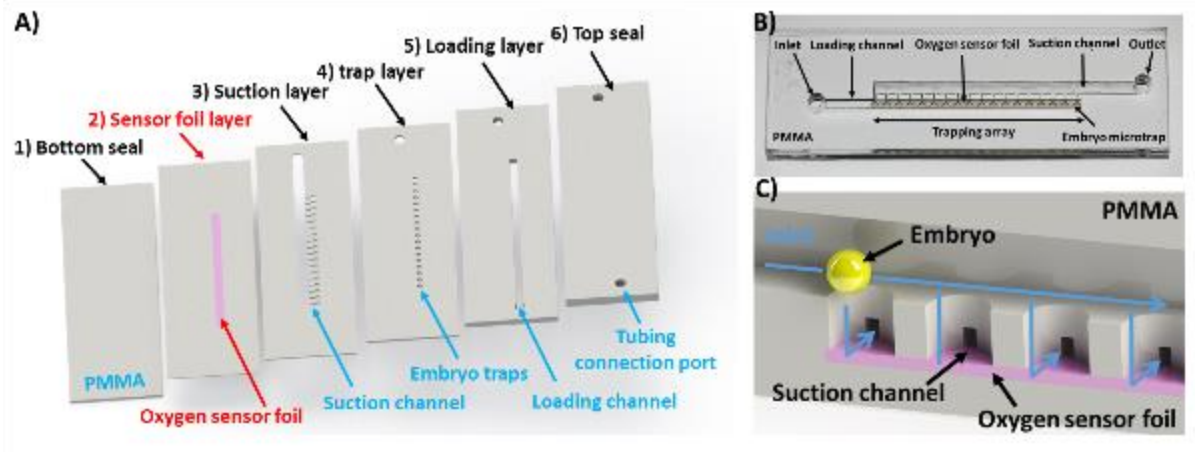


*Figure 5.8.1 Design of the microfluidic chip-based device. A) An exploded view of the chip device depicting all layers and features. The chip comprised six layers. Each layer was fabricated separately on a laser cutting machine. The second layer was a holder for fitting the oxygen sensor foil. All six layers were then thermally bonded together in a fan assisted oven. B) Macrophotograph of the chip-based device. All features are depicted. C) Cross-section view of the chip device, depicting embryo trapping and immobilising principles. Note that the oxygen sensor foil was located beneath the embryo traps, making all loaded embryos sit on it. Published in Ref 114. Reproduced with permission from John Wiley and Sons.*

Oxygen detection was achieved by using the Presens® VisiSens™ system that captures the signals from the sensor foil using a miniaturised digital microscope (Figure 5.8.2). Signals were then transformed in the analysis software (VisiSens Analytical 1) that calculates the oxygen level by comparing the values from the calibration with the readings from detected signals.

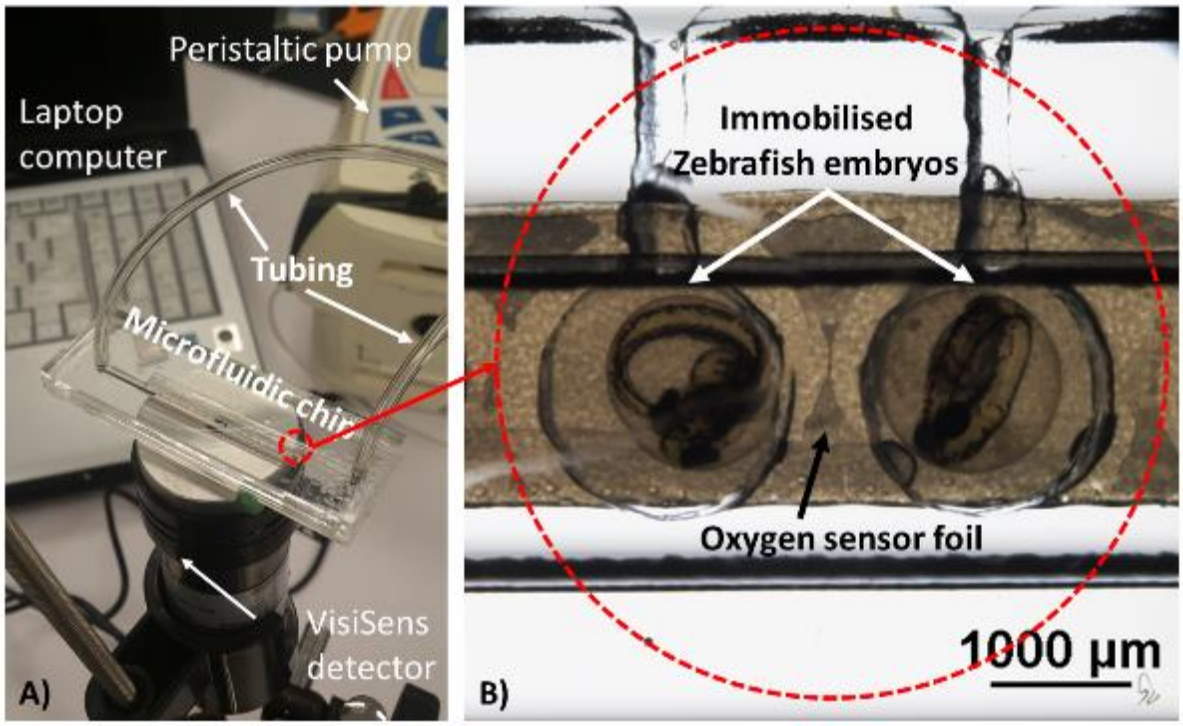


*Figure 5.8.2 Experimental set-up for real-time oxygen detection. A) Photograph of the experimental set-up showing the Presens VisiSens™ system associated with a microfluidic lab-on-a-chip device. The detection unit included a portable USB microscope with a 1.3MP camera, capable of imaging at 10x or greater magnifications. B) Magnified view of the microfluidic chip device loaded with 40 hour post fertilisation (hpf) zebrafish embryos. Note that the clear bright field view was effected by the oxygen sensor foil, but it has no effect on the experiment as the oxygen detection is based on fluorescence signals. Published in Ref 114. Reproduced with permission from John Wiley and Sons.*

### 5.8.2 Experimental validation

During the calibration of the detection system, air-saturated water (water bubbled with air) and anoxic water ($Na_2SO_3$, 5 g/L) were used to create an anoxic/normoxic boundary. In the bright field, the anoxic region and normoxic region can be clearly seen as orange and green areas, respectively. The contrast was greatly improved under a fluorescence view (Figure 5.8.3).

As a proof-of-concept experiment, I investigated the changes in oxygen gradient by adjusting the supply of oxygen under the demands of zebrafish embryo metabolism. Embryos at 40 hour post fertilisation (hpf) were loaded onto the chip device, followed by a continuous flow for on-chip culture. By altering the flow rate, the oxygen concentration changed in the approximate contact zones (region of interest, ROI) of the zebrafish

embryos. ROI was determined by direct observation of embryo position from bright field images, followed by outlining the entire chorion area in the fluorescent images (Figure 5.8.3). It was observed that in the absence of a continuous supply of oxygen, the oxygen level quickly plummeted around the embryo (Figure 5.8.3).

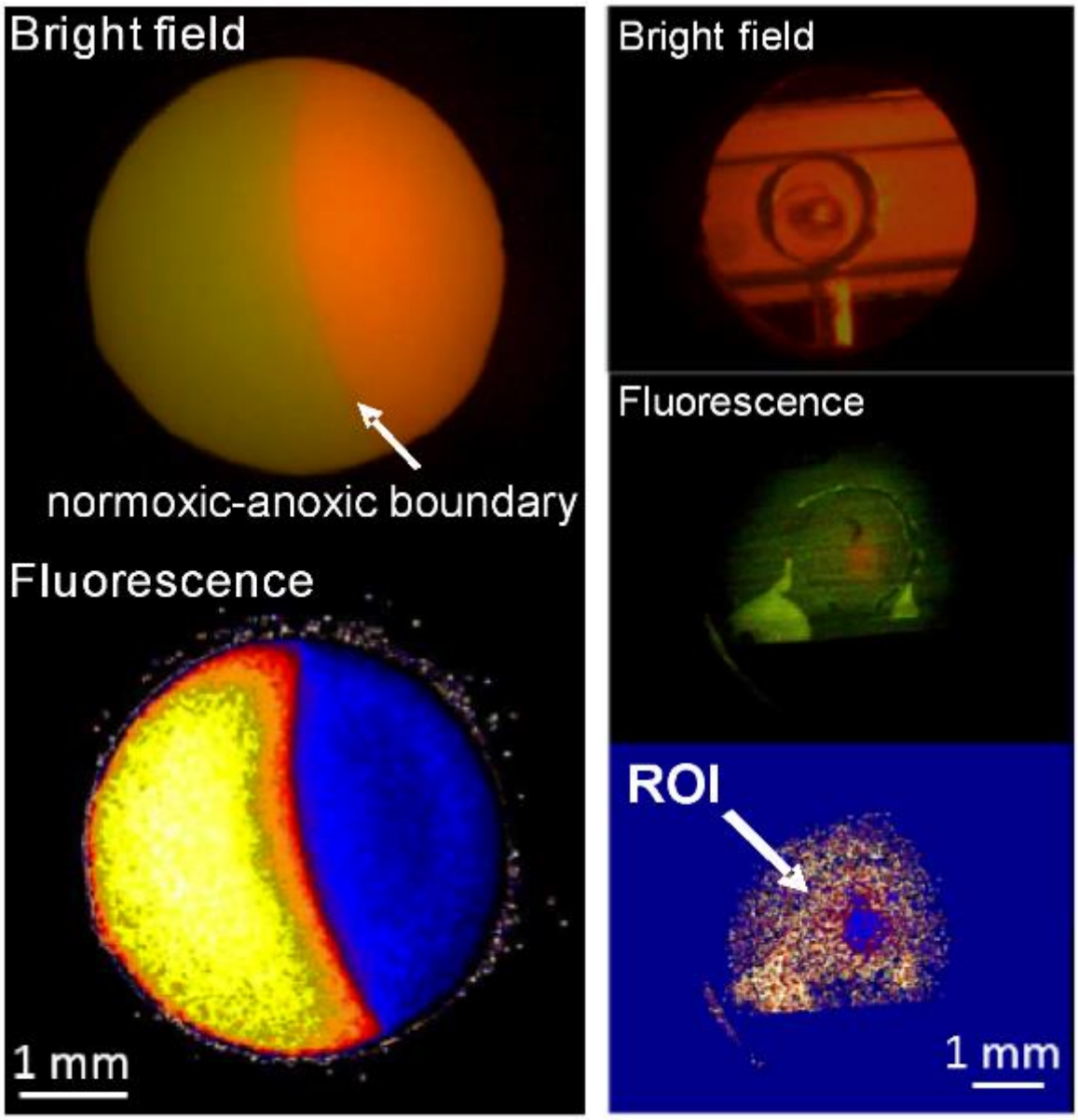


*Figure 5.8.3 Oxygen gradient detection using embedded sensor foils on a microfluidic chip-based device. (Left) Comparing image taken from bright field (upper panel) and fluorescence view (lower panel) in respond to a drop of anoxic water on the oxygen sensing foil. The boundary of normoxic (green) and anoxic (orange) regions can be clearly observed in the bright field, however, the boundary can be more clearly to observe using fluorescence. It is worth noting the excessively high fluorescence signals on the bottom left image, indicating an unfavourably high oxygen diffusion rate*

*from air to water. This phenomenon indicated that calibration of the oxygen sensor is not possible in the atmospheric environment. (Right) Real-time images (top- bright field, middle- fluorescence, and bottom- calculated oxygen level) of a zebrafish embryo with oxygen gradients due to a reduced flow rate. Published in Ref 114. Reproduced with permission from John Wiley and Sons.*

Next, I characterised how oxygen gradients could be affected by the presence of fish embryos during the halt and reintroduction of oxygen saturated water. In the experiment the flow of oxygen saturated water was halted and then continued through perfusion after two minutes. As a result, oxygen levels kept decreasing steadily over time until nearly depleted. After the perfusion restarted, it was found that oxygen level slowly recovered in the first minute and then rapidly jumped back to saturation (Figure 5.8.4 A).

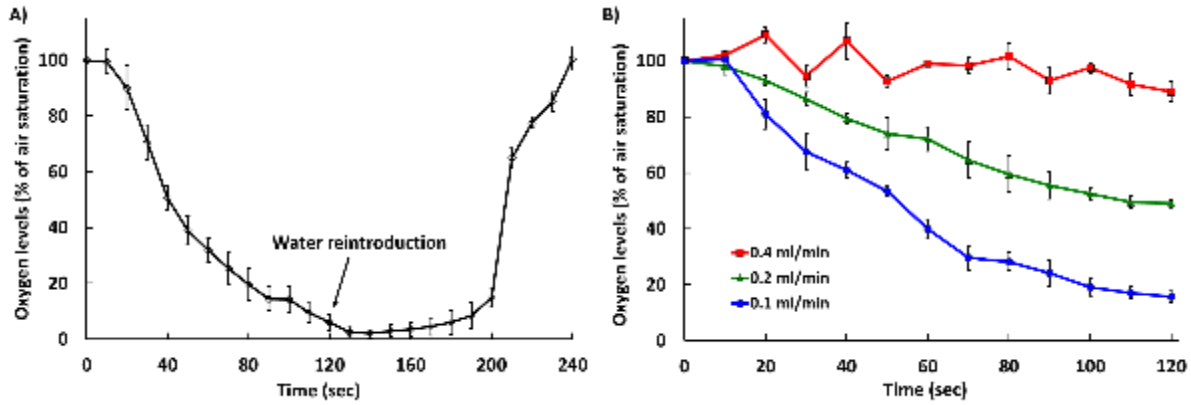


*Figure 5.8.4 Relationship between the fluidic flow and the oxygen gradient in the air impermeable microfluidic chip. A) Oxygen level (% air saturation) as a function of time (seconds) during the halt and reintroduction of water flow to zebrafish embryos at 40 hpf. Flow rate for water reintroduction was 0.4 mL/min. B) The effect of flow (0.4, 0.2, and 0.1 mL/min) on oxygen levels over the time in approximate (contact) zones of 40 hpf zebrafish embryos. Published in Ref 114. Reproduced with permission from John Wiley and Sons.*

Lastly, I investigated the oxygen gradient as a function of different flow rates. At the flow rate of 0.4 mL/min, oxygen levels were relatively constant over the period of 120 second. In comparison, when the flow rate was reduced to 0.2 or 0.1 mL/min, oxygen levels declined from nearly 100% to 60% or 20%, respectively (Figure 5.8.4 B). This result indicated a demand of oxygen required by on-chip culturing embryos.

## 5.9 Interfacing with a high-throughput imaging cytometry

As zebrafish embryo bioassays are gaining an increasing amount of interest, a high-throughput and automated experimental system is urgently demanded. Current zebrafish embryo assays are low throughput because a standard zebrafish embryo biotest is an image-based analysis. The changes in embryonic phenotypes during the experiment are usually recorded as images and then proceed to image analysis. Therefore, the acquisition of high quality images is one of the most important steps in the assay. Yet this is not an easy task, as zebrafish embryos are spherical and their body trunks are curled inside the chorion, making the imaging extremely difficult and time-consuming.

Recently the TROPHOS® Plate Runner HD™ (Trophos, Inc., Marseilles, France) - a high-speed multichannel imaging cytometer - was developed for this purpose. It equipped with a high speed camera capable of acquiring images at a resolution of up to 67 mega pixels with a depth of field of 40 µm. The imaging cytometer is thus able to acquire images for each well of 96-well plates in three fluorescent channels within 25 minutes. Because of the high resolution, changing objective lenses become unnecessary for imaging and magnifications can be conducted digitally in post-imaging steps without loss of information.

This equipment is a very desirable accompaniment to the lab-on-a-chip embryo trapping array for high-throughput screening. With all outstanding capabilities, the imaging cytometer, however, is only adaptable with standard multiwell plates. Hence, in this section, I modified and expanded the previous chip device to be compatible with the cytometer.

### 5.9.1 High density fish embryo trapping array

The expanded version of the embryo trapping array was designed to fit the exact same space as a conventional 96-well microtitre plate (127 mm × 85 mm). Each chip consisted of 12 independent microfluidic manifolds for zebrafish embryo loading, immobilising, and culturing, as described in chapter 3. Herein, the embryo traps were designed to feature a total circumference and distribution of the wells on standard 96-well microtitre plate for any plate readers that accept multi-well plates (Figure 5.9.1 A). In particular, each image taken from a well from a 96-well plate covered three embryos immobilised in the traps (Figure 5.9.1 B).

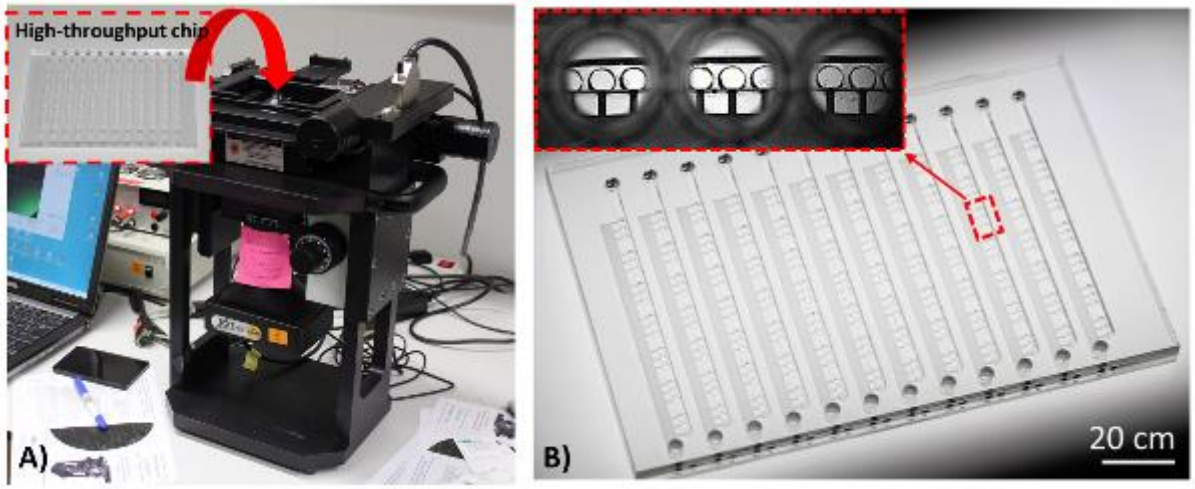


*Figure 5.9.1 Lab-on-a-chip technology for high-throughput zebrafish embryo immobilisation, microfluidic flow-through culture and time-lapse imaging. A) The high-speed multichannel imaging cytometer TROPHOS Plate Runner HD (Trophos, Inc.). Inset: A high-throughput zebrafish embryo trapping array adaptable to the imaging cytometer. B) Photograph depicting the high-throughput chip-based device. It contained 12 independent fluidic manifolds. Inset: Overlay of a 96-well plate with a chip-based device.*

### 5.9.2 Experimental validation

To validate the technology, an experiment was performed to test the quality of images taken from the fluidic device. Transgenic *Tg(fli1a:EGFP)* embryos were loaded onto a chip-based system at the 16 hpf before the development of intersegmental vessels (ISVs). The developing embryos were then continuously perfused in a close-loop cycle at a continuous flow rate of 0.4 mL/min with E3 media. On the chip, ISVs were fully developed at 40 hour post fertilisation, in line with the control experiment where the embryos were cultured in standard Petri dishes.

The presence of ISV can be clearly viewed in the images taken from the imaging cytometer, with a minimum amount of autofluorescence from the chip device (Figure 5.9.2). Acquired images were further digitally magnified five times and the details of the embryo could still be seen clearly, thanks to the chip device that immobilised the fish embryos. This result proved that the chip device fit well with the high-resolution image cytometer and was ready to perform zebrafish embryo bioassays.

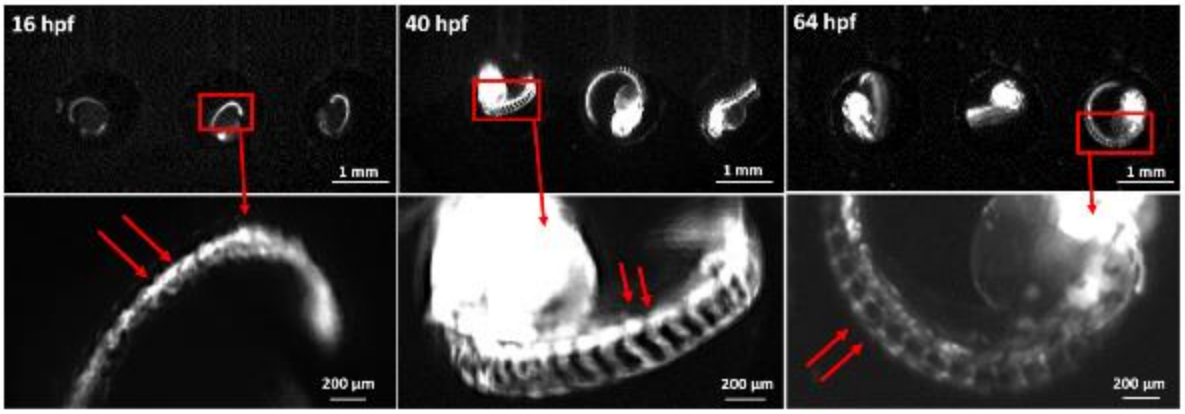


*Figure 5.9.2 Assessment of imaging quality of the cytometer, taken images from the chip-based device and depicting Tg(fli1a:EGFP) zebrafish embryos cultured under continuous microperfusion. High-resolution visualisation of patterns of intersegmental vessels (ISV) was conducted using multichannel imaging cytometer TROPHOS Plate Runner HD. Transgenic embryos were arrayed and immobilised at 16 hpf. ISV can be clearly viewed at 40 hpf. Digitally magnified images also showed high definition.*

### 5.9.3 3D printed fluidic interface

During the experiment, I realised that the high-throughput chip device was very difficult to use because of the increased effort necessary for tubing connections and leakage prevention. This issue is in fact not only apparent in this particular case, but also is a common issue experienced by many lab-on-a-chip devices.

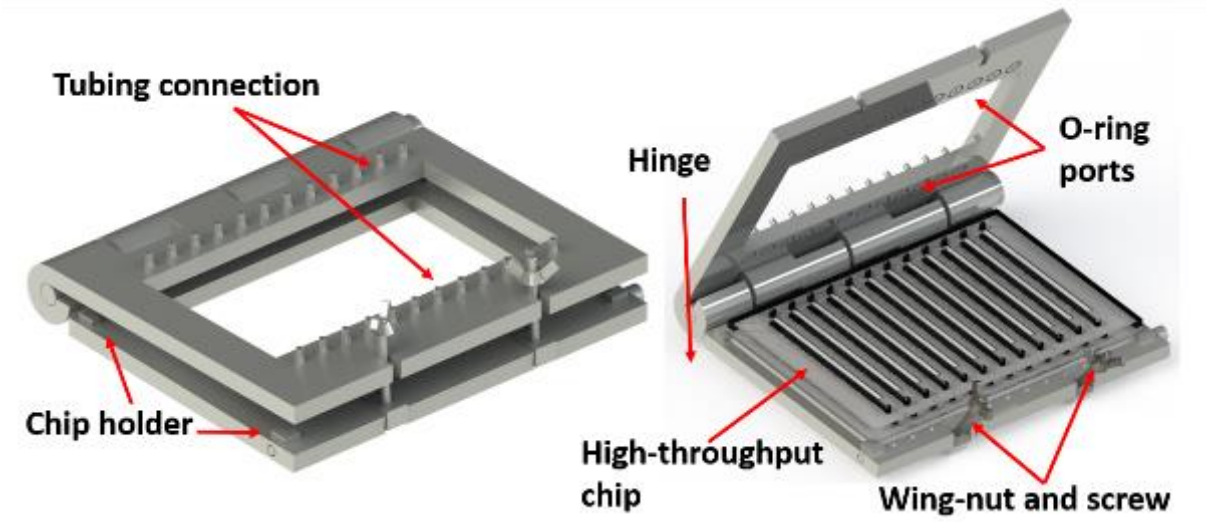


*Figure 5.9.3 Photo realistic rendering images of the fluidic interface. All functional features depicted. It sandwiches the high-throughput chip device in the middle interfacing between the culturing chip and the external tubing.*

To address this problem, a proof-of-concept 3D printed fluidic interface was prototyped for convenient chip positioning, tubing connections, and image acquisition. The interface comprised of a hinge-based cradle to fix the chip device and two arrays of integrated barb connectors that extend the inlets and outlets of the chip for tubing interconnections. Each connector was surrounded by a notch that held a rubber O-ring to seal the gap between the cradle interface and the chip device. To secure the sealing of the fluid interconnection, a mechanic locking system was integrated into the device. The bottom layer of the cradle was bundled with two small hinge holders carrying two screws together with two wing-nuts. To use the cradle device, simply place the chip device onto the holder, close the hinge and tighten the two wing-nuts. Image acquisition could be accessed via the top and bottom surface that were left empty (Figure 5.9.3).

*Figure 5.9.4 Macrophotograph of 3D printed fluidic interface with the HTS chip device. The interface was fabricated by Stereolithography (SLA) 3D printing technology using VisiJet SL Clear material. Published in Ref 112. Reprinted with permission from © 2015 American Chemical Society.*

The prototype was 3D printed using Stereolithography, allowing a high quality finish of all small features (Figure 6.3.4). The smallest feature was the wall of the connection nozzles with only 0.2 mm thickness, nonetheless, it was accomplished successfully without any imperfections. Although 3D printing materials are toxic to the aquatic organism and are not suitable for fabricating lab-on-a-chip devices directly, as discussed in chapter 4, they can still contribute to the device manufacture as long as they are not directly or largely in touch with the fluids. The contact of the material in the connection nozzles is neglectable, as evidenced by the validation test, showing no mortalities throughout the experiment (Figure 5.9.2).

## 5.10 Summary and discussion

In this project, I present a microfluidic lab-on-a-chip device for zebrafish embryo toxicity assays. The automated arraying and immobilisation of embryos on the chip-based device simplified specimen handling and accelerated image acquisition. The chip device allowed embryo on-chip culturing on a one-embryo-in-one-trap basis, which improved time-lapse imaging for tracking every single embryo. The toxicity test can be performed under continuous flow-through conditions over 48 hours without disturbing the development of the specimens.

The further developments and modifications were performed for advanced applications of the chip device. Firstly, an additional layer holding an oxygen sensor foil was integrated to the embryo chip, enabling a visualised measurement of oxygen level in real-time. Secondly, a high-throughput chip was fabricated by integrating 12 individual fluidic manifolds onto a plate-based device that was the exact size of a 96-well multititre plate. The device seamlessly fit to a high-resolution image cytometer that can screen up to 252 embryos in less than 10 minutes. Thirdly, a 3D fluidic interface was prototyped for a rapid and leak-free experimental set-up for the high-throughput device. This made the use of the microfluidic system increasingly user-friendly and effortlessly.

**Design of the lab-on-a-chip device**

The viability of the embryos under a microperfusion condition is of utmost concern in the chip design. Computational fluid dynamics (CFD) simulations were performed to show that, under a constant flow rate of 400 µL/min, the embryos were exposed to a low water pressure and a very low shear stress. According to previous work by Wlodkowic and co-workers, the maximum shear stress value from the simulation was at least two orders of magnitude lower than the value reported to damage cells[115].

Another concern when using microperfusion fish embryo toxicity test (µFET) is that all embryo culture chambers are mutually connected, which opens up the possibility of cross contamination. This situation is, in fact, minimised by having individual suction microchannels for each of the embryo trap. When a dead embryo releases waste, the waste would be directly flushed out of the chip device via the suction manifold (Figure 5.10.1).

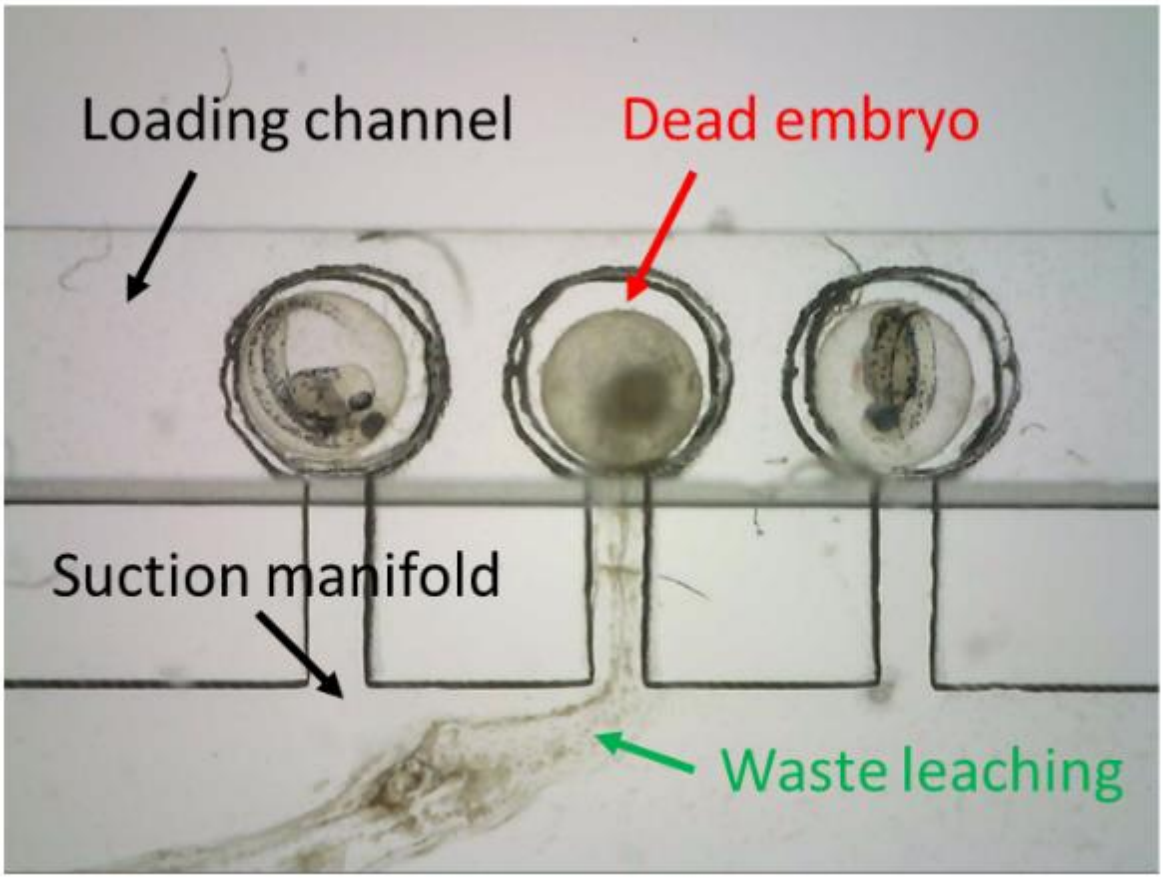


*Figure 5.10.1 Automatic clearance of embryo waste during the microperfusion culture. Each embryo culture chamber was connected to a suction microchannel. Any waste produced from unhealthy embryos would be flushed out of the culture chamber without cross contamination.*

**Comparison between FET and iFET**

Most of the toxicity results in the experiment were scored using both the FET method ($LC_{50}$) and the iFET ($EC_{50}$) method. Compared with the standard FET method, the iFET not only focuses on lethal endpoints, but also includes sub-lethal endpoints. Therefore, the iFET is a more sensitive scoring method for identifying the effects of toxicants. Compared with the $LC_{50}$ values, $EC_{50}$ values were at least 20% higher (Figure 5.10.2). The difference becomes significant for compounds that cause few mortalities, but severe developmental abnormalities. For example, xanthine alkaloid caffeine, known to be a potent antagonist of adenosine receptors, induced iFET $EC_{50}$ value 3.5 times higher than the FET $LC_{50}$ value.

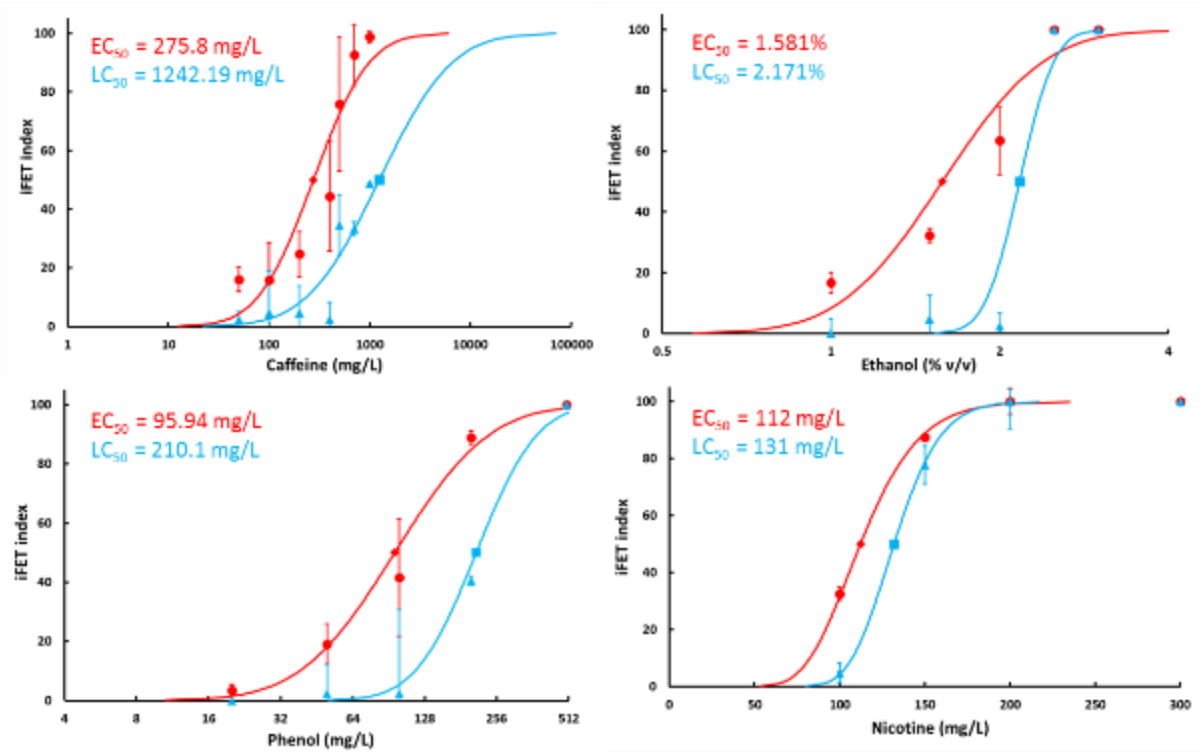


*Figure 5.10.2 Comparison of scoring methods between FET (lethal) and iFET (lethal and sub-lethal/teratogenic) endpoints after exposure to several compounds. Experiments were performed on chip-based devices for 48 hours. Note that iFET calculations include FET mortality parameters and introduces nine sub-lethal parameters. It increases the sensitivity of a standard fish embryo toxicity test.*

**Comparison between microperfusion and static experiment**

The results confirmed that the microperfusion fish embryo toxicity assay (µFET) obtained comparable results to conventional FET assays performed in multi-well plates when testing reference toxicants. Linear correlation analysis between the two experimental setups yielded $R^2$ value of more than 0.9 (Pearson and Lee linear correlation test ($p<0.01$)) (Figure 5.10.3). When testing compounds that are unstable in static conditions, such as nicotine, the microperfusion system displayed a higher toxicity than the static system. This result indicated that the chip-based microperfusion system is more reliable in these toxicity tests than static conditions.

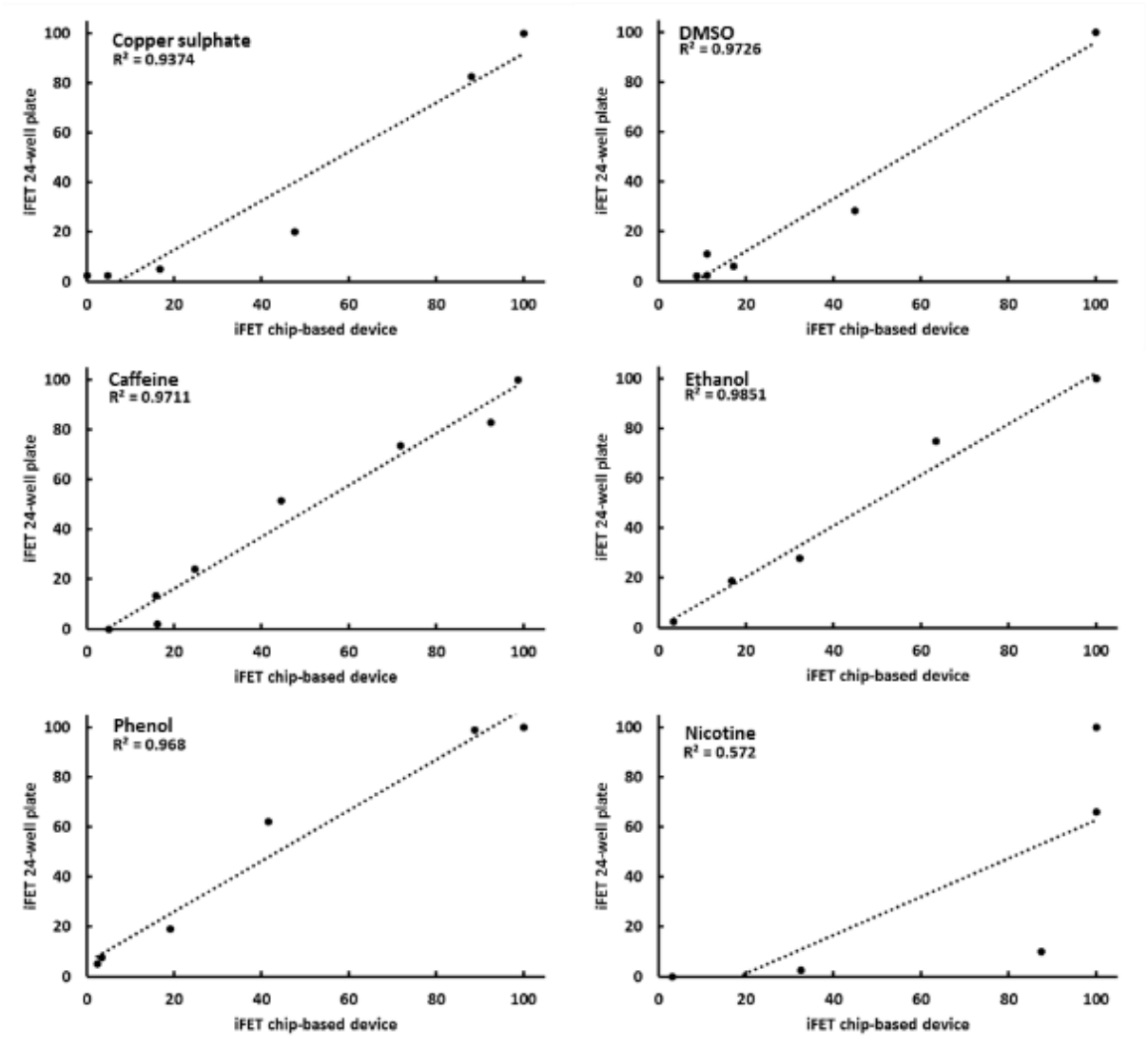


*Figure 5.10.3 Linear correlation analysis between chip-based microperfusion experiments and plate based static experiments. Lab-on-a-chip experiments were performed under continuous microperfusion at a flow rate of 400 µL/min for 48 hours. Note the excellent agreement between the two experiments when testing standard reference chemicals. Also note a bad correlation when testing unstable compound (nicotine) where chip-based device showed higher toxicity. Published in Ref 112. Adapted with permission from © 2015 American Chemical Society.*

**Limitations**

The major limitation of using the microfluidic embryo array in toxicity tests is the maximal test duration. To perform chip-based experiments, the test duration was reduced from a standard 96 hours to 48 hours. Some compounds, in particular non-polar and highly

hydrophobic compounds, may not reach internal equilibrium concentrations within 48 h of exposure. However, the reduced exposure duration was necessary because the embryo array was designed to immobilise fish embryos within the chorion. Zebrafish embryos normally hatch between 48 hpf and 72 hpf, and hatched embryos would swim out of the device and deteriorate the experiment.

Nevertheless, the necessity for 96 h of toxicant exposure is debatable. To start with, it is believed that the ideal time point for toxicant penetration of zebrafish embryo is shortly after 24 hpf. After this time point, the chorion of the embryo hardens and it becomes increasingly difficult for compounds to penetrate the developing embryos. There is no solid example of slowly penetrating and equilibrating drugs in zebrafish. Generally, they penetrate well early or very poorly. The early developmental processes are easier to perturb than late processes.

Secondly, in many countries outside the EU, complex and prohibitive Animal Ethics permits are required for any tests performed on hatched embryos. Animal Ethics is not required only for unhatched embryos. This profoundly limits deployment of OECD TG 236 test protocols that must often be modified to adhere to Animal Ethics regulations.

Thirdly, key responses, lethal and sub-lethal endpoints can be already observed in unhatched embryos cultured with toxicants for up to 48 h, as evidenced by the previous work (Table 5-1)[39].

*Table 5-1 Lethal and sub-lethal endpoints of zebrafish*[39]

| | Exposure time | | | |
|---|---|---|---|---|
| | **24 h** | **48 h** | **96 h** | **120 h** |
| **Lethal endpoints** | | | | |
| Coagulation | √ | √ | √ | |
| Tail not detached | √ | √ | √ | |
| No somite formation | √ | √ | √ | |
| No heartbeat | | √ | √ | |
| Lack of hatching | | | | √ |
| **Sublethal developmental endpoints** | | | | |
| Completion of gastrula | | | | |
| Formation of somites | √ | | | |
| Development of eyes | √ | √ | √ | |
| Spontaneous movement | √ | √ | √ | |
| Heartbeat/blood circulation | | √ | √ | |
| Heartbeat frequency | | √ | √ | |
| Pigmentation | | √ | √ | |
| Formation of edemata | | √ | √ | |
| **Teratogenicity endpoints** | | | | |
| Malformation of the head | √ | √ | √ | |
| Malformation of sacculi/otoliths | √ | √ | √ | |
| Malformation of tail | √ | √ | √ | |
| Malformation of heart | √ | √ | √ | |
| Modified chorda structure | √ | √ | √ | |
| Scoliosis | √ | √ | √ | |
| Rachitis | √ | √ | √ | |
| Yolk deformation | √ | √ | √ | |
| General growth retardation | √ | √ | √ | |
| Length of tail | | | | √ |

# 6 Development of a highly integrated and automated microfluidic total analysis system (µTAS)

## 6.1 Introduction

The emerging microfluidic lab-on-a-chip technologies have addressed many issues in cell-based and organism-based pharmaceuticals and toxicant screening. The technologies are based on two major concepts: by miniaturising the test vessels, the consumption of samples is greatly reduced; and by applying a flow throughout the fluidic system, a more accurate test result is achieved. Nevertheless, using lab-on-a-chip technology is not as popular as expected[116]. The major obstruction is actually the difficulty in operation. This is ironic because lab-on-a-chip technology is meant to be convenient to use, but it is not the case in most current designs. Many lab-on-a-chip prototypes can be rather referred as chips-in-the-lab, because the chips themselves cannot stand alone, they require many associated sensors and actuators to operate the entire system (Figure 6.1.1). More attention should be focused on developing a miniaturised analysing system with integrated functions.

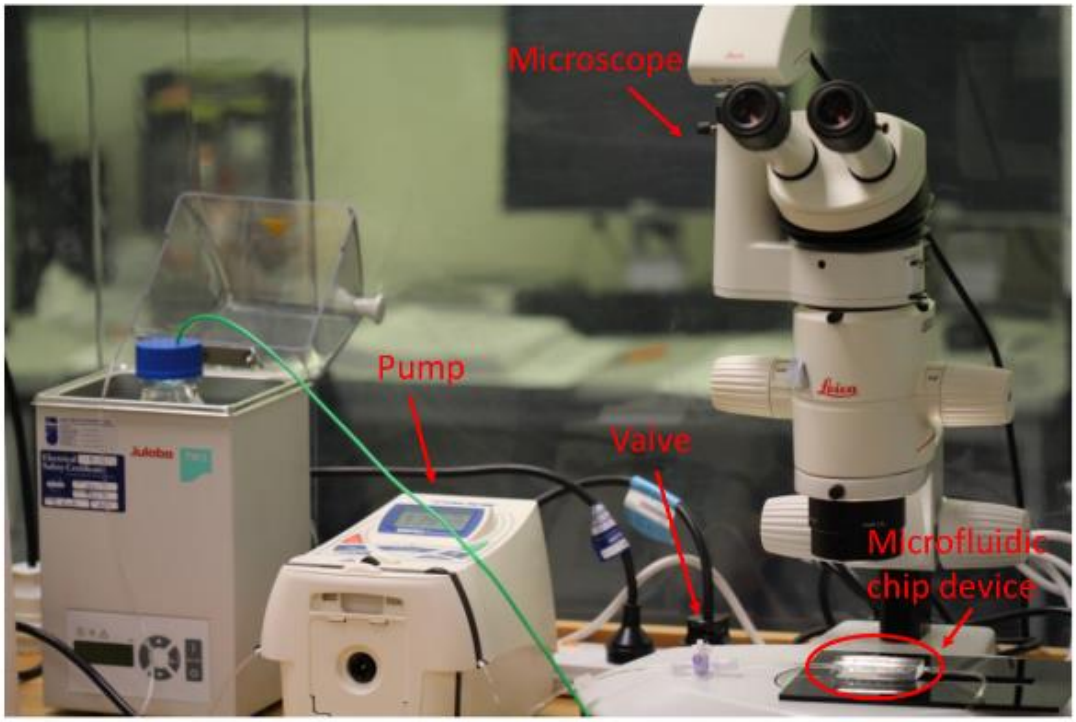


*Figure 6.1.1 A standard experimental set-up for using a microfluidic lab-on-a-chip device. Although the chip itself is miniaturised, it requires bulky detectors and fluidic actuators to be operated. There is little automation involved and the throughput is very low.*

In this chapter, a series of miniaturised pumps and valves were developed to efficiently and effectively actuate the high-throughput system. And finally, I integrated all the units, together with the chip device described in the previous chapter, and presented a prototype of a microfluidic total analysis system.

## 6.2 Miniaturised microfluidic actuators

To operate a high-throughput microfluidic device requires a substantial amount of technical support, especially for the fluidic actuators. For example, the device described in section 5.9 had 12 individual fluidic manifolds, meaning an array of 12 pumps is needed. Currently, there is a lack of pumps for microfluidic high-throughput screenings, which need to be inexpensive, reliable, and capable of running with low volumes. In this regard, I customised a series of peristaltic pumps and valves by using robotic servo motors combined with 3D printing technologies.

### 6.2.1 Miniaturised peristaltic pump

Selection of pumps is one of the most important considerations in running a microfluidic system. Commonly used pumps for lab-on-a-chip devices include peristaltic pumps, syringe pumps, and piezoelectric pumps. Their difference in terms of performance was the pulsation intensity and the range of flow rates. In this section, I designed and manufactured a series of customised peristaltic pumps because they are relatively simple: simple to make, simple to use, and simple to maintain. The pump design was based on using Dynamixel servos (Robotis Ltd.) as the actuator of the pump, using metal bearings as the rollers, and using 3D printing to fabricate a pump head.

A range of Dynamixel servos, i.e. AX-12A, AX-18A, MX-28T, and MX-64T, was investigated. Each servo has a different size, max torque, and max speed, which enables the pump series to be very versatile for broader applications. Taking the pump design using AX-12A, as an example, the pump comprised of four major components: i) a servo actuator, ii) a 3D printed pump head, iii) a 3D printed roller holding a number of metal bearings, and iv) tubing and connectors (Figure 6.2.1).

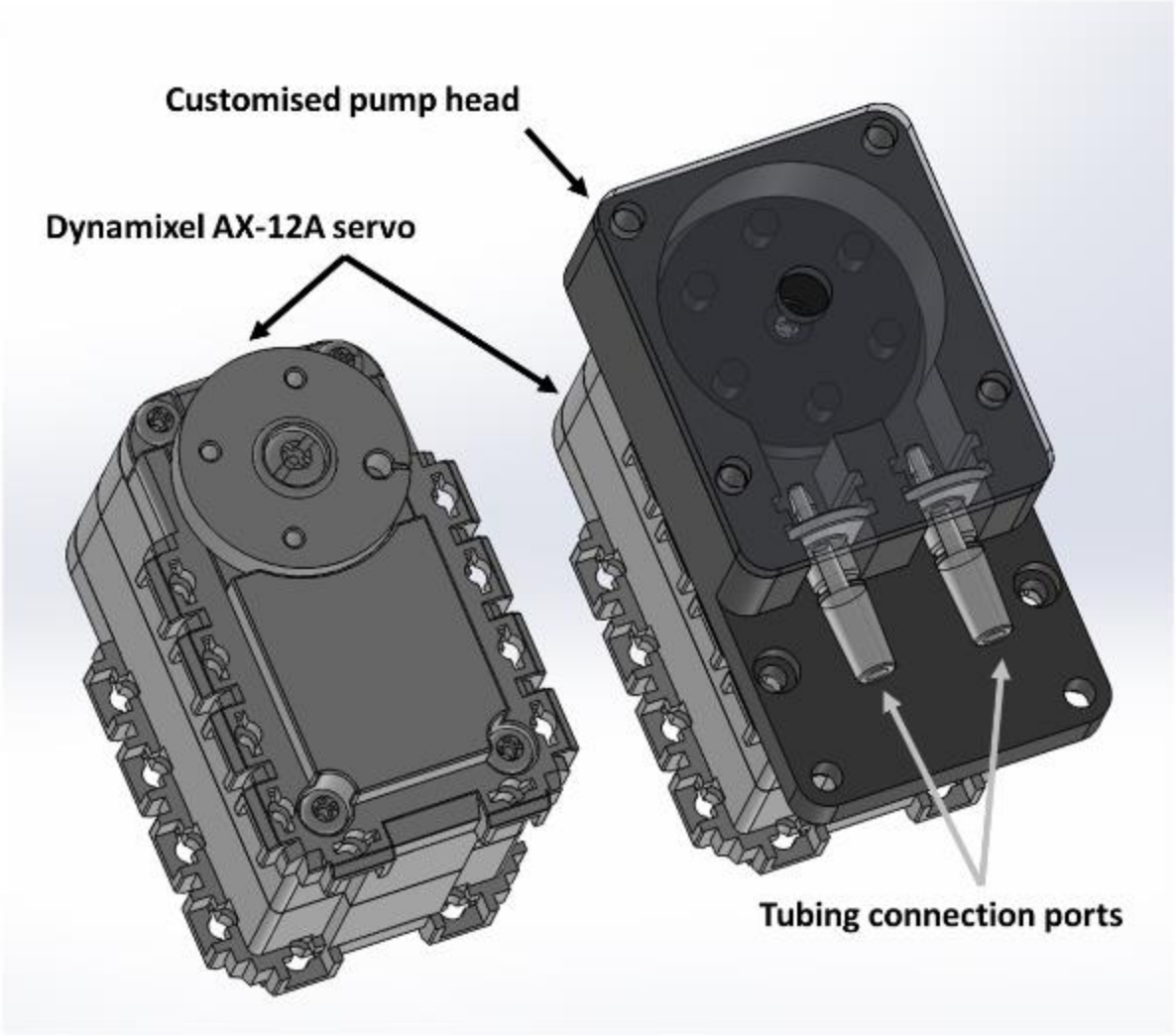


*Figure 6.2.1 Computer aided design (CAD) of the miniaturised peristaltic pump based on a Dynamixel AX-12A servo motor. The customised pump head and the roller holder were 3D printed.*

The pumping speed and pulsation were restricted by the servo actuators, but they can be tuned and compensated for by the design of the pump head. The number of rollers is an important parameter in this regard. Many small rollers can reduce the pulsation, but will also reduce the maximum flow rate, while a few of large rollers increase the flow rate but introduce substantial pulsations. In the design, the pump head and rollers were interchangeable, as to fit into extensive applications. Figure 6.2.2 presented a few examples of the pump designs using different combinations of servo actuators and pump heads.

Thanks to the powerful servo actuators and the associated microcontroller (CM-530, Robotis), the pump is fully controllable and programmable under a PC software environment.

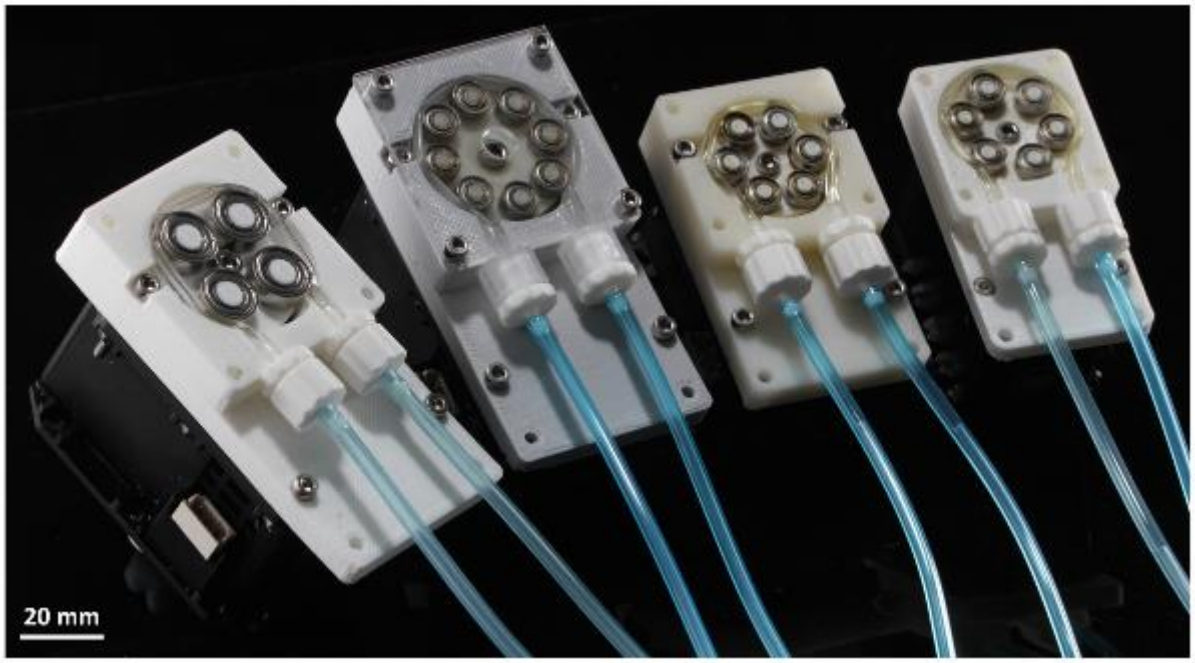


*Figure 6.2.2 Variant designs of customised pumps. From left to right: 1) Four-roller pump head with Dynamixel MX-64T servo, 2) eight-roller pump head with Dynamixel MX-64T servo, 3) six-roller pump head with Dynamixel MX-28T servo, and 4) six-roller pump head with Dynamixel AX-12A or AX-18A servo.*

The reliability of the pumps was assessed and the linear range between the flow rate and rolling speed was determined for each actuator (Figure 6.2.3). The pump using AX-18A had the highest maximum flow rate with a widest linear range, followed by MX-64T, AX-12A, and MX-32T. However, both AX-18A and AX12A could not achieve a low flow rate because they do not have enough torque at a low speed. On the contrary, MX-64T and MX-32T do not have a fast speed, but they are high in torque and powerful enough to achieve a flow rate as small as 75 µL/min.

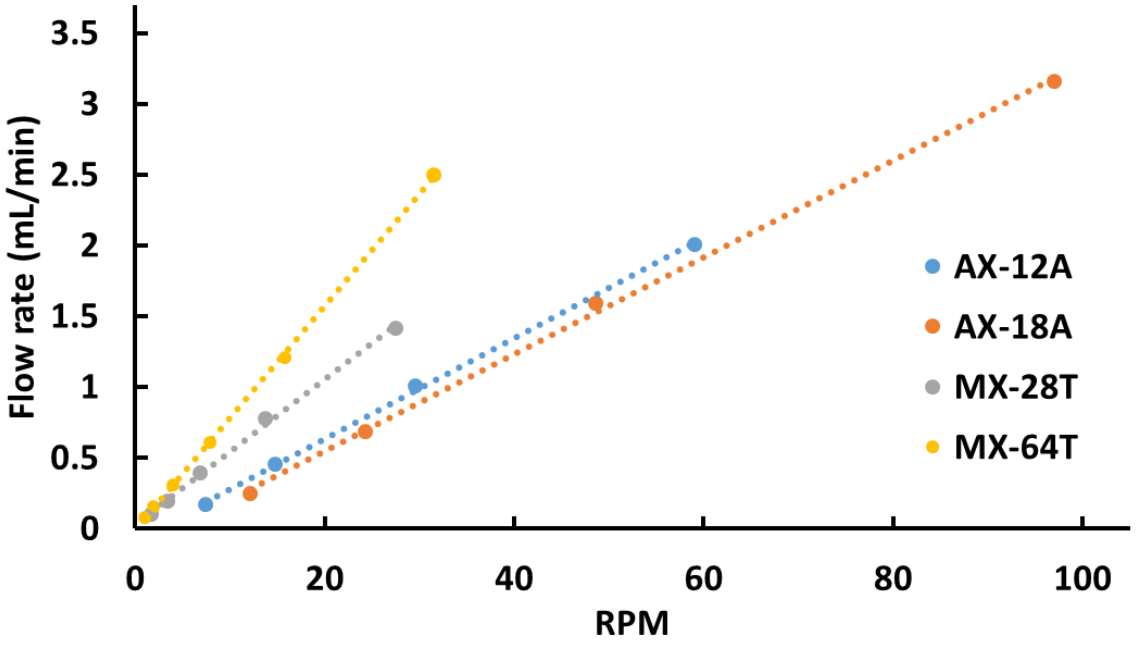


*Figure 6.2.3 Calibration curves of pumps using different servos, depicting the relationship between flow rate and pump speed (revolution per minute, RPM). All pumps had a linear correlation from at least 0.1 mL/min to 1.5 mL/min, which is sufficient for most applications in perfusion experiments.*

### 6.2.2 Pinch valve

Valve is one of the commonly used fluidic actuators in microfluidics. However, a programmable pinch valve is currently still rare. In this regard, I prototyped a pinch valve based on the Dynamixel AX-12A servo actuator. Similar to the pumps, the valve consisted of four major components: i) a servo actuator, ii) a 3D printed head, iii) a 3D printed pinch arm with a metal bearing as a pusher, and iv) tubing and connectors (Figure 6.2.4).

The valve was actuated by a CM-530 microcontroller (Robotis, Ltd). Like the pumps, the valve is also fully programmable under a PC software environment. The only difference was that the valve was operated in a “servo mode” instead of a “wheel mode” for the pump. In servo mode, the movement of the actuator could be more finely controlled. Note that AX-12A was a weak actuator that has a relatively low torque. However, in this experiment I found that it was enough to hold up to the pressure, until the tubing connector failed first. Hence, no further designs using other servo actuators were attempted.

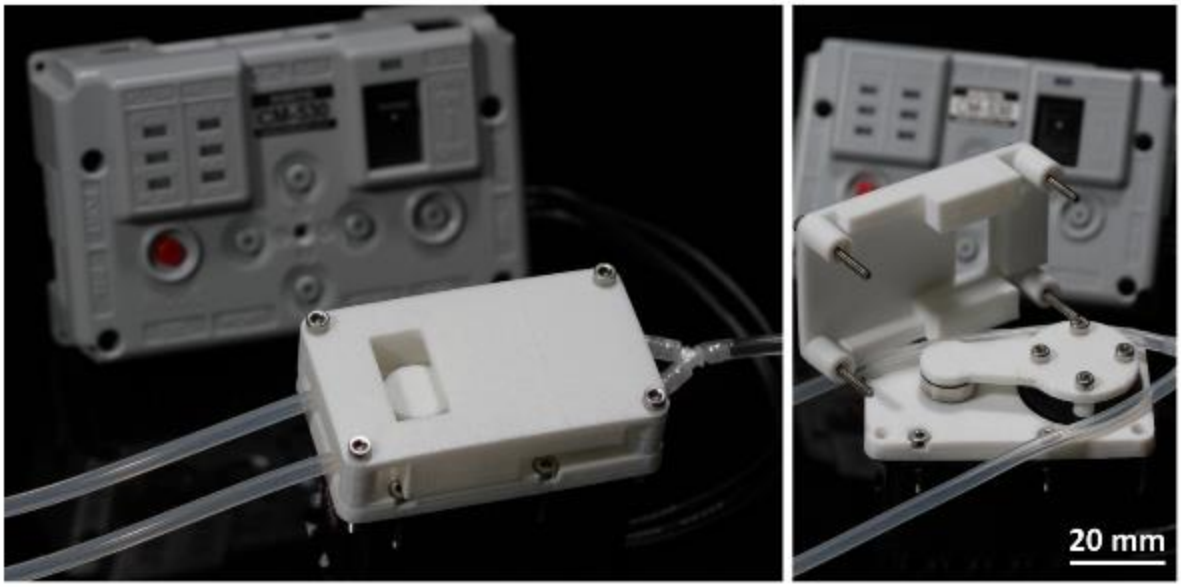


*Figure 6.2.4 Customised two-way pinch valve based on Dynamixel AX-12A servo. The pusher arm and the cover lid were 3D printed.*

## 6.3 Microfluidic total analysis system (μTAS)

To wrap up the study, I set out to design and manufacture an affordable and highly customisable analysis platform for zebrafish embryo bioassays. By integrating innovative technologies, such as microfluidics, robotics, and 3D printing, the microfluidic total analysis system miniaturised and automated all experimental procedures, including sampling, long-term flow-through culture, and detection.

The system was separated into two parts. The first part was the organism culturing system, which included a high-throughput chip with a fluidic interface, arrays of fluidic actuators, and an auxiliary miniaturised microscope (Figure 6.3.1). The utility and function of the chip and interface device were described above. Note that the fluidic actuation system was highly customisable and can be expanded to include additional pumps as required. A rack for pumps and fluidic reservoirs was prototyped using thermoplastic PMMA.

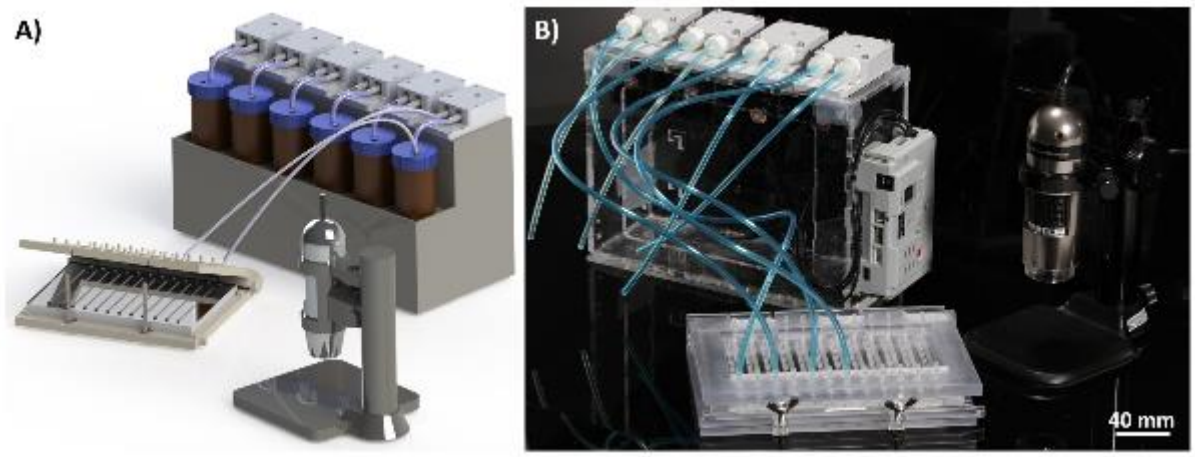


*Figure 6.3.1 Microfluidic pump array associated with a high-throughput chip interface and a miniaturised microscope. A) A photo realistic rendering image B) A macrophotograph depicting the experimental set-up.*

The second part of the system was an automated analysis platform. The core of the platform was a servo actuated rack-and-pinion stage, mounting the fluidic interface together with the chip device for automated image acquisition. As a proof-of-concept prototype, a simplified version of the stage that only moved alone one-dimension was manufactured. As such, the fluidic interface was also simplified to cradle one chip with one fluidic manifold. The rack-and-pinion system was actuated by an AX-12A servo. Two microcontrollers (CM-530, Robotis) were embedded on to the stage for controlling the moving system and fluidic actuators. Finally, a high-resolution miniaturised microscope (DinoLite, Taiwan) was placed under the stage, imaging the chip device from the bottom (Figure 6.3.2). The prototype was fabricated using thermal plastic PMMA.

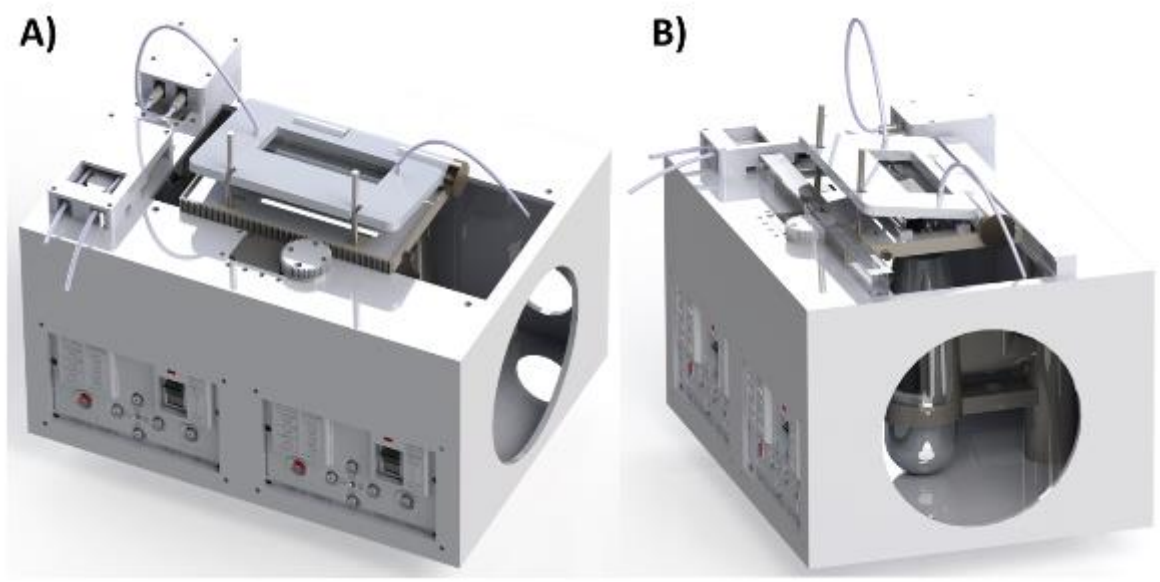


*Figure 6.3.2 Photo realistic rendering images of the microfluidic total analysis system (µTAS). The system comprised of a one dimensional rack-and-pinion moving stage, an embedded peristaltic pump, an embedded two-way valve, and a miniaturised microscope. A miniaturised fluidic interface was fit to the moving stage together with the lab-on-a-chip device. The system was controlled by two CM-530 microcontrollers (Robotis Ltd.).*

In the primary experiment, the moving stage was set to move at an interval of two seconds, each time covering three embryo traps, throughout the entire chip device. Afterwards, the stage moved to the original spot for the next imaging task. The system performed with great reproducibility in positioning the imaging regions after iterative tests (Figure 6.3.3).

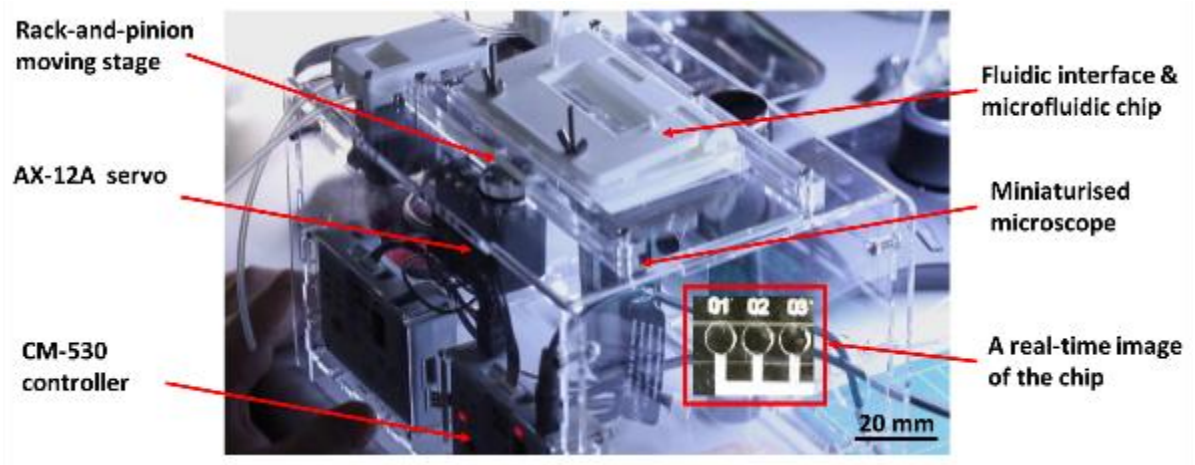


*Figure 6.3.3 Prototype of the microfluidic total analysis system (µTAS). All features are depicted. Inset: a window from a computer running the image capturing software, showing a real-time view of the chip device.*

## 6.4 Summary and discussion

In this chapter, more advanced technologies for automated and high-throughput zebrafish embryos bioassays were presented. To be able to actuate a high-density microfluidic system, a series of highly customised peristaltic pumps were manufactured. Robotic servo motors were selected as actuators that are powerful and accurate to provide continuous flows to the system. Lastly, I prototyped a microfluidic total analysis system that integrated all the aforementioned features into a platform, together with a moving stage and an imaging system, allowing automated image acquisition for high-throughput zebrafish embryo bioassays.

Although using microfluidics for high-throughput screening has garnered an increasing amount of interest, the development of the fluidic actuators was falling behind demand. Currently commercialised pumps were either not accurate enough or extremely expensive, which are unsuitable for batch experiments. In this regard, a cost-effective and miniaturised pump array was presented. It used robotic servos as the actuators, which are robust and precise. The pump head was customised and fabricated using 3D printing and was interchangeable among different servos for a variant of flow control requirement. Unfortunately, the prototypes were still very primitive, as the durability of the pumps were limited by the plastics used in 3D printers. A pump head made in rigid materials, such as metal or alloy, would be ideal.

There is also a lack of an automated, high-throughput and inexpensive total analysis system for zebrafish embryo biotests. Letamandia and co-workers present a system, but it was expensive and not user-friendly[68]. Currently, The Union Biometrica system based on work from Pardo-Martin and co-workers was commercialized. However, it was designed mainly for zebrafish larvae analysis[69]. This system is not broadly adapted because of significant cost and limited scope of use. As far as I know no real units have yet been delivered and only demo units are currently available after five years of development. Under this circumstance, the advantage of this study with a miniaturised and customisable device will be exploited.

# 7 Conclusions

The development of zebrafish embryo as a model organism for bioassays has attracted a great amount of interest in the biomedical and environmental research communities. However, there is a lack of available technology that allows automated and high-throughput screenings under flow-through conditions. The main objective of this thesis is to address this problem. I first I explored the use of 3D printing to rapidly fabricate lab-on-a-chip devices for zebrafish embryo assays and found a potentially underestimated biocompatibility issue in 3D printing materials. Following up, I investigated the toxicity profiles of a range of 3D printing materials by using standardised biotests. Next, I developed and fabricated a biocompatible lab-on-a-chip device for automated embryo loading, arraying, and culturing on a microperfusion chip. Finally, I modified and expanded the chip device for high-throughput screening purposes; I prototyped a microfluidic total analysis system using a miniaturised and automated imaging platform for zebrafish embryo bioassays.

## 7.1 Achievement and impact

In chapter 3, the feasibility of using 3D printing to accelerate the fabrication of microfluidic lab-on-a-chip devices was investigated. Compared with conventional rapid prototyping technologies, I demonstrate that selected stereolithography technologies can achieve superior feature production, comparable levels of optical transparency, and user-friendly manufacture of prototypes. However, I for the first time, reported that caution needs to be exercised because most of the tested 3D printing materials were found to be toxic and cause significant developmental abnormalities, as evidenced by zebrafish embryo biotests. This work suggested that using 3D printing technologies enables us to rapidly prototype innovative devices for related research, but current 3D printing materials should not be directly exposed to aquatic biological specimens in the long-term. As 3D printing technologies attract an increasing amount of interests in scientific research, this preliminary work created instructive information for potential users when choosing 3D printing systems.

As a follow up, chapter 4 presented an extensive toxicity profiling on a panel of common polymers used in 3D printing applications. This work, for the first time, conducted an in-

depth and multispecies toxicity test, indicating potential dangers and limitations in fabrication of biocompatible devices using the FDM, SLA, and MJM 3D printing systems. Moreover, a pioneering chemical analysis successfully revealed two chemical compounds existing in the materials and causing the toxicities. This research provided guidance to the scientists selecting biocompatible 3D printing materials and it also established an effective and efficient method to assess the toxicity of unknown materials.

To avoid using toxic 3D printing material in making lab-on-a-chip devices, chapter 5 presented the design and validation of an innovative lab-on-a-chip technology for automated zebrafish embryo biotests performed on immobilised fish embryos cultured under a continuous microfluidic perfusion. It is acknowledged that a microfluidic lab-on-a-chip systems, such as this work, where the most tasks are conducted automatically without disturbing the test specimens or causing sudden changes to their environment, will perform more productively than conventional static and manual bioassays. Moreover, the application of the technology developed in this thesis is not limited to manipulation of zebrafish embryos. With simple modifications in size and dimension, the device should be suitable for other aquatic small model organisms, including Xenopus oocytes and sturgeon embryos. On top of that, a few more advanced lab-on-a-chip devices were prototyped with customised equipment for automated and high-throughput zebrafish embryo screening tests. A proof-of-concept microfluidic living embryo array system was fabricated to enable *in situ* Fluorescence Ratiometric Imaging (FRIM) on developing zebrafish embryos for kinetic quantification of oxygen gradients. It is reasonable to envisage that integration of microfluidic chip-based technologies with FRIM represents a noteworthy direction to miniaturise and revolutionise research on metabolism and physiology *in vivo*. Moreover, a high-throughput microfluidic device was presented for zebrafish embryo bioassays. The device was conceptually designed to seamlessly interface with a fluorescent imaging cytometer for rapid and high-resolution imaging. I hope this work will pave the way for the next generation of microfluidic bio-instrumentation for real-time and high-throughput whole-organism analysis, with broad applications in drug discovery and ecotoxicology.

In chapter 6, a miniaturised microfluidic total analysis system was customised that integrated a lab-on-a-chip device, a fluidic interface, an array of fluidic actuators, a camera,

and a programmed moving stage. This prototype will prospectively become a highly customisable and cost effective bio-instrument for zebrafish research communities.

## 7.2 Limitation and future work

An extensive study on 3D printing material toxicity profiling was performed using standard biotests on aquatic model organisms. The result showed that 3D printing materials are very toxic in the aquatic environment, but how would they affect soil or vegetation remains unknown. More tests should be conducted in this direction.

A primary chemical analysis was performed to identify and quantify the compound existing in the polymer water extract using GC-MS. Although few compounds were identified, I believe that more substances exist in the water sample, as the current extraction method was restricted by the solvent used for the liquid-liquid extraction. Future studies should be conducted using more or a combination of solvents for extraction. More detection technologies, including LC-MS or NMR, could be used for identification.

A microfluidic zebrafish embryo trapping array was demonstrated to be capable of loading, immobilising, and culturing live embryos in a microperfusion environment. It was also designed to be able to unload all the embryos from the chip device at the end of experiment. However, the unloading performance was not very consistent in the validation experiment. Embryos were found clogged at the inlet of the channel and torn after recovery. As the unloading function was required by many of our collaborators, a modification in the fluidic inlet and loading channel will be conducted in future work.

A prototype of a microfluidic total analysis system was fabricated. It has a rack-and-pinion moving stage that could be programmed for automated imaging. The prototype is, however, very primitive in that the stage can only move along one dimension. In future work, a robotic system with two or more servo actuators could be integrated to the stage to allow the positioning to occur freely on the X-Y plane for imaging of high-throughput chip devices.

# References


[1] Wlodkowic, D., Khoshmanesh, K., Akagi, J., Williams, D. E., and Cooper, J. M., "Wormometry-on-a-chip: Innovative technologies for in situ analysis of small multicellular organisms," Cytometry Part A, 79A(10), 799-813 (2011).

[2] Ségalat, L., "Invertebrate Animal Models of Diseases as Screening Tools in Drug Discovery," ACS Chemical Biology, 2(4), 231-236 (2007).

[3] Persoone, G., and Wells, P. G., "Artemia in aquatic toxicology: a review," Artemia research and its applications, 1, 259-275 (1987).

[4] Nunes, B. S., Carvalho, F. D., Guilhermino, L. M., and Van Stappen, G., "Use of the genus Artemia in ecotoxicity testing," Environmental Pollution, 144(2), 453-462 (2006).

[5] Persoone, G., Baudo, R., Cotman, M., Blaise, C., Thompson, K. C., Moreira-Santos, M., Vollat, B., Törökne, A., and Han, T., "Review on the acute Daphnia magna toxicity test–Evaluation of the sensitivity and the precision of assays performed with organisms from laboratory cultures or hatched from dormant eggs," Knowledge and management of aquatic ecosystems(393), 01 (2009).

[6] Watson, S., Juttner, F., and Koster, O., "Daphnia behavioural responses to taste and odour compounds: ecological significance and application as an inline treatment plant monitoring tool," Water Science & Technology, 55(5), 23-31 (2007).

[7] Baillieul, M., and Blust, R., "Analysis of the swimming velocity of cadmium-stressed Daphnia magna," Aquatic Toxicology, 44(4), 245-254 (1999).

[8] Bahrndorff, S., Michaelsen, T. Y., Jensen, A., Marcussen, L. F., Nielsen, M. E., and Roslev, P., "Automated swimming activity monitor for examining temporal patterns of toxicant effects on individual Daphnia magna," Journal of Applied Toxicology, n/a-n/a (2015).

[9] Untersteiner, H., Kahapka, J., and Kaiser, H., "Behavioural response of the cladoceran Daphnia magna Straus to sublethal Copper stress—validation by image analysis," Aquatic Toxicology, 65(4), 435-442 (2003).

[10] Zon, L. I., and Peterson, R. T., "In vivo drug discovery in the zebrafish," Nature Reviews Drug Discovery, 4(1), 35-44 (2005).

[11] Robert, J., and Cohen, N., "The genus Xenopus as a multispecies model for evolutionary and comparative immunobiology of the 21st century," Developmental and comparative immunology, 35(9), 916-23 (2011).

[12] Adams, D. S., Tseng, A. S., and Levin, M., "Light-activation of the Archaerhodopsin H(+)-pump reverses age-dependent loss of vertebrate regeneration: sparking system-level controls in vivo," Biology open, 2(3), 306-13 (2013).

[13] Pratt, K. G., and Khakhalin, A. S., "Modeling human neurodevelopmental disorders in the Xenopus tadpole: from mechanisms to therapeutic targets," Disease models & mechanisms, 6(5), 1057-65 (2013).

[14] Scott, E. K., "The Gal4/UAS toolbox in zebrafish: new approaches for defining behavioral circuits," Journal of neurochemistry, 110(2), 441-56 (2009).

[15] Blackiston, D., Shomrat, T., Nicolas, C. L., Granata, C., and Levin, M., "A second-generation device for automated training and quantitative behavior analyses of molecularly-tractable model organisms," PLoS One, 5(12), e14370 (2010).

[16] Gerlai, R., "Associative learning in zebrafish (Danio rerio)," Methods Cell Biol, 101, 249-70 (2011).

[17] Sison, M., and Gerlai, R., "Associative learning performance is impaired in zebrafish (Danio rerio) by the NMDA-R antagonist MK-801," Neurobiol Learn Mem, (2011).

[18] Blackiston, D. J., and Levin, M., "Aversive training methods in Xenopus laevis: general principles," Cold Spring Harbor protocols, 2012(5), (2012).

[19] Pittman, J. T., and Lott, C. S., "Startle response memory and hippocampal changes in adult zebrafish pharmacologically-induced to exhibit anxiety/depression-like behaviors," Physiology & behavior, 123, 174-9 (2014).
[20] Harper, C., and Lawrence, C., [The Laboratory Zebrafish] CRC Press, (2012).
[21] Chakraborty, C., Hsu, C. H., Wen, Z. H., Lin, C. S., and Agoramoorthy, G., "Zebrafish: A Complete Animal Model for In Vivo Drug Discovery and Development," Current Drug Metabolism, 10, 116-124 (2009).
[22] Rihel, J., Prober, D. A., Arvanites, A., Lam, K., Zimmerman, S., Jang, S., Haggarty, S. J., Kokel, D., Rubin, L. L., and Peterson, R. T., "Zebrafish behavioral profiling links drugs to biological targets and rest/wake regulation," Science, 327(5963), 348-351 (2010).
[23] Mandrekar, N., and Thakur, N. L., "Significance of the zebrafish model in the discovery of bioactive molecules from nature," Biotechnology letters, 31(2), 171-179 (2009).
[24] Crawford, A. D., Liekens, S., Kamuhabwa, A. R., Maes, J., Munck, S., Busson, R., Rozenski, J., Esguerra, C. V., and de Witte, P. A., "Zebrafish bioassay-guided natural product discovery: isolation of angiogenesis inhibitors from East African medicinal plants," PloS one, 6(2), e14694 (2011).
[25] Bowman, T. V., and Zon, L. I., "Swimming into the Future of Drug Discovery: In Vivo Chemical Screens in Zebrafish," ACS Chemical Biology, 5(2), 159-161 (2010).
[26] Taylor, K. L., Grant, N. J., Temperley, N. D., and Patton, E. E., "Small molecule screening in zebrafish: an in vivo approach to identifying new chemical tools and drug leads," Cell Communication and Signaling, 8(1), 11 (2010).
[27] Selderslaghs, I. W., Van Rompay, A. R., De Coen, W., and Witters, H. E., "Development of a screening assay to identify teratogenic and embryotoxic chemicals using the zebrafish embryo," Reproductive toxicology, 28(3), 308-320 (2009).
[28] Ahmad, F., Noldus, L. P., Tegelenbosch, R. A., and Richardson, M. K., "Zebrafish embryos and larvae in behavioural assays," Behaviour, 149(10-12), 10-12 (2012).
[29] Rubinstein, A. L., "Zebrafish assays for drug toxicity screening," (2006).
[30] Parng, C., Seng, W. L., Semino, C., and McGrath, P., "Zebrafish: a preclinical model for drug screening," Assay and drug development technologies, 1(1), 41-48 (2002).
[31] Eimon, P. M., and Rubinstein, A. L., "The use of in vivo zebrafish assays in drug toxicity screening," (2009).
[32] Ma, A. C., He, B., Guo, Y., and Leung, A. Y., "Modeling Tumor Angiogenesis with Zebrafish."
[33] van Ham, T. J., Mapes, J., Kokel, D., and Peterson, R. T., "Live imaging of apoptotic cells in zebrafish," The FASEB Journal, 24(11), 4336-4342 (2010).
[34] Ghotra, V. P., He, S., de Bont, H., van der Ent, W., Spaink, H. P., van de Water, B., Snaar-Jagalska, B. E., and Danen, E. H., "Automated whole animal bio-imaging assay for human cancer dissemination," PloS one, 7(2), e31281 (2012).
[35] Tran, T. C., Sneed, B., Haider, J., Blavo, D., White, A., Aiyejorun, T., Baranowski, T. C., Rubinstein, A. L., Doan, T. N., Dingledine, R., and Sandberg, E. M., "Automated, quantitative screening assay for antiangiogenic compounds using transgenic zebrafish," Cancer research, 67(23), 11386-11392 (2007).
[36] Serbedzija, G. N., Flynn, E., and Willett, C. E., "Zebrafish angiogenesis: a new model for drug screening," Angiogenesis, 3(4), 353-359 (1999).
[37] Lawson, N. D., and Weinstein, B. M., "In Vivo Imaging of Embryonic Vascular Development Using Transgenic Zebrafish," Developmental Biology, 248(2), 307-318 (2002).
[38] Li, Y., Huang, W., Huang, S., Du, J., and Huang, C., "Screening of anti-cancer agent using zebrafish: comparison with the MTT assay," Biochemical and biophysical research communications, 422(1), 85-90 (2012).
[39] Lammer, E., Carr, G. J., Wendler, K., Rawlings, J. M., Belanger, S. E., and Braunbeck, T., "Is the fish embryo toxicity test (FET) with the zebrafish (Danio rerio) a potential alternative for the

fish acute toxicity test?," Comparative Biochemistry and Physiology Part C: Toxicology & Pharmacology, 149(2), 196-209 (2009).
[40] CARVAN, M. J., Dalton, T. P., Stuart, G. W., and Nebert, D. W., "Transgenic zebrafish as sentinels for aquatic pollution," Annals of the New York Academy of Sciences, 919(1), 133-147 (2000).
[41] Nerbert, D., "Use of reporter genes and vertebrate DNA motifs in transgenic zebrafish as sentinels for assessing aquatic pollution," Environmental Health Perspectives, 110(1), A15 (2002).
[42] Kusik, B. W., Carvan III, M. J., and Udvadia, A. J., "Detection of mercury in aquatic environments using EPRE reporter zebrafish," Marine Biotechnology, 10(6), 750-757 (2008).
[43] Scholz, S., Fischer, S., Gündel, U., Küster, E., Luckenbach, T., and Voelker, D., "The zebrafish embryo model in environmental risk assessment—applications beyond acute toxicity testing," Environmental Science and Pollution Research, 15(5), 394-404 (2008).
[44] [OECD Guidelines for the Testing of Chemicals 236], (2013).
[45] Hwang, H., and Lu, H., "Microfluidic tools for developmental studies of small model organisms –nematodes, fruit flies, and zebrafish," Biotechnology Journal, 8(2), 192-205 (2013).
[46] Yanik, M. F., Rohde, C. B., and Pardo-Martin, C., "Technologies for micromanipulating, imaging, and phenotyping small invertebrates and vertebrates," Annual review of biomedical engineering, 13, 185-217 (2011).
[47] Lammer, E., Kamp, H. G., Hisgen, V., Koch, M., Reinhard, D., Salinas, E. R., Wendler, K., Zok, S., and Braunbeck, T., "Development of a flow-through system for the fish embryo toxicity test (FET) with the zebrafish (Danio rerio)," Toxicology in Vitro, 23(7), 1436-1442 (2009).
[48] Quantification, G., [Lab on Chip PCR].
[49] University, R., [Wallet-sized labs the next big thing], (2014).
[50] Funfak, A., Brösing, A., Brand, M., and Köhler, J. M., "Micro fluid segment technique for screening and development studies on Danio rerio embryos," Lab on a Chip, 7(9), 1132-1138 (2007).
[51] Son, S. U., and Garrell, R. L., "Transport of live yeast and zebrafish embryo on a droplet ("digital") microfluidic platform," Lab on a chip, 9(16), 2398-2401 (2009).
[52] Paik, P., Pamula, V. K., Pollack, M. G., and Fair, R. B., "Electrowetting-based droplet mixers for microfluidic systems," Lab on a Chip, 3(1), 28-33 (2003).
[53] Paik, P., Pamula, V. K., and Fair, R. B., "Rapid droplet mixers for digital microfluidic systems," Lab on a Chip, 3(4), 253-259 (2003).
[54] Shen, Y.-c., Li, D., Al-Shoaibi, A., Bersano-Begey, T., Chen, H., Ali, S., Flak, B., Perrin, C., Winslow, M., and Shah, H., "A student team in a University of Michigan biomedical engineering design course constructs a microfluidic bioreactor for studies of zebrafish development," Zebrafish, 6(2), 201-213 (2009).
[55] Wielhouwer, E. M., Ali, S., Al-Afandi, A., Blom, M. T., Olde Riekerink, M. B., Poelma, C., Westerweel, J., Oonk, J., Vrouwe, E. X., Buesink, W., vanMil, H. G. J., Chicken, J., van 't Oever, R., and Richardson, M. K., "Zebrafish embryo development in a microfluidic flow-through system," Lab on a Chip, 11(10), 1815-1824 (2011).
[56] Yang, F., Chen, Z., Pan, J., Li, X., Feng, J., and Yang, H., "An integrated microfluidic array system for evaluating toxicity and teratogenicity of drugs on embryonic zebrafish developmental dynamics," Biomicrofluidics, 5, 024115 (2011).
[57] Choudhury, D., van Noort, D., Iliescu, C., Zheng, B., Poon, K.-L., Korzh, S., Korzh, V., and Yu, H., "Fish and Chips: a microfluidic perfusion platform for monitoring zebrafish development," Lab on a Chip, 12(5), 892-900 (2012).
[58] Zheng, C., Zhou, H., Liu, X., Pang, Y., Zhang, B., and Huang, Y., "Fish in chips: an automated microfluidic device to study drug dynamics in vivo using zebrafish embryos," Chemical Communications, 50(8), 981-984 (2014).

[59] Akagi, J., Khoshmanesh, K., Evans, B., Hall, C. J., Crosier, K. E., Cooper, J. M., Crosier, P. S., and Wlodkowic, D., “Miniaturized Embryo Array for Automated Trapping, Immobilization and Microperfusion of Zebrafish Embryos,” PLoS ONE, 7(5), e36630 (2012).
[60] Khoshmanesh, K., Akagi, J., Hall, C. J., Crosier, K. E., Crosier, P. S., Cooper, J. M., and Wlodkowic, D., “New rationale for large metazoan embryo manipulations on chip-based devices,” Biomicrofluidics, 6, 024102 (2012).
[61] Tan, W.-H., and Takeuchi, S., “A trap-and-release integrated microfluidic system for dynamic microarray applications,” Proceedings of the National Academy of Sciences, 104(4), 1146-1151 (2007).
[62] Wang, K. I. K., Bonnetat, A., Andrews, M., Salcic, Z., Akagi, J., and Wlodkowic, D., "Automatic image analysis of zebrafish embryo development for lab-on-a-chip." 194-199.
[63] Akagi, J., Khoshmanesh, K., Hall, C. J., Crosier, K. E., Crosier, P. S., Cooper, J. M., and Wlodkowic, D., “Fish on Chips: Automated Microfluidic Living Embryo Arrays,” Procedia Engineering, 47(0), 84-87 (2012).
[64] Akagi, J., Khoshmanesh, K., Hall, C. J., Cooper, J. M., Crosier, K. E., Crosier, P. S., and Wlodkowic, D., “Fish on Chips: Microfluidic Living Embryo Array for Accelerated In Vivo Angiogenesis Assays,” Sensors and Actuators B: Chemical, (2012).
[65] Wang, K. I. K., Salcic, Z., Yeh, J., Akagi, J., Zhu, F., Hall, C. J., Crosier, K. E., Crosier, P. S., and Wlodkowic, D., “Toward embedded laboratory automation for smart lab-on-a-chip embryo arrays,” Biosensors and Bioelectronics, 48(0), 188-196 (2013).
[66] Akagi, J., Zhu, F., Hall, C. J., Khoshmanesh, K., Kalantar-Zadeh, K., Mitchell, A., Crosier, K. E., Crosier, P. S., and Wlodkowic, D., "Dynamic analysis of angiogenesis in transgenic zebrafish embryos using a 3D multilayer chip-based technology." 86151B-86151B-9.
[67] Akagi, J., [Development of Lab-on-a-chip devices for Automated Manipulation of Zebrafish] University of Auckland, (2014).
[68] Letamendia, A., Quevedo, C., Ibarbia, I., Virto, J. M., Holgado, O., Diez, M., Belmonte, J. C. I., and Callol-Massot, C., “Development and validation of an automated high-throughput system for zebrafish in vivo screenings,” PloS one, 7(5), e36690 (2012).
[69] Pardo-Martin, C., Chang, T.-Y., Koo, B. K., Gilleland, C. L., Wasserman, S. C., and Yanik, M. F., “High-throughput in vivo vertebrate screening,” Nature methods, 7(8), 634-636 (2010).
[70] Chang, T.-Y., Pardo-Martin, C., Allalou, A., Wahlby, C., and Yanik, M. F., “Fully automated cellular-resolution vertebrate screening platform with parallel animal processing,” Lab on a Chip, 12(4), 711-716 (2012).
[71] Skommer, J., and Wlodkowic, D., “Successes and future outlook for microfluidics-based cardiovascular drug discovery,” Expert opinion on drug discovery, 10(3), 231-244 (2015).
[72] Masuzawa, T., “State of the Art of Micromachining,” CIRP Annals - Manufacturing Technology, 49(2), 473-488 (2000).
[73] Qin, D., Xia, Y., and Whitesides, G. M., “Rapid prototyping of complex structures with feature sizes larger than 20 μm,” Advanced Materials, 8(11), 917-919 (1996).
[74] Xia, Y., and Whitesides, G. M., “Soft Lithography,” Angewandte Chemie International Edition, 37(5), 550-575 (1998).
[75] Xia, Y., and Whitesides, G. M., “Soft lithography,” Annual review of materials science, 28(1), 153-184 (1998).
[76] Weibel, D. B., DiLuzio, W. R., and Whitesides, G. M., “Microfabrication meets microbiology,” Nature Reviews Microbiology, 5(3), 209-218 (2007).
[77] Waldbaur, A., Rapp, H., Länge, K., and Rapp, B. E., “Let there be chip—towards rapid prototyping of microfluidic devices: one-step manufacturing processes,” Analytical Methods, 3(12), 2681-2716 (2011).
[78] Hull, C. W., [Apparatus for production of three-dimensional objects by stereolithography] Google Patents, (1986).
[79] Takagi, T., and Nakajima, N., "Photoforming applied to fine machining." 173-178.

[80] Ikuta, K., and Hirowatari, K., "Real three dimensional micro fabrication using stereo lithography and metal molding." 42-47.
[81] i.materialise, [3D Printing Technologies: Stereolithography], (2015).
[82] Ho, C. M. B., Ng, S. H., Li, K. H. H., and Yoon, Y.-J., "3D printed microfluidics for biological applications," Lab on a Chip, (2015).
[83] Choi, J.-W., Ha, Y. M., Choi, K., and Lee, S. H., "Fabrication of 3-dimensional microstructures using dynamic image projection." 339, 473-478.
[84] Wu, S., Serbin, J., and Gu, M., "Two-photon polymerisation for three-dimensional micro-fabrication," Journal of Photochemistry and Photobiology A: Chemistry, 181(1), 1-11 (2006).
[85] Technologies, D. M., "3D print - FDM," (2015).
[86] Huang, T., Qu, X., Liu, J., and Chen, S., "3D printing of biomimetic microstructures for cancer cell migration," Biomedical Microdevices, 16(1), 127-132 (2014).
[87] Bertassoni, L. E., Cecconi, M., Manoharan, V., Nikkhah, M., Hjortnaes, J., Cristino, A. L., Barabaschi, G., Demarchi, D., Dokmeci, M. R., and Yang, Y., "Hydrogel bioprinted microchannel networks for vascularization of tissue engineering constructs," Lab on a Chip, 14(13), 2202-2211 (2014).
[88] McDonald, J. C., Chabinyc, M. L., Metallo, S. J., Anderson, J. R., Stroock, A. D., and Whitesides, G. M., "Prototyping of Microfluidic Devices in Poly(dimethylsiloxane) Using Solid-Object Printing," Analytical Chemistry, 74(7), 1537-1545 (2002).
[89] Bonyar, A., Santha, H., Ring, B., Varga, M., Kovacs, J. G., and Harsanyi, G., [3D Rapid Prototyping Technology (RPT) as a powerful tool in microfluidic development] Elsevier Science Bv, Amsterdam(2010).
[90] Bonyár, A., Sántha, H., Varga, M., Ring, B., Vitéz, A., and Harsányi, G., "Characterization of rapid PDMS casting technique utilizing molding forms fabricated by 3D rapid prototyping technology (RPT)," International Journal of Material Forming, 7(2), 189-196 (2014).
[91] Han, K.-H., "Reliability aspects of packaging and integration technology for microfluidic systems," Device and Materials Reliability, IEEE Transactions on, 5(3), 452-457 (2005).
[92] Paydar, O., Paredes, C., Hwang, Y., Paz, J., Shah, N., and Candler, R., "Characterization of 3D-printed microfluidic chip interconnects with integrated O-rings," Sensors and Actuators A: Physical, 205, 199-203 (2014).
[93] Au, A. K., Lee, W., and Folch, A., "Mail-order microfluidics: evaluation of stereolithography for the production of microfluidic devices," Lab on a Chip, 14(7), 1294-1301 (2014).
[94] Preechaburana, P., and Filippini, D., "Fabrication of monolithic 3D micro-systems," Lab on a Chip, 11(2), 288-295 (2011).
[95] Shallan, A. I., Smejkal, P., Corban, M., Guijt, R. M., and Breadmore, M. C., "Cost-effective three-dimensional printing of visibly transparent microchips within minutes," Analytical chemistry, 86(6), 3124-3130 (2014).
[96] Kitson, P. J., Rosnes, M. H., Sans, V., Dragone, V., and Cronin, L., "Configurable 3D-Printed millifluidic and microfluidic 'lab on a chip'reactionware devices," Lab on a Chip, 12(18), 3267-3271 (2012).
[97] Rogers, C. I., Qaderi, K., Woolley, A. T., and Nordin, G. P., "3D printed microfluidic devices with integrated valves," Biomicrofluidics, 9(1), 016501 (2015).
[98] Anderson, K. B., Lockwood, S. Y., Martin, R. S., and Spence, D. M., "A 3D Printed Fluidic Device that Enables Integrated Features," Analytical Chemistry, 85(12), 5622-5626 (2013).
[99] Begolo, S., Zhukov, D. V., Selck, D. A., Li, L., and Ismagilov, R. F., "The pumping lid: investigating multi-material 3D printing for equipment-free, programmable generation of positive and negative pressures for microfluidic applications," Lab on a Chip, 14(24), 4616-4628 (2014).
[100] Erkal, J. L., Selimovic, A., Gross, B. C., Lockwood, S. Y., Walton, E. L., McNamara, S., Martin, R. S., and Spence, D. M., "3D printed microfluidic devices with integrated versatile and reusable electrodes," Lab on a Chip, 14(12), 2023-2032 (2014).

[101] Walczak, R., and Adamski, K., “Inkjet 3D printing of microfluidic structures—on the selection of the printer towards printing your own microfluidic chips,” Journal of Micromechanics and Microengineering, 25(8), 085013 (2015).
[102] Bhargava, K. C., Thompson, B., and Malmstadt, N., “Discrete elements for 3D microfluidics,” Proceedings of the National Academy of Sciences, 111(42), 15013-15018 (2014).
[103] Bolch, C. S., and Blackburn, S., “Isolation and purification of Australian isolates of the toxic cyanobacteriumMicrocystis aeruginosa Kütz,” Journal of Applied Phycology, 8(1), 5-13 (1996).
[104] Wigh, A., Bony, S., Devaux, A., Gonzalez-Ospina, A., and Domenjoud, B., "Proposal for a sub-lethal toxicity test using zebrafish embryo." Poster presentation (WE026).
[105] Zhu, F., Skommer, J., Macdonald, N. P., Friedrich, T., Kaslin, J., and Wlodkowic, D., “Three-dimensional printed millifluidic devices for zebrafish embryo tests,” Biomicrofluidics, 9(4), 046502 (2015).
[106] [OECD Guidelines for the Testing of Chemicals 201], (2002).
[107] Zhu, F., Skommer, J., Friedrich, T., Kaslin, J., and Wlodkowic, D., "3D printed polymers toxicity profiling: a caution for biodevice applications." 96680Z-96680Z-7.
[108] Yamaji, K., Kawasaki, Y., Yoshitome, K., Matsunaga, H., and Sendo, T., “Quantitation and human monocyte cytotoxicity of the polymerization agent 1-hydroxycyclohexyl phenyl ketone (Irgacure 184) from three brands of aqueous injection solution,” Biological and Pharmaceutical Bulletin, 35(10), 1821-1825 (2012).
[109] Zhu, F., Wigh, A., Friedrich, T., Devaux, A., Bony, S., Nugegoda, D., Kaslin, J., and Wlodkowic, D., “Automated Lab-on-a-Chip Technology for Fish Embryo Toxicity Tests Performed under Continuous Microperfusion (µFET),” Environmental science & technology, (2015).
[110] Karlsson, J., von Hofsten, J., and Olsson, P.-E., “Generating Transparent Zebrafish: A Refined Method to Improve Detection of Gene Expression During Embryonic Development,” Marine Biotechnology, 3(6), 522-527 (2001).
[111] Meier, J. K., Gosau, M., Müller, S., Moralis, A., Liebsch, G., and Prantl, L., [Perfusion Monitoring in Microvascular Flaps: Fluorescence Imaging Applied as a Method to Discover Vessel Thrombosis.], (2012).
[112] Meier, J. K., Prantl, L., Muller, S., Moralis, A., Liebsch, G., and Gosau, M., “Simple, fast and reliable perfusion monitoring of microvascular flaps,” Clinical hemorheology and microcirculation, 50(1-2), 13-24 (2012).
[113] Kellner, K., Liebsch, G., Klimant, I., Wolfbeis, O. S., Blunk, T., Schulz, M. B., and Gopferich, A., “Determination of oxygen gradients in engineered tissue using a fluorescent sensor,” Biotechnology and bioengineering, 80(1), 73-83 (2002).
[114] Zhu, F., Baker, D., Skommer, J., Sewell, M., and Wlodkowic, D., “Real‐time 2D visualization of metabolic activities in zebrafish embryos using a microfluidic technology,” Cytometry Part A, 87(5), 446-450 (2015).
[115] Wlodkowic, D., Faley, S., Zagnoni, M., Wikswo, J. P., and Cooper, J. M., “Microfluidic Single-Cell Array Cytometry for the Analysis of Tumor Apoptosis,” Analytical Chemistry, 81(13), 5517-5523 (2009).
[116] Whitesides, G. M., “The origins and the future of microfluidics,” Nature, 442(7101), 368-373 (2006).